Investigation of isocyanate-based dual-cure resins and their suitability for additive manufacturing

Inaugural-Dissertation

zur

Erlangung des Doktorgrades

der Mathematisch-Naturwissenschaftlichen Fakultät

der Universität zu Köln

vorgelegt von

Anne Fischer geb. Hansen

aus Mechernich

Köln, 2021

Abstract

The development of materials for vat photopolymerization printing technologies has gained increasing attention within the last ten years. To date, the choice of materials for this printing technology is limited to photopolymers that tend to result in highly crosslinked, but usually brittle material properties. In this work, a dual-cure approach was developed, with the target to improve the overall material properties of 3D printed objects. For this purpose, the orthogonal and sequential polymerization of acrylate- and polyisocyanate based precursors was investigated. Photosensitive polyurethane acrylates were synthesized and mixed with low viscous polyisocyanates. The sequential polymerization was triggered by UV-light and heat, respectively. The reaction of the isocyanate groups in the heat, resulted in a polyurea network, confirmed by infrared spectroscopy. The morphology of resulting combined networks was systematically investigated by dynamic mechanical analysis and atomic force microscopy and showed that phase-separated morphologies with two distinct glass transition temperatures were formed, leading to a 10 fold increase in toughness in comparison to the neat polymeric networks. First printing trials showed the feasibility of the resin system for vat photopolymerization. The approach was extended to the sequential polymerization of isocyanate terminated prepolymers and low viscous acrylates. Varying the crosslinking densities of each polymeric network resulted in different morphologies as well as thermomechanical properties. Typical elastomers were obtained by a low crosslinking density of both polymeric networks. Cyclic loading-unloading measurements on 3D printed specimen showed the energy elastic behavior of the materials and an elongation at break of 101 % and a tensile strength of 3.4 N·mm^{-2} were achieved. A dual-cure resin based on acrylate-functionalized polyisocyanates was evaluated and resulted in thermally- and chemically stable 3D printed materials with the option to generate adoptable and catalytically active surfaces. The suitability of this resin to 3D print chemical reaction ware was demonstrated.

In summary, the results obtained in this work show the tuneability and variability of combining acrylate- and polyisocyanate precursors, contributing to the increasing demand of new and improved materials for vat photopolymerization.

Kurzfassung

Die Entwicklung von lichtempfindlichen Harzen die in der Stereolithographie zum Einsatz kommen, hat in den letzten 10 Jahren an Interesse gewonnen. Die derzeitigen Harze resultieren oftmals in spröde Materialeigenschaften, was der hohen Vernetzungsdichte der bei der Polymerisation entstehenden Netzwerke zuschulden ist. Die Entwicklung von neuen Materialien mit verbesserten Eigenschaften ist daher von großem Interesse und steht im Fokus dieser Arbeit. Zu diesem Zweck wurden Acrylate und Isocyanate miteinander kombiniert, die in einem sequentiellen Polymerisationsprozess zur Reaktion gebracht wurden. Dazu wurden lichtsensitive Polyurethanacrylate hergestellt und mit Polyisocyanaten vermischt. Die Initiierung der radikalischen Polymerisation der Acrylate erfolgte mittels UV Licht und die Reaktion der Isocyanate mittels Wärmezufuhr. Die Reaktion der Isocyanate resultierte in ein Polyharnstoff Netzwerk, wie mittels Infrarot Spektroskopie gezeigt werden konnte. Die Morphologie der resultierenden kombinierten Netzwerke wurde systematisch mittels Rasterkraftmikroskopie und dynamisch mechanischer Analyse untersucht. Es konnte gezeigt werden, dass phasenseparierte Netzwerke mit zwei Glasübergangstemperaturen entstanden sind, die zu einer 10-fachen Erhöhung der Zähigkeit im Vergleich zu den reinen Materialien geführt hat. Die Anwendung des entwickelten Harzsystems im 3D Druck konnte erfolgreich gezeigt werden. Weiterhin wurde das Konzept auf Isocyanat-terminierte Prepolymere, in Kombination mit niedrig viskosen Acrylaten ausgeweitet. Insbesondere wurde der Einfluss der Vernetzungsdichten der beiden Polymerphasen auf die Morphologie sowie die thermomechanischen Eigenschaften untersucht. Es konnte gezeigt werden, dass niedrige Vernetzungsdichten beider Polymerphasen zu energie-elastischen Materialien führen. Das gedruckte Bauteil verfügt über eine Dehnung von 101 % und eine Zugfestigkeit von 3.4 N·mm^{-2}. Weiterhin erfolgte die Synthese einer hybriden Struktur, die sowohl lichtsensitive Acrylat-, als auch reaktive Isocyanat-Gruppen enthält. Die Verwendung dieser Struktur als Basismaterial für den 3D Druck von chemisch stabilen Bauteilen wurde gezeigt, ebenso wie die Möglichkeit, die Oberfläche des 3D gedruckten Bauteils in einem nachgelagerten Prozessschritt zu funktionalisieren. Der Einsatz dieses Harzes für das Drucken chemischer Experimente wurde anhand einer Modellreaktion gezeigt.

Die Ergebnisse dieser Arbeit zeigen, dass die Kombination von Acrylaten und Isocyanaten ein breites Eigenschaftsprofil liefern und so zu verbesserten Eigenschaften von 3D gedruckten Bauteilen führen.

Table of Contents

List of Abbreviations

2C	Two component
1C	One component
3D	Threedimensional
ABP	4-aminobenzophenone
AC	Acrylic network
AFM	Atomic force microscopy
AM	Additive manufacturing
AN	Acrylic network
ATR	Attenuated total reflection
a.u.	Arbitrary units
BBOT	2,5-bis(5-tert-butyl-2-benzoxazolyl)thiophene
BHT	Butylated hydroxytoluene
CL	crosslinked
CN	Combined network
CLIP	Continous liquid interface printing
Conc.	Concentration
COS	Cross sectional skeleton
DBA	Dibutylamine
DBTL	Dibutyltin dilaurate
DCM	Dichloromethane
DLP	Digital light processing
DMA	Dynamic mechanical analysis
DMF	Dimethylformamide
DPGDA	Dipropylene glycol diacrylate
DSC	Differential scanning calorimetry
FDM	Fused deposition modelling
FFF	Fused filament fabrication
FT-IR	Fourier-transform infrared
GPC	Gel permeation chromatography
HCl	Hydrocloric acid
HDI	Hexamethylene diisocyanate

HEA	Hydroxyethyl acrylate
HEMA	Hydroxyethyl methacrylate
HSS	High speed sintering
iCN	Inverse combined network
IPDI	Isphorone diisocyanate
IPN	Interpenetrating network
LCD	Liquid crystal display
MDI	Methylenediphenyl diisocyanate
MeOD	Deutrated methanol
NCO	Isocyanate group
n.d.	Not determined
NMR	Nuclear magnetic resonance
PA	Polyamide
PC	Polycarbonate
PDI	Pentamethylene diisocyanate
PDI	Polydispersity index
PEC	Polyethercarbonate
PEG	Polyethylene glycol
PEGDA	Polyethylene glycol diacrylate
PET	Polyethylene terephtalate
PP	Polypropylene
PPG	Polypropylene glycol
pTHF	Polytetrahydrofurane
PU	Polyurethane
PUA	Polyurethane acrylate
Ref.	Reference
SANS	Small angle neutron scattering
SAXS	Small angle X-ray scattering
SLA	Sterelothography apparatus
SLS	Selective laser sintering
STL	Standard triangulation language
TDI	Toluene diisocyanate
Tg	Glass transition temperature
THF	Tetrahydrofurane

THFA	Tetrahydrofurfuryl acrylate
TEM	Transmission electron microscopy
TPE	Thermoplastic elastomer
TPU	Thermoplastic polyurethane
Vis	Visible
VOC	Volatile organic compound
VPP	Vat photopolymerization
wt%	Weight percent

1 Introduction

In our everyday life, we are surrounded by the interaction of light and matter: It is the reason why nature blossoms anew every year, why our body is able to produce vitamin D and why we can see the world as colorful as it is. Researchers have harnessed the interaction of light and matter to develop innovative technologies that have become indispensable in today's world.

One of these innovative technologies is radiation curing, which has been intensively investigated since the 1960's.[1] It can be defined as the polymerization (crosslinking) of monomers, requiring a photon to initiate a chain propagation.[2] For the first time, solvents were eliminated for the preparation of coatings, adhesives and printing inks, which is one reason why this technology has experienced a steadily steep growth since then.

As Lambert and Beer have already taught us in 1729, the penetration of light through a material is limited, which is the reason why radiation curing was and (somehow) still is restricted to applications with low layer thicknesses.[3,4] But as early as 1974, the researcher David Jones published an article poking fun at a process that should evolve as the Stereolithography process in the 1980s, enabling the formation of a three-dimensional object by radiation curing.[5]

The idea is simple: a three dimensional digital model is sliced into multiple layers. These information are sent to a printer, filled with a photosensitive resin. Each layer is then cured step by step using UV light, finally leading to a three dimensional object.

Although there has been earlier literature, Charles W. Hull is regarded as the inventor of the process that he patented as the Stereolithography Apparatus (SLA) in 1986.[6] In 1989, two competitive printing technologies, fused filament fabrication and selective laser sintering were developed and since then, 3D printing experienced a steady growth.[7] For stereolithography, however, it took more than 20 years before the first affordable 3D printers were available. Next to the engineering part of the process, researchers started to develop and improve printable materials, trying to mature the technology from simple prototyping to the manufacturing of functional parts.

The development did not stop until now – it is rather more topical than ever. In many senses, 3D printing has the potential to revolutionize the way parts are manufactured.[8] Complex geometries and a high level of individualization are the key advantages of this technology. The intention of

this thesis is to contribute to the continuous improvement of 3D printing by developing new resin systems for the fabrication of three-dimensional objects by radiation curing.

2 State of the Art

The following chapter summarizes the relevant literature that represents the basis for the investigations performed within this thesis.

2.1 Additive Manufacturing

Additive manufacturing (AM) which is frequently called 3D printing, represents a flexible processing technique for a huge variety of materials such as polymers, metals and ceramics.[9] It refers to the production of three dimensional structures in a layer by layer fashion. Compared to traditional manufacturing technologies, 3D printing offers several advantages, including the fabrication of complex geometries with high precision, flexibility in design as well as personalized customization.[10] Especially the variety of available polymer materials has enabled the development of a wide range of printing methods. Extensive literature is available about the current status, challenges and future applications of additive manufacturing.[9–12] A short overview is given in the following section.

Depending on the physical state of the polymer, different methods exist to fabricate a three dimensional object via 3D printing. The main technologies are fused filament fabrication (FFF), frequently referred to as fused deposition modelling (FDM), powder bed fusion such as selective laser sintering (SLS) as well as high speed sintering (HSS), and vat photopolymerization (VPP) techniques, such as digital light processing (DLP) and stereolithography apparatus (SLA).[13] Polymeric powders, filaments and sheets are processed in FFF as well as in powder bed fusion, while in VPP the polymeric material is produced during the printing process by the light induced polymerization of suitable precursors.[9]

For all printing technologies, the design of a three dimensional digital model precedes the printing process. After construction, the digital model is converted into a cross-sectional sliced model e.g. by using Standard Triangulation Language (STL). This file contains the information of each layer that will be printed.[14] In a further step, the file is translated into an instruction set for the printer which is subsequently send to the printer, that can start the fabrication of the object.[11]

In FFF, polymer filaments and foils are extruded through a so called 'hot-end', where the polymer strain is melted and is selectively deposited through a nozzle on a build platform, as schematically

illustrated in Figure 1. Inexpensive machines and materials make FFF attractive in the do-it-yourself sector, as well as in the industry for the manufacturing of functional parts. High anisotropy and poor adhesion between the layers are the main drawbacks of this technology.[15]

In SLS, polymer powders are selectively sintered using a laser as energy source (Figure 1). The laser scans the first layer of a powder bed and the polymer particles are melted and fused together. Subsequently, a new powder layer is applied and the process is repeated. The advantage of powder bed fusion technologies is that no support structures are needed, as the printed objects are stabilized by the non-sintered powder. After the print job, the powder is removed, yielding the desired object.[13]
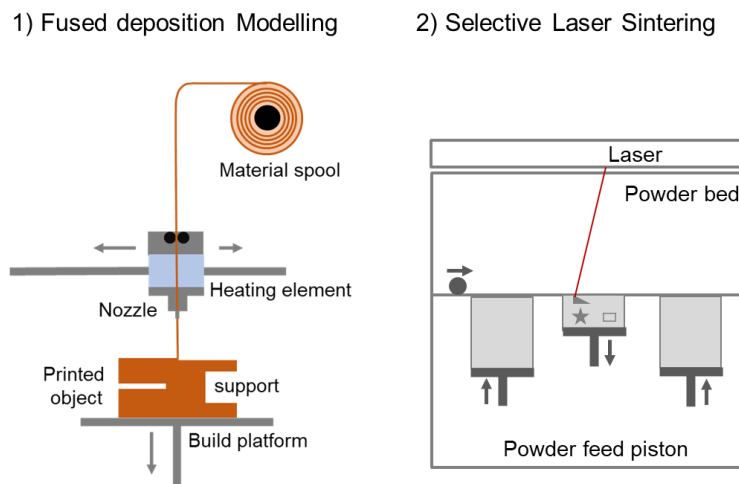
Figure 1. Schematic illustration of fused deposition modelling (adopted from Ref. 16) and selective laser sintering (inspired by Ref. 17).

In VPP, photosensitive oligomers and monomers are selectively cured by the exposition to a light source. The active polymerization process to yield the 3D printed object is particularly attractive with regard to high levels of build resolutions (10 to 100 nm), excellent surface quality, high strength between the layers and the fabrication of clear objects.[11]

In the following chapter, the different polymer classes that find application in 3D printing are described with their corresponding physical properties.

2.1.1 Classes of Polymers used in Additive Manufacturing

In general, polymer solids can be divided into different categories based on their physical behavior, as schematically illustrated in Figure 2.[18]

Figure 2. Schematic illustration of the four different polymer classes. Figure inspired by Ref. 19.

Thermoplastic polymers are non-crosslinked polymers that consist of linear and branched polymer chains, which are associated via intramolecular forces. They have a melting point and thus can be reversibly deformed by heating above the melting temperature. This effect is used in classical injection molding as well as in FFF and SLS printing technologies. Examples are polypropylene (PP), polyethyleneterephtalate (PET) and polyamide (PA).[20]

In contrast to that, elastomers are weakly crosslinked polymer networks with long polymers between the crosslinking points. They have a glass transition temperature (T_g) below room temperature and cannot be reprocessed by melting, as in the case of thermoplastics. As their glass transition temperature is well below the temperature of use, elastomers show rubber-elastic material properties after crosslinking.[21]

Prominent examples are silicone- and natural rubber. In principle, elastomers can be formed in vat photopolymerization (VPP) based printing technologies, however, due to their low crosslinking density and high number of monomer repeating units, they are difficult to access via VPP.

Thermosets are highly crosslinked polymers with a T_g above their temperature of use and similar to elastomers, cannot be reprocessed by melting. The high number of crosslinks or sterically hindered monomers limits the mobility of the polymer chains, causing a high glass transition temperature. Residing in the glassy state, thermosets are usually rather hard and brittle. Examples

are polyepoxides and specific polyacrylates.[22] In VPP, thermosets are the materials that result upon the active polymerization during the printing process.

A special class of materials are thermoplastic elastomers (TPE) that combine elastomeric properties with the re-processibility of thermoplastic materials. Instead of chemical crosslinking points these materials feature physical crosslinks. These physical interactions are generated by phase-separated block-copolymers that contain soft segments with low glass transition temperature and hard segments with either a high glass transition temperature or a melting temperature well above the temperature of use, of which the latter can also be of crystalline nature. Examples are thermoplastic polyurethanes (TPU) with a crystalline polyurethane hard block and a low T_g polyester, polyether or polycarbonate soft block, as well as thermoplastic polystyrene-*block*-copolymers (TPS), containing a high T_g polystyrene hard block and a polybutadiene or polyethylene soft block.[23] These types of polymers can be processed by FDM and SLS printing technologies.

While thermoplastics and thermoplastic elastomers are processed in FFF and SLS printing technologies, elastomers and thermosets are produced during vat photopolymerization based techniques upon the light induced polymerization of photo-sensitive precursors. As this thesis deals with the development of photo-resins for use in VPP, this technology will be described in more detail in the next section.

2.1.2 Vat Photopolymerization

Vat photopolymerization (VPP) based printing technologies have gained increasing interest in a huge variety of applications such as tissue engineering[24,25], dentistry[26], microfluidics[27], sensors and actuators[28], hydrogels[29], chemical engineering[30,31], catalysis[32,33] and many more. One major reason is the high resolution that can be obtained in comparison to other additive manufacturing techniques.[11] VPP makes use of photopolymers that are selectively cured, layer-by-layer, upon the selective exposition to a radiation source. For this purpose, either a laser, as in SLA, or a digital light mask, as in DLP are used as light sources. The light source can either be placed above or beneath the resin bath, leading to so called top-down or bottom-up printer setups, respectively.[34] Both setups are illustrated in Figure 3.
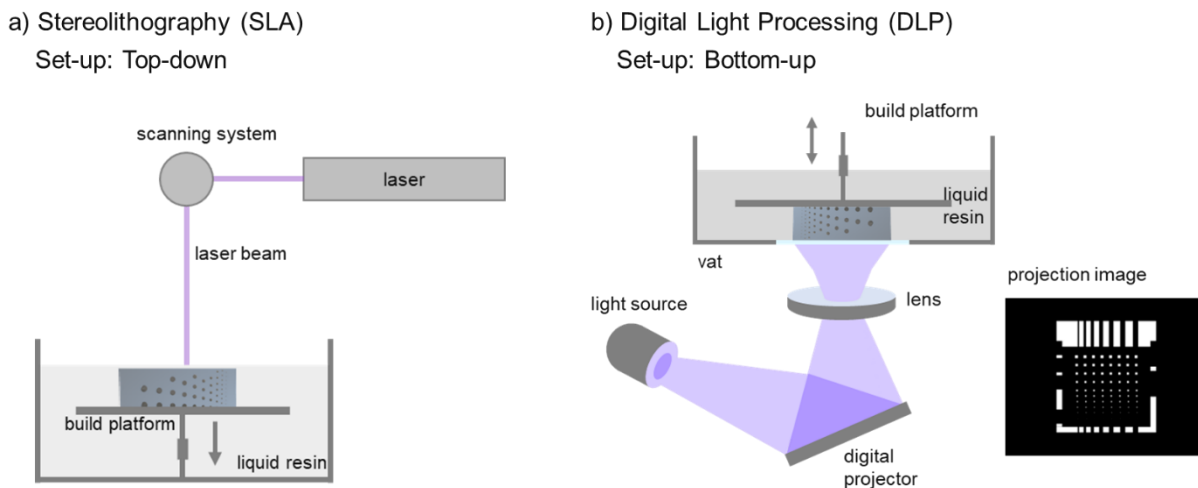
Figure 3. Schematic illustration of vat photopolymerization based printing techniques. a) Stereolitography with a top-down printer setup. b) Digital light processing with a bottom-up printer setup. Figures inspired by Ref. 35.

In SLA, a UV laser cures the layer of the photopolymer point by point, while in DLP a whole layer is projected at a time in form of black and white images. The accuracy of the printed part depends on the projector resolution in DLP, which is limited to the resolution of the digital screen. In SLA the accuracy depends on the condensed laser beam diameter, offering a higher resolution compared to DLP. In terms of printing speed, DLP is faster, as the surface patterned exposure from a DLP projector allows to expose the entire x,y-image at a time, in contrast to the dynamic writing of the laser beam, that scans the surface point by point.[34] The z-axis resolution that relates to the depth of cure is controlled by the photoinitiator as well as the parameters of irradiation, such as wavelength and power of the light source as well as the exposure time.[9] Typically, shorter exposure times apply in SLA due to the higher photon density of the scanning laser, while longer exposure times are needed in DLP due to a lower energy density of the light source.

There are different printer setups are available.[34] A top-down printer is exemplarily illustrated for the stereolithography apparatus (Figure 3). Herein, the build platform is placed in the vat that contains the photosensitive resin and a laser scans the surface of the photopolymer point by point from above, inducing a local polymerization. After one layer is cured, the build platform moves down and the next layer is cured. This process is repeated until the build is completed.

In contrast to that, in a bottom-up version (exemplarily for DLP), the build-platform moves down into the vat that contains the photosensitive resin and the image is projected through a transparent window at the bottom of the vat, thus selectively triggering the polymerization of the photopolymer. After curing of one layer, the build-platform moves up and the printed part is detached from the vat window, the resin flows back and the process can be repeated until the final

object is completed. One drawback of this approach is the periodic detachment of the printed part from the vat window after each layer, which can result in stresses and deformation.[12,34]

For a top-down approach, no detachment step is needed, however, the resin required for each printing process needs to match the build volume and the height of the intended product. As a result, the layer thickness is more difficult to control.[36] This is why usually higher resolutions can be obtained with the bottom-up approach with 10 μm to 100 μm, in comparison to 50 μm to 100 μm for the top-down printer setup.[11]

The printer setups are steadily improving towards industrial manufacturing. This includes the development of printers with larger resin vats to enable the fabrication of large objects, favored by improved high-resolution DLP systems. The development of a comparably new vat photopolymerization technique, referred to as continuous liquid interface printing (CLIP), by DeSimone and co-workers increases the printing speed. In this process, a permeable window on the bottom of the vat is used, that allows the diffusion of oxygen through the vat. Oxygen inhibits the solidification of the resin and the adhesion to the vat window. This so-called 'dead-zone' between the window vat and the printed part enables the continuous elevation of the build platform during the printing process, without a delamination step after each layer.[37,38] Much faster printing speeds can be obtained and additionally, this process improves the bottom-up approach by eliminating the periodic detachment of the printed part.[39] Technologies without a detachment step are especially attractive for the printing of soft materials, as for example elastomers.

For all techniques, support structures are needed to print overhanging parts. After printing, the parts are removed from the build platform and are cleaned to remove excess resin. The printed object has not yet achieved full cure, which is why it is frequently referred to as green body in this state. The term green body is frequently used in additive manufacturing and has been adopted from ceramics. It is defined by IUPAC as an "object formed from a preceramic material prior to pyrolysis."[40] To raise the conversion of the photopolymers captured in the product build, a UV post-curing step is usually included. Depending on the photopolymer system, further post-processing steps are employed to obtain the final 3D printed object with its ultimate mechanical properties.

Each technology requires the adjustment of the photosensitive resin to the processing parameters, with special focus on the wavelength and power of the light source. The photoinitiating system in the resin is essential and needs to be matched to the light source that is used or the light source has to be chosen according to the desired photoinitiating system. The

reactivity of the resin is further important when considering the different exposure times and energy densities of the printer setups. Although the CLIP technology increases the printing speed, this printing process is limited to the polymerization of photosensitive resins that are inhibited by oxygen, as otherwise the continuous elevation of the printed object would not be possible.

Along with the improvement of the printer setups, the development of photosensitive resins plays an important role to pave the way of vat photopolymerization based printing techniques from rapid prototyping to industrial manufacturing. In the following sections, relevant material classes and material design parameters for use in VPP, targeting functional applications of additive manufacturing technologies will be discussed in further detail.

2.2   Photocuring of Polymer Formulations

Light represents a powerful energy source for the rapid transformation of a liquid resin into a solid by formation of an insoluble polymer network.[41,42,43] Functional monomers and oligomers react via cationic or radical polymerization mechanisms to form crosslinked polymer networks, initiated via photoinitiator molecules that decompose upon the exposition to light. Specific monomers that follow a radical curing mechanism are characterized by their robustness and fast reaction rates.

As the curing formulation is usually solvent-free and the reaction can be performed at ambient temperatures, photocuring represents the technology of choice in an ever growing field of applications such as in coatings and adhesives,[44] dental fillings and printing inks.[45]

A typical radiation curable liquid resin, following a radical curing mechanism, comprises three major components:[46]

- Carbon-carbon (C=C) double bond containing mono- or multifunctional prepolymers or oligomers
- Low viscous C=C functional co-reactive monomers
- A suitable photoinitiating system

Functional prepolymers usually contain backbones based on polyethers, polyesters, polyurethanes or polysiloxanes that largely determine the final mechanical properties of the UV cured material. Low molar mass mono- or multifunctional co-reactive monomers are added to dilute the higher viscous oligomer to appropriate viscosities, as well as to adjust the crosslinking

density of the intended polymer network. Photoinitiators are added to initiate the polymerization reaction. By absorbing light of a specific wavelength, the photoinitiator forms reactive intermediates such as radicals or cations.[47] These reactive intermediates are then capable of initiating the polymerization of functional monomers and oligomers to form a polymer.[48] A detailed description of the absorption process and the following photochemical and -physical processes is given in literature.[49,50,51] It is necessary for the initiating process that the emission of the light source overlaps with the absorption band of the photoinitiator, in order to ensure the formation of reactive intermediates. Thus, the photoinitiator has to be chosen according to the light source or vice versa. The photoinitiator concentration is further important with regard to the power of the radiation source and the exposure time.

Most photocuring reactions proceed via a radical chain growth polymerization, as in the case of the radical polymerization of C=C double bond carrying monomers like (meth)acrylates and vinyl monomers. The most common types of photoinitiating systems that are used to initiate this type of curing reactions are Norrish type I and Norrish type II photoinitiators. The first decomposes via direct cleavage from the excited state of a light sensitive molecule, while in the latter, a sensitizer abstracts a hydrogen from a co-initiator in order to generate radicals.[52]

The two different mechanisms are illustrated in Figure 4, exemplarily for an acylphosphine oxide (Norrish type I initiator) and benzophenone with triethylamine as co-initiator (Norrish type II initiator), respectively. Acylphosphine oxides have shown to undergo a fast photolysis, leading to benzoyl and phosphinoxyl radicals that are both capable of initiating the polymerization reaction.[52] In contrast, the ketyl radical of benzophenone is inactive towards the initiation of the reaction. The benzophenone abstracts a hydrogen from the triethylamine that acts as donor molecule. The formed α-amino alkyl radical is then able to initiate the polymerization reaction.

Norrish type I: direct cleavage
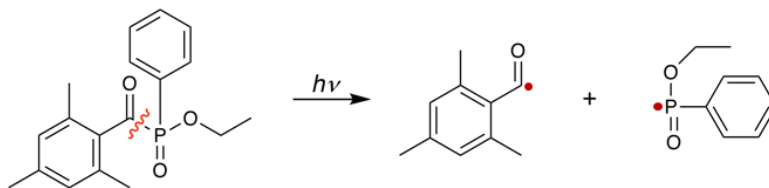
Norrish type II: sensitization
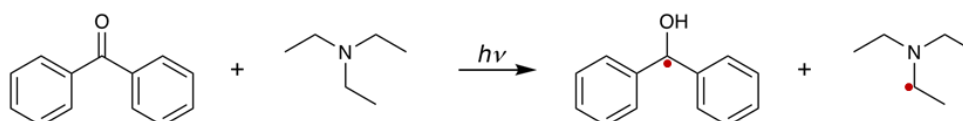
Figure 4. Formation of radical intermediates via direct cleavage (Norrish type I) and sensitization (Norrish type II).

The propagation step of the polymerization mechanism of acrylates, initiated by the radical intermediates is illustrated in Figure 5.
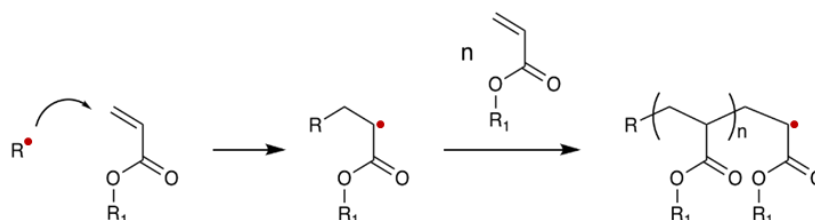
Figure 5. Schematic illustration of the radical propagation step in the radical polymerization mechanism of acrylates.

Upon absorption of light, the initiator forms intermediate radicals that add to an acrylic C=C double bond, leading to the formation of a reactive monomer radical. Chain propagation takes place by further addition of monomers. The chain growth reaction is terminated either by a radical combination of two growing radical chain ends or via a disproportionation reaction, yielding a reactive C=C double bond end-group and a saturated chain end.

The polymerization proceeds fast and thus only little control over molar mass and polydispersity of the resulting polymer is obtained. Upon vitrification the polymerization reaction stops, thus un-cured monomers remain entrapped in the acrylic network. Typical conversions are in the order of 90 %.[53] Although acrylates usually provide high polymerization rates, enabling the phase change from liquid to solid within seconds in a radical polymerization process, a major drawback

lies in the high volume shrinkage as well as the inhibition of the polymerization reaction by oxygen.[54]

Epoxides represent another class of materials that are frequently used in photocuring polymerization reactions, following a cationic curing mechanism.[55] No oxygen inhibition and only little shrinkage are the main advantages of epoxy resins. However, they still find less application due to high moisture sensitivity, limited choice of monomers, slow reaction rates and high cost, in comparison to the widely used acrylates.[56] Other photocuring materials are based on thiol-ene click reactions that in contrast to the photoinduced chain growth, follow a step growth polymerization mechanism, but are even less employed in industrial applications.[57,58]

With the rise of available UV laser technologies in the late 1980ies, it became possible to locally induce a photopolymerization by selectively irradiating defined areas on a given liquid surface. This development has been the starting point of vat photopolymerization based techniques, enabling to produce 3D objects out of a liquid phase.[6] To this point, photopolymers have been predominantly used for 2D applications. Thus, with the use of these materials for the fabrication of bulk objects, the development of new materials has been subject of intensive investigations, equally in industrial and academic research. The thesis deals with the development of photocurable resins for use in vat photopolymerization based techniques, with special focus on digital light processing following a bottom-up printing process. Important considerations regarding the material requirements from a processing point of view, the existing photo-resins, their polymerization mechanisms and the resulting mechanical properties are given in the following sections.

2.3   Processing of Photopolymers in Vat Photopolymerization

The processing of photopolymers in vat photopolymerization based techniques requires to consider specific processing conditions, that partially differ from those of earlier applications of photopolymers in coatings and adhesives. Usually, photopolymers have been applied as thin films via standard spray, roll, cast or printing application with the focus on achieving a fast and full conversion of the reactive species into polymer networks. In VPP, however, where three dimensional bulk objects are produced by a layer by layer selective curing of the monomers, a curing reaction should only occur in an intended voxel of a liquid phase. In areas that are not lightened, the reaction must not spread, in order to reach the intended resolution. Typically, inhibitors that scavenge the radicals are employed to avoid this so-called "dark-curing".

Multiple layers need to be cured and adhere to each other to obtain a three dimensional object, in contrast to the curing of only a single layer. To obtain a good interlayer bonding, it is necessary that the curing of one layer proceeds into the previous cured layer, resulting in the chemical linkage of layers. However, at the end of the printing process the final part needs to achieve full conversion to be used in diverse applications. A UV flood post-processing step is often applied to obtain a full conversion, however, as the penetration depth of light is limited, it is challenging to reach the inner part of the object. One strategy to guarantee a full monomer conversion is thus the addition of thermal initiator molecules.[59] Upon the thermal post-treatment of the printed object, residual monomers can be cured. A quantitative conversion of the monomers is further important to reach the ultimate mechanical properties of a given material.

The physical characterization of photocurable resins in their liquid state is thus necessary to find the right processing parameters and to judge its overall suitability for a printing technology. The photopolymer in its solid and crosslinked state determines the final mechanical properties of the material and thus the field of possible applications. The understanding of the dependencies of the transformation process from a liquid into a crosslinked polymer is essential to develop a resin formulation.

When developing a formulation, the photoinitiator needs to match the light source of the printer. Typically, light sources with wavelengths of 365 nm, 385 nm and 405 nm are available for DLP, regardless of the printer setup. For most printer setups, limitations with regard to viscosity apply, in order to enable the successful processing of the material. Typical viscosities are < 5 Pa·s for both, bottom-up and top-down printer setups.[60,61] Higher viscosities prevent a fast enough back-flow of the resin in bottom-up printer setups and make it difficult to achieve the self-levelling of the resin in top-down approaches. A high viscosity thus directly impacts the efficiency of the printing process. In a bottom-up printer setup, high viscosities further increase the detachment forces, when the polymerized material is separated from the transparent window at the bottom of the printer.

Low resin viscosities of < 1 Pa·s in combination with fast build rates are highly advantageous in order to enable the formation of a stable polymer network within seconds. At the same time, a fast reaction rate is often associated with a high polymerization shrinkage. A high volume shrinkage during the printing process is undesired, as the intention is to obtain a 3D printed part at true scale. Achieving a sufficient green strength of the object produced is essential. As the exposure time of the resin to UV light during the printing process is short, usually not all monomers are reacted, thus requiring a post-processing of the printed object with UV light to obtain a fully cured

object. However, it is important to obtain a stable green body, as otherwise the 3D printed part would collapse during printing, especially in the case of a bottom-up printer setup, due to the periodic detachment of the build part from the vat during printing.

For an easy and safe handling of the photo-resin, low odor, low irritation and low toxicity of the starting materials are advantageous.

There exists a huge variety of suitable materials for use in VPP techniques. Prominent examples of formulations featuring higher performance are often based on acrylic oligomers, containing polyurethane building blocks, diluted with co-reactive monomers.[45,62–65] Since the material properties in the solid state determine the final application, the correlation between the processability and composition of the resin material such as reactivity and viscosity with the resulting material properties need to be investigated and well understood in order to develop photo-resins that meet the demands for the manufacturing of functional materials.[66,67,28]

2.3.1 Mechanical Properties of Thermosets

In general, crosslinked polymer networks are obtained during vat photopolymerization. Once photopolymers are in their crosslinked solid state, they are insoluble, non-meltable and only degrade upon cleavage of covalent chemical bonds upon thermal treatment.

Depending on the degree of crosslinking, polymer networks can be divided into thermosets that are usually strongly crosslinked and elastomers that are characterized by long polymer chains with only few crosslinking points.

To gain knowledge about the thermal behavior of such crosslinked materials, typically their modulus is measured in dependence on the temperature by dynamic mechanical analysis.[68] Herein, the sample is deformed by applying a periodic low strain in the region of a linear material response, while the temperature is gradually increased, starting from temperatures well below the glass transition temperature of the sample. As response of the applied strain, the stress is measured.

In case of a purely elastic material, the stress and strain waves are in phase (0 °), which means they oscillate without any energy loss. For purely viscous materials, there is a shift in the phase angle of 90 ° between excitation and response, which means that the excitation energy is entirely dissipated as heat. The material flows, and deforms irreversibly.[69]

Most materials, including polymers, change their behavior over temperature from a predominantly energy elastic state below the glass transition temperature, over a viscoelastic state during phase transitions to a potentially viscous state upon melting or degrading at higher temperatures.[70]

The data derived from dynamic mechanical analysis (DMA) allow the determination of fundamental material parameters such as the storage and the loss modulus (E' and E'') as well as the loss factor ($tan\delta$) over temperature that are defined as

$$E' = \frac{\sigma_0}{\varepsilon_0} \, cos\delta \tag{1}$$

$$E'' = \frac{\sigma_0}{\varepsilon_0} \, sin\delta \tag{2}$$

and

$$tan\delta = \frac{E''}{E'} \tag{3}$$

with σ_0 being the stress and ε_0 being the strain applied to the sample.

The storage modulus E' represents the elastic response of the material to the periodic deformation. The loss modulus E'' relates to the viscous response of the material to the periodic deformation. The relation between these two parameters is given by the loss factor. A high loss factor indicates that the material dissipates energy like a viscous fluid, whereas in materials with a low loss factor, the elastic behavior predominates. The dependence of the storage modulus on the temperature is schematically illustrated in Figure 6, comparing a strongly crosslinked thermoset with a glass transition temperature at about 100 °C, a toughened thermoset with a glass transition temperature at about room temperature and an elastomer, with a glass transition temperature at about -50 °C.
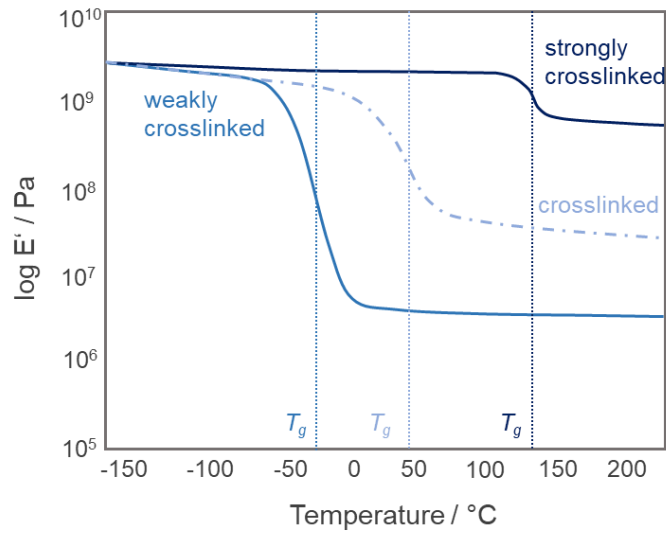
Figure 6. Modulus in dependence of the temperature for a weakly crosslinked elastomer and a strongly crosslinked thermoset. Modified according to Ref. 70.

At temperatures below their respective glass transition temperature, all polymers are in their glassy state and the dissipation of energy is restricted, as the translational and rotational internal movements of the molecular chains are frozen and thus inhibited in their movement. Upon temperature increase, the modulus rapidly declines at the glass transition temperature and the mobility of the molecular chains increases. After the glass transition temperature, the polymer enters an area of stable modulus. Strongly crosslinked thermosets usually possess high glass transition temperatures. In contrast to that, elastomers are characterized by their low glass transition temperature. The area above the glass transition temperature is often related to the rubbery plateau, in which the material shows entropy-elastic behavior. The value of E' in the rubbery plateau, refers to the crosslinking density and the end-to-end distance between two crosslinking points with

$$\frac{E'}{3} = G'_R = \nu RT \tag{4}$$

where G'_R is the relaxed rubbery modulus, R is the universal gas constant, T is the temperature and ν is the number of crosslink sites per unit volume.[71]

The main difference between these crosslinked polymer classes is their respective modulus at the temperature of use. The modulus is controlled by the type of polymer (chain flexibility) and the crosslinking density. While elastomers, being based on flexible polymer chains, are already in the rubbery plateau, thermosets are still in their glassy state. As a result, hard and brittle material

properties prevail for the latter, as the movement of the polymer chains and the dissipation of energy are severely restricted.

Tensile test measurements depict the deformation behavior of thermosets at a certain temperature e.g. room temperature.[72,73] The tensile stress σ is defined as force F per area A_0 of a sample, where for the most simple case, A_0 is supposed to be constant over the experiment.

$$\sigma = \frac{F}{A_0} \tag{5}$$

The resulting strain ε is defined as the quotient of the change in length Δl and the original length l_0 of a sample with

$$\varepsilon = \frac{l - l_0}{l_0} = \frac{\Delta l}{l_0} \tag{6}$$

According to Hook's Law, the tensile stress is directly proportional to the strain, with

$$\sigma = E \cdot \varepsilon \tag{7}$$

The constant E represents the complex modulus, that is frequently referred to as Young's modulus. Hook's law is only valid in the linear regime of a tensile curve, which is why the Young's modulus is determined at low strains, typically between 0.05 % and 0.25 %. Typical stress-strain curves for elastomers, thermosets and tough thermosets are illustrated in Figure 7.
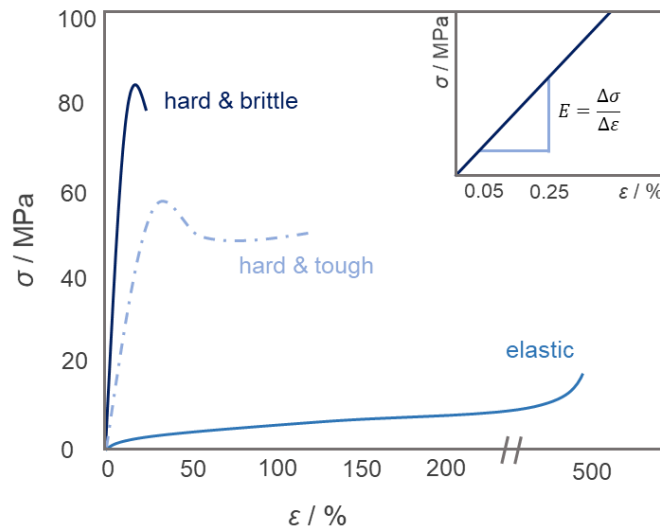
Figure 7. Stress-strain diagram of selected polymers. Modified according to Ref. 74.

Elastomers are characterized by their high extensibility and the ability to completely recover after application of a strain force. The deformation of elastomers is directly linked to their thermal properties.[75,76] Their thermodynamically unique behavior is usually achieved upon weak crosslinking of high molar mass polymers. Strongly crosslinked thermosets usually possess high Young's-moduli with low strains at break and often suffer brittle fracture.[77] Engineering applications require materials that have high values for strength and stiffness, while at the same time avoiding brittle fracture. Toughness, which is the opposite to brittleness, is often defined as the area under the stress-strain curve[78]

$$\tau = \int_0^{\varepsilon_b} \sigma \, d\varepsilon \tag{8}$$

where ε_b is the elongation or strain at break. High toughness is an indicator for a good resistance against crack growth and can thus help to prevent brittle fracture.[74] However, the increase in toughness typically goes in hand with a decrease in strength and stiffness, as illustrated in Figure 7. After reaching a yield point, the sample undergoes permanent plastic deformation. A compromise is needed to design the materials according to the desired applications, where tensile strength and toughness (elasticity/energy dissipation) are closely matched to the intended application profile.

2.3.2 Processing-Property Relation

The processing requirements of inks in 3D printing (viscosity, reactivity, resulting green strength) and the resulting polymer networks strongly correlate with the final material properties. To go beyond the current limitations of polymers produced via VPP, it is necessary to understand the interdependencies.[79]

A fast polymerization rate of a liquid resin into its solid state is highly desired in VPP to obtain an efficient production process by enabling short exposure times and thus, fast layer build rates. The polymerization rate can be affected by the number of initiated chains on the one hand and the reactivity of monomers on the other hand. Short exposure times are typically achieved in a combination of highly reactive monomers, low viscosities (fast flow rate), a high initiator concentration and the presence of crosslinking monomers.[62] This combination effectively prevents the build-up of longer polymer chains between networking points. This means that only low end-to-end distances (R_{max}) between the crosslinking points can be obtained, resulting in a finite extensibility of the sample when applying a strain force.[79,80] As a consequence, highly crosslinked and often brittle thermosets are formed during the printing process. The end-to-end distance R_{max} is defined as

$$R_{max} = b \cdot N \tag{9}$$

with b being the monomer length and N being the number of monomers between crosslinks.[81]

To obtain more flexible products by VPP, one solution is to increase the monomer length R_{max} of the corresponding precursor. Increasing the molar mass of the precursors enables the printing of less crosslinked materials or even materials with highly designed crosslinking density. Choosing the right end functionality is important. For that purpose often acrylate instead of methacrylate reactive end-groups are used as precursors as well as highly reactive acrylic co-reactive monomers.[82] Combinations of acrylic and methacrylic functionalities are also known for improved combined polymerization rates.

Low resin formulation viscosities are another essential requirement for the processing of resins in VPP. In theory, the viscosity of a polymer is proportional in a power law to the molar mass, as defined by the semi-empirical Mark Houwink equation with

$$[\eta] = K \cdot M^\alpha \qquad (10)$$

where $[\eta]$ is the intrinsic viscosity, K and a are constants dependent on the nature of the macromolecule, solvent and temperature and M is the viscosity average of the molar mass.[83] This means that increasing the molar mass of a precursor molecule will typically lead to an increase in viscosity. However, the Mark Houwink equation does not include molecular interactions of the polymer chains e.g. hydrogen bonding. Prominent examples are polyurethanes that possess strong hydrogen bonding between the urethane functional groups.[84] This is especially relevant when these interactions are not statistically distributed, but concentrated as for example at the reactive moieties of a radiation curable precursor. This includes polyurethane acrylates, that are frequently used in radiation curing applications. These interactions further influence the viscosity and usually lead to a significant increase, in comparison to precursors with less molecular interactions as for example within polyester acrylates.[85]

Increasing the molar mass of the precursor is limited by the viscosity restrictions of the given application. Also, the build-up of long polymer chains by increasing the number of monomers N is limited by short exposure times during the printing process. The importance of this contradiction is further enhanced by the fact that in general, the mechanical properties, specifically the toughness of a polymer increases, as the molar mass between the crosslinking points increases.[86,87] Especially elastomeric materials that are characterized by long polymer chains with only few crosslinking points, are difficult to access via VPP, as a high green strength is necessary to prevent the collapse of the object during printing.

It is thus necessary to develop new strategies that bypass the restrictions imposed on the resins, such that improved mechanical properties can be provided.[88] There are already existing concepts that try to circumvent these issues from both a technical point of view that improves existing printer-setups as well as from a material point of view.

One of the simplest methods is the printing at elevated temperatures. Viscosity η and temperature T are related via the Arrhenius-Andrade relation by

$$\eta = \eta_0 \cdot e^{\frac{E_A}{R \cdot T}} \qquad (11)$$

with η_0 being a material constant, E_A being the activation energy and R being the universal gas constant.[89] Accordingly, the viscosity decreases exponentially with increasing temperature. However, at higher temperatures there is the risk of a premature thermally initiated radical polymerization of the acrylic functions, which is why temperature can only be increased in a controlled way.

Another approach to avoid high viscosities is by diluting high molar mass polymers with non-reactive solvents.[90,91] However, this usually requires complex post-processing steps to get rid of the solvent, as a fast removal can lead to crack formation and degradation of the polymer network. Additionally, a large volume shrinkage is to be expected that directly correlates to the amount of solvent used.

Another approach is the design of low viscous oligomeric acrylates, that can be printed directly, without the addition of any reactive diluent.[92] Owing to the fact that inhomogeneous and highly crosslinked polymer structures are formed by UV curing of (meth)acrylate based resins, an improvement of the homogeneity has been achieved by using addition-fragmentation chain transfer agents in order to control the polymerization process and to increase the toughness of the final material.[93,94] The addition of the mediator, however, leads to an increase in curing times.

Finally, the combination of two different polymerization reactions has become popular to form polymer networks that exceed the properties of conventional thermosets, which has been well studied within the last decade. Many applications of photopolymers have been facing similar challenges concerning processing-property paradigms.[95,96] By combining two polymerization reactions, at least one reaction needs to take place in the printer to form a stable green body. However, the second reaction can also take place outside the printer, as for example by a thermal post-treatment step of the printed part. This broadens the choice of useful reactions and allows to extend the potential property range of the 3D printed bulk material. In this thesis, dual-cure resin systems will be investigated, combining acrylate radical curing reactions with isocyanate based thermal curing. The following section gives a detailed introduction into the chemistry of polyurethanes.

2.4 Chemistry of Polyurethanes

Since the development of the di-isocyanate polyaddition reaction by Otto Bayer, polyurethanes (PU) have experienced a steadily increasing relevance in research and industrial applications.[97] Generally, an urethane functional group is formed by the reaction of a hydroxy-group with an isocyanate. For the polymerization reaction usually oligomeric di-alcohols, frequently called polyols are reacted with (poly)isocyanates via a polyaddition reaction. Depending on the functionality of the precursors, linear thermoplastics, crosslinked elastomers or thermosets are obtained. The huge variability and good commercial availability of different polyols and isocyanates, enables the cost-effective production of polyurethanes that cover a broad range of mechanical properties. This is why polyurethanes are widely used in industrial applications.[98,99]

2.4.1 Isocyanates

Isocyanate groups are formally esters of isocyanic acid and have been extensively studied in the last decades.[100–102] Although many different synthesis routes have been described, the prevalent route to synthesize isocyanates still is by phosgenation of primary amines, as illustrated in Figure 8.

Figure 8. Schematic illustration of the synthesis of isocyanates by phosgenation.

Only few isocyanates have gained industrial relevance and are produced on a large scale. The most frequently used aromatic isocyanates are methylenediphenyl diisocyanate (MDI) and toluene diisocyanate (TDI), while hexamethylene diisocyanate (HDI), isophorone diisocyanate (IPDI) and hydrated methylenediophenyl diisocyanate ($H_{12}MDI$), represent the most common aliphatic examples (Figure 9). A novel biobased isocyanate is pentamethylene diisocyanate (PDI), representing an alternative for fossil fuel sourced HDI without a loss in final material properties.[103]
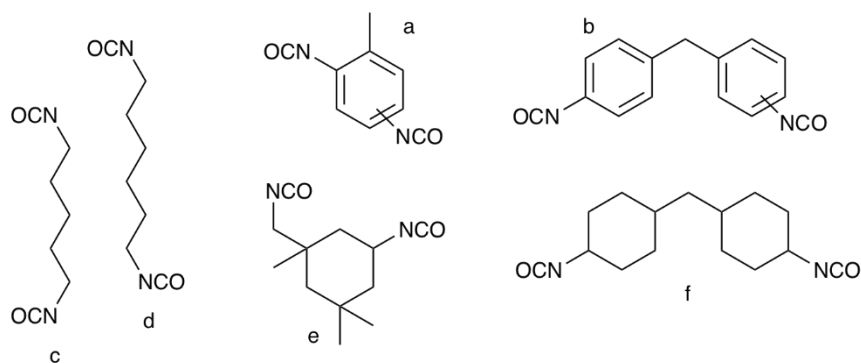
Figure 9. Examples of industrial relevant aromatic and aliphatic isocyanates: a) toluene diisocyanate (TDI), 2,4- and 2,6-isomers; b) methylenediphenyl diisocyanate (MDI), 4,4'- and 2,4'-isomers; c) pentamethylene diisocyanate (PDI); d) hexamethylene diisocyanate (HDI); e) isophorone diisocyanate (IPDI); f) hydrated methylenediphenyl diisocyanate (H$_{12}$MDI).

In general, diisocyanates are extremely reactive and readily react with a lot of potential reaction partners. Due to the combination of a low viscosity and comparably high vapor pressure, the monomeric diisocyanate species are classified as toxic substances. One of the world's worst chemical industrial disasters, the Bhopal gas tragedy has been caused by a gas leak of the monofunctional methyl-isocyanate in 1984, where 2259 people died and more than half a million people were injured.[104]

While the products from the reaction of diisocyanates are typically safe to use and find many applications in households (mattresses, artificial leather coatings, household glues, tool handles, elastic fabrics etc.) and even in medical and orthopedic applications (casting plaster, orthopedic inlays, corrective aligners etc.), the processing of diisocyanates in industrial applications is highly regulated. To better control the risks in applications such as coatings and adhesives, isocyanates are first converted into higher molar mass polyisocyanates that are physiologically more benign.[105]

Containing two cumulated double bonds, the reactivity of the isocyanate group is based on strong polarization of the adjacent oxygen and nitrogen heteroatoms, which ultimately leads to a large electrophilicity of the central carbon, as shown by the resonance structures in Figure 10.[106]
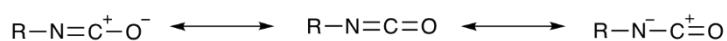
Figure 10. Resonance structures of the isocyanate group.

Depending on the nature of the rest group R, the reactivity of the isocyanate group can be readily manipulated. Electron withdrawing groups for example, further reduce the electron density at the

carbon atom, increasing the reactivity. This is why the reactivity of aromatic isocyanates is largely enhanced over aliphatic ones. The electrophilic character of the isocyanate group enables a huge variety of reactions, which is the main reason why isocyanates are used in so many applications. Typical reaction partners are nucleophiles that contain an *active hydrogen*, such as alcohols and amines, as well as thiols and carboxylic acids. The latter two are used to a lesser extent. A reaction with water is also commonly applied, especially in the production of foams. The most common reactions of isocyanates with the corresponding reaction partners are illustrated in Figure 11.
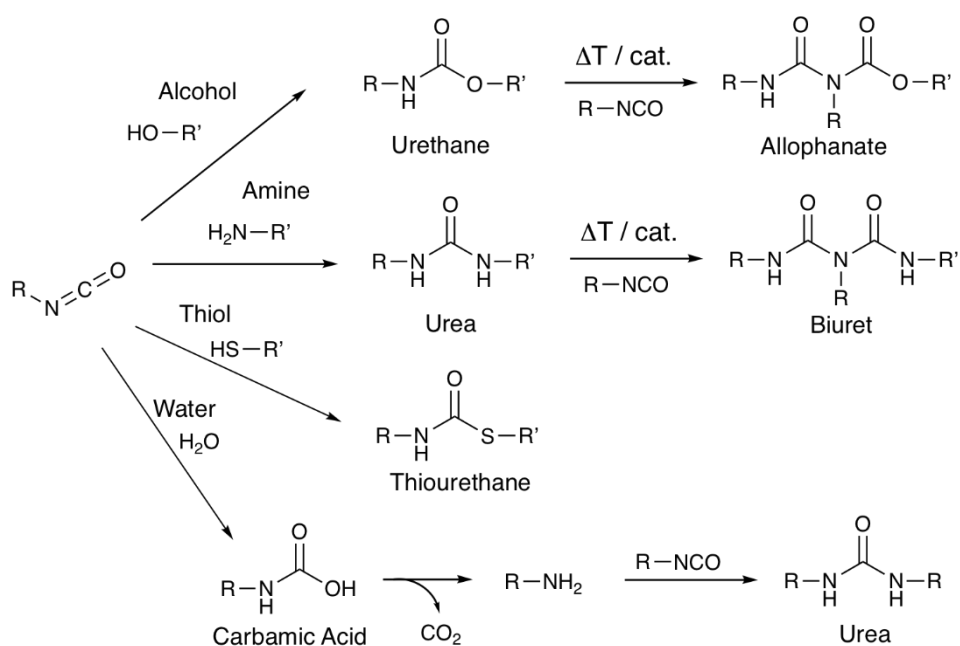
Figure 11. Reactions of Isocyanates with hydrogen containing nucleophiles. Alcohol to urethane, urethane to allophanate. Amine to urea and urea to biuret. Thiol to thiourethane. Water to carbamic acid (instable) to amine and CO_2, amine to urea. Modified according to Ref. 106.

In general, the hydrogen containing nucleophile attacks the electrophilic carbon of the isocyanate, followed by a hydrogen transfer to the nitrogen, resulting in thermodynamically stable carbonyl containing compounds. The resulting products are urethanes (carbamate esters), ureas, thiourethanes and amides in case of reaction with alcohols, amines, thiols and carboxylic acids, respectively.[106] The reaction with water results in the formation of carbamic acid that readily dissociates upon carbon dioxide (CO_2) formation, resulting in a primary amine that reacts with a second isocyanate to form a stable urea. This kind of reaction is often used in foams or moisture-curable polyurethanes, where the in situ generated carbon dioxide has the function of a blowing agent.[107] Beyond that, some of the reaction products are still capable of reacting with the isocyanate group, as they still contain active hydrogens. Urethane and urea adducts for example,

result in the formation of allophanates and biurets, respectively (Figure 11). However, these reactions tend to occur less readily and usually catalysts and/or higher temperatures are required.[108] The relative reaction rates of the corresponding hydrogen active compounds towards the isocyanate groups are listed in Table 1 as a rule of thumb.[109] The values are normalized with respect to the water – isocyanate reaction.

Table 1. Relative reaction rates of non-catalyzed reactions of nucleophilic, hydrogen containing compounds with the isocyanate groups, taken from reference [109]. The corresponding values are normalized with respect to the water-isocyanate reaction.

Hydrogen active compound	Relative reaction rate
Primary aliphatic amine	1000
Secondary aliphatic amine	200-500
Primary aromatic amine	2-3
Primary hydroxyl	1
Water	1
Secondary hydroxyl	0.3
Urea	0.15
Tertiary hydroxyl	0.005
Urethane	0.001

Amines in general are by far the most reactive nucleophiles towards the isocyanate group, with decreasing relative reaction rates from primary aliphatic amines, over secondary aliphatic amines to primary aromatic amines. Primary hydroxyl groups as well as water follow with reaction rates that are 1000 fold slower compared to primary aliphatic amines. Urea and urethanes are the tail end. Owing to the different reaction rates and the huge variety of reaction partners and products, catalysis plays an essential role in isocyanate chemistry, especially in terms of selectivity.[110]

Commonly, organic tertiary amines[111] and organometallic salts[112,113,114] are used. Of these, dibutyltin dilaurate (DBTDL or DBTL) is used most frequently and has been described as the 'workhorse of the urethane catalysis.'[115] It represents the benchmark catalyst, which is related to the high catalytic activity combined with a high selectivity towards the urethane formation. However, potential toxicity concerns are the major drawback of DBTL, which is why researchers world-wide are searching for appropriate alternatives, having a similar activity as well as selectivity.[110,116,117]

Isocyanates further undergo homocyclization reactions, resulting in the formation of polyisocyanates. [105,118] These have two advantages, on the one hand, the vapor pressure of the isocyanates is reduced, reducing toxicity concerns and on the other hand, higher isocyanate functionalities are obtained, enabling higher crosslinking densities in polymer structures. A

selection of isocyanate reactions leading to polyisocyanates are illustrated in Figure 12, exemplarily based on hexamethylene diisocyanate. Polyisocyanates based on HDI are especially interesting because of the low viscosities of the resulting isocyanate reaction products in comparison to IPDI and $H_{12}MDI$ based reaction products. The industrially most important examples are the formation of cyclic trimers (isocyanurate and imminooxadiazinedione) and dimers (uretdione), where three or two isocyanate molecules react to form a cyclic structure.
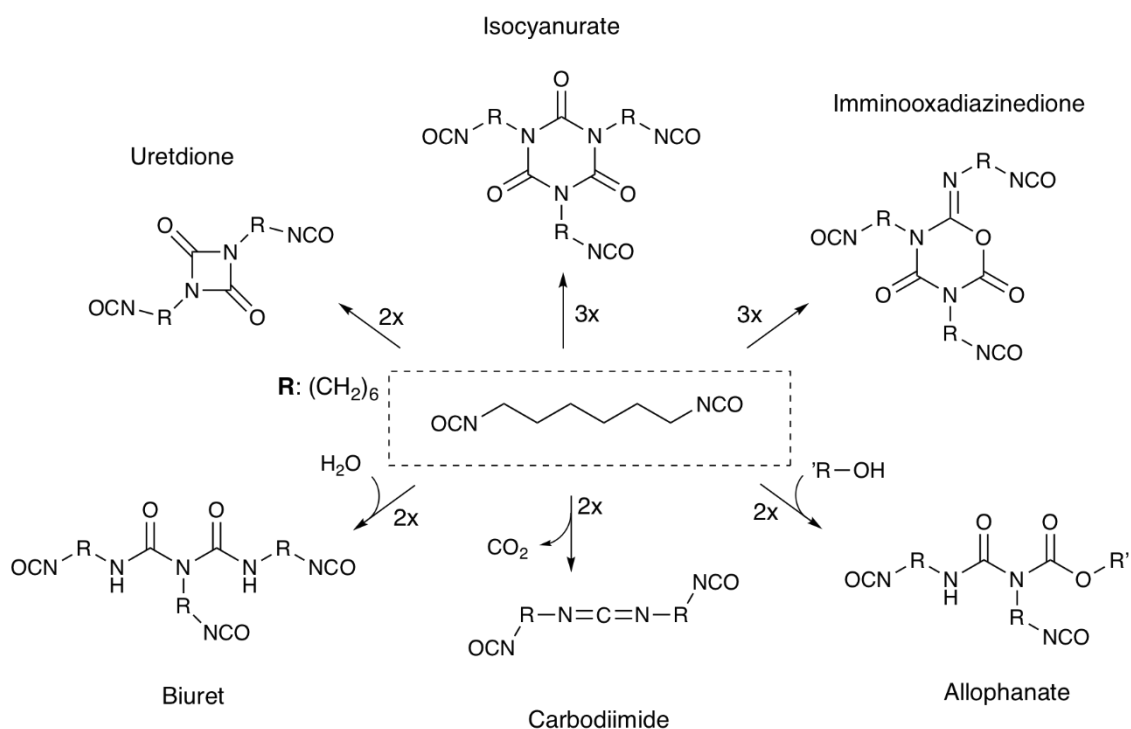
Figure 12. Reactions of hexamethylene diisocyanate resulting in polyisocyanates (idealized structures) such as: Isocyanurate, imminooxadiazinedione, allophanate, carbodiimide, biuret and uretdione. Adopted from Ref. 118.

Other options are the formation of polyisocyanates with an allophanate or biuret structure. Herein, two isocyanate groups react with each other and additionally, an alcohol or water is added, resulting in the respective allophanate and biuret structures. Carbodiimides are also accessible from isocyanates upon the separation of carbon dioxide.[118]

Especially, the trifunctional isocyanurate ring is highly thermodynamically stable, which is related to the symmetrical ring structure and the hyperconjugated π-system parallel to the ring plane.[119,120] This stability is the reason why this material class is gaining increasing interest in the formation of polyurethane networks, especially with regard to applications where high chemical and thermal stability is required.[121,122] The synthesis of soluble polyisocyanurate structures affords that the isocyanates are only partially reacted to higher molecular structures. This is why

excess monomeric diisocyanate needs to be removed after successful synthesis. However, as a result, the polyisocyanurates do not occur in the form of well-defined compounds as illustrated in Figure 12, but always as oligomeric mixtures with a molar mass distribution.

For the cyclotrimerization of isocyanates, a catalyst is required. Prominent examples are (alkali) metal alkoxides[100], metal carboxylates[123], (hetero) carbenes[124] and trialkyl phosphines[125], some of which are exemplarily illustrated in Figure 13.
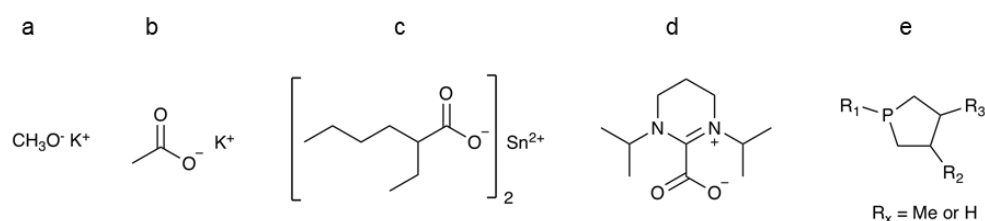
Figure 13. Selection of common catalysts used for the cyclotrimerization of isocyanates. a) potassium methoxide, b) potassium acetate, c) tin octanoate, d) CO_2 protected N-heterogenic carbene, e) trialkyl phosphines.

2.4.2 Polyols

Polyols represent the most important co-reactants for isocyanates to yield polyurethane materials.[126] Common polyols are polyether polyols, such as polyethylene glycol (PEG), polypropylene glycol (PPG) or polytetratydrofurane (pTHF), aromatic and aliphatic polyester polyols, based on phthalic acid, adipic acid or maleic acid or polycarbonate polyols. The corresponding structures are schematically illustrated in Figure 14.
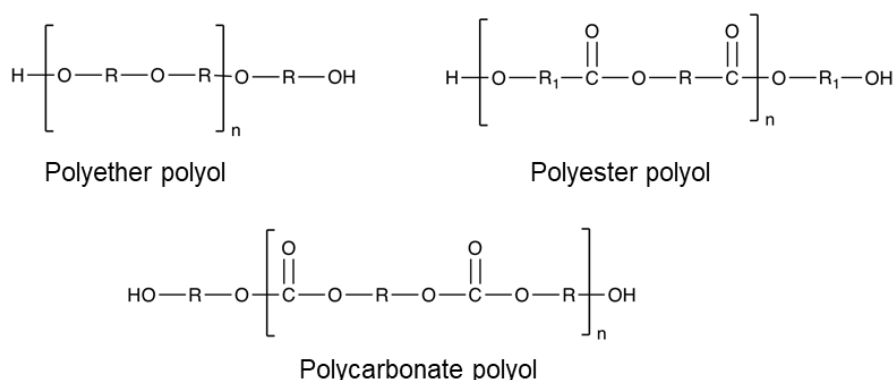
Figure 14. Schematic illustration of selected polyols.

The choice of the polyol highly depends on the requirements of the polyurethane for the final application. Important characteristics are the molar mass, the glass transition temperature, the viscosity as well as the functionality.[127]

Polyether polyols possess little oxidative stability, which is why they are usually used for interior applications only. However, they demonstrate excellent hydrolytic stability. In contrast to that, polyesters possess little hydrolytic stability, but are stable against oxidation, which is why they are used in outdoor applications. In terms of UV stability, aliphatic polyols are the preferred choice, as aromatic moieties yellow upon exposure to UV light.[127] Polycarbonates are both, hydrolytically, as well as oxidatively stable. Polyether polyols as well as aliphatic polycarbonate polyols possess a rather low viscosity, making them attractive from a processing point of view, especially for solvent-free applications.[109] A new class of polyols based on the incorporation of CO_2 into a polyether polyol, leading to polyether carbonate polyols, represents an attractive sustainable alternative for the preparation of polyurethanes.[128,129]

2.4.3 Polyurethane Materials

High reactivity, thermodynamically stable reaction products as well as a huge variety of reaction partners are among the reasons why isocyanate-based reactions are the materials of choice for the preparation of tailored polymeric materials. The most industrial relevant polyurethanes are formed by the step growth polymerization reaction of (poly)isocyanates with polyols and water. Depending on the functionality of the precursors, different sorts of polymeric structures can be formed, which can generally be divided in physically associated and chemically crosslinked polymer networks. Thermoplastic polyurethanes (TPU) belong to the group of physically associated networks and are characterized by phase segregation of block copolymers and strong hydrogen bonding of the urethane structure. The resulting three dimensional network is of physical nature, enabling the re-processability of TPU's at elevated temperatures. A detailed description of TPU materials can be found in literature.[130–133] In this thesis, chemically crosslinked and thus covalent polyurethane networks will be the subject of investigation, which is why the most common synthesis strategies and the resulting material properties will be discussed in greater detail. However, matching the properties of TPU like materials, starting from the liquid phase in a vat photopolymerization is a highly regarded target for the development of polyurethane based photocurable resins and of this work, respectively.

The most common synthetic strategy to work with isocyanates is the two component (2C) approach of mixing polyisocyanates with another reactive species, mainly polyols. Due to the

reactivity of isocyanates, the components are physically separated before application, and only upon mixing, a fast polymerization reaction with short curing times takes place. A three dimensional network is formed, when the reactive groups are employed stoichiometrically and the average functionality of both components is > 2. Accordingly, to achieve crosslinked networks, the polyisocyanate precursors as described in section 2.4.1 are ideally suited, as they provide high functionalities of ≥3. Such components are commonly used as crosslinkers in the formation of covalent PU networks, as schematically illustrated in Figure 15.[134]

Getting the stoichiometry of the two components right is essential to ensure the full conversion of the functional groups via polyaddition reaction, in order to reach the ultimate mechanical properties of the material. A good miscibility as well as an adequate mixing of the two components is another fundamental requirement for the successful use of two component systems.

A more consumer friendly approach utilizes so called one component (1C) polyurethane formulations (Figure 15). 1C formulations have the advantage that no mixing step prior to application is needed, thus ensuring that both components are already mixed in the right stoichiometry and the ultimate mechanical properties are reached. This can be realized by reversibly inactivating the isocyanate group with a so-called blocking agent. Blocking agents are monofunctional active hydrogen containing nucleophiles that are thermodynamically stable at low temperatures, but decompose upon temperature exposure.[135,136]
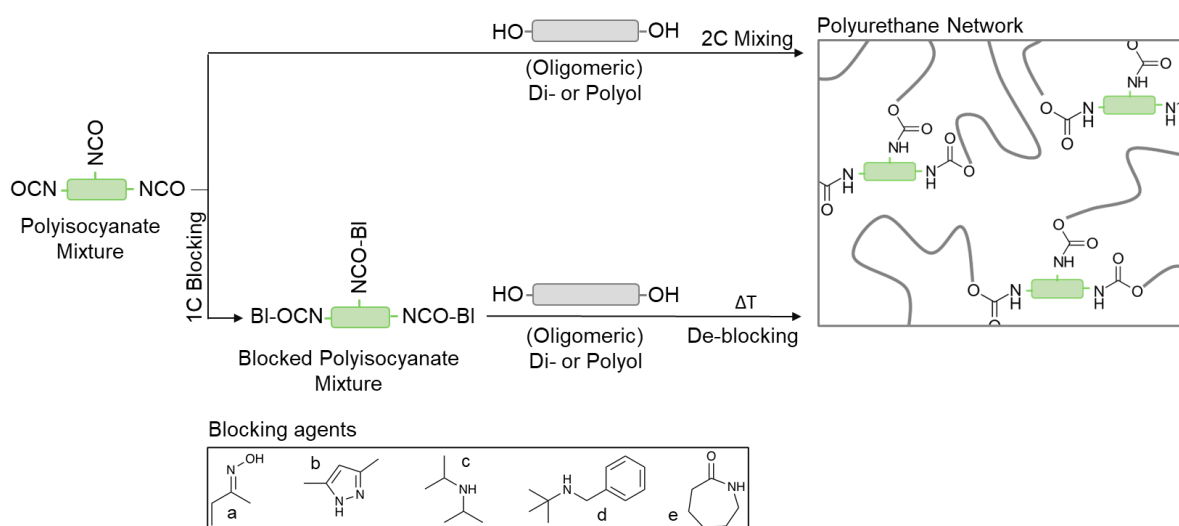

Figure 15. Schematic illustration of common covalent polyurethane crosslinking mechanisms, starting from one and two component formulations. Figure inspired by Ref. 134.

Common examples for blocking agents (Figure 15 a-e) are butanone oxime, 3,5-dimethylpyrazole, diisopropylamine, benzyl tert-butylamine and caprolactam. The use of blocked isocyanates has the advantage of long open times to process the polyurethane formulation and a reaction taking place at will. Upon deblocking, the isocyanate is again formed in situ and directly undergoes the curing reaction with the desired reaction partner.

To balance storing stability and reactivity, usually high temperatures are required to obtain a successful through-cure, which again limits the scope of applications of blocked 1C curing systems to heat resistant substrates. In comparison to 2C systems, longer curing times are observed due to the more complex reaction profile. In case of using volatile blocking agents, their release at higher temperatures results in the formation of volatile organic compounds (VOC), which can cause concerns regarding the environmental evaluation of these solutions and working place hygiene aspects.

To circumvent the release of VOC's, but still enable a stable 1C formulation, latent polyurethane catalysts that only trigger the reaction of isocyanates with reactive species upon application of a certain stimulus, have gained increasing interest and are subject of academic and industrial research.[137,138] Latent reactive catalysts are typically combined with isocyanates with sufficiently low reactivity that need a catalyst for curing in an acceptable time.

Another crosslinking mechanism which has been amongst others intensively studied by Piet Driest, is the crosslinking via reaction of isocyanates with each other i.e. by trimerization, as schematically illustrated in Figure 16.[134] In this case, the final crosslinking reaction exclusively involves the reaction of isocyanate groups, rendering the addition of other reaction partners redundant.[121,139] Precursors for this type of curing, are either solely based on polyisocyanates or based on isocyanate functional prepolymers, that are formed upon sub-stochiometric reaction of monomeric diisocyanates with polyols. The crosslinking by trimerization has several advantages compared to the other systems.[140,141] As only one component is involved in the reaction, no mixing is required, no stoichiometry issues occur, that can potentially negatively influence the overall mechanical properties and no release of chemicals occurs as in blocked isocyanate 1C systems.

Since a (latent) catalyst needs to be added prior to application, strictly speaking the trimerization reaction does not provide for a one component system. When using longer chain functional isocyanate precursors, the viscosity is comparably high, while at the same time the low isocyanate functionality causes longer curing times, which, in combination, may limit the scope of application.
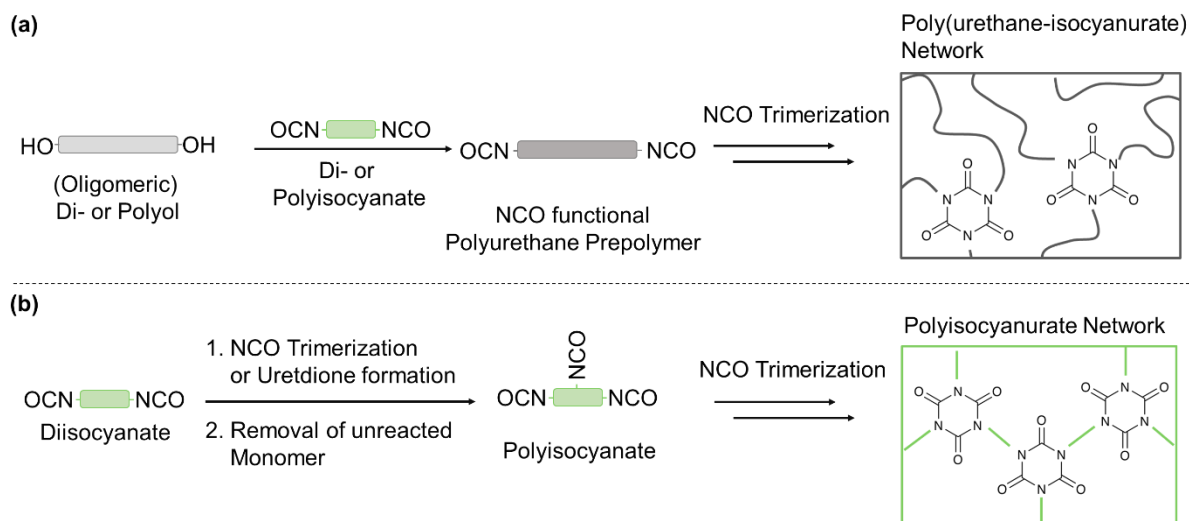
Figure 16. Schematic illustration of the formation of Isocyanurate networks. a) Formation of a Poly(urethane-isocyanurate) network by the trimerization of an NCO-functional polyurethane prepolymer. b) Formation of a polyisocyanurate network based on the trimerization of a polyisocyanate. Figure inspired by Ref. 134.

The various crosslinking opportunities as well as the broad range of available starting materials form the basis for the versatility of polyurethane chemistry.[98,142,143] Especially, polyurethane networks containing isocyanurate rings as a crosslinking unit demonstrate high thermal stability and chemical resistance against various media.[121,144,145] In a direct comparison, polyurethane materials regularly outperform e.g. UV cured (meth)acrylate networks in terms of toughness and durability. However, if the application requires the curing via UV light, as for example in stereolithography or UV coatings, polyurethanes can be combined with radiation curing moieties. The modification of polyurethanes to enable a light based curing mechanism is discussed in the next section.

2.4.3.1 Polyurethane acrylates

Polyurethane acrylates have been extensively studied in the last decade.[146–149] They are frequently used in coatings, adhesives and more recently in stereolithography, to improve the mechanical properties of radiation curing formulations.[62] Acrylated urethanes are considered to combine the high abrasion resistance, toughness and tear strength of polyurethanes with the weatherability of acrylates.[150] Oligomeric urethane acrylates can easily be prepared by the reaction of isocyanate functional prepolymers with hydroxyl containing acrylate monomers, such as hydroxyethyl(meth)acrylate (HE(M)A), as schematically illustrated in Figure 17.

In a typical process, an isocyanate functional prepolymer is prepared by the sub-stochiometric reaction of a polyol with a di- or polyisocyanate. Subsequent reaction with a hydroxyl containing monomeric acrylate, leads to the light curable polyurethane acrylate.
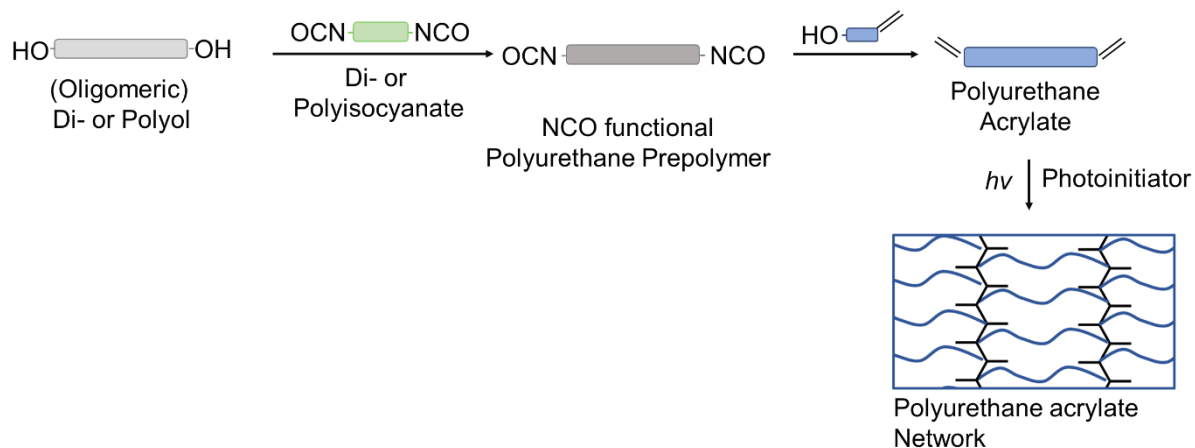
Figure 17. Schematic illustration of the preparation of polyurethane acrylates. Figure inspired by Ref. 134.

The curing of polyurethane acrylates is initiated via the UV induced radical polymerization of the acrylic double bonds, leading to a three dimensional polyurethane acrylate network.[151] As the viscosity of these materials is usually high due to hydrogen bonding, these oligomeric acrylates are commonly diluted with co-reactive acrylic monomers and oligomers to reduce the viscosity and increase the reactivity of these formulations. Light sensitive polyurethane acrylates are frequently used in VPP. However, they also represent an ideal candidate to be combined with thermally curable isocyanate precursors, leading to a so-called dual-cure resin. The investigation of dual-cure resins based on polyurethane acrylates, in combination with thermally curable isocyanates will be the subject of this work. A detailed overview of dual-cure thermosets in general, as well as the resulting morphology will be given in the following chapter.

2.5 Dual-Cure Thermosets

One prominent strategy in VPP and in general in coating and adhesive applications is the use of dual-cure resin systems, employed to improve the performance of crosslinked materials derived from low molar mass resins. A dual-cure resin is characterized by a combination of two different polymerization processes that either take place simultaneously or sequentially.[152] These reactions can be triggered by similar or different stimuli, such as temperature or UV light.[153] While the use of dual-cure resins represents a classical approach for the toughening of thermoset materials,[154] it is further frequently employed in radiation cured coatings and adhesives to ensure a sufficient cure of the non-illuminated areas.[155]

Most combinations of polymers result in heterogenous structures, which is related to the enthalpy driven low miscibility of polymer precursors. However, specifically the heterogeneity of these polymer blends makes these kind of materials attractive.

By combining e.g. elastomers with thermosets, a synergism in terms of improved tensile and tear strength as well as damping/toughness characteristics can be obtained.[156] If the volume of the hard phase dominates, the material is typically toughened. If the elastic phase dominates, the tear strength of the elastic phase is generally improved. Thus, the combination of two polymer networks can range from a filler-reinforced elastomer, over a leathery material to a rubber reinforced (high impact) thermoset, depending on which of the two phases predominates.[157] In co-continuous networks, both phases contribute to the properties of the blend in all directions, which can additionally effect the mechanical properties. The general concept and the resulting networks of dual-cure resins are schematically illustrated in Figure 18.
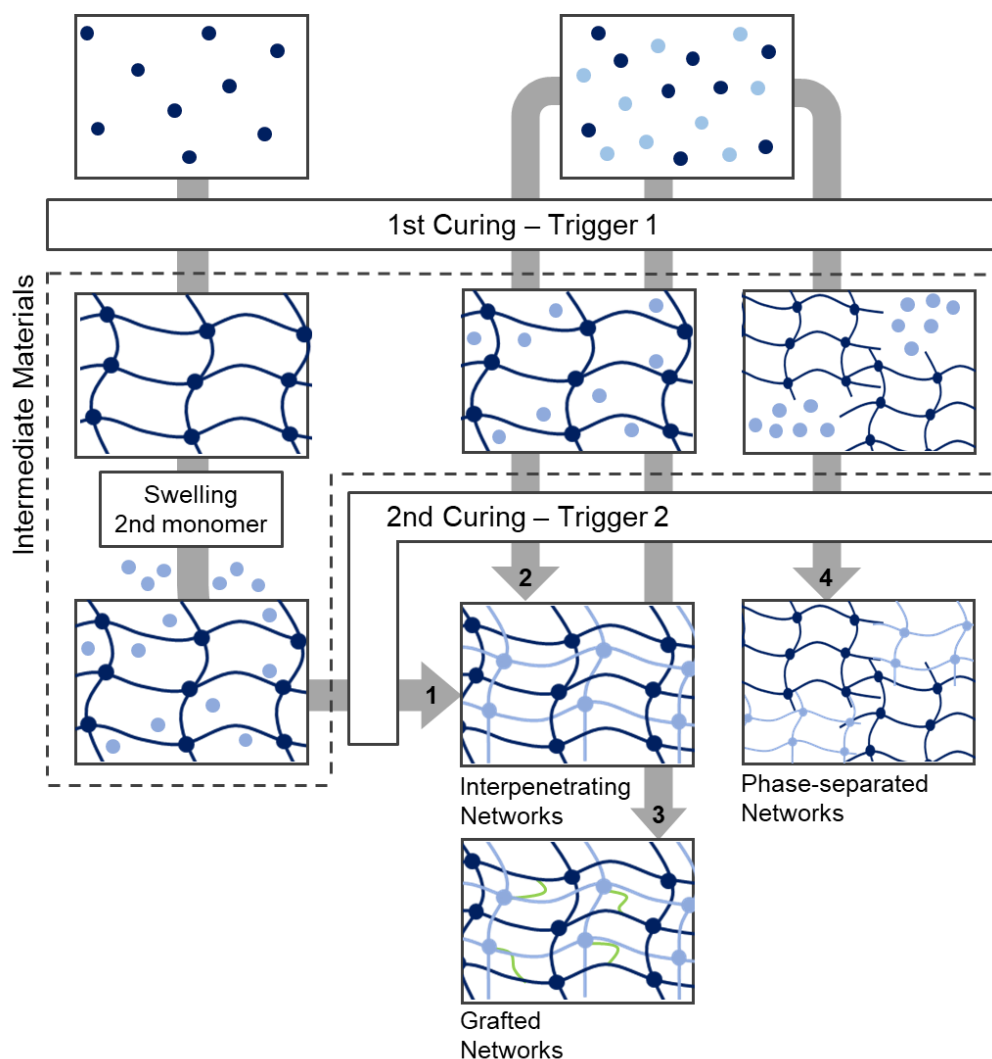
Figure 18. Schematic illustration of a sequential dual-cure process. Figure inspired by reference 153.

What is often referred to as the formation of an interpenetrating network (IPN) involves the curing of a first type of monomer, that is subsequently swollen by a second type of monomer, which is eventually polymerized and crosslinked (1). As a result, the two networks are not chemically linked to each other, but are physically interpenetrating. [158] This approach is often used for the formation of tough hydrogels and in most examples, UV light is used as stimuli for both curing reactions.[159,160]

Another dual-cure approach represents the direct mixing of two types of monomers, followed either by a subsequent or a simultaneous polymerization. A sequential polymerization requires that the two reactions proceed selectively and independently from each other, which is frequently referred to as orthogonal. The miscibility of the two types of monomers, as well as of the developing crosslinked polymers plays an essential role for the resulting network structure.[161]

In the case, that the second monomer remains at least partially miscible in the polymer network formed by monomer one, an interpenetrating network is formed upon the second polymerization reaction (2). However, often, a polymerization induced phase separation is observed that is related to an enthalpy-driven reduction of the compatibility with increasing degree of polymerization, accompanied by an increasing network density of the first and second type of monomers.[162] As a consequence, at least partially phase-separated network structures evolve (4).

Depending on the monomer functionality, it is possible to introduce hybrid molecules, that are able to participate in both curing reactions. By mutually linking the polymeric phases to each other, the domain sizes of the separated phases can be reduced, or phase separation can be even completely avoided (3). The resulting internetwork grafting, typically improves the transparency of the final material.[163,164]

A simultaneous and orthogonal polymerization of two types of monomers affords two different types of reaction kinetics, e.g. those of chain and step growth polymerization. Depending on the reactivity of monomers and the choice of catalyst/initiators, both reactions can be triggered by the same stimulus (e.g. UV light or heat).[165] The differential kinetics of the two polymerization reactions have significant influence on the expected outcome with respect to phase separation and thus, to the ultimate properties. In tendency fast (polymerization reaction is faster than phase separation kinetics) and simultaneous reactions yield interpenetrating networks with smaller phase separation.[164]

In general, the products derived from dual-cure resins do not necessarily result in the formation of interpenetrating networks. Defined by IUPAC, an interpenetrating network corresponds to: "A polymer comprising two or more networks which are at least partially interlaced on a molecular scale but not covalently bonded to each other and cannot be separated unless chemical bonds are broken."[166]

Factors such as the miscibility of the monomers, phase separation during mixing or during polymerization as well as the feed ratio of the monomers are essential factors that determine the evolution of the final network structure.

Historically, interpenetrating networks have been extensively studied in the late 1960s. Meyer and Widmaier have focused their research of IPN's on the relation between synthesis and morphology[163,167], while Klempner and Frisch pioneered the use of IPN's based on polyurethane combinations (mainly with polymethylmethacrylate) for energy absorbing materials.[157,168] A

series of review articles has been written by Sperling and his co-workers, that comprehensively summarize the advances within the course of time.[158,165,169–171,172]

With time, the strict definition of interpenetrating networks has become broader, as investigations have shown, that IPN's do not necessarily interpenetrate on a molecular scale but may also exhibit dual-phase continuity.[172] A fundamental understanding of the morphology of dual-cure networks, being interpenetrating or not, is important, as the morphology is largely responsible for the mechanical properties of the resulting material.

Figure 19 gives an overview of typical morphologies that can be obtained upon polymerizing two types of monomers. Depending on the compatibility of the polymerized networks and the feed ratio of monomers employed, various phase morphologies of the polymeric networks can be expected. The resulting morphologies correlate to the physical properties such as the glass transition behavior and the dependence of the loss factor on the temperature, as can be measured by dynamic mechanical analysis.[157,173]
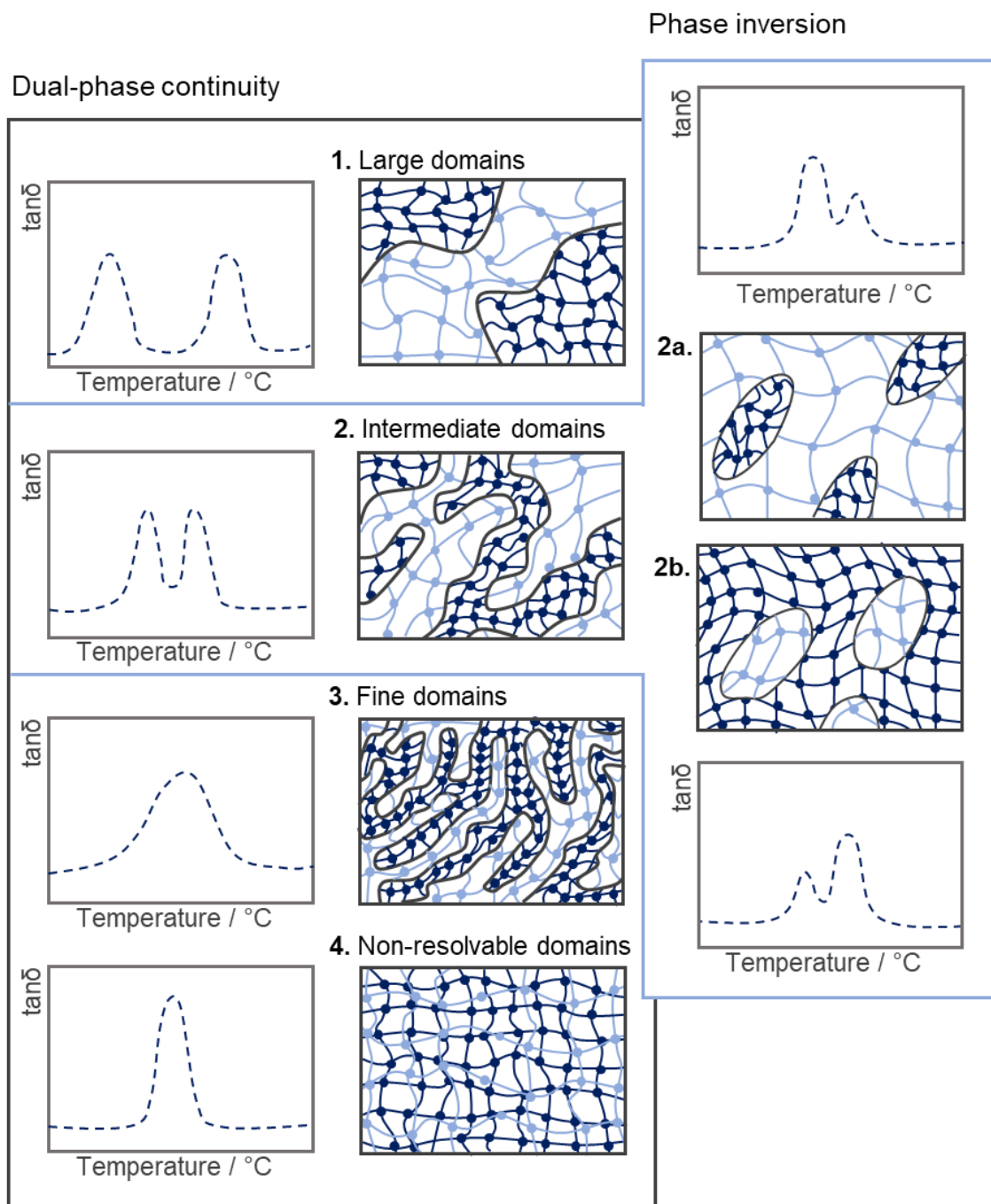
Figure 19. Schematic illustration of the potential morphology evolution of interpenetrating networks. The drawing was designed based on the descriptions of IPN's by Klempner and Frisch.[168]

Dual-cure resin systems mostly involve the combination of two polymer networks in which one is in the glassy state, while the other is in the rubbery state at use temperature.

The following four morphology states are conceivable for an even feed-ratio of the monomers, as proposed by Klempner and Frisch[168] (see also Figure 19):

1. The domain sizes of the two networks are large, in the magnitude of a few micrometers. Each material has a distinct glass transition temperature that are well separated from each other.

2. The domains of the two networks are of intermediate size, in the magnitude of hundreds of nanometers. Each material still has a distinct glass transition temperature, however they are shifted inwardly.

3. The domain sizes are small, in the magnitude of tens of nanometers. The material has one broad intermediate glass transition temperature, that stretches the region between the two polymer networks.

4. Individual domain sizes are not resolvable anymore. The material has one sharp glass transition temperature.

The even feed-ratio of two monomers that form incompatible networks from homogenous monomer blends often results in a material with dual-phase continuity (co-continuous structures). The domains of both phases are interconnected and build up elongated domains, that extend throughout the sample.[171] Upon formation of the first network, spinodal decomposition takes place, which leads to the phase separation.[158,161] The degree of de-mixing is dependent on the miscibility of the two polymer blends, as well as the miscibility of the second type of monomer in the first network.[174] Co-continuous structures can be formed over a certain interval of volume fractions.[175] In case of a sufficient change of the feed-ratio, phase inversion may take place, as schematically illustrated in Figure 19 for case 2 (intermediate domains). Depending on the monomer ratio, either phase one is continuous (2a) or phase two is continuous (2b) and the result is a matrix-dispersed particle structure.

It is not trivial to analyze interpenetration of networks as such. Although imaging methods such as transmission electron microscopy (TEM) or atomic force microscopy (AFM) can give information about the morphology, interpenetration on a molecular level cannot be evidenced.[176] Small angle neutron scattering (SANS) as well as small angle x-ray scattering (SAXS) can be used to get information about the interface that has been formed between the phase-separated regions, i.e. sharp or diffuse interfaces, and further enables to determine the total interface area.[177] With SANS, the resolution of heterogeneities on the magnitude of a few angstroms can be determined.[178]

The most common way to qualitatively analyze the level of interpenetration on a molecular scale involves the determination of the storage- and loss modulus in dependence on the temperature by a DMA measurement. The inward shift of the two glass transition temperatures of the

independent neat material networks represents good evidence of at least partial interpenetration.[167]

The turbidity of the received samples can be determined by the scattering of light and is another indication for phase separation and phase size.[179]

A huge variety of dual-cure resin systems resulting in heterogenous morphologies, has evolved over the past decade, as there are many polymerization reactions that can be combined. Prominent examples are a combination of click polymerization reactions that include nucleophilic ring-opening reactions, photochemical addition of thiols to alkenes and alkynes as well as carbonyl addition of thiols to isocyanates.[153,180] Photoinitiated thiol-ene reactions followed by a thermal thiol-epoxy reaction, represent an extensively studied dual-curing resin system[181–183], as well as the thermal and photochemical curing of isocyanate and acrylate functionalized oligomers.[184,155] Another prominent example represents the simultaneous UV curing of acrylates and epoxides.[185,186]

Transferring the dual-cure concept to a vat photopolymerization based system, requires the adaption to the processing requirements that have been described in Chapter 2.3. Three different dual-curing processes will be discussed in detail, with regard to VPP:

1) The simultaneous activation of two polymerization processes

2) The sequential activation of two polymerization processes and

3) Special dual-cure polymerization options, involving post-functionalization.

Figure 20 schematically lists the basic photochemical and thermal reactions that have been exploited in VPP to date. Essentially, at least one monomer type must proceed via a radiation induced polymerization mechanism in order to be applicable in VPP.
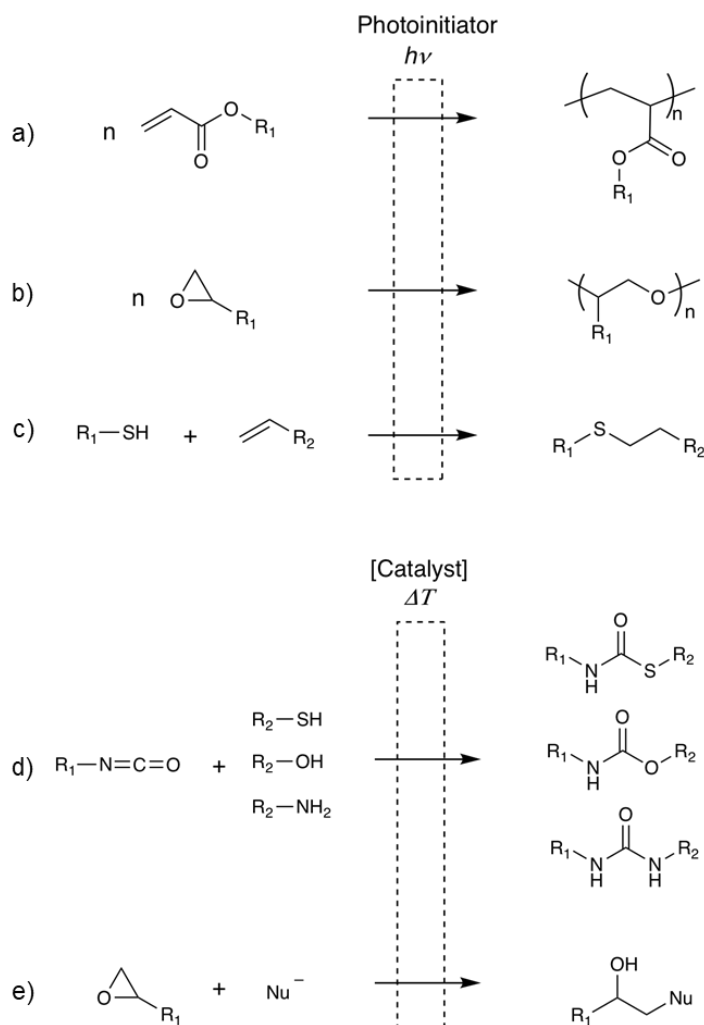
Figure 20. Schematic illustration of light- and heat induced polymerization reactions frequently used in vat based photopolymerization. a) radial polymerization of acrylates, b) cationic polymerization of epoxides, c) radical induced thiol-ene addition, c) addition reaction of isocyanates with hydrogen containing nucleophiles, d) curing reaction of epoxides with nucleophiles.

The most prominent dual-cure example used in VPP is the simultaneous polymerization of acrylates and epoxides, following a radical chain growth polymerization and a cationic step growth polymerization, respectively. The resin needs to contain independent radical and cationic photoinitiating systems that are both activated by the light source of the printer. The fast reaction rate of (meth-)acrylates is combined with the lower curing speed of the epoxides.

The polymerization of the (meth)acrylic species controls the build time of the 3D printed object due to the high curing speed, while the role of the epoxides is to provide material properties and increase the accuracy of the build product due to their lower curing shrinkage and thus reduced distortion of the 3D printed part.[187] Dark curing is avoided, as the fast curing (meth-)acrylates confine the illuminated voxel, in which the cationic polymerization of the epoxides takes place. As

the cationic polymerization of epoxides is not inhibited by oxygen in comparison to the radical polymerization of the acrylates, the overall oxygen inhibition can be reduced by combining the two monomers.[185]

Using this approach, Boydston and co-workers managed to print multi-material objects, by selectively triggering the polymerization of an acrylate and an epoxide, leading to a heterogenous network structure containing stiff epoxide and soft acrylate moieties.[188] This approach enabled the fabrication of spatially controllable mechanical properties. Zhou and co-workers used a similar approach, by simultaneously triggering the cationic polymerization of epoxides as well as the radical polymerization of acrylates using liquid crystal display (LCD) irradiation, leading to an interpenetrating polymer network.[189] They further showed, that a heat treatment after printing was essential to enable a full curing of the epoxide and thus to obtain ultimate properties.

Wenjuan and co-workers studied the accuracy of epoxy/acrylate hybrid systems in stereolithography and evaluated the corresponding shrinkage factor of the fabricated part that was less than 2 %.[187]

These examples show that hybrid acrylate/epoxy systems in combination have a high synergism in terms of reaction rate, accuracy and oxygen inhibition.

The research group lead by Timothy E. Long has developed a variety of different strategies to improve the mechanical properties of 3D printed parts.[24,190] Amongst others, they investigated a dual-cure 3D printing resin, based on the chain growth polymerization of acrylates and a simultaneous step growth polymerization via thiol-ene coupling.[191] The use of thiol-ene coupling allows for the controlled formation of long and linear polymer chains between the crosslinking points. The properties of the final 3D printed part provided increased elongations due to the decrease in crosslinking density obtained via chain extension, enabling the fabrication of elastomeric like material properties. [192]

The use of sequential polymerization processes expands the amount of reactions that can be combined, as they are not limited to photo-induced polymerization machanisms. Improved mechanical properties for 3D printed parts have been obtained by Qi and co-workers that used a dual-cure resin based on photocurable acrylates and thermally curable epoxides.[193] The resulting 3D printed parts showed improved fracture stress and a higher Young's modulus in comparison to the purely acrylate and epoxy resins.

Turri and co-workers used a similar approach and achieved to produce 3D printed composites filled with up to 30 % carbon fibers, by using a UV assisted 3D printing process.[194,195]

Another dual-cure combination has been exploited by the company Carbon Inc.. They exploited a technology that has been initially developed for coatings.[184] The technology makes use of inactive blocked isocyanates, that are re-activated at elevated temperatures. As isocyanate blocking agent, 2-(tert-butylamino)ethyl methacrylate was used. The methacrylic functionality of the blocking agent reacts with co-reactive monomers to form an acrylic polymer network during the printing process. Upon an increase in temperature after printing, the isocyanate is re-activated by the instable bond of the blocking agent, enabling the formation of a second network upon reaction of the isocyanate with available chain extenders such as diols or preferably primary or secondary amines. This enables the formation of a second thermoplastic network structure by strong hydrogen bonding of the resulting urethanes or urea upon heat exposure.[196,197] Using this technology, 3D printed parts with 300 % elongation at break and 6 MPa tensile strength have been obtained.[198] However, the material pocesses a broad glass transition temperature, which means that the material properties differ with changing temperature.

Another novel approach has been demonstrated by Chu and co-workers. They used a dual-cure resin based on biobased acrylates and 2-hydroxyethyl acrylate (HEA) in combination with 1,6-hexamethylene diisocyanate (HDI).[199] During the UV curing step, the acrylic network is formed, while upon temperature exposure, the HDI reacts with the hydroxy group of HEA to form a urethane network with strong hydrogen bonding properties. The resin comprises a molecule with functional groups, that are able to participate in both curing reactions. However, during the thermal reaction, no second network structure is formed, but the crosslinking density is increased, which leads to an increased glass transition temperature and thus to improved mechanical and thermal properties.

One major drawback of this approach is the use of the highly volatile and toxic HDI monomer as well as the toxic HEA monomer. Additionally, a premature reaction of HDI with HEA cannot be fully excluded, which may lead to an increase in viscosity already during printing.

A similar approach has been developed by Wu and co-workers.[200] They used an acrylate resin containing hydroxy groups that enables a second thermal curing reaction. However instead of using monomeric HDI, they employed the hexamethylene diisocyanate trimer, which, due to higher viscosity and lower vapor pressure can be handled safely and at the same time further increases the crosslinking density due to a functionality of > 3. Upon the addition of the

polyurethane based crosslinker, they were able to increase the glass transition temperature from 85 °C to 120 °C.

While the sequential polymerization of acrylates and epoxides yielding interpenetrating networks has been studied for application in 3D printing, the sequential curing of acrylates and isocyanates, without the use of hybrid molecules that connect both networks, has not been investigated so far and will be introduced in chapter 4.2 of this work.

Dual-cure resins have further been used to produce 3D printed objects with self-healing properties, that can be partially reprocessed. For this purpose Zhang, and his co-workers polymerized a diacrylate resin containing β-hydroxyl groups as well as acrylamide, enabling a transesterification reaction at elevated temperatures.[201] A similar approach has been demonstrated by Ge and his co-workers. Although the materials are not fully meltable, they show unique self-healing properties and partial reprocessability.[202]

Another interesting feature that can be exploited from dual-cure resins is the surface functionalization of the fabricated 3D printed object. Yang and co-workers integrated a vinyl-terminated initiator into the resin mixture, enabling post-printing surface-initiated atom transfer radical polymerization (ATRP).[203] That way, they grew polymer brushes of poly(ethylene glycol) methacrylate on the surface for improved biocompatibility of the structural material. [204,205]

Thiol-yne chemistry has further been used to selectively functionalize 3D printed parts by using off-stoichiometric amounts for the step growth polymerization, leaving functional groups for a post-printing step.[206] Chiappone et. al proved the concept by functionalizing an azide terminated squaraine dye via click reaction with available alkyne groups, analyzed by the use of fluorescence measurements.[207] Fourkas and co-workers made use of unreacted acrylates that after printing, undergo highly selective Michael additions with diamines. Upon a second post-curing reaction they were able to metallize the amine-modified structures.[208]

Especially dual-cure resins containing hybrid structures, are well suited to enable a surface functionalization. A resin comprising partially acrylated hexamethylene diisocyanate trimer will be presented in Chapter 4.1, where the isocyanate groups were subsequently used to functionalize a sensitizer for photooxygenation reactions on the surface. The same resin enabled on the other hand the fabrication of highly chemically resistant 3D printed structures by a simple reaction of the isocyanate groups with water upon urea formation.[209]

In conclusion, dual-cure resins have been successfully used to influence the ultimate mechanical properties of 3D printed structures, to improve reaction rates and shrinkage, to enable the incorporation of self-healing properties and re-processibility as well as to post-process the surface of finished parts.

The conceptualization of the design of dual-cure resin systems based on acrylates and isocyanates will be in the focus of this thesis. Depending on the functionality of the monomers employed, it is the target to demonstrate their potential for the fabrication of toughened thermosets, flexible and elastomeric-like materials as well as highly chemically resistant and functionalized thermosets.

3 Task

Vat photopolymerization (VPP) based printing techniques are gaining increasing interest for the production of functional parts, providing objects with high feature resolution and complex geometry. The growing technology affords a steady improvement of the printing hardware itself as well as of the photopolymers that can be printed.[210,211]

Owing to the fact that photopolymers have been extensively optimized for 2D applications such as coatings and adhesives, the use of this technology to result in materials with bulk properties is not necessarily intuitive. Thus, it does not surprise that new material concepts, new polymer structures and networks are required to improve the properties of cured photopolymers, enabling their use also as functional bulk objects.

Several prerequisites from a processing point of view have to be fulfilled in order to adopt photopolymers for VPP:[34,45]

- Low viscosities are essential in order to enable a sufficient backflow of the resin during printing.
- Fast reaction rates and high monomer conversion are desirable to keep printing times short.
- The printed object should match the scale of the virtual model and shrink as little as possible.
- High green strength is also important so that the 3D printed part does not collapse under the force applied during the printing process.

To fulfil these requirements, usually oligomeric, difunctional acrylates are combined with co-reactive, mono-or multifunctional monomers to adjust the viscosity, as well as the crosslinking density of the intended part. The amount of co-reactive diluent is typically high to achieve appropriate printing viscosities and multifunctional precursors are needed to obtain sufficient green strength during the printing process. The resulting network structure is usually highly crosslinked, with only low number of monomer repeating units between the crosslinking points. Consequently, these materials suffer brittleness.

The goal to increase the toughness and flexibility of a printed product results in a processing-property paradigm: The use of high molar mass precursors, leading to less crosslinked but tough material properties is limited, as this would result in a high viscosity of the printing formulation. Short exposure times are preferred, but limit to build-up a high number of monomer repeating units, that would be necessary to reduce the crosslinking density of the final part.[79,212]

To enable the fabrication of though thermosets and even elastomers by designing polymer networks with lower crosslinking densities, dual-cure resin systems have gained increasing attention.

In general, dual-cure resins describe the simultaneous or sequential curing of two different polymerization reactions.[180] Employed in vat photopolymerization, usually the first reaction builds up a continuous network with sufficient green strength via light induced polymerization in the printer. This is followed by a second, independent polymerization reaction, that can also take place outside the printer. As the second reaction is not limited to light-initiated fast curing reactions, the choice of potential polymerization reactions is significantly broadened and allows to extend the potential property range of the 3D printed bulk material.

Based on this general concept, this thesis deals with the development of new dual-cure resin systems for application in 3D printing with the goal to achieve:

     1. Thermosets with a high solvent resistance by surface post-functionalization

     2. Tough thermosets

     3. Elastomers

The investigated new dual-cure resin systems for 3D printing applications are based on photocurable acrylates and thermally curable isocyanates. The use of hybrid molecules, able to participate in both curing reactions, are investigated as well as formulations based on the two types of monomers with strictly orthogonal polymerization mechanisms, as summarized in Figure 21.

Dual-cure hybrid molecules are employed to design surface-functionalized and solvent resistant 3D printed parts, e.g. for use in reaction containers for chemical synthesis applications (1).[209]

Formulations containing two sets of independently polymerizable monomers comprising photocurable acrylate functional polyurethane prepolymers and thermally curable low viscous polyisocyanates are investigated to produce toughened thermosets (2).

Reversely, a combination of thermally curable isocyanate based prepolymers in combination with photocurable monomeric acrylates is employed for the preparation of elastomers (3).

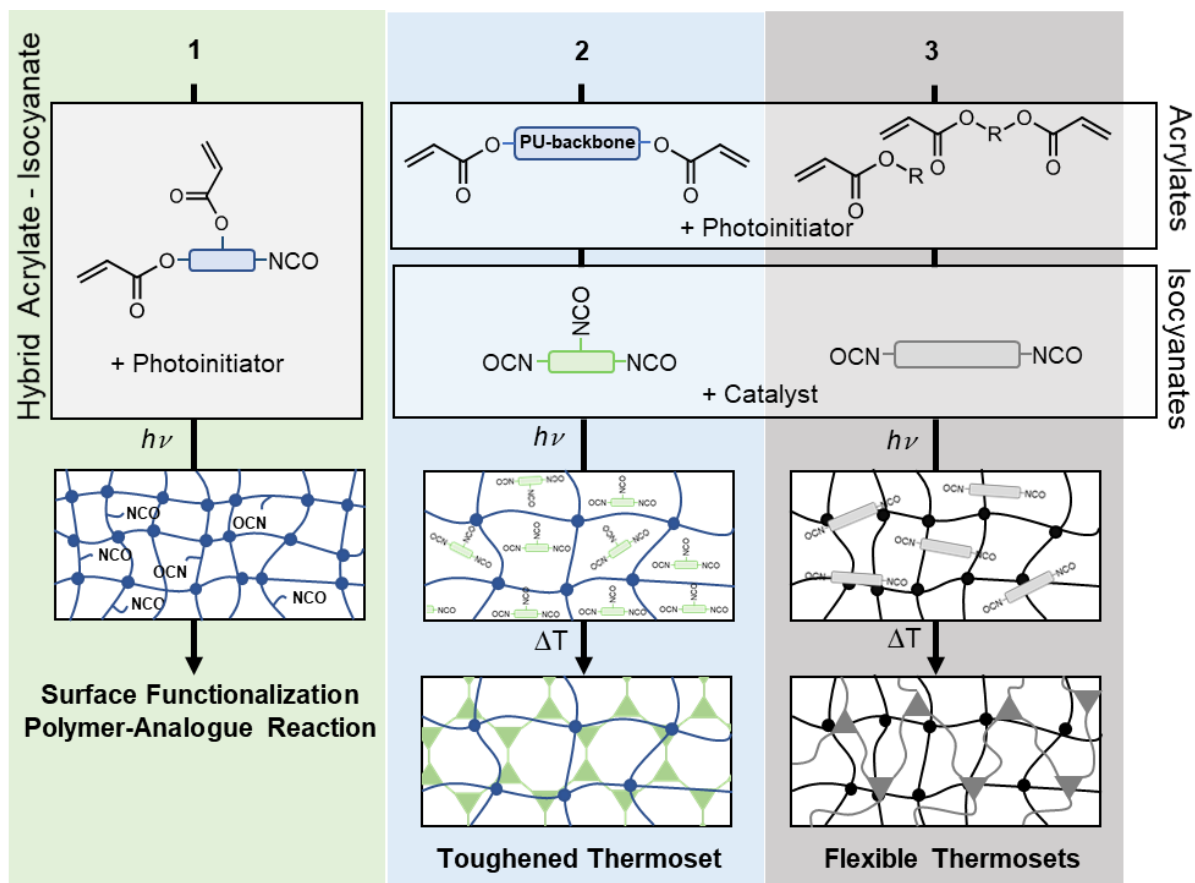Figure 21 schematically illustrates the concept for this thesis.

Figure 21. Schematic illustration of the working concept.

4   Results and Discussion

The following chapter is organized around the results of the three material classes that were investigated within this thesis.

In section 4.1 the development of solvent resistant and surface-functionalized thermosets based on hybrid polyisocyanato-acrylate resins is presented and the potential use of this material in chemical synthesis application is demonstrated.[209] Section 4.2 shows the development of orthogonal dual-cure resins based on acrylates and isocyanates, aimed at producing toughened thermosets. Section 4.3 focuses on the use of dual-cure systems of acrylates and isocyanates for the development of elastomers.

4.1   Surface-Functionalized Thermosets with Application as Flow Reactor

Surface-functionalized and solvent resistant thermosets are of high interest for the additive manufacturing of microfluidic devices or containers for chemical synthesis.[213] The advantage of using additive manufacturing (AM) for this application is given by the high degree of freedom in design, where complex geometries with inherent control over size, shape and integrated function can be obtained.[27,214–216] The use of dual-cure reactions to integrate additional function e.g. in the form of catalytically active surfaces, has been proven to be highly versatile in multistep chemical processes.[217–219] Especially, vat photopolymerization based printing techniques enable the option for easy post-functionalization of 3D printed parts.[203,204,220] When applying AM technology to produce qualified chemical reaction ware or fluid handling systems, the resistance against the exposition to organic solvents is essential.[221,222] Only few examples have been demonstrated to print suitable chemically resistant devices with VPP, as presented by Rapp and co-workers.[223,224,225]

In the following section, a hybrid dual-cure resin is presented that combines the option to design catalytically active surfaces with a high chemical and temperature stability in one resin formulation.[209]
For this purpose, a partially acrylated polyisocyanate with pending isocyanate functions is used as base material. Upon the VPP printing process the acrylate functional groups undergo a radical

polymerization reaction, resulting in a thermoset green body or scaffold, providing sufficient strength as well as pending reactive isocyanate functionalities.

Two post reactions are performed on the remaining isocyanate function, of which one leads to the formation of a highly solvent resistant 3D printed part, while the other results in a catalytically active surface. As proof of concept, a flow reactor is printed and functionalized that can be used for the photooxygenation reaction of citronellol. Two aspects are considered to be important: The flow reactor should withstand the harsh conditions during the intended catalytic reaction in aggressive solvents without degradation. The photooxygenation of citronellol should result in the corresponding hydroperoxide products, in dependence on the amount of catalytically active species on the reactor surface.

This section is based on the publication "From 3D to 4D printing: A reactor for photochemical experiments using hybrid polyurethane acrylates for vat-based polymerization and surface functionalization" by Anne Hansen, Melissa Renner, Thomas Büsgen, and Axel G. Griesbeck, published in 2020 in *Chemical Communications,* volume 56 on pages 15161 to 15164. The conduction of the photooxygenation reaction in the flow reactor was performed by Melissa Renner.

4.1.1   Synthesis, Characterization and Selection of Hybrid Polyurethane Acrylates

Hybrid polyisocyanato-acrylates were synthesized by partial reaction of the isocyanurate trimer of hexamethylene diisocyanate (HDI-Trimer, **1**), with a hydroxy (meth-)acrylate, i.e. 2-hydroxyethyl methacrylate (HEMA, **2**). Herein, the isocyanate group reacts with the hydroxyl function of HEMA upon formation of an urethane. The isocyanate content and accordingly the double bond content was adjusted by deploying different amounts of HEMA, as schematically illustrated in Figure 22. The corresponding structures were analyzed by ^{1}H-NMR analysis. The isocyanate content was measured using back titration of the functional isocyanate groups. The corresponding values are given in Table *2*, together with the viscosity of the resulting products.
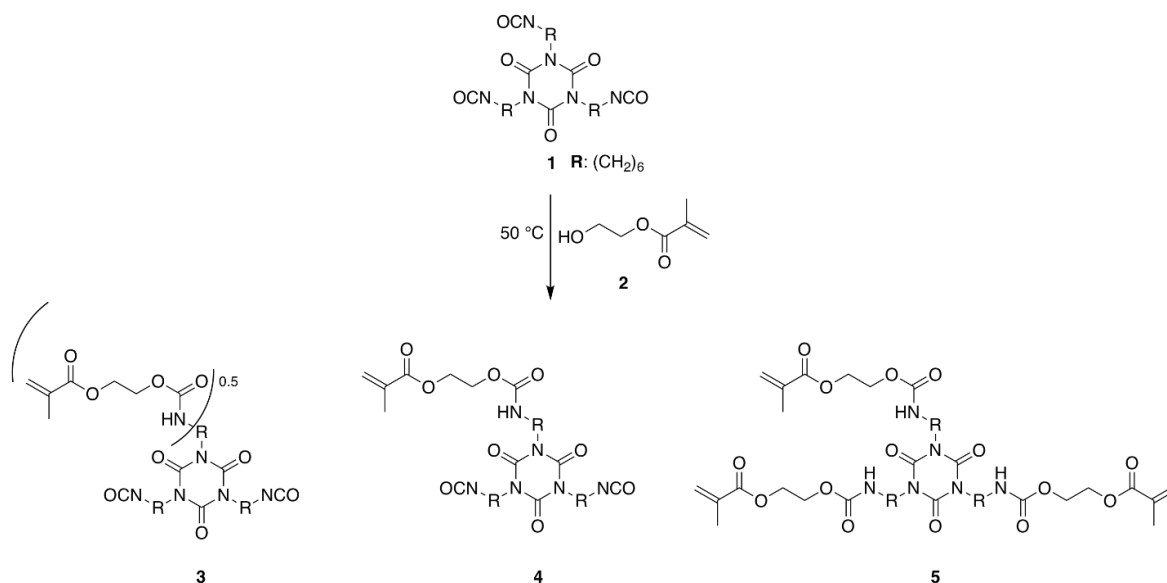
Figure 22. Reaction of HDI-Trimer (1) with different amounts of 2-hydroxyethyl methacrylate (2) leading to hybrid polyisocyanurate isocyanato-acrylates (3,4) and a polyisocyanurato acrylate (5).

Different amounts of HEMA were reacted with HDI-Trimer. For structures **3** and **4** not all isocyanate groups were converted. The amount of HEMA was adjusted to lead to a statistical conversion of 0.5 isocyanate groups per isocyanurate trimer for **3**. For **4**, statistically 1 isocyanate group was converted. The reactions yielded mixtures of HDI-Trimer, HDI-Trimer containing one, two or three HEMA functions. For **5**, all isocyanate groups were stoichiometrically reacted with HEMA. The viscosity of the reaction products increases with increasing conversion of the isocyanate groups. Table 2 gives the NCO-content, the conversion, as well as the resulting viscosity. Figure 23, shows the viscosity in a logarithmic scale in dependence on the isocyanate conversion.

Table 2. Isocyanate content, conversion and viscosity of the acrylated HDI-trimers.

#	NCO-content / %	Viscosity / mPa·s	Conversion / %
1	23.5	1200	0.00
3	17.3	3830	26.4
4	12.6	10680	46.4
5	0.04	420700	99.8

The exponential increase in viscosity can be attributed to the effect of increasing hydrogen bonding of the urethane groups formed. While the viscosity of structure **3** with 3830 mPa·s is almost low enough to be directly printed using VPP, the fully acrylated HDI trimer with a viscosity

of 420700 mPa·s, does not show sufficient reflow to be used in a high volume fraction in a VPP formulation. For structure **4,** an intermediate viscosity of 10680 mPa·s was obtained.
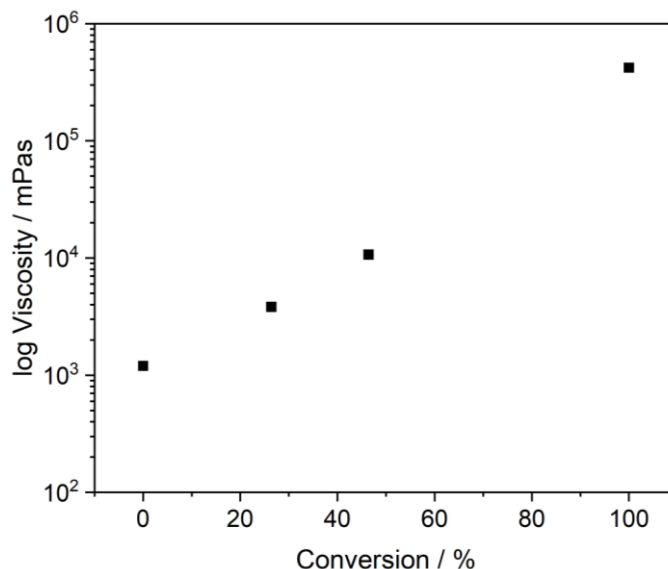
Figure 23. Viscosity in dependence of the isocyanate conversion of the prepared acrylated HDI-Trimers. The viscosity increases with increasing urethane functionality and conversion and with decreasing isocyanate content.

The conversion of the isocyanate groups can be easily adjusted to yield a desired viscosity, as well as to the desired NCO-content, respectively. This tuneability facilitates to find the desired balance between viscosity and availability of reactive isocyanate groups, allowing for a good control of immobilized e.g. catalyst concentrations for later reactions. For printing tests, structure **4** was chosen, providing an optimal balance between the number of acrylic double bonds for the UV induced polymerization reaction, viscosity and the amount of isocyanate groups available for post-printing functionalization reactions.

4.1.2 3D Printing and Post-Treatment of Hybrid Polyurethane Acrylates

For printing trials, structure **4** was diluted with 30 % di(propylene glycol) diacrylate (DPGDA, **6**) in order to achieve appropriate printing viscosities. DPGDA was chosen as it increases the crosslinking density and thus helps to obtain a printed part with high green strength. The formation of a dense and highly crosslinked network is especially relevant for applications in flow chemistry, to avoid swelling upon the exposition to solvents. The glass transition temperature of the DPGDA homopolymer amounts to 105 °C and thus imparts temperature stability upon co-polymerization with the acrylated HDI-Trimer, by increasing the resulting T_g of the thermoset. As photoinitiator, a blend containing three different acylphosphine oxides (**7a-c**) was used and was

added to the mixture (1 wt%). The blend is ideally suited for UV LED curing at 385 nm and has the ability to result in a non-yellowing system upon photobleaching. A non-yellowing and transparent system is of special interest for applications in flow chemistry, where light induced reactions are targeted. The mixture was then printed on a 385 nm DLP printer. The printing process as well as the relevant structures are schematically illustrated in Figure 24.
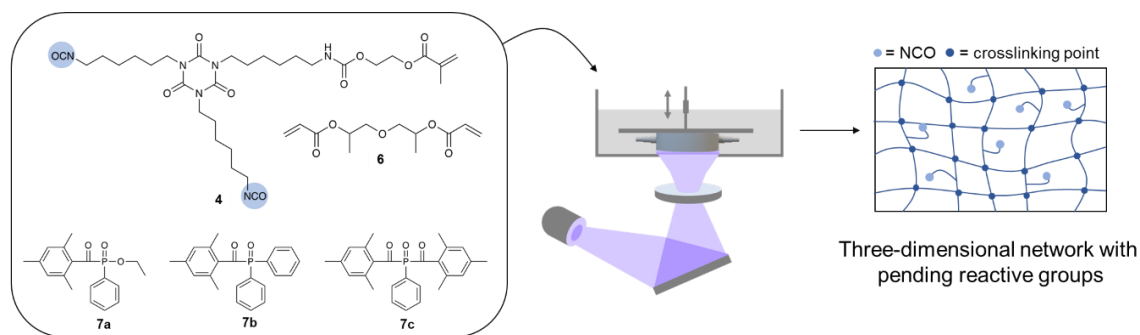
Figure 24. Schematic illustration of the printing process of the hybrid polyurethane acrylate, diluted with di(propylene glycol) diacrylate to yield 3D printed objects with pending reactive isocyanate groups.

The corresponding printing parameters are given in the experimental section (Chapter 6.3). The 3D printed part was washed with dried isopropanol as a sufficiently inert solvent to remove excess resin. As a first post-printing reaction, to yield high solvent resistance, the 3D printed part was immersed into hot water. The isocyanate groups reacted with water upon carboxylation, yielding CO_2 and a primary amine. As the reactivity of primary amines towards the isocyanate group is about 1000 times greater than the reactivity of water, the amine preferably reacts with another isocyanate group upon the formation of an urea group.[106]

This reaction lead to a direct linkage between the pending isocyanate groups by formation of a urea group and thus increased the crosslinking density and the glass transition temperature of the resulting polymer. Urea groups are well known for their high chemical resistance due to their high tendency to form stable hydrogen bonds between urea groups and thus offer an easy access to solvent resistant 3D printed parts. The reaction was monitored by the decrease of the isocyanate absorption band at 2265 cm^{-1}, accompanied by an increase in the N-H-deformation vibration at 1640 cm^{-1} of the urea group. The corresponding FT-IR spectra are given in Figure 25a. Dynamic mechanical analysis was measured before and after water treatment to determine the mechanical properties in dependence on the temperature, as illustrated in Figure 25b.
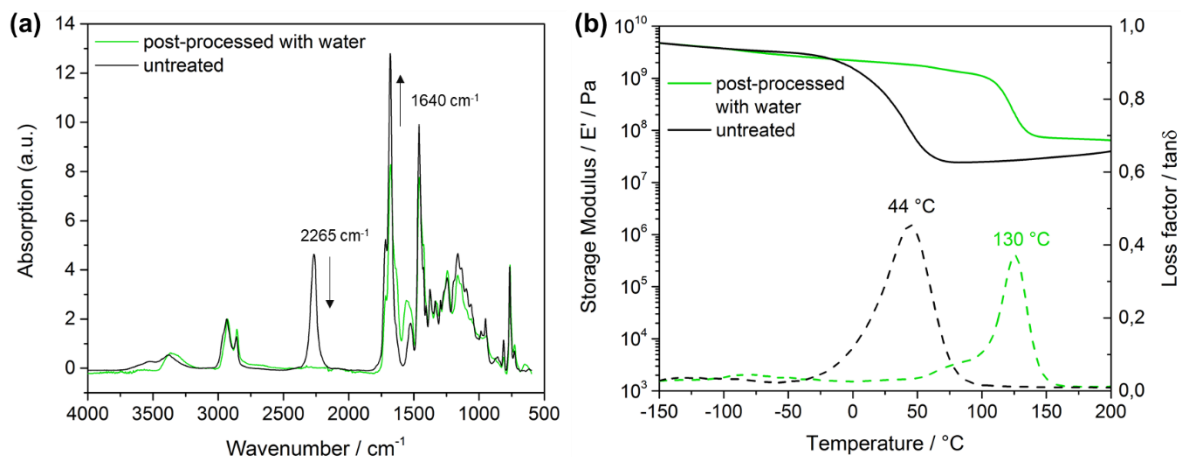
Figure 25. a) FT-IR spectrum and b) dynamic mechanical analysis of the 3D printed part before and after treatment with water.

The effect of the post-treatment with water can be observed in the temperature-dependent modulus of the material. The untreated 3D printed part that still contains isocyanate groups on the surface, has a glass transition temperature at about 44 °C, as determined by the peak maximum in the *tanδ* curve. The storage modulus gradually starts to decrease from about 0 °C onwards and reaches the plateau modulus at about 75 °C. As the isocyanate groups are not crosslinked yet, the short and flexible pending isocyanate side chains have a softening effect on the material, which influences the glass transition temperature. After treatment with water, the glass transition temperature is shifted to 130 °C, indicating that a further crosslinking reaction i.e. the intended urea formation took place. The pending side chains reacted with each other and the ability of those links to interact via strong hydrogen bonding with other urethane and urea groups resulted in an increase of the softening point and the crosslinking density. However, a local maximum in the *tanδ* curve at about 75 °C can still be observed. This may be related to an incomplete turnover of the isocyanate groups inside the bulk 3D printed object, assuming that depending on the part thickness, the water molecules did not penetrate through the whole sample under the given post-reaction conditions and thus, urea formation predominantly took place on the surface of the printed part.

In order to use the products derived from the post-processed hybrid resin for chemical synthesis applications, the chemical stability is essential. This is why the solvent resistance of the final material was investigated by determining the solvent uptake. Small blocks (10 mm x 10 mm x 2 mm) were printed and post-processed with water. Subsequently, the blocks were immersed in water, ethanol, dichloromethane (DCM), dimethylformamide (DMF), tetrahydrofurane (THF), toluene and acetone, each, for 24 h. The weight of the blocks was

determined before and after exposition to the solvents, enabling the calculation of the solvent uptake. Two commercially available resins ('Tough' and 'Durable' of the company Formlabs) were also printed and treated accordingly, in order to compare the solvent resistance to typical VPP resins. The results are illustrated in Figure 26.
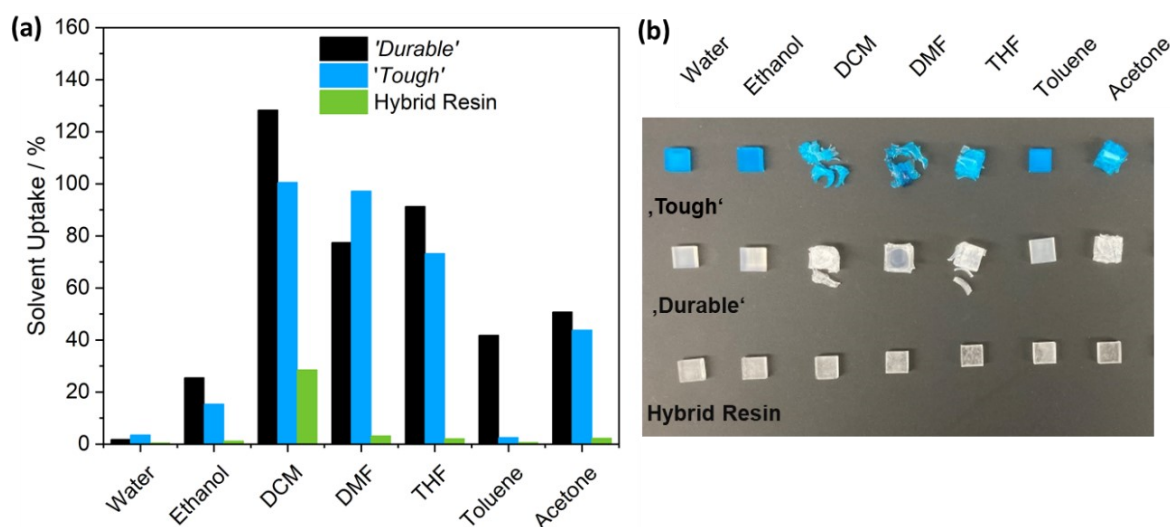
Figure 26. a) Solvent uptake of printed blocks after 24 h in water, ethanol, dichloromethane (DCM), dimethylformamide (DMF), tetrahydrofurane (THF), toluene and acetone. The two commercially available Formlabs resins 'Tough' and 'Durable' are compared to the new hybrid resin. b) Photo of the printed blocks after exposition to the seven solvents. Left figure reproduced from Ref. 209 with permission from the Royal Society of Chemistry.

The two commercially available and printed resins show high solvent uptakes of more than 20 % in weight in nearly all solvents apart of water. Especially in DCM, DMF and THF, the corresponding solvent uptake is more than 80 %. In contrast to that, the solvent uptake of the printed and post treated hybrid resin is well below 5 % in all solvents apart of DCM. However, with 28 % in DCM, the solvent uptake is much lower compared to 'Tough' and 'Durable'. The photo in Figure 26b shows the printed blocks after solvent treatment. It can be observed that in case of the commercial materials, the printed blocks were already falling apart after the exposition to DCM, DMF, THF and acetone, indicating that degradation took place. The hybrid resin stayed stable and no macroscopic degradation was observed. The stability in combination with a low solvent uptake makes the hybrid material ideally suited for the printing of the intended flow reactor.

The transmittance is also a crucial factor when it comes to microfluidic applications that target photocatalytic reactions. This is why UV-vis measurements were conducted on post-treated 3D printed parts with a thickness of 500 μm. Figure 27 illustrates the transmittance between 200 nm and 800 nm for two samples that were printed using different photoinitiator concentrations. As

the employed photoinitiator blend has an absorption maximum at 300 nm, with a local maximum at about 400 nm, it influences the transmittance of the 3D printed part at that wavelength. As illustrated in Figure 27, a decrease in the photoinitiator concentration from 1 wt% to 0.5 wt% results in an improved transmittance of 90 % between 450 nm to 800 nm and further, to an increased transmittance at 350 nm of 78 %.
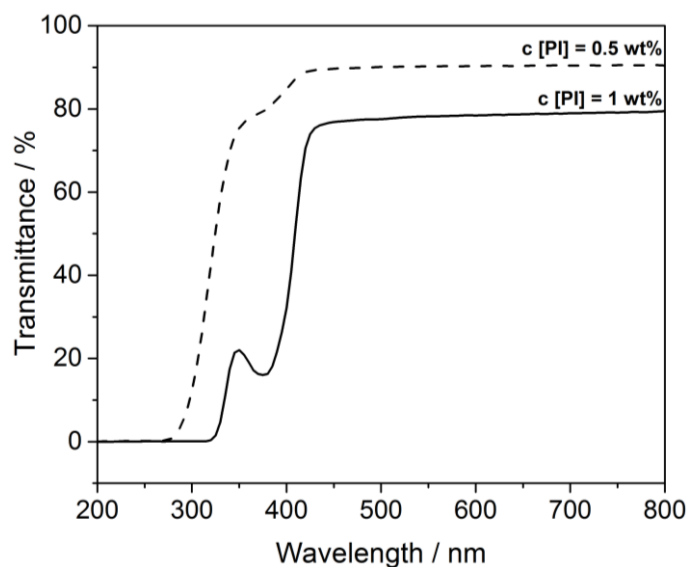
Figure 27. UV-vis transmittance of the 3D printed part, post treated with water with 500 μm thickness. The photoinitiator (PI) concentration was varied from 0.5 wt% to 1 wt%.

To obtain transparent 3D printed parts, the photoinitiator concentration should be chosen to be as low as possible to minimize photo-absorption of the cured resin in the critical wavelength area for a reaction. However, it should be sufficiently high in order to guarantee a high monomer conversion and appropriate exposure times during the printing process.

The pending isocyanate groups further represent a versatile option to obtain catalytically active surfaces. A flow reactor was printed and locally functionalized with 4-aminobenzophenone (ABP), gaining a photo-catalytically active surface to enabling photooxygenation reactions. The functionalization with 4-aminobenzophenone is presented in the following section.

4.1.3 Surface Functionalization and Application as Flow Reactor

The hybrid resin formulation based on structure **4** was applied for the printing of a flow reactor, suited to conduct chemical reactions on a small lab scale. The design, as well as the STL-file was provided by Renner.[226]

After printing, one part of the reactor was post-cured with water to achieve a chemically stable material, while a second part was functionalized with 4-aminobenzophenone before post-curing with water, to achieve a catalytically active surface. As model reaction and proof of concept for this new experimental flow reactor setup, the photooxygenation of citronellol was chosen, as this reaction is one of the best known examples of photochemical reactions.[209,227]

As schematically illustrated in Figure 28, the flow reactor consists of two parts, a body and a cover that are joined together before application. The reactor body contains the reaction chamber, with small inlet and outlet channels to provide connectors for a hose, enabling the feed and effluent of the reaction solution. The reactor cover has a round elevation in the middle that is immersed into the reaction solution upon joining the two parts.
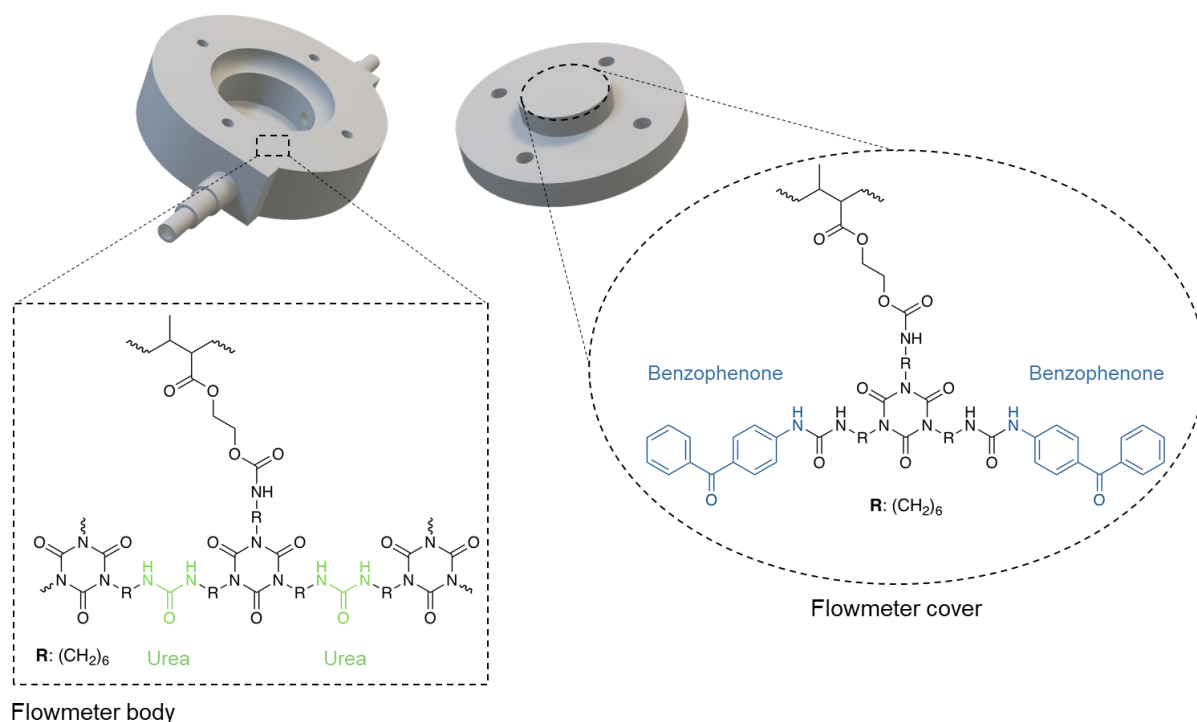
Figure 28. Schematic illustration of the flow reactor and the corresponding structures. The flow reactor body has urea groups on the surface that make the reactor resistant against the exposition to solvents. The flow reactor cover is locally functionalized with 4-aminobenzophenone, enabling the conduction of photochemical reactions.

Both parts were printed in one print job with the given hybrid formulation. After printing and washing with isopropanol, the reactor body was immersed into hot water for 4 hours to form a stable urea surface upon the reaction of the isocyanate groups with water.

To covalently bind the sensitizer to the reactor cover surface, a benzophenone derivative i.e. 4-aminobenzophenone was used. Benzophenone acts as triplet sensitizer in the photooxygenation reaction of citronellol. Upon the absorption of light with a wavelength of 350 nm, benzophenone enables the formation of singlet oxygen upon energy transfer to ground state oxygen.[228] The primary amine of ABP is reactive towards the isocyanate group and thus enables the direct linkage of the sensitizer to the reactor surface. As demonstrated in the work of Renner, the formation of urea does not negatively influence the absorption efficiency of the benzophenone function at 350 nm and the covalently bound benzophenone is still active as sensitizer.[229]

For the functionalization reaction, a concentrated solution of 4-aminobenzophenone in chloroform was prepared and applied to the center of the reactor cover. To finalize the reaction after evaporation of the solvent, the reactor cover was placed in the oven over night at 120 °C. Commonly, the reaction of a primary amine with an isocyanate takes place immediately and already at room temperature. However, since the T_g of the green body after printing was already higher than room temperature and the reactivity of the primary amine is reduced due to the position on the aromatic ring of the conjugated electron system of benzophenone, the reaction was performed at higher temperatures to ensure a sufficient degree of functionalization. The functionalization of the reactor cover with 4-aminobenzophenone was monitored by FT-IR measurements, as illustrated in Figure 29.
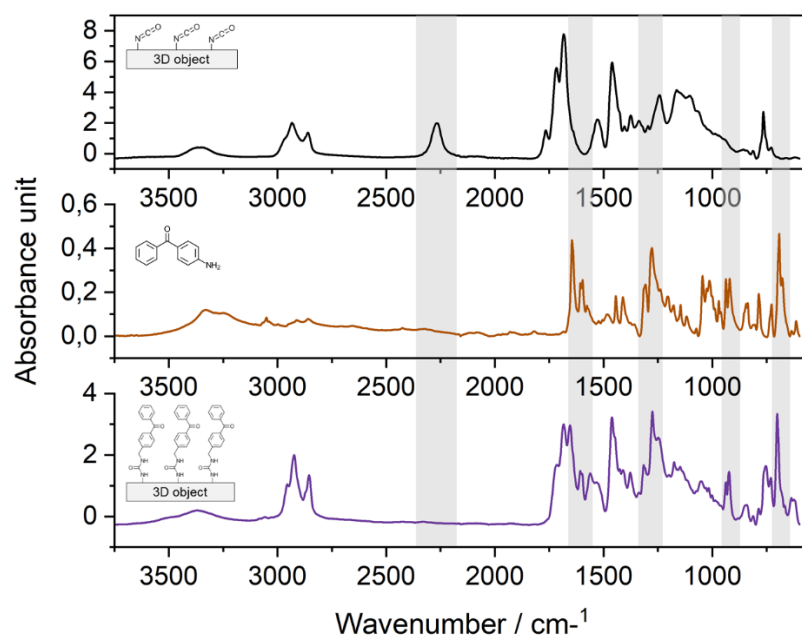
Figure 29. FT-IR measurement to prove the functionalization of the reactor cover with 4-aminobenzophenone. Top: 3D printed part with pending NCO-groups. Middle: 4-aminobenzophenone. Below: 3D printed part functionalized with 4-aminobenzophenone.

The top spectrum gives the 3D printed object directly after printing. The absorption of the isocyanate stretching vibration can be observed at 2265 cm^{-1}. The isolated peak allows to follow the reaction with 4-aminobenzophenone. The spectrum of 4-aminobenzophenone is illustrated in the middle of Figure 29 and the spectrum below illustrates the functionalized reactor surface. In the latter, the stretching vibration of the isocyanate group at 2265 cm^{-1} disappeared, indicating that a near quantitative reaction of the primary amine of ABP with the isocyanate group took place. The appearance of the characteristic N-H deformation vibration of the urea group at 1560 cm^{-1} and other absorption peaks specific for the benzophenone derivative, further prove that the ABP is covalently bonded to the reactor surface.

In order to quantify the activity of the flow reactor, it is necessary to determine the amount of ABP on the surface. For this purpose, the isocyanate content of a 3D printed block of known size was determined directly after printing, using titration experiments. This enabled the calculation of the amount of isocyanate per accessible surface area. On the assumption that the ABP reacts quantitatively with the isocyanate groups on the surface, it is thus possible to estimate the amount of sensitizer on the reactor cover. A detailed calculation as well as the assumptions made can be found in the experimental part in chapter 6.1. The concentration of isocyanate groups on the elevation in the middle of the reactor cover was determined to be about 0.016 mmol·cm^{-2}.

As example reaction, the photooxygenation reaction of citronellol was conducted in the flow reactor by Dr. Melissa Renner from the University of Cologne. Figure 30 schematically illustrates the experimental setup, the formation of singlet oxygen upon energy transfer of ABP to ground state oxygen, as well as the reaction equation of the photooxygenation of citronellol leading to the corresponding hydroperoxides **9a** and **b**.
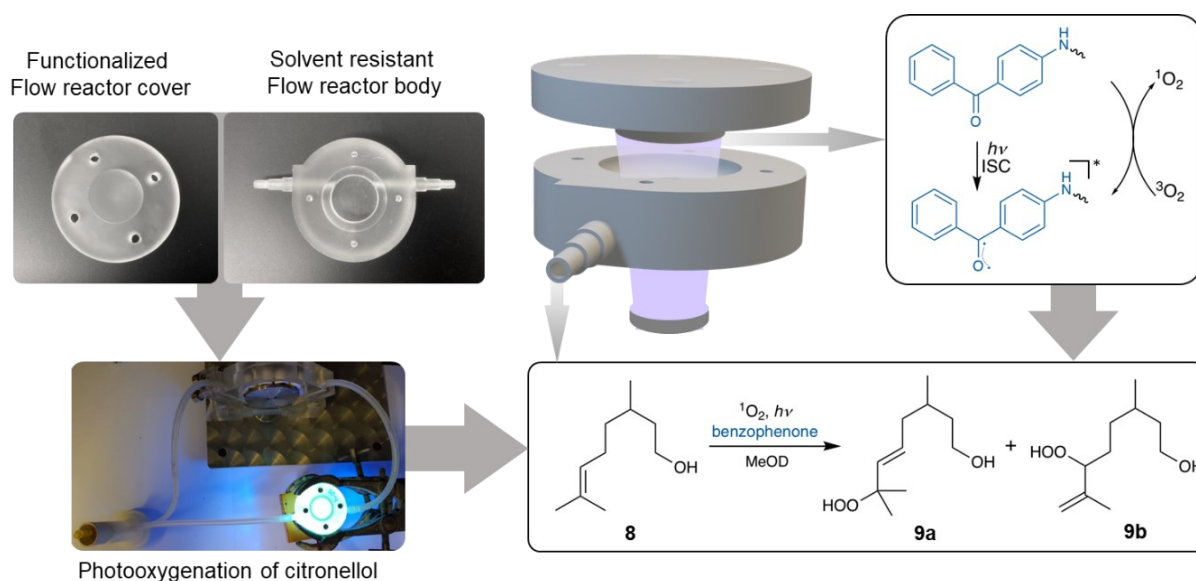
Figure 30. Schematic illustration of the photooxygenation of citronellol in the 3D printed flow reactor. Modified according to Ref. 209 with permission from the Royal Society of Chemistry.

After printing and performing the corresponding post-printing reactions, the two parts of the reactor were joined and the photooxygenation reaction of citronellol was conducted in the reactor. The reactor was used as a continuous loop reactor. The reaction solution containing citronellol (**8**) in deuterated methanol (MeOD) (0.30 mol·L^{-1}), was directed through silicone tubes into the reactor by the use of a peristaltic pump. The reactor was placed directly in front of an LED light source with a wavelength of 365 nm. At this wavelength, the bottom of the reactor body with a thickness of 500 μm has a transmittance of 80 % and thus enables the penetration of light to the reactor cover, where the ABP is covalently bonded to the surface. The ABP absorbs the light and singlet oxygen is formed upon energy transfer (intersystem crossing (ISC)) of benzophenone to ground state oxygen, resulting in the formation of the hydroperoxides **9a** and **9b**.

In order to compare the results and to evaluate the reproducibility of the reaction, three flow reactors (**1** to **3**) were printed and prepared, accordingly. The reaction conditions were similar for all reactions, only the exposure time was varied. The conversion of citronellol was determined by ^{1}H-NMR analysis, directly from the crude reaction solution, and no further isolation of the reaction products was performed. In order to check if the reactor can be used multiple times, flow reactor **2** was used for three consecutive cycles (**2**, **2.1**, **2.2**). The results were compared to the conduction of the reaction with benzophenone in solution as a reference. To that regard, the photooxygenation reaction was performed in an NMR tube that was exposed to the same light source. To correspond with the assumed functionalization level of the flow reactor cover,

benzophenone was used at a concentration of $4.2 \cdot 10^{-3}$ mol·L^{-1} in deuterated methanol, providing an absolute reactive ingredient quantity of 0.026 mmol. The exposure times as well as the turnover of the reactions are summarized in Table 3.

Table 3. Results and reaction conditions for the photooxygenation reaction of citronellol in the printed and post-processed flow reactors, compared to a homogenous reaction in solution as a standard.

#	Exposure time / h	Turnover / %
Reference	14	20
1	7	10
2	14	27
	21	38
	28	51
2.1	14	40
2.2	14	23
3	7	7
	14	12

The reference measurement with benzophenone in solution results in a turnover of 20 % after a reaction time of 14 h. Using flow-reactor two, a slightly higher turnover compared to the reference reaction was obtained (27 %). The multiple usage of this reactor resulted in an even higher output after the second cycle (40 %) and again to a similar output in the third one (23 %). However, for flow reactor 3 a turnover of only 12 % was obtained after 14 hours of reaction time.

The turnover of the reactions seems to vary in dependence on the flow reactor used. From these results, a quantitative conversion of all isocyanate groups on the reactor surface with ABP cannot be safely assumed for every performed functionalization reaction (**1** to **3**). Although the isocyanate group is fully reacted according to FT-IR measurements the actual amount of ABP on the reactor surface is difficult to quantify and thus may differ within each tested flow reactor. Later results in the work indicate that side reactions of the aliphatic isocyanate group with moisture from the air before or during functionalization with ABP may occur. Since the reactor covers were not handled under inert conditions, this potentially resulted in a varying degree of functionalization.

The successful multiple use of flow reactor 2 and the turnover achieved, suggest that the ABP is not fully consumed during the reaction. However, more experiments made under more carefully

controlled reaction conditions are needed in order to be able to make an exact and statistically relevant statement. With regard to the reference in solution, it can be stated that in principal, the immobilization of ABP to the reactor surface can achieve comparable turnovers. For better comparison, especially with regard to the effective light concentration, the reference measurement should also be repeated in a non-functionalized flow reactor of the same build.

4.1.4 Summary

A dual-cure hybrid resin was successfully used to print a solvent resistant and surface functionalized flow reactor that was used for the photooxygenation of citronellol, as a proof of concept on a model system.

The versatility of dual-cure hybrid resins to provide pending reactive isocyanate groups that are available for multiple reactions after printing, was demonstrated. That way, it was possible to obtain highly solvent resistant 3D printed objects with complex geometries and locally functionalized catalytically active surfaces from the same base resin by variation of post-printing conditions.

Upon printing of a flow reactor and performing a post-printing functionalization with 4-aminobenzophenone, it was possible to conduct the photooxygenation of citronellol in the flow, while irradiating with UV light through the bottom of the transparent reactor body. Two aspects were considered important for the proof of concept: 1. The flow reactor should withstand the harsh conditions of the photooxygenation reaction of citronellol in aggressive solvent without degradation. 2. The citronellol should be effectively converted into the hydroperoxides by irradiation through a sufficiently transparent reactor wall.

In conclusion, it can be stated that the expectations on the performance of the additively manufactured flow reactor were exceeded. The flow reactor withstood the exposition to deuterated methanol and light of 365 nm for more than 24 hours without degrading. The turnover of citronellol to the corresponding hydroperoxides at this exposure time was similar and in some cases even higher in comparison to the reference measurement, where benzophenone was used as sensitizer in solution.

The use of an isocyanate functional hybrid resin in VPP has enabled a controlled surface functionalization and property modification of a printed object by selected post-printing reactions. This technology has proven to be well suited for producing a complex and demanding flow reactor, for use in surface catalyzed photochemical synthesis applications.

4.2   Toughened Thermosets

Multiphase, heterogenous polymers are the materials of choice when it comes to the toughening of thermosets. Single-phase thermosets are usually in their glassy state at use temperature. As a result, they provide brittle and notch-sensitive materials.[230] One reason to produce multiphase thermosets is to incorporate a low glass transition temperature polymeric phase, as then, a part of the resulting material composition may provide sufficient mobility to absorb energy and allows the cured object to withstand higher impacts without fracturing. To reduce brittleness, many strategies involve the incorporation of a toughener, e.g. by the addition of preformed rubber particles as a separate phase, by the co-polymerization of two or more types of monomers or by the fabrication of interpenetrating and/or phase-separated polymer networks.[154]

In VPP, thermoset materials are formed by an active polymerization of photosensitive resins. To mature the technology from prototyping to the manufacturing of functional parts, the toughening of the resulting material is of high relevance.

To improve the material properties of objects fabricated via VPP, dual-cure resin systems have gained increasing interest. Most frequently, the simultaneous polymerization of acrylates and epoxides has been investigated, as well as the sequential polymerization of acrylates and epoxides.[188,231] The sequential curing of acrylates and isocyanates has solely been employed with hybrid molecules that take part in both curing reactions.[199,200] The sequential curing of acrylates and isocyanates that strictly follows an orthogonal curing mechanism to result in the formation of two distinct polymer phases, has not been presented in literature and will be introduced in the following section.

For this purpose, oligomeric polyurethane acrylates (PUA) are prepared by a synthesis route that allows for the formation of well-defined and low viscous structures. Different oligomeric diols are employed to alter the mechanical properties of the PUA. The novelty of the concept is the dilution of the PUA with low viscous polyisocyanates, instead of using co-reactive monomeric acrylates. The target is to enable a sequential polymerization process, in which the PUA builds a continuous acrylic network during the printing process, in which the isocyanate is entrapped.

Upon a thermal curing step, the isocyanates then react with themselves, building a thermoset based on isocyanurate ring structures. The controlled formation of multiphase heterogenous

networks and in particular the incorporation of a second polyurethane phase, is expected to significantly improve the toughness of the resulting material.

4.2.1 Synthesis, Characterization and Selection of Polyurethane Acrylates

Several polyurethane acrylate prepolymers (PUA) were prepared by a synthetic procedure that allows for a high control of their respective molar mass. Four PUA with polyols differing in structure and molar mass were prepared to alter the mechanical properties of the resulting material. For this purpose, polypropylene glycol (PPG) with 1000 g·mol^{-1} and 2000 g·mol^{-1}, a polycarbonate (PC) with 1000 g·mol^{-1} and a polyether carbonate (PEC) with 1000 g·mol^{-1} were used.

To achieve a high control of the molar mass during the polyaddition reaction, in a first reaction step, isocyanate terminated prepolymers were synthesized by using a diisocyanate in a molar excess of 15 : 1, with respect to the polymeric diol component. As a result, mainly the 2:1 adduct (diisocyanate : polyol) was formed, while the formation of 3:2 and higher adducts was statistically suppressed. The polyols were reacted with the diisocyanate at 100 °C under a nitrogen atmosphere. The excess amount of diisocyanate was removed by distillation using a thin film evaporator, leading to isocyanate terminated difunctional prepolymers. In a subsequent synthesis step, the remaining isocyanate groups of the prepolymers were reacted stoichiometrically with a monofunctional hydroxy acrylate, yielding the corresponding polyurethane acrylates. The progress of the reaction was monitored by titration of the excess isocyanate groups. The synthetic procedure is schematically illustrated in Figure 31, exemplarily with hexamethylene diisocyanate (HDI) as diisocyanate component, polypropylene glycol (PPG) as oligomeric diol and 2-hydroxyethyl methacrylate (HEMA) as capping agent.
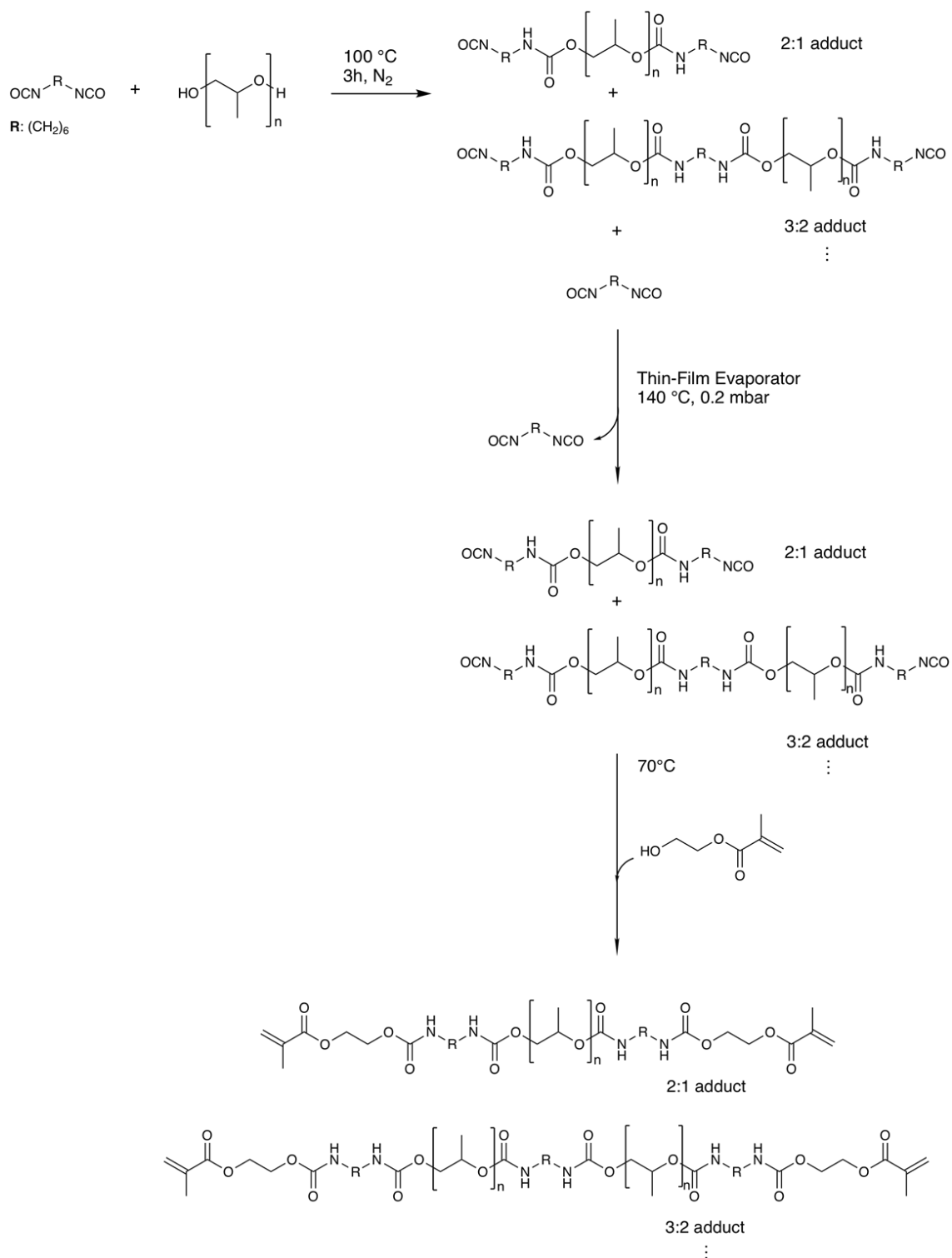
Figure 31. Reaction scheme of the synthesis of polyurethane acrylates. First, the polyol is reacted with a large excess of HDI. To remove the remaining HDI monomer, a thin film evaporator is used. In the last step, the product is reacted with 2-hydroxyethyl methacrylate, yielding the desired polyurethane acrylates.

Using the monomeric diisocyanate in a high excess, increases the probability that the isocyanate selectively reacts with one diol molecule, resulting predominantly in the 2:1 adduct. The distribution of isocyanate terminated prepolymers can be predicted using the Schulz-Flory probability distribution with

$$P_x(NCO) = p^{x-1} \cdot (1-p) \tag{12}$$

The probability P_x *(NCO)* corresponds to the substance quantity of each adduct, *x* is an odd natural number and the probability for a chain growth p corresponds to the ratio between the amount of polyol and isocyanate.[232] In case of using the isocyanate in an excess of 15:1, the resulting distribution of the homologues was calculated. The results are illustrated in Table 4.

Table 4. Predicted distribution of the mass average molar mass of the resulting polyurethane acrylates, using the Schulz-Flory distribution, with a ratio between isocyanate and oligomeric diol of 15:1.

Adduct	P_x (NCO) [%]
2:1	87.85
3:2	10.98
4:3	1.07
5:4	0.09

Based on the calculations, 87.85 % of the 2:1 adduct and only 10.98 % of the 3:2 adduct are expected to be formed during synthesis. The amount of higher homologues can be neglected. Thus, a high degree of control over the molar mass of the resulting structures as well as of the polydispersity can be expected. By controlling the chain length towards short chains, the viscosity of the polyurethane acrylates can be reduced to a minimum.

Table 5 gives the compositions of the four polyurethane acrylates synthesized accordingly. As isocyanate component, hexamethylene diisocyanate was used for all polyurethane acrylates. The polyol component was varied with regard to the molecular structure, as well as the molar mass. All resulting isocyanate prepolymers were end capped with 2- hydroxyethyl methacrylate, yielding the corresponding polyurethane acrylates, further referred to as PUA 1 to PUA 4.

Table 5. Composition of the polyurethane acrylates.

#	Isocyanate	Polyol	Hydroxy acrylate
PUA 1	HDI	PC 1000	HEMA
PUA 2	HDI	PEC 1000	HEMA
PUA 3	HDI	PPG 1000	HEMA
PUA 4	HDI	PPG 2000	HEMA

The resulting methacrylate functional polyurethanes were obtained in the form of clear and viscous resins, except for the polycarbonate containing PUA 1 that crystallized upon cooling. The structures were analyzed by ^{1}H-NMR spectroscopy (see experimental section). The corresponding molar masses as well as the molar mass distributions were determined by gel permeation chromatography (GPC) and were compared to the predicted Schulz-Flory distribution.

The GPC measurements confirmed the control of the molar mass during prepolymer synthesis. The chromatograms are exemplarily given for PUA 4 in Figure 32, including the polyol, the NCO-terminated prepolymer (ISO-Prep.) as well as the final PUA.
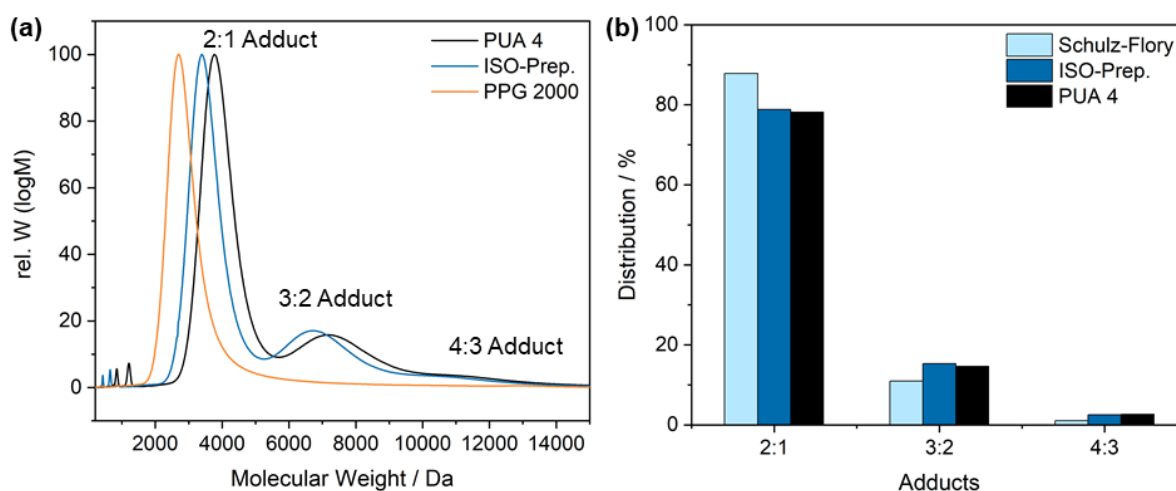
Figure 32. a) Gel permeation chromatography of the polyol, the ISO-prepolymers as well as the resulting PUA. b) The predicted Schulz-Flory distribution in comparison to the experimentally obtained distributions of the ISO prepolymer and the final PUA.

As predicted by the Schulz-Flory distribution, predominantly the 2:1 adduct was formed and only small fractions of higher homologues are present. No significant change in the distribution was observed after end-capping with 2-hydroxyethyl methacrylate.

Owing to the controlled reaction conditions, the resulting molar mass distributions are mainly dependent on the molar mass distributions of the oligomeric diols employed. The measured molar masses M_n as well as the polydispersities $Đ$ of the final PUA's are summarized in Table 6.

Table 6. Molar masses and polydispersities of the polyurethane acrylates, determined by GPC and end-group titration of the isocyanate terminated prepolymer. In the latter, the molar mass of HEMA has been added to obtain the molar mass of the PUA.

#	Polyol	Đ Polyol	$M_{n, GPC}$ [g·mol^{-1}]	Đ PUA	$M_{n, titration}$ [g·mol^{-1}][b)
PUA 1	PC 1000	1.7	2150	1.8	1550
PUA 2	PEC 1000	1.2	2350	1.5	1560
PUA 3	PPG 1000	1.1	2290	1.2	1600
PUA 4	PPG 2000	1.1	3460	1.3	2520

In case of PUA 1 with the PC as diol, a comparably broad distribution of 1.8 was obtained, which can be related to the molar mass distribution of the pure polycarbonate (1.7). For all other PUA's, well defined polymers were obtained with polydispersities below 1.5 and with only a slight increase compared to the corresponding polyols employed. The average molar masses according to the GPC measurements of the three PUA with polymeric diols of 1000 g·mol^{-1} are in a similar range. Next to GPC measurements, the molar masses were determined by end-group analysis of the isocyanate groups before reaction with HEMA. The resulting molar masses are lower compared to the ones determined by GPC, which can be related to the fact that the GPC is a relative analytical method. The values obtained depend on various parameters such as the solubility in the eluent in comparison to the standard styrene polymer, which was used for calibration of the GPC. This is why the numbers obtained by means of end-group analysis were considered to be more appropriate.

The viscosity is an essential parameter for the development of photosensitive resins with application in VPP. Ideally the printing resin should not exceed 5 mPa·s to ensure good printability. This is one of the key hindrances when wanting to incorporate toughness into such formulations, as they in many cases lead to a steep increase in viscosity. By suppressing the evolution of long polymer chains, it was possible to reduce the viscosity of the PUA's to a minimum.

However, the structure and the molar masses of the polyols that were employed, further influenced the viscosity, due to intra- and intermolecular interactions. The change in viscosity

during the synthetic procedure for the different PUA is illustrated in Figure 33. The dotted lines between the data points function as guide to the eye.
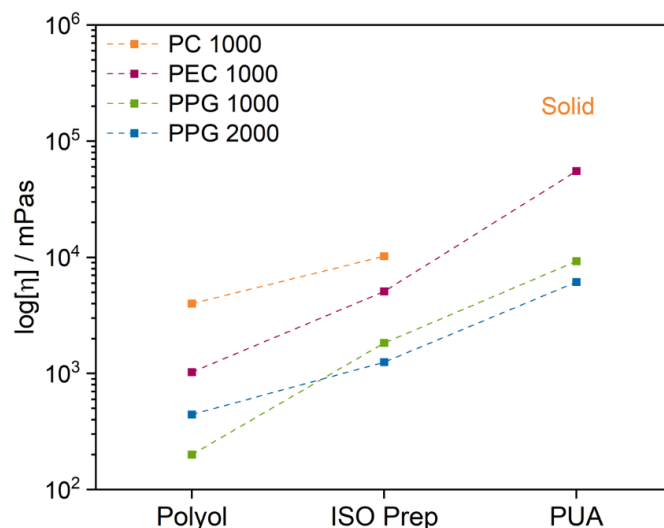
Figure 33. Viscosities of the polyols, the isocyanate terminated prepolymers (ISO Prep) and the corresponding polyurethane acrylate, in dependence on the type of polyol.

The viscosity of the polyols with a constant molar mass of 1000 g·mol^{-1} gradually increases from polyether (200 mPa·s), over polyether carbonate (1030 mPa·s) to polycarbonate (4000 mPa·s). The rigid and polar character of the polycarbonate groups, as well as the stronger intra- and inter-polymer chain interactions lead to the higher viscosities of the polycarbonate and the polyether carbonate in comparison to the pure propylene glycol based polyethers.[233] The viscosity of the polyethers increases with increasing molar mass from 200 mPa·s to 443 mPa·s, respectively.[234]

The urethane groups that were formed upon reaction of the isocyanates with the polyols, result in an increase in the viscosity for all polyurethane acrylates, which can be related to intra and inter-polymer chain interactions such as hydrogen bond formation. An increase in viscosity related to entanglement can be excluded as the prepolymers are well below the critical mass for entanglements.[79] The viscosities of the PPG containing NCO-terminated prepolymers show a reverse effect upon the urethane formation. The PUA with the higher molar mass PPG (2000 g·mol^{-1}) results in a lower viscosity (6130 mPa·s) than the one with the PPG of 1000 g·mol^{-1} (9240 mPa·s).

This effect can be related to the ratio between the amount of flexible polyol and the number of urethane groups. In case of the ISO prepolymer 4, the number of urethane groups, related to the overall molar mass is lower compared to ISO prepolymer 3. Interactions in form of hydrogen

bonding are thus less pronounced. Upon the reaction with HEMA, two additional urethane groups are formed, that in all cases lead to an increase in the viscosity. The polycarbonate containing PUA 1, crystallized upon cooling and is a solid at room temperature.

Next to the material properties in the liquid state, the corresponding mechanical properties of crosslinked PUA's were investigated. The materials themselves possess a viscosity that is too high to allow a direct printing. This is why the properties of the PUA's in the solid state were investigated based on UV cured films. For this purpose, the PUA's were mixed with the photoinitiator 2-hydroxy-2-methylpropiophenone (Omnirad 1173) and films were applied onto a glass substrate, followed by the exposition to UV light using high energy mercury lamps. The PUA's polymerized upon light exposure and formed transparent polymer networks.

The mechanical properties were determined by dynamic mechanical analysis (DMA) as well as tensile tests, illustrated in Figure 34 and Table 7.
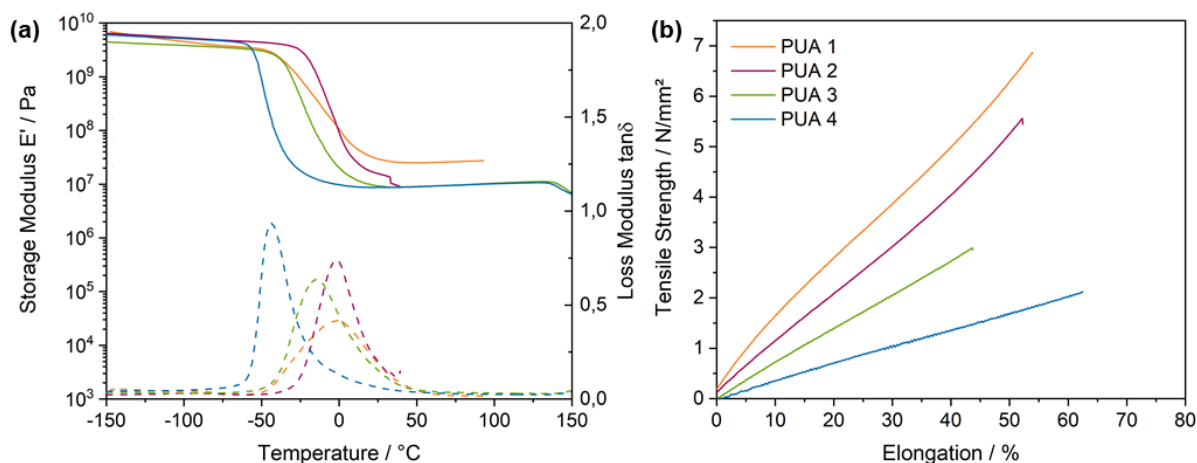
Figure 34. a) Dynamic mechanical analysis and b) Tensile tests of UV cured polyurethane acrylates containing different polymeric diols.

All PUA networks have a glass transition temperature below 0 °C, as determined by the peak maximum of the loss factor in the DMA curves.

The PUA based on the PPG with 2000 g·mol^{-1} has the lowest T_g of -43 °C which is related to the high amount of flexible PPG segments in the polymer backbone. The PPG based PUA, with 1000 g·mol^{-1} has a T_g of -15°C, while the polycarbonate and polyether carbonate based PUA's have a T_g of -2 and -0.5 °C, respectively.

The tensile tests show the quasi-static mechanical behavior of the networks at room temperature. Herein, the tensile strength as well as the Young's modulus increase with increasing amount of polycarbonate in the backbone, while the elongation at break almost stays constant for all materials, indicating the influence of a similar crosslinking density. The PUA with the 2000 g·mol^{-1} PPG is even softer compared to the PUA with the 1000 g·mol^{-1} PPG. The area under the tensile curve corresponds to the absorbed energy per volume until breaking occurs. Thus, both carbonate containing PUA's have an improved capability of absorbing energy in comparison to the PPG containing PUA. This can be related to inter- and intra-polymer chain interactions of the carbonate group and also reflects the form and position of the loss factor curve.

Table 7. Young's modulus (E_{mod}), tensile strength (σ), elongation at break (ε) and glass transition temperature (T_g) of the PUA networks measured by tensile testing and dynamic mechanical analysis (numbers in brackets give the standard deviation, 5 samples were measured per entry).

#	E_{mod} [Nmm^{-2}]	σ_b [Nmm^{-2}]	ε_b [%]	T_g [°C]
PUA 1	14.8	6.9	53.9	-0.5
	(2.0)	(0.7)	(5.9)	
PUA 2	9.3	5.6	52.3	-2
	(1.8)	(0.8)	(6.7)	
PUA 3	n.d.	2.9	43.7	-15
		(0.9)	(10.2)	
PUA 4	n.d.	2.1	62.5	-43
		(0.6)	(18.7)	

Although the PUA's that contain polycarbonate in the backbone give better mechanical properties compared to the PPG containing PUA's, the latter are better suited in terms of processibility in VPP. Especially the PUA containing the PPG with 2000 g·mol^{-1} is attractive, as only a little amount of reactive diluent is needed to achieve appropriate printing viscosities. This is why further investigations were performed with PUA 4.

4.2.2 Characterization and Selection of Polyisocyanates

The second key part of the new dual-cure concept, besides identifying a flexible PUA, is to identify a low viscous polyisocyanate that is suited to dilute PUA 4 to appropriate printing viscosities, while being able to polymerize via a thermally induced reaction of the isocyanate group to form a thermoset based on isocyanurate ring structures. That way highly crosslinked, transparent, as well as chemical and temperature resistant networks can be formed. In the printing formulation, they are intended to build-up a second polymeric phase with a high glass transition temperature, featuring as a well-distributed hard filler to reinforce the continuous acrylic thermoset phase. The

miscibility of the polyurethane acrylate and the polyisocyanate should be high to form homogenous mixtures.

Figure 35 gives the idealized structures of four commercially available low viscous polyisocyanates, that were considered as appropriate diluents for PUA 4.

Figure 35. Molecular structures of commercially available HDI-based polyisocyanates.

All four substances that are commercially available in a technical grade, show a structure based on hexamethylene diisocyanate with different functional groups (allophanate, asymmetric trimer, uretdione and biuret). The viscosities as well as the isocyanate contents of the polyisocyanates under evaluation are illustrated in Table 8. The uretdione has the lowest viscosity of 150 mPa·s and is therefore best suited as a diluent. The allophanate as well as the asymmetric trimer, with viscosities of 500 mPa·s and 730 mPa·s, respectively, are also suitable to dilute the PUA 4 to appropriate printing conditions, while the biuret structure with 2500 mPa·s is borderline to achieving the desired printing viscosities below 5000 mPa·s.

Technical products of the allophanate-, the uretdione- as well as the biuret structure are mixtures of higher homologues comprising other polyisocyanates, such as the polyisocyanurate, with the presented structures being the main component. However, this means that they are not strictly difunctional, but possess an isocyanate functionality between 2.5 and 3. The functionality of the polyisocyanates directly influences the crosslinking density of the thermoset that forms upon the thermal reaction of the isocyanate groups and is thus of relevance for the material properties of the final polymer network.

Table 8. Viscosity and isocyanate content of commercially available HDI-based polyisocyanates.

HDI based polyisocyanate	Viscosity [mPa·s]	Isocyanate Content [%]	Functionality
Uretdione	150	21.8	2.5
Allophanate	500	20	2.5
asym. Isocyanurate	730	23.5	3
Biuret	2500	23	2.5

PUA 4, with a viscosity of 6130 mPa·s was mixed with the corresponding polyisocyanates in a 1:1 weight ratio and the resulting viscosities were measured. A weight ratio between the two components of 1:1 was chosen, to allow the acrylic phase to remain the continuous phase in order to obtain a stable acrylic scaffold during the printing process. As expected, the mixture with the uretdione results in the lowest formulation viscosity of 2100 mPa·s (F1), followed by the allophanate containing mixture with 2990 mPa·s (F2). The asymmetrical trimer and biuret containing mixtures result in viscosities of 3780 mPa·s (F3) and 7560 mPa·s (F4), respectively. Homogenous mixtures were obtained for the allophanate and the uretdione, indicating a good miscibility of the ingredients. In contrast to that, the mixtures containing the asymmetrical isocyanurate as well as the biuret structures turned opaque, indicating heterogeneity of the composites. Thus, in terms of processibility as well as homogeneity, the uretdione and the allophanate are appropriate as diluents for the polyurethane acrylate. However, with regards to safe operations, the use of an uretdione-based polyisocyanate as a reactive diluent can be problematic. Apart from the trimerization reaction of free isocyanate groups, the uretdione functional group can also cleave upon temperature exposure during the post-curing step, potentially releasing some volatile hexamethylene diisocyanate monomer. As the allophanate is more stable at higher temperatures and further shows good compatibility with the acrylic prepolymer, it was chosen as the preferred diluent for the following discussed dual-cure resin formulations.

4.2.3 Screening of Dual-Cure Isocyanate-Acrylate Resins

For the preparation of combinatorial networks, a photoinitiator is needed to trigger the photopolymerization reaction of the PUA, while a catalyst is needed to initiate the trimerization reaction of the isocyanate groups. As photoinitiator, 2-hydroxy-2-methyl-1-phenylpropanone (Omnirad 1173) with an absorption maximum of about 250 nm was chosen, corresponding to the emission spectrum of the mercury lamps that were used as light source to trigger the

polymerization. A concentration of 3 wt% related to the amount of acrylate in the system was used, in order to guarantee a full conversion of the acrylate groups. Tin(II) ethylhexanoate was chosen as trimerization catalyst, with a concentration of 0.75 wt% with regard to the amount of isocyanate, according to literature.[121]

To prepare the resin formulations, PUA 4, allophanate, photoinitiator and catalyst were thoroughly mixed using a speedmixer. Different PUA 4 and allophanate weight ratios were applied, as given in Table 9, which are further referred to as blends 1 to 4.

The pure polyurethane acrylate plus photoinitiator (Ref.2), as well as the pure allophanate plus catalyst (Ref. 1) function as reference materials. The different formulations with the corresponding viscosities are given in Table 9.

Table 9. Ratios of PUA to polyisocyanate and the resulting viscosities.

#	PUA 4 [wt%]	Allophanate [wt%]	Viscosity [mPa·s]
Ref. 1	0	100	500
Blend 1	33.3	66.7	2043
Blend 2	50	50	2988
Blend 3	60	40	4080
Blend 4	66.7	33.3	4822
Ref. 2	100	0	6779

In all cases, homogenous and clear mixtures were obtained, indicating a good miscibility of the two components. The viscosity of the formulations increases linearly with decreasing amount of allophanate.

In a subsequent step, the blends were cured using a standard UV curing coating process. The production of films in a UV curing coating line helps to efficiently screen the application and to investigate the curing properties of the formulations while trying to emulate the printing process as well as possible, considering the viscosity restrictions, as well as the post-curing conditions concerning temperature and the presence of air.

For this purpose, 400 μm films of the corresponding formulated blends were applied onto glass substrates and were exposed to mercury lamps. Subsequently, the films were placed into the oven at 100 °C for 17 hours, to ensure full conversion of the isocyanates. Ref. 2 was prepared in a similar way, but was only exposed to UV light. For Ref. 1, it was not possible to obtain a film by simply

placing a mixture of the allophanate with the catalyst into the oven. The isocyanate reacted with air humidity, resulting in a foaming of the material, due to the evolution of carbon dioxide. Therefore, reference 1 was prepared by placing the catalyst containing allophanate between two glass plates. That way, the trimerization reaction of the isocyanate groups was allowed to take place under the exclusion of humidity.

Interestingly, the heat induced reaction of the isocyanates in blends 1 to 4 did not result in a foaming of the material. The preceding photopolymerization seems to provide a good stabilization for the subsequent reaction of the polyisocyanates and hinders the formation of blisters.

As the sequential polymerization of formulation 1 to 4 results in the formation of combined networks, they are further referred to as Combined Networks 1 to 4 (CN 1 to 4), indicating the polymerized state of the samples.

After the UV curing process, a polymerization induced phase separation was observed for all samples, except for the reference materials. The polymerization of the polyurethane acrylate leads to an increase in viscosity, which is why it is reasonable to assume that the liquid isocyanate turned incompatible in the crosslinked PUA network. The miscibility of the isocyanate might thus be significantly reduced in comparison to the non-crosslinked PUA. The phase separation after the first polymerization reaction can be followed by transmission measurements, as illustrated in Figure 36. With an increasing amount of isocyanate, the transmission of light of the resulting first networks decreases in comparison to the clear reference samples, indicating a higher phase separation and/or the formation of larger domains.

After the second thermal curing, the turbidity remained high, indicating that stable phase-separated networks were formed upon the sequential polymerization process. Figure 36 shows images of the fully cured combined networks, layered as 10 mm squares on a black background with the letters '3D-PRINTING' to provide a guide to the eye. It can be seen, that with increasing amount of isocyanate, the turbidity of the samples increases.
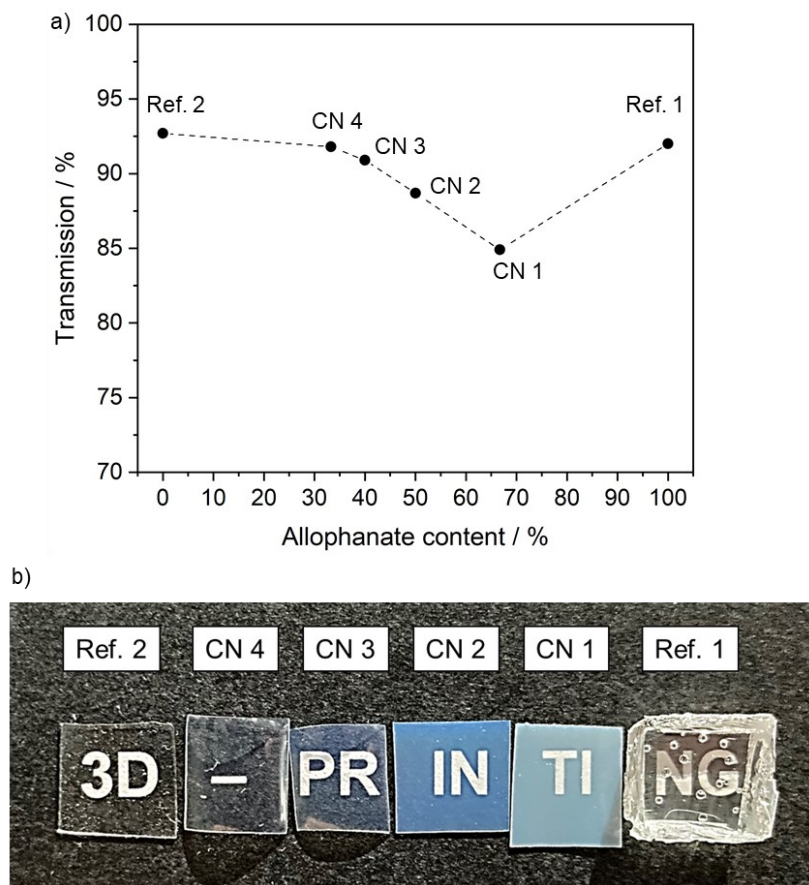
Figure 36. a) Transmission measurement after the first polymerization reaction (UV curing) b) Images of the combined networks after the two-step sequential polymerization process.

It seems that in case of the PUA network being the matrix with only a low volume of the polyisocyanurate network present, the transmission of the samples is still high, while in case of the isocyanurate network being the matrix in the presence of only a low volume of the polyurethane acrylate, the transmission decreases. This leads to the assumption that the polyisocyanurate has a higher compatibility with the crosslinked PUA matrix and forms a separated phase of smaller domain size than a PUA network formed inside a polyisocyanurate matrix. AFM and DMA measurements were performed to further prove this hypothesis.

4.2.3.1 Structural Characterization

Both polymerization reactions were monitored by ATR-FT-IR spectroscopy, with special focus on the second, heat-induced reaction of the isocyanate groups. The second reaction can be easily followed by the isolated isocyanate stretching vibration at 2265 cm^{-1}, as illustrated in Figure 37, exemplarily for sample CN 2.

The full disappearance of the isocyanate absorption peak indicates that the reaction is quantitative. The control of the residual isocyanate peak by FT-IR measurements was further used to optimize the post-processing conditions by variation of reaction time and temperature.
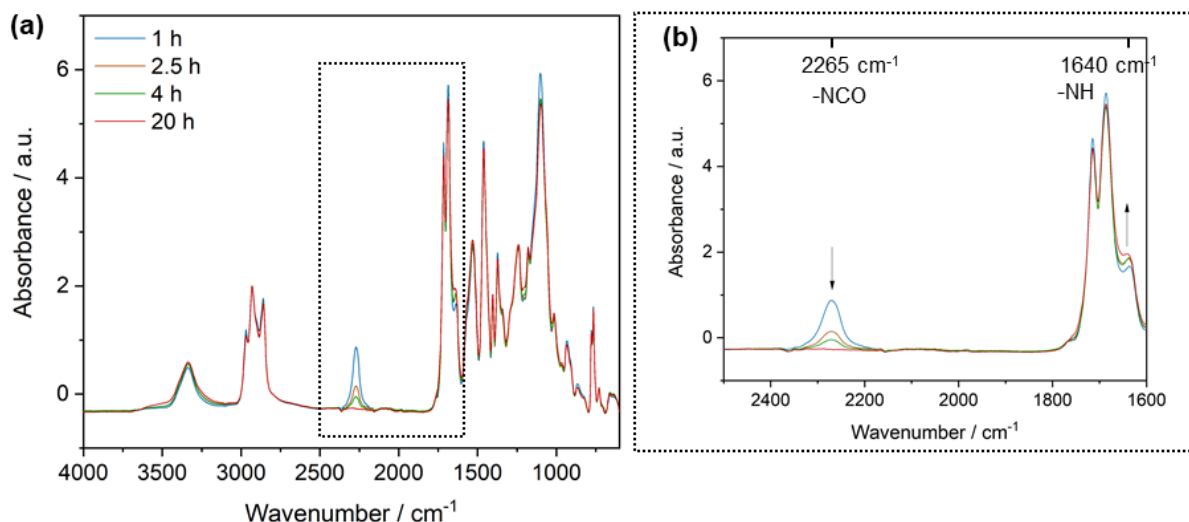

Figure 37. FT-IR spectra following the second heat-induced polymerization reaction of the isocyanate groups of the sample CN 2 after UV polymerization and curing at 100 °C in dependence of the curing time.

The spectrum shows a gradual decrease of the stretching vibration of the isocyanate groups with time. After 20 h of heat treatment, the peak is not detectable anymore, indicating a full conversion of the isocyanate groups. At the same time, an increase of the absorption peak at 1640 cm^{-1} is observed, which can be attributed to the N-H-deformation vibration of the urethane group. The carbonyl stretching vibration of the isocyanurate ring at 1690 cm^{-1}, however, does not significantly increase as would have been expected in case of a trimerization as the targeted crosslinking reaction. The evolution of the absorption peak at 1640 cm^{-1} indicates that urea has been predominantly formed instead of the isocyanurate ring structure. As no isocyanate reactive components have been added and no water was present in the reaction mixture, the urea formation might be related to the reaction of the isocyanate groups with humidity from the air. This further implies that the selectivity of the selected tin(II)ethylhexanoate for the trimerization reaction in presence of non-treated air, is not high enough towards the intended isocyanurate formation. The reaction of isocyanate groups with water usually goes in hand with the formation of blisters, due to CO_2 formation. Surprisingly, no blister formation was observed during and after the second polymerization reaction and homogenous films were obtained.

The polyurea formation requires the reaction of an isocyanate group with water, generating a free amine as well as CO_2. The free primary amine then directly reacts with another free isocyanate group, forming a linear linkage between the isocyanate molecules. The main difference to the polyisocyanurate is that two isocyanates react with each other, forming a linear linkage, while an isocyanurate formation affords the reaction of three isocyanates, leading to a crosslinking point. In terms of thermomechanical properties, a polyurea thus behaves differently compared to a polyisocyanurate network. Next to a lower crosslinking density, a lower glass transition temperature of the material may be expected. Since the isocyanate functionality of the employed allophanate is larger than 2, still a crosslinked network will be formed upon urea formation, also due to strong hydrogen interaction between the urea groups. In order to get a detailed understanding of the resulting networks, the thermomechanical properties were investigated by DMA measurements.

4.2.3.2 Thermomechanical Properties

The thermomechanical properties of CN 1 to 4, as well as of the two reference samples were measured using dynamic mechanical analysis. Figure 38 illustrates the results of the DMA measurements, providing a) the storage modulus, b) the loss modulus and c) the loss factor in dependence on the temperature. In d) the minimum of $tan\delta$ between the two glass transition temperatures is observed in dependence on the allophanate content.
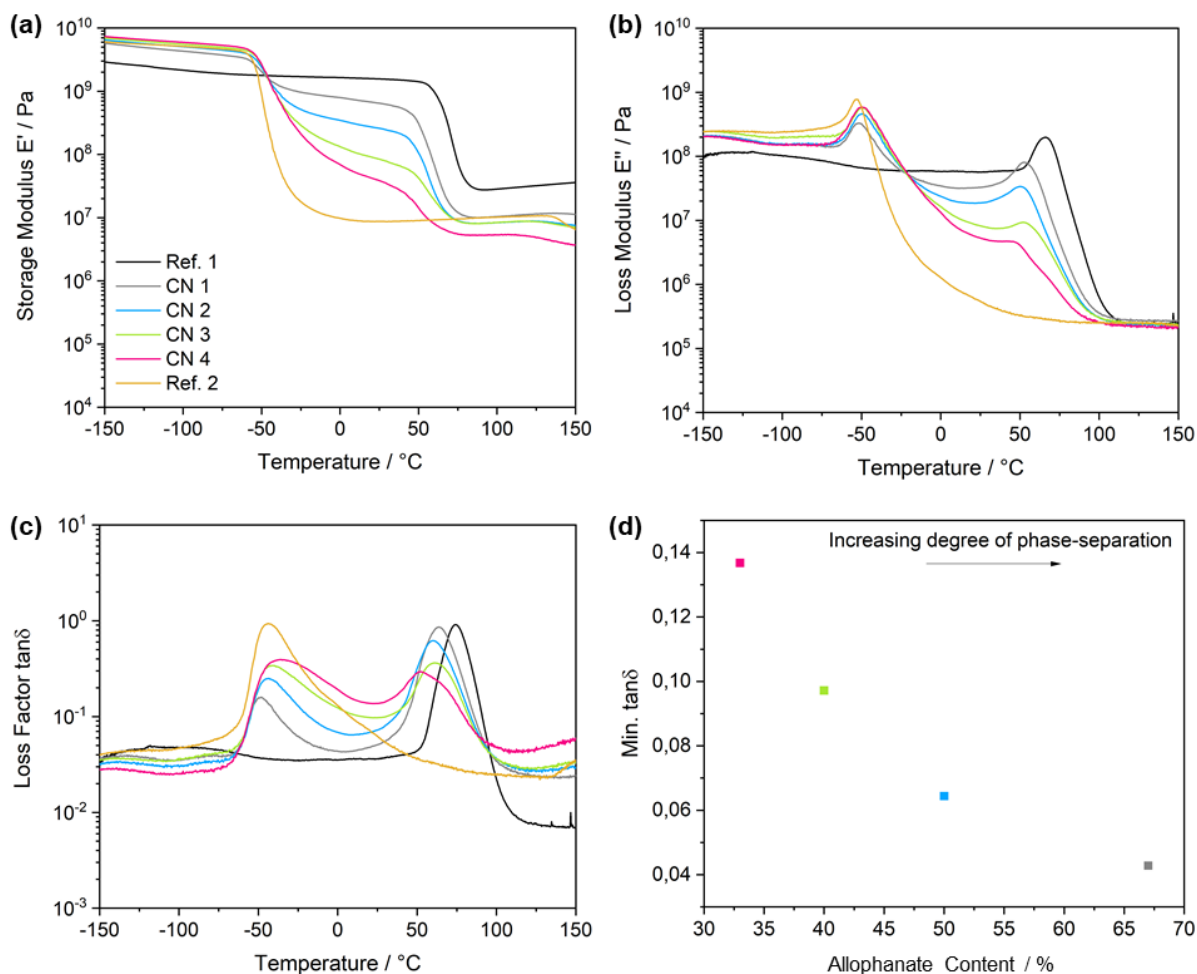
Figure 38. Dynamic mechanical analysis of combined networks 1 to 4, as well as the corresponding references giving a) the storage modulus b) the loss modulus and c) the loss factor in dependence on the temperature. d) illustrates the minimum *tanδ* between the two glass transition temperature in dependence on the isocyanate content.

For reference 2, the storage modulus rapidly decreases at about -43 °C from about $5.5 \cdot 10^9$ Pa to $9 \cdot 10^6$ Pa, entering a plateau modulus at higher temperatures. Reference 1 has a high modulus of $2.5 \cdot 10^9$ Pa until the modulus rapidly decreases at about 74 °C, resulting in a plateau modulus of $3 \cdot 10^7$ Pa, which is three times higher compared to the acrylic network. The maximum of the loss factor curve represents the glass transition temperature of the material, that is -43 °C for the PUA network and 74 °C for the isocyanurate network, respectively. This means that the polyurethane acrylate network represents a soft material with a glass transition temperature below room temperature, while the isocyanate based network provides a hard and highly crosslinked material with a glass transition temperature above room temperature.

Upon combination of the two liquid precursors in varying weight ratios, the resulting cured networks CN 1 to 4 possess two well separated glass transition temperatures. This is indicated by

two distinct changes in the storage and loss modulus in dependence on the temperature, as well as in the two maxima of the loss factor curve. Herein, the transition at low temperature corresponds to the soft polyurethane acrylate network while the one at higher temperatures corresponds to the isocyanate based urea/isocyanurate network, which is mainly based on a polyurea in case of CN 1 to 4 and polyisocyanurate based in case of reference 1.

In all cases where two distinct glass transition temperatures can be observed, phase-separated networks have formed. Between these two transitions, the storage modulus stays almost constant for CN 1 and CN 2 and the loss factor is low (< 0.1), providing energy elastic behavior. This is advantageous when it comes to technical applications where the mechanical properties are required to stay constant within a broad temperature range, as for example in dynamic applications like a shoe sole and static applications like in seals. In VPP to date, soft materials with a constant plateau modulus and good physical properties are difficult to access. Usually, the solution for a so-called 'four-season material' is a broad glass transition temperature around room temperature, thus providing toughness over a large temperature range, but at the same time significantly changing the modulus over use temperature.

For CN 3 and CN 4, the storage modulus gradually decreases between the two glass transition temperatures, and no stable plateau modulus is obtained, indicating that the phases are not perfectly separated, but may interpenetrate on a molecular scale. This is further illustrated by the loss factor curve, that does not decrease to comparably low values between the two glass transition temperatures as in CN 1 and CN 2. This means that in this temperature region, more energy is absorbed under a forced strain and the material properties are more viscoelastic.

The first glass transition temperature of all combined networks is in the same order of magnitude like the reference 2 sample at -43 °C. Deviations can be explained by measurement errors and might be related to a partial interpenetration of the two polymeric phases. In contrast to that, the second glass transition temperatures of CN 1 to CN 4, are shifted to lower temperatures by about 10 °C for CN 1 to CN 3 and by even 20 °C for CN 4, compared to the isocyanurate network of reference 1. This can be related to a lower network density of the second polymeric phase due to more urea instead of isocyanurate formation, to an increased mixing of the two polymer networks or to smaller domain sizes of the isocyanate based network and thus to higher homogeneity.

As already figured out in the structural characterization of the combined networks, a different network builds up in case urea bonds are preferentially formed instead of urethanes. It seems reasonable to assume that a polyisocyanurate network was formed in reference 1, which was

prepared under the exclusion of moisture and air, while in case of the combined networks, a polyurea network was formed, as the reaction was conducted under air. The shift in the glass transition temperature is likely related to the fact that the urea network has a glass transition temperature at about 60 °C, which is proven below. Additionally, the T_g shift can be explained by a partial interpenetration of the networks, especially for sample CN 4. Besides the larger shift to lower temperatures, a less steep slope of the storage modulus of the second transition implies a better mixing of the two phases.

In order to get a deeper understanding of the structure of the second network, a third reference material in form of a polyurea network was prepared. For this purpose, the allophanate based isocyanate was reacted with a stoichiometric amount of water in such a way that the free amines, generated upon the isocyanate-water reaction, have another available isocyanate group to form an urea linkage. FT-IR spectroscopy and DMA measurements were performed and compared to the combined networks (exemplarily to sample CN 2), as well as to reference 1. The results are illustrated in Figure 39.
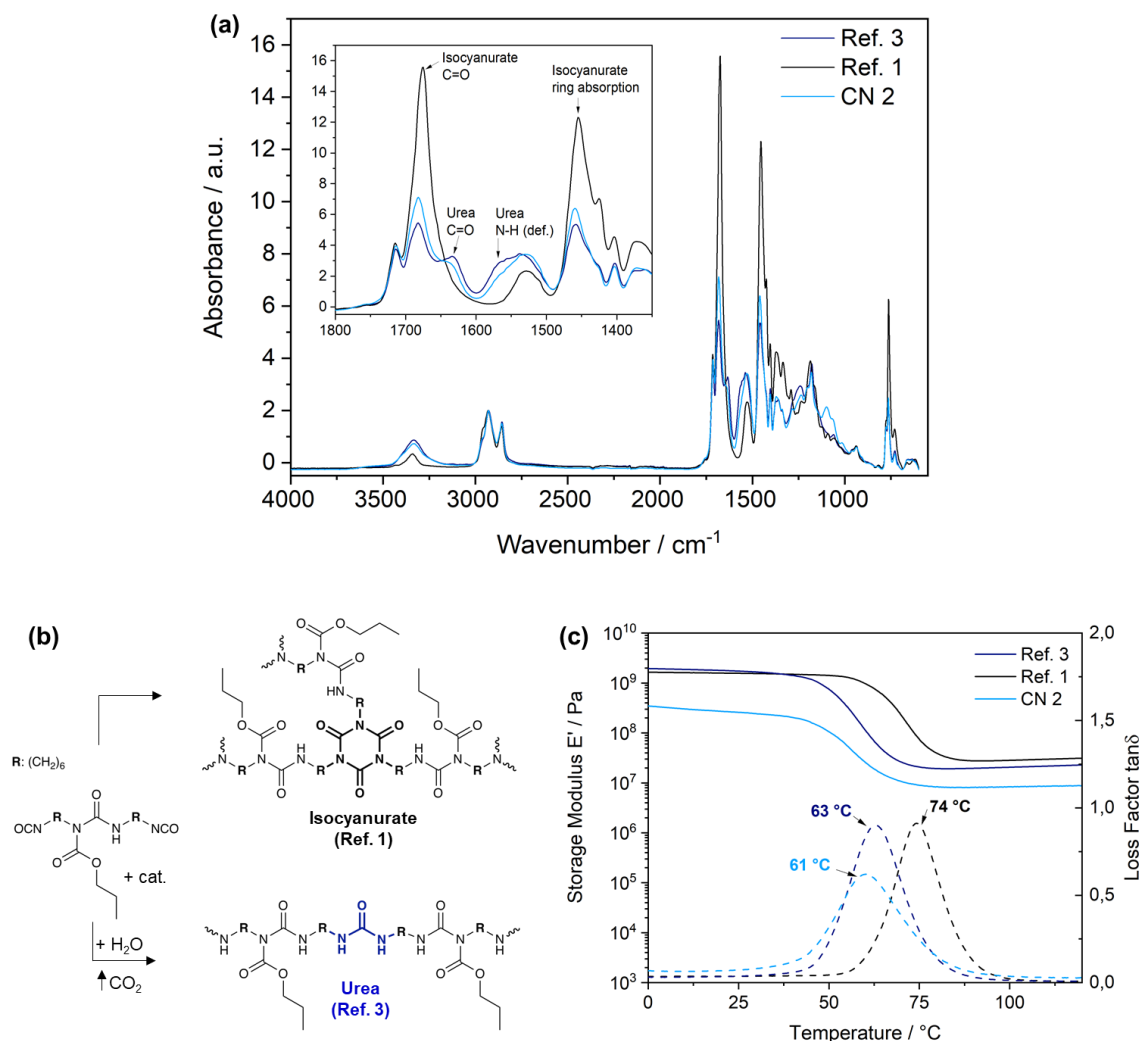
Figure 39. a) FT-IR spectra of the polyisocyanurate, the polyurea and the combined network. b) Structures of the polyurea and polyisocyanurate network. c) dynamic mechanical analysis of the polyisocyanurate, the polyurea and the combined network.

The FT-IR spectra were used for a qualitative analysis of the different network structures. The results reveal (Figure 39 a), that for the polyisocyanurate network (Ref. 1) the characteristic absorption band of the carbonyl stretching vibration at 1675 cm⁻¹ is observed, as well as the ring absorption band at 1450 cm⁻¹. For the urea network (Ref. 3), at 1630 cm⁻¹ as well as at 1560 cm⁻¹ the typical absorption bands of the carbonyl stretching vibration as well as the N-H deformation vibration, respectively, are noticed. Comparing the reference spectra with the spectrum of sample CN 2, it can be seen that the formation of the second network is more likely to correspond to a polyurea network.

The characteristic urea absorption bands evolve at 1630 cm⁻¹ and 1560 cm⁻¹. However, it cannot be excluded that a certain amount of polyisocyanurate network structure was formed as well.

81

The formation of the two network structures is illustrated in Figure 39 b). In case of a polyisocyanurate formation, the isocyanate groups of three allophanate based polyisocyanates react with each other to form the trimer ring, ultimately leading to a densely crosslinked network. In contrast to that the urea network is formed upon reaction of an isocyanate group with water, leading to a primary amine by separation of CO_2. The primary amine then directly reacts with another isocyanate group of the allophanate based polyisocyanate to build an urea. As the technical grade of the allophanate was used with a functionality of 2.5, also in the case of a polyurea formation, a crosslinked network evolves.

The DMA measurements further reveal that crosslinked network structures have been build up for Ref. 1 and Ref. 3. As expected, the crosslinking density of the urea network (Ref. 3) is lower compared to the polyisocyanurate network (Ref. 1). The glass transition temperature of the polyisocyanurate network is at 74 °C, while the urea network has a T_g at 63 °C. The second glass transition of sample CN 2 is at 61 °C. Thus, also with regards to the thermomechanical properties, the network structure that evolves during the second polymerization reaction is more likely corresponding to a polyurea network.

In order to evaluate whether the two phases are interpenetrating on a molecular scale or whether the phases are clearly separated, a model was used to calculate the dynamic mechanical analysis data of the combined networks CN 1 to CN 4.

Calculations were performed that predict the morphology evolution, based on the material properties of the neat polymer phases that are combined. To differentiate between dispersed and co-continuous structures at similar compositions, dynamic mechanical analysis can be a useful method. In case of dual phase continuity, both phases contribute equally to the storage modulus in dependence on the temperature, whereas in dispersed structures, the overall modulus is dominated by the matrix component.[175]

In literature, different models have been developed to calculate the modulus-temperature dependence of polymer blends, taking into account co-continuous as well as matrix-dispersed particle morphologies, where the phases are completely separated. Takayanagi and co-workers developed a model method to interpret the viscoelastic properties of polymer blends for matrix-dispersed particle morphologies.[235] Their work is based on Kerner's equation in which the modulus of the two phase system is related to the elastic constants of the continuous and dispersed phase.[236] The model is based on the assumption that the dispersed phase is in the shape

of spherical particles and the two phases perfectly adhere to each other.[236] Figure 40a illustrates the qualitative behavior of a two phase material for spheres in a continuous matrix.[175]
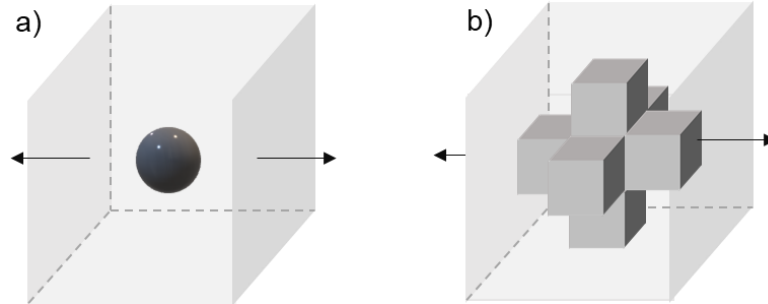

Figure 40. Qualitative behavior of a two phase material. Micromechanical model for a) spheres in continuous matrix and b) dual-phase continuity (co-continuity). Figure inspired by Ref. [237] and [235].

In case that the dispersed particles are spheres and assuming that each phase has the modulus of the neat material (neglection of interphase), the following equation can be applied to predict the modulus of the resulting composite

$$\frac{1}{E} = \frac{1 - \sqrt[3]{v_2}}{E_2} + \frac{\sqrt[3]{v_2}}{E_2 v_2^{\frac{2}{3}} + E_1(1 - v_2^{\frac{2}{3}})},$$

(13)

with E_1 and E_2 being the moduli of the matrix and filler phase, respectively, v_2 being the volume fraction of the filler particles and E being the effective modulus of the composite material.[235,236]

For co-continuous blends, a different model is needed, as the interconnectivity between the two phases is not incorporated in the matrix-dispersed particle approach. Veenstra and co-workers have developed a model that describes the case for dual-phase continuity, that is comparable to the COS (Cross Orthogonal Skeleton) model proposed by Kolarik.[237,238] Instead of spheres embedded in a matrix, three orthogonal bars of component 1 in a unit cube, where the remaining volume is occupied by component 2, are used to describe the co-continuity, as schematically illustrated in Figure 40 b.

As co-continuity is not necessarily limited to an equal volume fraction of the two components, Veenstra extended the COS model, taking into account the different influences of a weak and a stiff

component on the modulus of the composite. Next to the parallel model of serial-linked parts they introduced a series model of parallel linked parts, resulting in the following equations for the determination of the modulus

$$E_a = \frac{(a^4 + 2a^3b) \cdot E_1^2 + 2 \cdot (a^3b + 3a^2b^2 + ab^3) \cdot E_1E_2 + (2ab^3 + b^4) \cdot E_2^2}{(a^3 + a^2b + 2ab^2) \cdot E_1 + (2a^2b + ab^2 + b^3) \cdot E_2} \quad (14)$$

$$E_b = \frac{a^2bE_1^2 + (a^3 + 2ab + b^3) \cdot E_1E_2 + ab^2E_2^2}{bE_1 + aE_2} \quad (15)$$

with $v_s = 3a^2 - 2a^3$ and $b = 1 - a$, where a relates to the volume fraction of the soft phase. E_a applies for the case that the stiff component dominates (volume fractions between 50-100 %) and E_b for the case that the stiff component is the minor phase (0-50 %).[237] In case of an equal volume fraction of the two phases, an average value of E_a and E_b can be used to calculate the effective modulus of the blend, with E_1 and E_2 being the moduli of the neat polymer networks.

These models can be useful for the prediction of the mechanical properties of two-phase systems. To predict the mechanical properties of the combined networks shown earlier, the storage modulus of the neat PUA network as well as of the neat polyurea network were used as basis. The polyurea network was chosen as reference, as it has previously shown that the polyurea formation is the predominant reaction mechanism of the second curing reaction instead of the intended polyisocyanurate formation. The storage modulus in dependence on the temperature of both reference measurements is illustrated in Figure 41.
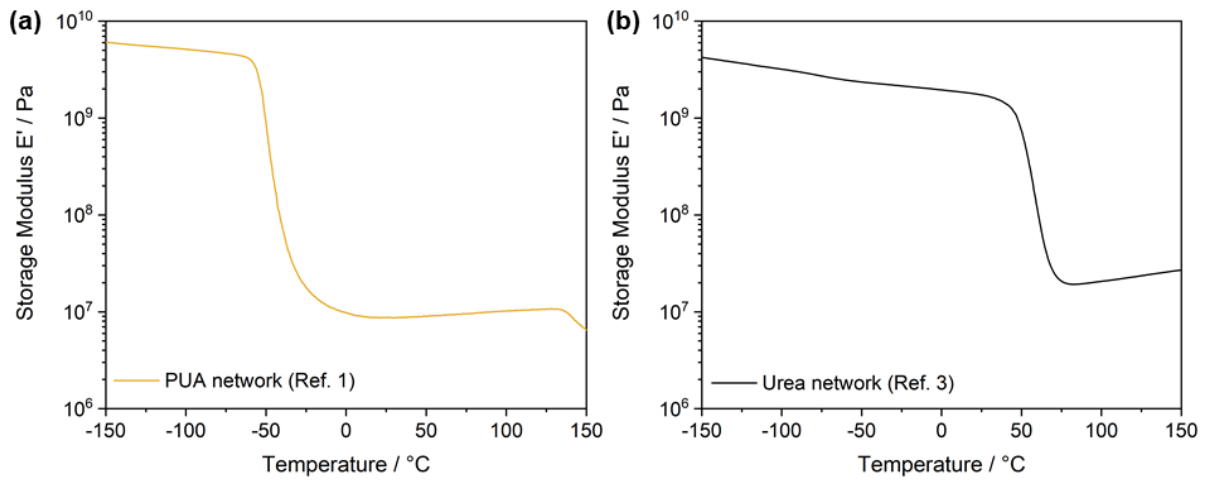
Figure 41. Experimental DMA measurements giving the storage modulus in dependence on the temperature of the PUA network (a) as well as of the polyurea network (b).

The storage moduli E' in dependence on the temperature were used to calculate the moduli of the combined networks. Depending on the volume fractions of polyurethane acrylate and polyurea, the two references were either assumed to be the matrix phase, corresponding to E_1 or the dispersed phase, corresponding to E_2 in the equation presented previously; a was chosen accordingly.

For CN 1, the polyurea is assumed to be the continuous phase and the matrix-dispersed model was applied. For CN 2, it is likely that dual-phase continuity prevails, which is why the co-continuous model was chosen to fit the data. For CN 3 and CN 4, the polyurethane acrylate was assumed to be the continuous phase and again the matrix dispersed model was applied for the calculations. The results of the fits are illustrated in Figure 42, in conjunction with the data determined experimentally.
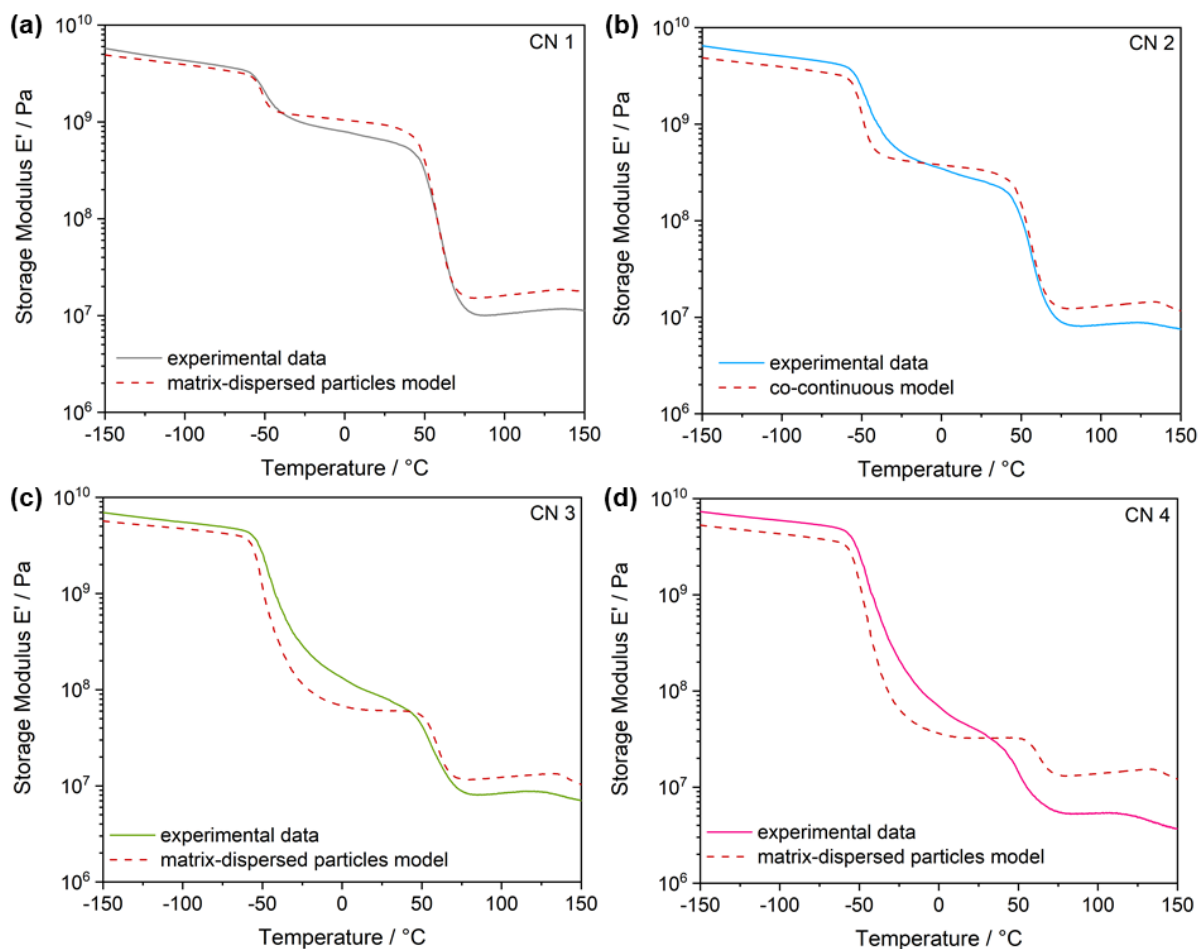
Figure 42. Experimental DMA measurements and calculated values giving the storage modulus in dependence on the temperature of samples a) CN 1, b) CN 2, c) CN 3 and d) CN 4.

For CN 1, the model represents a good fit for the combined network. The plateau modulus between the two glass transition temperatures is only a little shifted towards lower moduli for the experimental data, indicating a good fit of the model. The results for CN 2 illustrate that the co-continuous model is well suited to fit the data. However, it can be seen, that the storage modulus between the two glass transition temperatures continuously decreases in case of the experimental data, indicating that the phases are not fully separated but may interpenetrate on a molecular scale. As the model assumes that the phases are completely separated, deviations from this behavior can be related to an interpenetration of the two polymeric phases.

This interpenetration becomes even more pronounced for CN 3 and CN 4, where the experimentally determined storage modulus gradually decreases and no plateau modulus is obtained between the two glass transition temperatures. The experimental data deviate from the theoretical fits, which leads to the conclusion that the phases are not fully separated.

In all cases, the storage modulus in the rubbery plateau is much lower for the theoretical calculations compared to the experimentally determined values. As the storage modulus in the rubbery plateau can be regarded as a measure of the crosslink density, it might be the case that the two phases do not perfectly adhere to each other, which is one of the main assumptions of the model that was applied.

In conclusion it can be stated that based on the calculations it is likely that for CN 1, polyurethane acrylate particles are dispersed in a continuous polyurea matrix, while in the case of CN 2, both phases are likely to be equally distributed leading to dual-phase continuity. For CN 3 and CN 4, it is assumed, that the miscibility of the two polymer networks is higher compared to CN 1. This is why it is concluded that the domain sizes of the two phases is smaller, resulting in an inward shift of the two glass transition temperatures. To further support these assumptions, the morphology of Ref. 1 and 3, as well as of the four combined networks was investigated by AFM measurements.

4.2.3.3 Morphology

AFM measurements were performed to further investigate the morphology of the combined networks that can be correlated to the results obtained by the theoretical calculations of the storage modulus. The topographic images are illustrated in Figure 43.
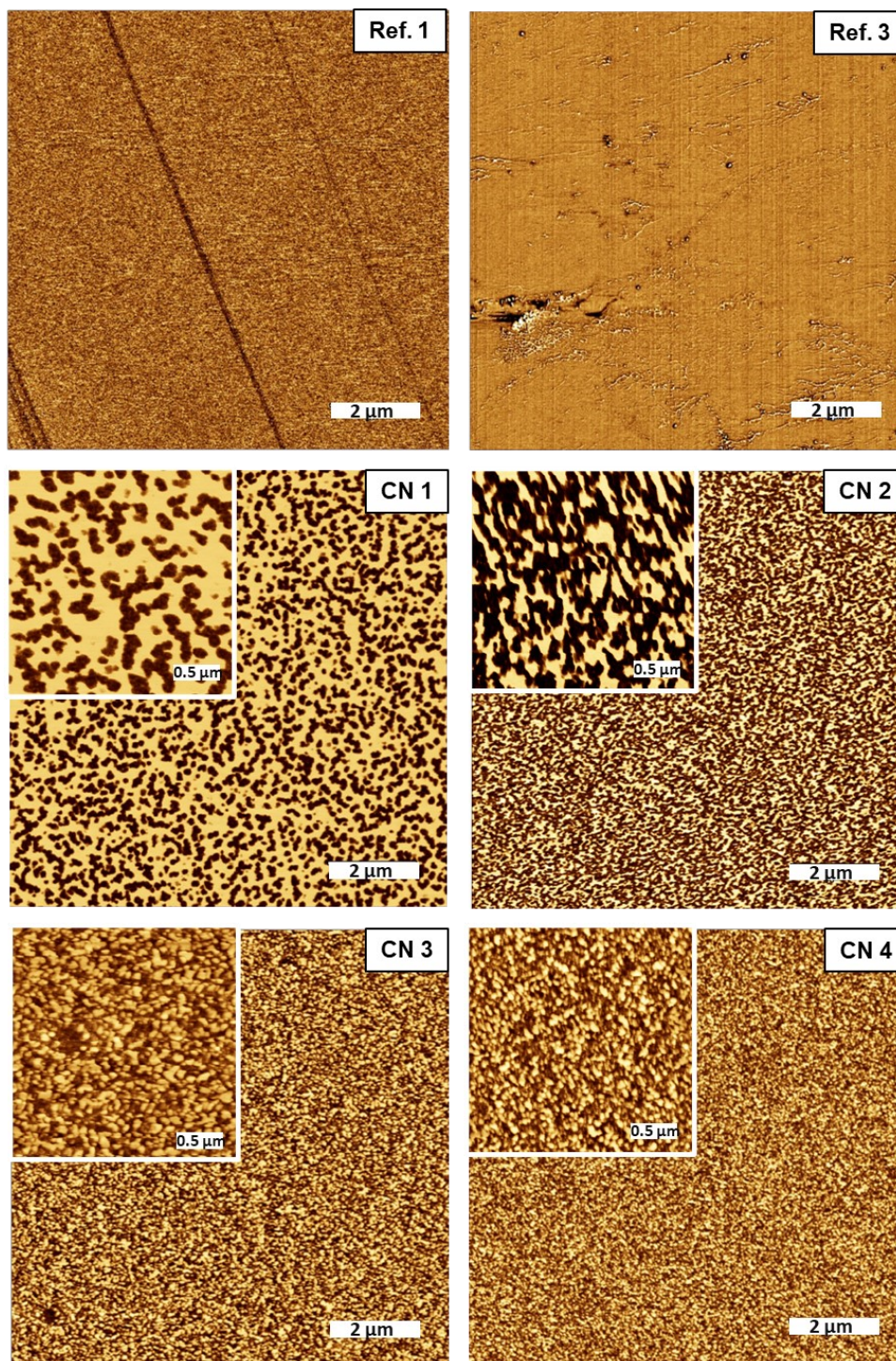
Figure 43. Topographic images of combined network 1 to 4 as well as the two reference samples.

In the corresponding topographic images, hard materials are illustrated with light color and soft materials with dark color. The reference material of the polyurea network (Ref. 3) shows a homogenous phase. In contrast to that, the pure PUA sample (Ref. 2) gives a finely distributed network with occasional hard domains and little soft segregation. This behavior can be attributed

to the structure of the PUA, that already itself contains soft and hard domains. The polypropylene glycol represents the soft segment, while the urethane groups, with the ability of strong hydrogen bonding, can be regarded as hard domains.

For CN 1, the topographic image clearly reveals that a phase-separated morphology has evolved, in which the polyurethane acrylate network is evenly distributed in the harder polyurea network. Individual PUA particles are round to oval and often string together in partially branched chains. The thickness of the PUA phase is on average 80 nm to 120 nm. The lengths of the particles range up to approximately 1.7 µm.

The AFM images of CN 2 illustrate that the PUA and the polyurea network are interconnected, resulting in dual-phase continuity. Domains of 940 nm x 230 nm are measured for the hard polyurea network, while for the soft PUA, domain sizes are a little bit smaller with 730 nm x 200 nm.

For CN 3 and CN4, a fine and homogenous distribution of polyurea particles in the PUA network can be observed, which is even finer for CN 4 compared to CN 3. Round polyurea particles have diameters of 40 nm to 140 nm for CN 3 and 30 nm to 90 nm for CN 4. The fine and nearly homogenous distribution of the polyurea particles explains their thermomechanical properties. The inward shift of the two glass transition temperatures can thus be explained by the domain sizes of the polyurea particles, that are likely to be in a regime what is called an interpenetrating network, as explained in chapter 0.

In conclusion it can be stated, that at low PUA concentrations, the PUA network is embedded in form of particles in the polyurea network, while at high PUA concentrations, phase inversion takes place and the polyurea phase is embedded in the PUA network. Smaller domain sizes are obtained in case the polyurea is the dispersed phase, indicating that the miscibility of low amounts of polyisocyanate in the PUA is higher than the miscibility of low amounts of PUA in the polyisocyanate.

The mechanical properties were further investigated to prove, if the toughness was increased upon the combination of the two polymer networks.

4.2.3.4 Mechanical Properties

To investigate the toughness of the combined networks in comparison to the neat polymer networks, tensile tests were performed. The area under a stress-strain curve can be used as a

measure of the toughness and was determined by integration.[74] The results are illustrated in Figure 44 and given in Table 10.
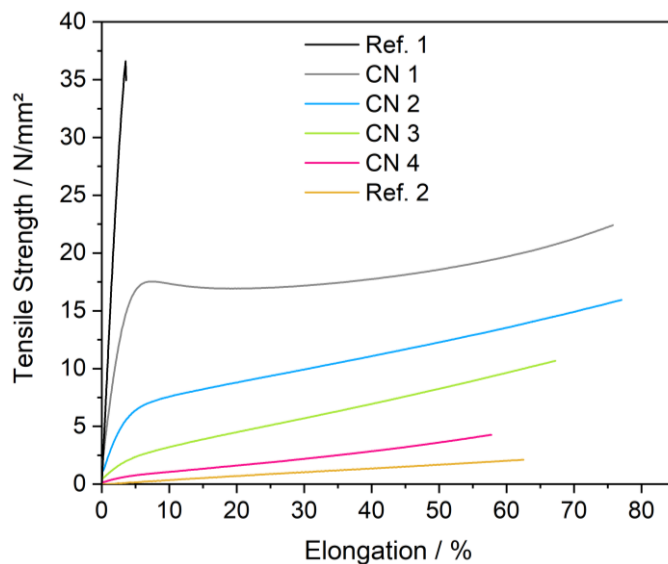

Figure 44. Stress-strain curves of the combined networks in comparison to Ref. 1 and Ref. 2.

The tensile tests reveal that as expected, the polyurea network is a rigid material with high tensile strength and high Youngs modulus, but low elongation at break. In contrast to that, the polyurethane acrylate is a soft material, with low tensile strength, but high elongation at break. The toughness (E/A), which is related to the integrated area below the stress-strain curve is low for both reference materials. Upon the combination of the two networks, a synergistic property profile can be observed.

Table 10. Young's modulus (E_{mod}), tensile strength (σ), elongation at break (ε) and toughness (defined as the energy per area E/A) of the combined networks as well as the corresponding references. Values in brackets indicate the corresponding errors, determined out of 5 samples per entry.

#	E_{mod} [Nmm^{-2}]	σ [Nmm^{-2}]	ε [%]	E/A [MJm^{-3}]
Ref. 3	1180	37	3.6	0.73
	(68)	(7.9)	(0.9)	
CN 1	365	22	67	13.6
	(15)	(1.1)	(6.6)	
CN 2	95	16	77	8.34
	(5.7)	(1.8)	(11)	
CN 3	25	11	67	4.14
	(3.9)	(0.7)	(4.3)	
CN 4	n.d.	4.3	58	1.27
		(0.5)	(4.6)	
Ref. 2	n.d.	2.1	63	0.67
		(0.6)	(19)	

In CN 1, the polyurethane acrylate phase is dispersed in the polyurea network as was shown by the DMA and AFM measurements. It can thus be regarded as a rubber-reinforced thermoset. The dispersed polyurethane acrylate particles, lead to a decrease in the Young's modulus as well as the tensile strength but to an increased elongation at break compared to the neat polyurea network.

CN 2 can be described as a leathery material, as both phases are equally dispersed, building a co-continuous network structure. The Young's modulus as well as the tensile strength is lower as for CN 1, while the elongation at break is in a similar range. Compared to the neat polyurethane acrylate network, the Young's modulus as well as the tensile strength have been significantly improved, without a loss in the elongation at break.

CN 3 and CN 4 can be regarded as filler-reinforced elastomers, as hard polyurea particles are dispersed in a soft and continuous polyurethane acrylate phase. Compared to the neat polyurethane acrylate network, the tensile strength as well as the Young's modulus have been improved with increasing amount of polyurea particles, while the elongation at break did not change.

This behavior confirms the assumption of a synergistic property profile when combining the two polymeric phases. The toughness increases from CN 4 to CN 1, in connection with an increasing amount of polyurea. Transferring the results to VPP, it can be stated, that CN 2 to CN 4 are well suited as printing material, while it is assumed to be difficult to obtain a stable green body with CN 1, which is discussed in more detail in the next section.

4.2.4 3D-Printing of Isocyanate–Acrylate Resins

For the printing process of the dual-cure resin system, it is assumed that the acrylate needs to build a continuous network to stabilize the build. The network can be co-continuous and homogenous, co-continuous and phase-separated or continuous with dispersed particles of the polyurea network. It was shown that co-continuity is obtained when applying the two types of precursors in an equal weight ratio, as in sample CN 2. Using the polyisocyanate in lower amounts like in samples CN 3 and CN 4, the acrylic network provides the continuous phase and it is assumed that a stable scaffold can be obtained during the printing process.

However, for CN 3 and CN 4, viscosity issues occur. Besides improving the mechanical properties, the polyisocyanate has the function to dilute the oligomeric polyurethane acrylate to appropriate printing viscosities. This means, the higher the amount of polyisocyanate, the lower the viscosity and the better the printability. Another feature that is interesting for VPP is to obtain a material showing phase separation. This is of interest for applications where the material should not change its mechanical properties with temperature. Phase separation is highest for CN 1. However, since no co-continuous morphology was obtained it is not suited as printing material. Based on these facts, CN 2 was chosen to be printed on a digital light processing printer to assess and compare the properties derived by printing.

To transfer the formulation to the printer, it was necessary to adapt the photoinitiator to the emission of the light source of the printer (405 nm). For this purpose, a ready-to-use photoinitiator mixture (Omnirad BL 750, IGM-Resins) containing three different phenyl phospine oxides with a suitable absorption spectra was chosen. The printing process further requires to add an inhibitor to avoid dark curing. Dark curing means the progression of the polymerization reaction in areas that are not illuminated. For this purpose, 2,5-bis(5-tert-butyl-2-benzoxazolyl)thiophene (BBOT) was used in an amount of 0.05 wt%, related to the amount of acrylate. The polyurethane acrylate as well as the polyisocyanate, the catalyst and the photoinitiator were thoroughly mixed, providing a homogenous and clear formulation which was poured into the resin bath of the printer.

The resin formulation containing tin(II) ethylhexanoate and Omnirad BL 750 turned out to be extremely light sensitive (reasons for this behavior were investigated in a separate work-stream but are not part of this work). Accordingly, the mixing of the formulation was performed in the dark.

In order to evaluate the printing parameters, photo-rheology was performed first. The light source of the photo-rheometer was 405 nm, which is similar to the light source of the printer. The light intensity of the light source in the printer was measured, enabling to set a similar intensity for the photo-rheology measurements. Additionally, the gap of the rheometer was set to 0.1 mm, corresponding to the thickness of one layer in the printing process. The time difference between the exposition to light and the crossover of storage- and loss modulus, further referred to as gel point, functioned as indication to choose the exposure time of the first layer for the printing process. Figure 45 gives the results of the photo-rheology measurements.
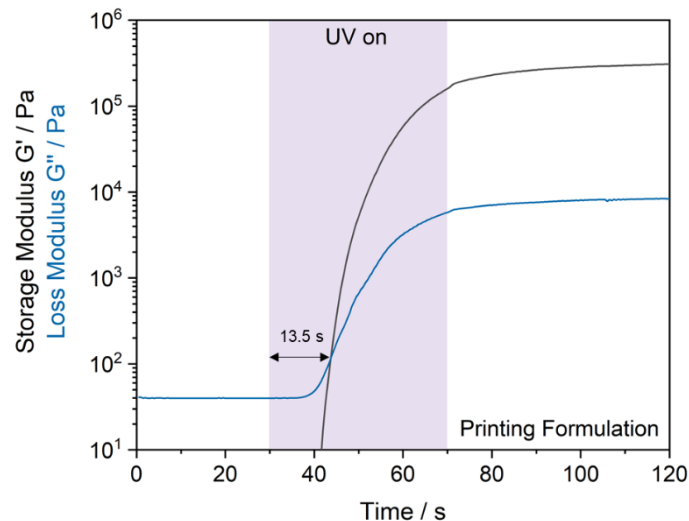

Figure 45. Photo-rheology measurements giving the storage- and loss modulus in dependence on the time and exposure to UV light.

The resin formulation was placed onto the rheometer and the storage- and loss modulus were measured. After 30 s, the UV light was turned on for 40 s. The loss modulus starts to increase after an induction period of about 10 s and is crossed by the storage modulus after 13.5 s.

This so called gel-point is of interest to determine the exposure time for the printing process. The final storage modulus is in the order of 10^5 Pa, which is sufficient to obtain adhesion to the build platform.

Tensile bars were chosen as printing objects, to enable the mechanical characterization of the resulting materials. The test specimen were printed flat, in x,y-direction. This has the advantage, that one print job is finished within a few minutes.

Figure 46. CAD-design file of a S2 tensile bar in the corresponding x,y-printing direction.

After printing, the 3D printed test specimen was carefully detached from the build platform and excess resin was removed. The obtained green body was stable and did not collapse during or after printing, proving the feasibility of the dual-cure, dual network concept.

The printed samples were subsequently placed in the oven at 100 °C for 17 h, in order to trigger the second curing reaction of the isocyanates. After the second polymerization was completed, the printed objects were completely white from the outside, while the inside was completely transparent. AFM and DMA measurements were performed in order to evaluate the morphology as well as the thermomechanical properties. The results are illustrated in Figure 47.
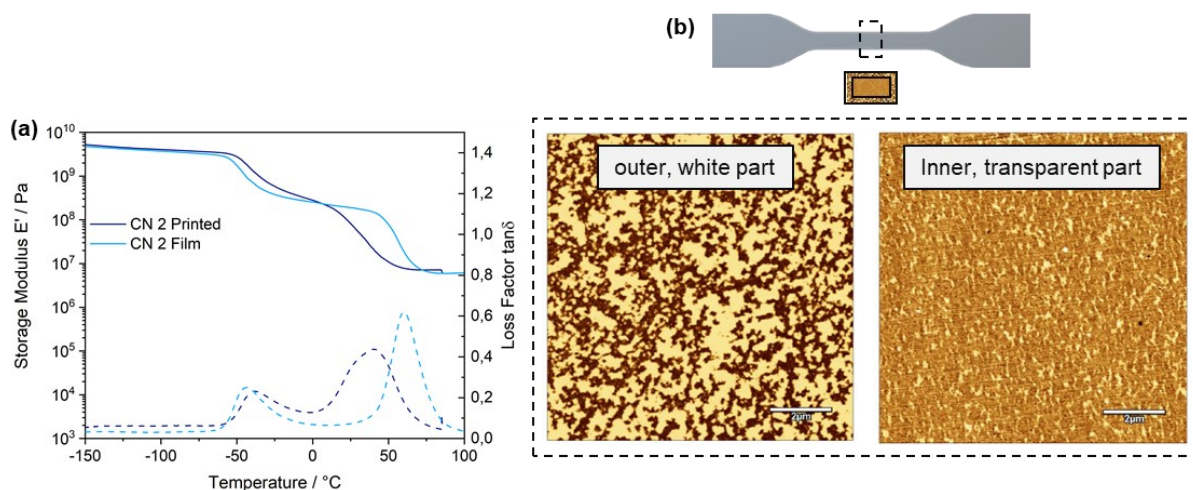

Figure 47. a) Comparison of the thermomechanical properties of the printed and casted film CN 2. b) AFM topographic images of the printed CN 2, giving the morphology of the outer, white part and the inner, transparent part.

The results illustrate that different morphologies have evolved. In the outer white part, the polyisocyanate based network provides the continuous phase and the polyurethane acrylate is

the dispersed phase. In the inner transparent part, the polyurethane acrylate provides the continuous phase and round to oval polyisocyanate based polyurea agglomerates are evenly dispersed.

One potential reason of this behavior may be related to the light intensity of the light source of the printer, which is much lower compared to the mercury lamps that were used for the screening test performed in chapter 4.2.3. It is thus reasonable to assume, that the reaction of the acrylates during the printing process is much slower and does not reach full conversion within the exposure time. Thus, the acrylate network is not able to entrap the isocyanate inside a cured voxel, which leads to the diffusion of the isocyanate to the surface. As a consequence, the outer part of the object contains an increased amount of isocyanate.

The DMA measurements of the 3D printed part in comparison to the casted film further illustrate an inward shift of the two glass transition temperatures, which is even more pronounced for the second glass transition temperature, corresponding to the isocyanate based network. It might be the case that the second curing reaction did not reach full conversion during post-curing.

4.2.5 Summary

In conclusion it can be stated that acrylic functional polyurethane prepolymers and low viscous polyisocyanates are well suited to formulate homogenous photocurable resins that can be used in vat photopolymerization, leading to phase-separated networks with improved toughness in comparison to the neat materials.

Formulations based on a polyurethane acrylate and the allophanate based polyisocyanate were investigated in great detail. The second curing reaction of the polyisocyanate was performed under heat exposure after the light induced radical polymerization of the acrylic prepolymer. It was found that against original design and expectation, no pure polyisocyanurate network formation took place, but predominantly a polyurea network was formed, likely by a reaction with water provided by the air during heating. The consequential network showed a lower crosslinking density and glass transition temperature than the intended polyisocyanurate network.

DMA and AFM measurements further proved that the sequential polymerization of the two types of monomers lead to the formation of phase-separated polymer networks with two distinct glass transition temperatures. The results were further determined by theoretical calculations of the storage modulus in dependence on the temperature. The theoretical calculations were based on a model that assumes a completely phase-separated morphology. The fits obtained were well suited

to describe the morphologies where the polyurea network was the predominant phase as well as for the co-continuous network structure. In case of the polyurethane acrylate being the predominant phase, the fit was less in line with the performed DMA measurements, indicating that the phases were not completely separated.

Tensile tests and the calculation of the toughness revealed that it was possible to reinforce the acrylic network upon the incorporation of the isocyanate based particles. Additionally, the polyurethane acrylate particles dispersed in the isocyanate based network lead to an elastification of the pure isocyanate based network. Thus, the target to obtain a toughened thermoset was successfully achieved.

First printing trials of the dual-cure resin formulation were successful.

4.3 Elastomers

The ability to reversibly deform at ambient temperatures when applying a strain-force, make elastomers unique materials that are used in a huge variety of applications, such as seals and tires.[239] A low glass transition temperature and long polymer segments with a high number of repeating units between crosslinks, resulting in a low crosslinking density are the key characteristics of elastomers.[76,240] For VPP, the preparation of an elastomeric 3D printed object is challenging and typically, highly crosslinked, high T_g and comparably brittle materials are produced.[241] Using high molar mass precursors for the manufacturing of elastomeric materials is restricted by the viscosity limitations of the printing process. Short exposure times between layers are preferred to achieve a high build speed, however restrict to build up a high number of monomers between crosslinks.[79]

Different strategies have been developed to circumvent these issues.[242–248] Amongst others, Long and his co-workers developed a printable resin based on the UV induced radical polymerization of acrylates and a simultaneous chain extension via thiol-ene coupling.[191] Taking a different path, the company Carbon Inc. makes use of reversibly blocked isocyanates to perform a secondary chain extension in a thermal post-processing step to create long-chain polyurethanes.[184,198] Recently, an interesting approach has been demonstrated by Wallin and co-workers. They developed 3D printable tough silicone double networks, by combining photocurable and condensation thiol-ene reactions.[61] The combination of two orthogonal curing mechanisms, resulting in materials where both polymeric phases exhibit low glass transition temperatures is

frequently used for the preparation of tough hydrogels.[249] The advantage in comparison to single phase materials is that under load, the weaker polymeric phase dissipates energy upon fracturing, while the second network remains intact and bears the load.[61,250]

Transferring this approach to VPP, combined networks are prepared in which both phases exhibit a low glass transition temperature. The intention is to obtain materials with elastomeric properties.

For this purpose, the dual-cure concept of using independently curable radical and isocyanate building blocks, as already described in chapter 4.2 was used to develop more flexible materials. However, instead of using low viscous polyisocyanates to dilute a high viscous polyurethane acrylate, monomeric mono- and diacrylates were chosen to dilute a higher viscous oligomeric difunctional isocyanate. The overall concept, however, remains similar: the acrylates build up a green body during the printing process, while the isocyanate prepolymers are dispersed in the acrylic matrix. In a subsequent step, taking place outside the printer, the isocyanates undergo a thermally induced curing reaction. The use of starting materials with reverse viscosities compared to chapter 4.2 is expected to strongly influence the properties of the resulting materials, giving access to a diverse and still unusual property profile for use in VPP based AM technologies, namely tough elastomers.

4.3.1   Selection and Characterization of Isocyanate Prepolymers

Isocyanate prepolymers were prepared using a similar method as already described in chapter 4.2. The monomeric isocyanate was used in a high molar excess in comparison to the respective polyol. After reaction, the excess monomeric isocyanate was distilled off and well-defined structures were obtained. In order to illustrate the variety of available precursors, also with regard to more sustainable alternatives, two prepolymers were prepared, as illustrated in Figure 48.
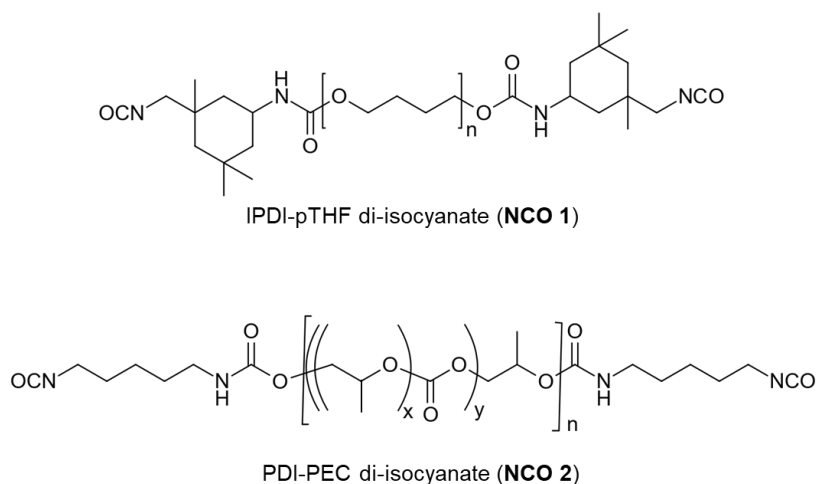
Figure 48. Chemical structure of isocyanate prepolymers.

For NCO 1, isophorone diisocyanate (IPDI) was used as diisocyanate which was reacted with polytetrahydrofuran (pTHF) (1000 g·mol^{-1}) as polyol component. The precursors were chosen based on the fact, that pTHF is frequently used in elastomers and, in combination with IPDI leads to a liquid prepolymer. For NCO 2, biobased pentamethylene diisocyanate (PDI) was chosen and was reacted with a polyether carbonate (PEC) (1000 g·mol^{-1}). The resulting structures were analyzed by GPC and by end-group titration to determine the molar mass as well as the molar mass distribution. The results are illustrated in Table 11.

Table 11. Viscosity, number average molar mass and polydispersity determined by GPC. NCO-content of isocyanate terminated prepolymers and molar masses determined by end-group titration.

#	η [mPa·s]	$M_{n, GPC}$ [g·mol^{-1}]	$Đ_{GPC}$	NCO [%]	$M_{n, titration}$ [g·mol^{-1}]
NCO 1	13100	2180	1.5	5.6	1500
NCO 2	7510	1980	1.3	5.8	1450

The molar masses of both prepolymers are in the same order of magnitude. The prepolymers were synthesized with the corresponding isocyanate in a high molar excess, leading to the formation of predominantly the 2:1 adduct (isocyanate : polyol). The viscosity is much higher for NCO 1 13100 mPa·s) in comparison to NCO 2 (7510 mPa·s). However, from experience it is assumed that appropriate printing viscosities can be obtained with both prepolymers by dilution with monomeric mono- and diacrylates in a subsequent formulation step.

To investigate the material properties of the pure prepolymers they were catalytically trimerized under heat exposure, and the resulting thermosets were analyzed by differential scanning

calorimetry (DSC). For this purpose, the corresponding prepolymers were mixed with tin(II) ethylhexanoate (0.75 wt%) as catalyst and were poured into a mold. The mold was placed into an oven at 100 °C for 17 h. The completion of the reaction was determined by FT-IR spectroscopy, monitoring the decrease of the isocyanate signal at 2265 cm^{-1}. The glass transition temperature of trimerized NCO 1 is -50 °C and for NCO 2, -22°C, as determined by DSC.

The DSC analysis of both crosslinked prepolymers confirms that they are in the rubbery plateau at room temperature, thus suitable for their intended use as one part of a dual-cure combinatorial elastomeric network.

4.3.2 Selection and Characterization of Acrylates

There is a huge variety of monomeric and oligomeric mono- and multifunctional acrylates that possess a broad range of mechanical properties.[251] The preparation of soft and elastomeric materials with a glass transition temperature below use temperature, requires the use of acrylates that possess a low glass transition temperature in their polymerized state. This is why polyethylene glycol diacrylates (PEGDA) was chosen as diacrylate component. In this study a PEGDA with an average molar mass of 700 g·mol^{-1} was used. In combination with a mono-acrylate it is possible to tune the resulting crosslinking density of the acrylic network. For this purpose Tetrahydrofurfuryl acrylate (THFA) was chosen, which is frequently used as an elastomeric component in acrylate based copolymers.[252]

The glass transition temperatures of the acrylates in the polymerized state were determined using DSC. Next to the neat acrylic materials, mixtures of both materials were cured and analyzed by DSC measurements in order to determine the mixed glass transition temperatures. To polymerize the acrylates, they were mixed with 2-hydroxy-2-methylpropiophenone as photoinitiator, and 400 μm films were applied onto glass substrates that were subsequently radically cured under high energy mercury lamps (details are given in the experimental section). The glass transition temperatures of the resulting networks are given in Table 12 and are further referred to as acrylic networks (AN 1 to AN 3).

Table 12. Glass transition temperature of acrylic networks.

wt%	AN 1	AN 2	AN 3
THFA	100	50	–
PEGDA 700	–	50	100
T_g [°C]	-31	-36	-41

The polymerized THFA has a glass transition temperature of -31 °C. The T_g of the PEGDA 700 network is lower and amounts to -41 °C. Upon combining the two monomers, a glass transition temperature of - 36 °C is obtained.

The acrylates thus represent well suited candidates for the preparation of low T_g elastomeric like polymer networks. The sequential curing of acrylates and isocyanates to result in combined polymeric networks is investigated in the next section.

4.3.3   Screening of Dual-cure Isocyanate - Acrylate Resins

In order to investigate the dual-cure isocyanate-acrylate resins, the crosslinking density of the acrylic phase was systematically varied, at constant isocyanate to acrylate weight ratio. For this purpose, NCO 1, as well as THFA and PEGDA 700 were mixed with 0.75 wt% tin(II)ethylhexanoate and 0.3 wt% 2-hydroxy-2-methylpropiophenone. Films of these mixtures were each applied onto glass substrates and were cured under UV light, followed by a thermal curing process at elevated temperatures. The variation of the mono- to diacrylate ratio of the resulting 'inverse' combined networks (iCN) is given in Table 13.

Table 13. Composition of inverse combined networks (iCN).

m [g]	iCN 1	iCN 2	iCN 3
NCO 1	5	5	5
PEGDA 700	2	3	4
THFA	3	2	1

Subsequently, DMA measurements were performed in order to investigate the influence of the crosslinking density of the acrylic phase on the final thermomechanical properties. The corresponding results are illustrated in Figure 49.
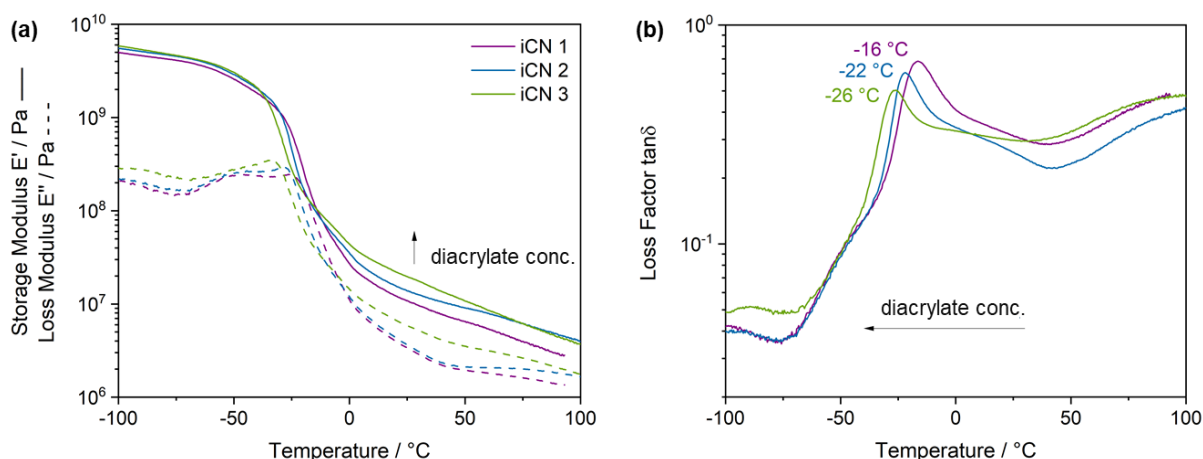
Figure 49. DMA measurements of the inverse combined networks (iCN). (a) Storage modulus and loss modulus in dependence on the temperature. (b) Loss factor in dependence on the temperature.

The left diagram in Figure 49 gives the storage- as well as the loss modulus in dependence on the temperature. With increasing amount of diacrylate the crosslinking density of the samples slightly increases from iCN 1 to iCN 3, as can be seen in the rubbery plateau above the glass transition temperature. The glass transition temperature of iCN 3 is lowest, which is a result of the lower glass transition temperature of PEGDA 700 compared to THFA. The right diagram gives the loss factor in dependence on the temperature. The glass transition temperatures were determined by the maximum of *tanδ* in the loss factor curve and increases from iCN 3 over iCN 2 to iCN 1, with - 26 °C, - 22 °C and -16 °C, respectively. The variation in the diacrylate to mono-acrylate ratio can be used to tune the mechanical properties by shifting the glass transition temperature and the crosslinking density in the rubbery plateau.

Interestingly, the storage moduli of the samples steadily decreases with temperature. This indicates that at least one of the phases is not fully crosslinked. As already worked out in chapter 4.2, the assumption suggests that instead of the intended trimerization reaction of the isocyanate groups at least partially a polyurea formation took place. With the use of PEGDA 700, the material is hydrophilic, which may lead to water-uptake of the network that then reacts with the isocyanate groups. As the isocyanate prepolymers prepared are strictly bifunctional, a polyurea formation would lead to a linear polyurea based thermoplastic elastomer, instead of the targeted crosslinked thermoset.

To prove this hypothesis, time dependent FT-IR spectroscopy of the second curing reaction was performed, exemplarily for iCN 2. The corresponding spectra are illustrated in Figure 50. Measurements were performed at t_0 (starting point before the film was placed into the oven), after 3 h and 20 h.
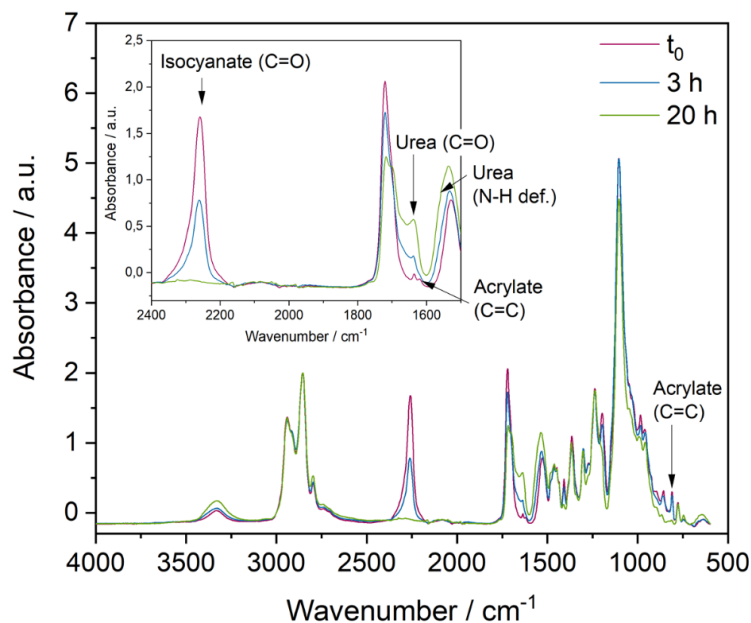
Figure 50. FT-IR spectroscopy of the second curing reaction in dependence on the time, exemplarily for iCN 2. t_0 represents the starting point, before the film was placed into the oven.

The progress of the reaction can be monitored by the decrease in the carbonyl stretching vibration of the isocyanate group at 2265 cm^{-1}. At the same time, the carbonyl stretching vibration of the urea group increases over time at 1640 cm^{-1}, as well as the N-H deformation vibration of the urea group at 1560 cm^{-1}. The results illustrate that also in this case, the polyurea formation is the predominant reaction taking place during the thermal curing, instead of the intended trimer formation. Also vibrations of the acrylic double bonds at 814 cm^{-1} and 1625 cm^{-1} are still visible at t_0 and after 3 h of reaction, indicating that the preceding radical polymerization was not completed and residual acrylic double bonds are still present. After 20 h, the vibration at 814 cm^{-1} fully disappeared, which means that the residual monomers evaporated or continued to react during the thermal curing.

In contrast to the dual-cure system described in the previous chapter, the functionality of the isocyanate based prepolymers is precisely two. Assuming the isocyanate prepolymers have mostly reacted by forming urea connections, as indicated by FT-IR measurements, a predominantly linear polymer is formed instead of a polymer network.

In order to obtain a stable rubbery plateau above the glass transition temperature, an allophanate polyisocyanate based on HDI with a functionality of 2.5, further referred to as allophanate was added as second isocyanate component that has already been used as diluent in chapter 4.2. The addition of the allophanate thus enables the formation of a crosslinked network of isocyanate

prepolymers, even if no trimerization reaction takes place. The compositions of the samples are given in Table 14.

Table 14. Composition of inverse combined networks (iCN) with addition of a multifunctional isocyanate as crosslinker to the second polymer phase.

m [g]	iCN 4	iCN 5	iCN 6
NCO1	7	5	3
Allophanate	3	5	7
PEGDA 700	5	5	5
THFA	5	5	5

The concentration of the acrylic monomers was kept constant and a weight ratio between diacrylate- to monoacrylate of 1:1 was chosen. The overall concentration between the acrylic- and isocyanate phase was kept constant at an even weight ratio (1:1). Within the second polymer phase, the ratio between the bifunctional isocyanate (NCO 1, f = 2) and the multifunctional isocyanate (allophanate, f = 2.5) was systematically varied, with 70 wt% to 30 wt% (iCN 4), 50 wt% to 50 wt% (iCN 5) and 30 wt% and 70 wt% (iCN 6), accordingly. DMA measurements were performed in order to investigate the thermomechanical properties in dependence on the crosslinking density of the second polymer phase. The results are shown in Figure 51.
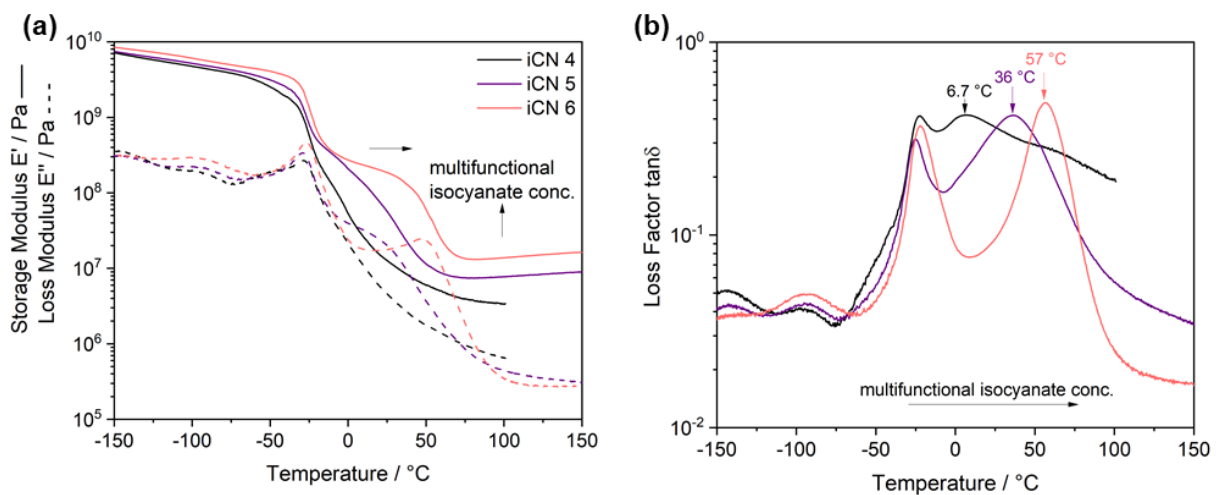

Figure 51. DMA measurements of iCN 4 to iCN 6, illustrating the influence of the addition of a crosslinker of the second polymer phase. a) Storage- and loss modulus in dependence on the temperature. b) Loss factor in dependence on the temperature.

The left diagram in Figure 51 gives the storage- and loss modulus in dependence on the temperature. On the right, the corresponding loss factor curves are illustrated. With increasing amount of multifunctional isocyanate the crosslinking density of the samples increases from iCN 4 to iCN 6. At the same time, the second glass transition temperature is shifted from 6.7 °C for iCN 4 to 36 °C for iCN 5 to 57 °C for iCN 6. This means that next to an increase in the crosslinking density, the material properties of the overall material significantly change. The incorporation of the multifunctional isocyanate thus leads to a different polymeric network, which has a more rigid character. This is further shown by the storage modulus between the two glass transition temperatures, which increases with increasing amount of multifunctional isocyanate.

In order to get a detailed understanding of the structure-property relations of the corresponding dual-cure systems, the morphology was investigated by AFM. The findings were correlated to the thermomechanical properties measured by DMA, which will be presented in the following chapter.

4.3.3.1 Morphology

In order to investigate the relation between structure and thermomechanical properties, a detailed AFM and DMA study was performed. For this, NCO 2 was chosen as base isocyanate functional prepolymer. The compositions of the samples are illustrated in Table 15, referred to as iCN 7 to iCN 13. The samples were prepared by mixing the components with 0.3 wt% 2-hydroxy-2-methylpropiophenone and 0.75 wt% tin(II)ethylhexanoate. Thin films (400 µm) were applied onto glass substrates, which were first UV cured, followed by a thermal curing at elevated temperatures.

Table 15. Composition and viscosities of the samples prepared to investigate the morphology by AFM and DMA measurements.

m [g]	iCN 7	iCN 8	iCN 9	iCN 10	iCN 11	iCN 12	iCN 13	Ref. 1	Ref. 2
NCO 2	5	5	5	10	7	3	–	5	–
Allophanate	5	5	5	–	3	7	10	5	–
PEGDA 700	3	5	7	5	5	5	5	–	5
THFA	7	5	3	5	5	5	5	–	5
η [mPa·s]	132	185	305	389	262	152	114	n.d.	n.d

The overall mass ratio between isocyanate and acrylate was kept constant at 1:1. For samples iCN 7 to iCN 9, the ratio between mono- to diacrylate was varied at a constant ratio of bi-functional to multi-functional isocyanate. For samples iCN 10 to iCN 13, the ratio between bi-functional to multifunctional isocyanate was varied at constant mono- to diacrylate ratio. Two reference samples were prepared, in each case with an equal weight ratio between the two different types of monomers. AFM as well as DMA measurements were performed in order to understand the thermomechanical properties in dependence on the morphology. The information obtained were employed to find a suitable formulation that can be printed by vat photopolymerization.

AFM phase contrast images of the two reference samples are illustrated in Figure 52. The phase contrast, the scale of which is shown next to the respective image, is an indication of the materials' capability to dissipate or store energy exerted from the AFM cantilever oscillation. The higher the value of the phase contrast, the more energy is stored, i.e. the materials is more elastic, while the lower the value of the phase contrast, the more energy is dissipated while the materials can be characterized as more viscous. In the literature phase contrast imaging is commonly applied to evaluate difference in materials properties (such as "soft-hard" domains) of a sample surface. Within the image area of 5 μm x 5 μm both reference samples show a homogenous phase distribution. When zooming in to 0.3 μm x 0.3 μm, a nanophase-separated morphology can be observed on both samples, as can be seen in the inlay images. This phase separation is believed to result from the use of different building blocks (bifunctional vs. multifunctional isocyanate and mono- vs. diacrylate) that are already present in the reference materials.
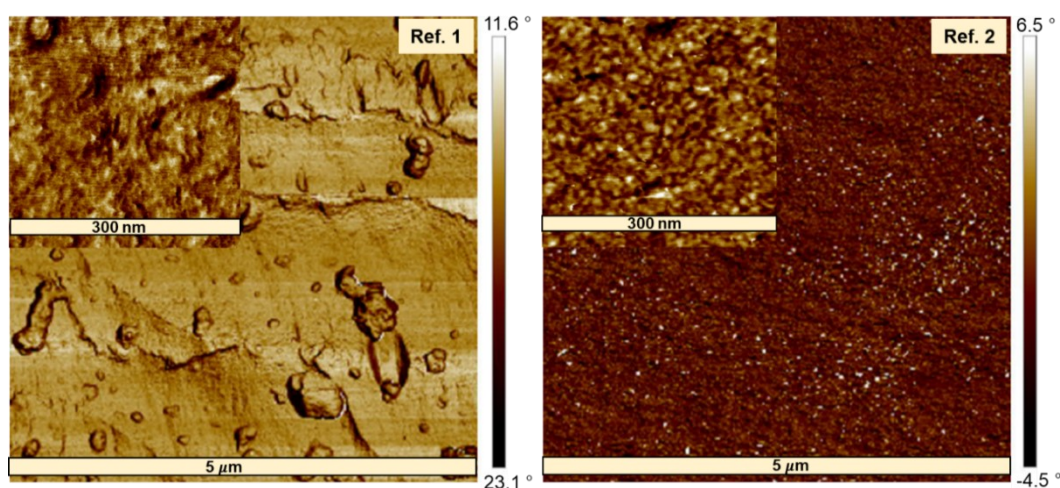

Figure 52. Representative AFM phase contrast images of reference samples 1 and 2.

No DMA measurements have been performed for the two reference samples. The acrylate reference network is too soft to be measured and already breaks upon clamping the test specimen. Test specimen of the isocyanate based networks were too thick to be clamped.

The crosslinking density of the acrylic phase was varied first, by changing the weight ratio between PEGDA 700 and THFA from 30 : 70 (iCN 7) over 50 : 50 (iCN 8) to 70 : 30 (iCN 9). Corresponding results of DMA and AFM measurements are illustrated in Figure 53.
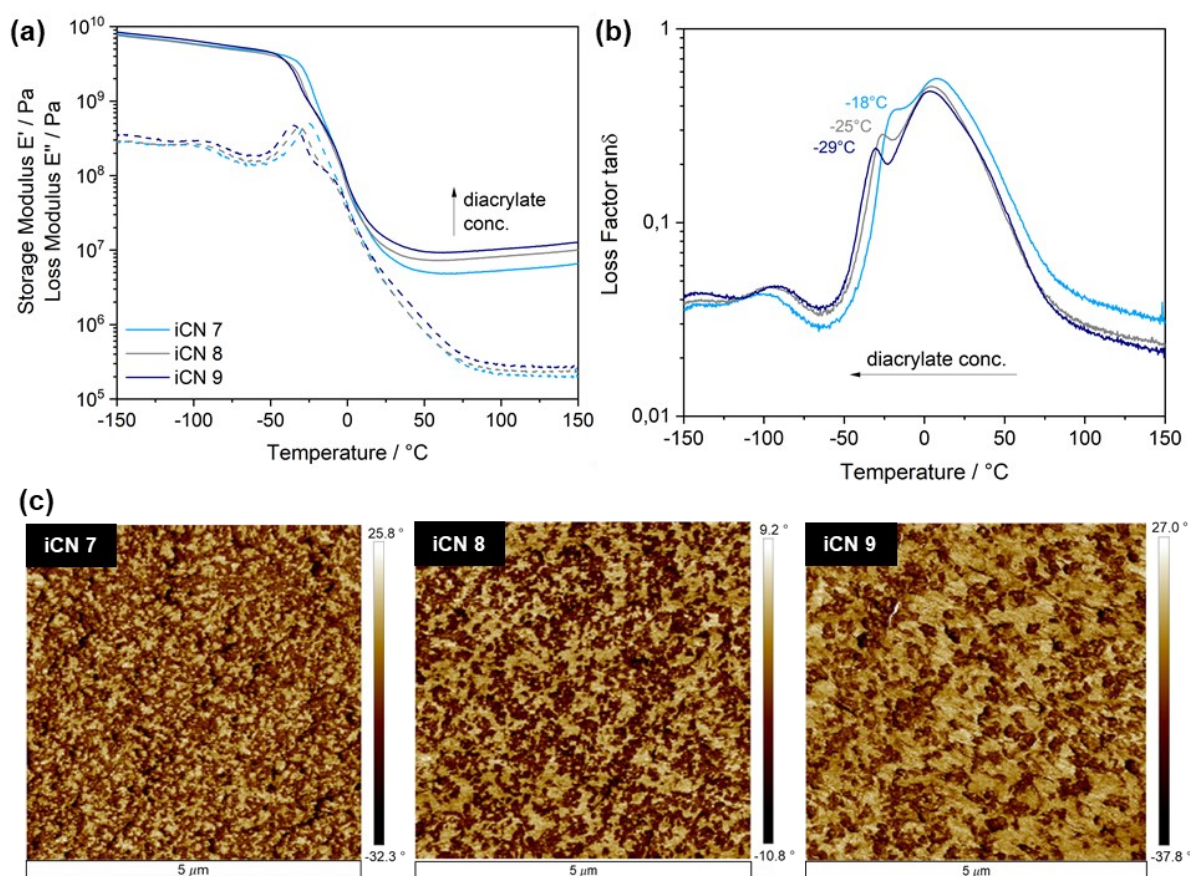

Figure 53. DMA measurements giving a) the storage- and loss modulus and b) the loss factor in dependence on the temperature for iCN 7 to 9; c) AFM phase contrast images for iCN 7 to 9.

According to AFM phase contrast images, phase-separated domains are seen in all three samples, which is in line with the observation of two glass transition temperatures in DMA measurements. In all cases, the lower T_g phase can be attributed to acrylate rich domains, while the higher T_g phase consists of polyurea rich domains. The change in the ratio between PEGDA 700 and THFA affects the crosslinking density of the acrylic network, resulting in an increasing modulus in the rubbery plateau from iCN 7 to iCN 9. The fact that in all three samples the acrylic phase is

contributing to the overall network density leads to the assumption that at least some co-continuity of the two networks prevails. In co-continuous networks, both phases contribute equally to the mechanical properties, while this is not the case for matrix-dispersed particle morphologies.

The lower glass transition temperature is shifted to even lower temperatures with increasing amount of PEGDA 700 from -18 °C to -29 °C, while there is no shift of the higher T_g. Thus, it is reasonable to assume that the shift in the lower glass transition temperature is dependent on the composition of the acrylic network. PEGDA 700 has a much lower glass transition temperature compared to THFA homopolymer, which explains the shift in T_g to lower temperatures with increasing amount of PEGDA 700. The fact that the loss modulus curves of the two materials are partially overlapping, makes it difficult to rule out the formation of smaller domains that would also result in one broad glass transition temperature and, in contrast, to the formation of similar phase separation, but different T_g of the acrylic phase.

The phase contrast images (Figure 53 c) give information about the morphology and the phase separation. Different morphologies are observed by changing the degree of crosslinking of the acrylic phase. For a low amount of PEGDA 700 (iCN 7), the acrylic phase is crosslinked to a lower degree and remains mobile, forming the continuous phase in which small isocyanate based network domains are dispersed. Increasing the bifunctional acrylic crosslinker concentration leads to the formation of co-continuous domains (iCN 8) where the elasticity of the acrylic network increases, resulting in a higher phase contrast, as evidenced by the increase of the area fraction from the high phase contrast domains. Further increase in the amount of acrylic crosslinkers eventually results in the continuous "hard" phase in iCN 9, where the isocyanate based network and the highly crosslinked acrylic materials form the continuous phase, while the less crosslinked acrylic domains are evenly distributed.

It is likely that the gel formation of the acrylic phase is dominating the morphology evolution, independent of the isocyanate phase. During the radical polymerization of the acrylates, the isocyanate is still in a liquid state and thus phase separation is forced by the gel formation of the acrylates, directing the morphology evolution. In case of high amounts of THFA, the polymerization is likely to be slow and large THFA chains build up, resulting in the formation of a continuous acrylate network. With increasing amount of PEGDA 700, the polymerization rate is believed to increase and a more dense acrylic network builds up, eventually leading to the isocyanate based network being the continuous phase. To verify this hypothesis, the gel formation of samples iCN 7 to iCN 9 was determined by photo-rheology, as illustrated in Figure 54. For this

purpose, the formulations were measured on a rheometer with in-situ curing ability. The UV light was switched on after 30 s of the measurement for 20 s, leading to an increase in the storage modulus after a short induction period. The gel point is reached when the storage modulus crosses the loss modulus. Subsequently auto-acceleration of the radical polymerization takes place, leading to a steep increase in the storage modulus.
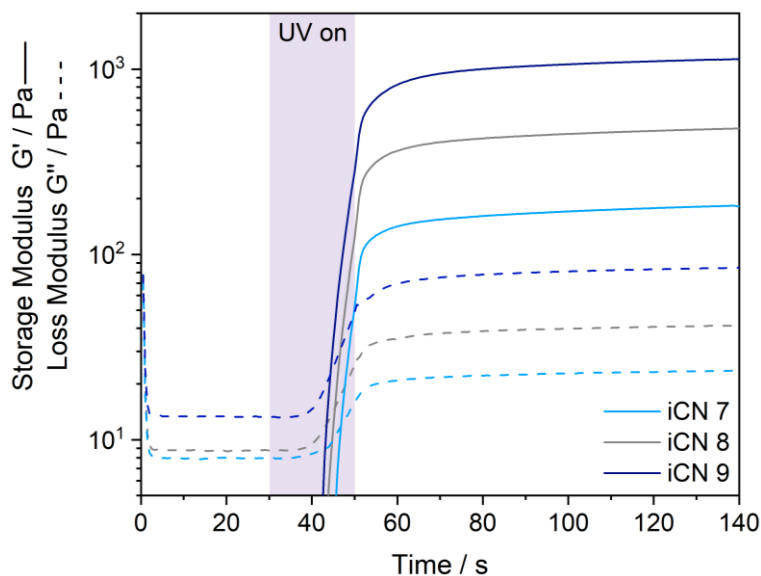

Figure 54. Photo-rheology of samples ICN 7 to ICN 9.

The results of the photo-rheology measurements show that sample iCN 9, containing the highest amount of diacrylate, reaches the gel point fastest (14 s), followed by iCN 8 (16 s) and iCN 7 (17 s), respectively. This proves that with increasing double bond functionality the radical polymerization is faster. The final moduli obtained further indicate that iCN 7 has a lower crosslinking density compared to iCN 9. The absolute storage moduli are comparably low for a crosslinked thermoset, which can be related to the fact that the isocyanate phase, which is still in its liquid state has a diluting effect on the network, consequently leading to a lower overall modulus. This behavior further explains and supports the morphology evolution of the combined networks.

In order to further understand the morphology of the combined networks, bearing analysis has been carried out in which the highest phase contrast determined from the image was defined as point 0 and the difference between each individual data points and point 0 was then plotted as statistical histograms, as shown in Figure 55 for samples iCN 7 to iCN 9. Two distinct peaks are obtained that differ in dependence on the amount of crosslinker of the acrylic phase. At low PEGDA

700 fractions, the soft phase is continuous, as indicated by the higher peak of the soft domain. An even ratio between PEGDA 700 and THFA (iCN 8) results in slightly higher peak height of the hard domain, indicating a co-continuous phase morphology. For sample iCN 9, the peak of the hard phase is obviously higher, which means that the hard phase becomes the continuous phase.
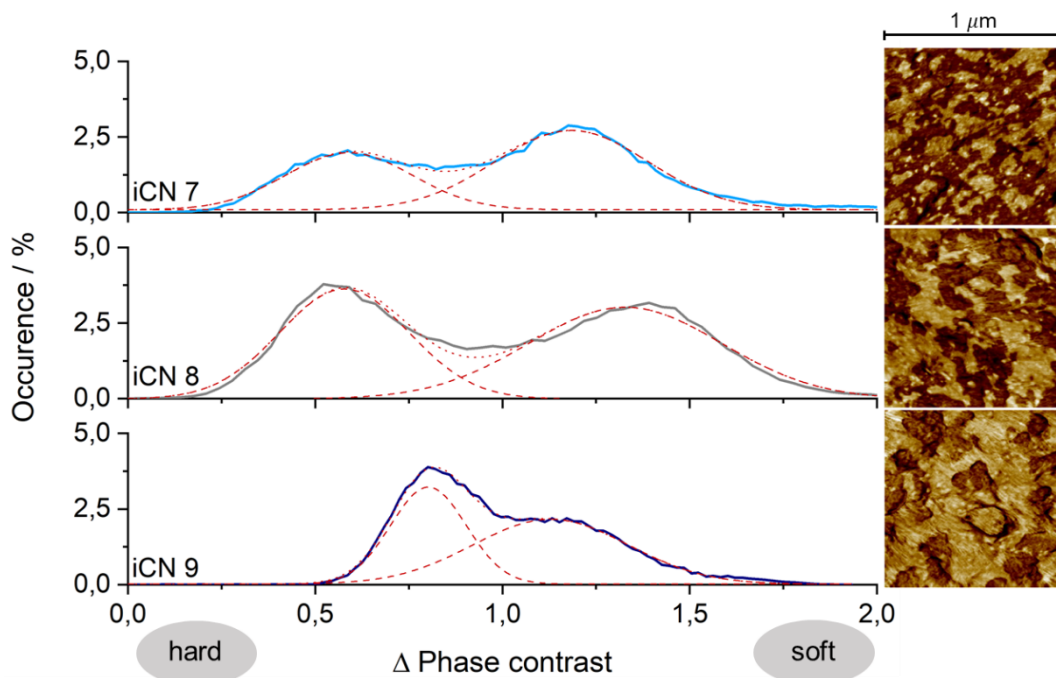

Figure 55. Bearing analysis of phase contrast images providing the distribution of the two phases for samples ICN 7 to 3.

The peak-to-peak distance is dependent on the degree of phase mixing as well as the difference in degree of crosslinking. No clear dependence of the degree of phase separation on the crosslinker concentration can be observed. It is observed that iCN 8 has the highest phase separation, followed by iCN 7. The sample with the highest amount of PEGDA 700 (iCN 9) has the lowest phase separation. This behavior may be related to thermodynamic and kinetic changes in miscibility during the reaction which have not been investigated in further detail.

Keeping the ratio between PEGDA 700 and THFA constant (50 : 50), the weight ratio between the bifunctional- and multifunctional isocyanate was systematically varied. The influence on the thermomechanical properties as well as the morphology was investigated by DMA and AFM measurements.

In Figure 56, the storage and loss moduli, as well as the loss factors are given in dependence on the temperature for samples iCN 10 to iCN 13 (with decreasing NCO 2 prepolymer and increasing

allophanate content from iCN 10 to iCN 13), as well as for iCN 8 (being the 1:1 ratio between NCO 2 and allophanate). The addition of the multifunctional isocyanate leads to an increase in the crosslinking density of the overall material, as confirmed by the increase in the storage modulus in the rubbery plateau. As already described earlier, in case no allophanate is added to the reaction mixture, it is likely that a linear polymer forms during the second polymerization reaction. This is the reason, why no stable rubbery plateau is obtained in case of iCN 10, as the sample breaks at 50 °C.
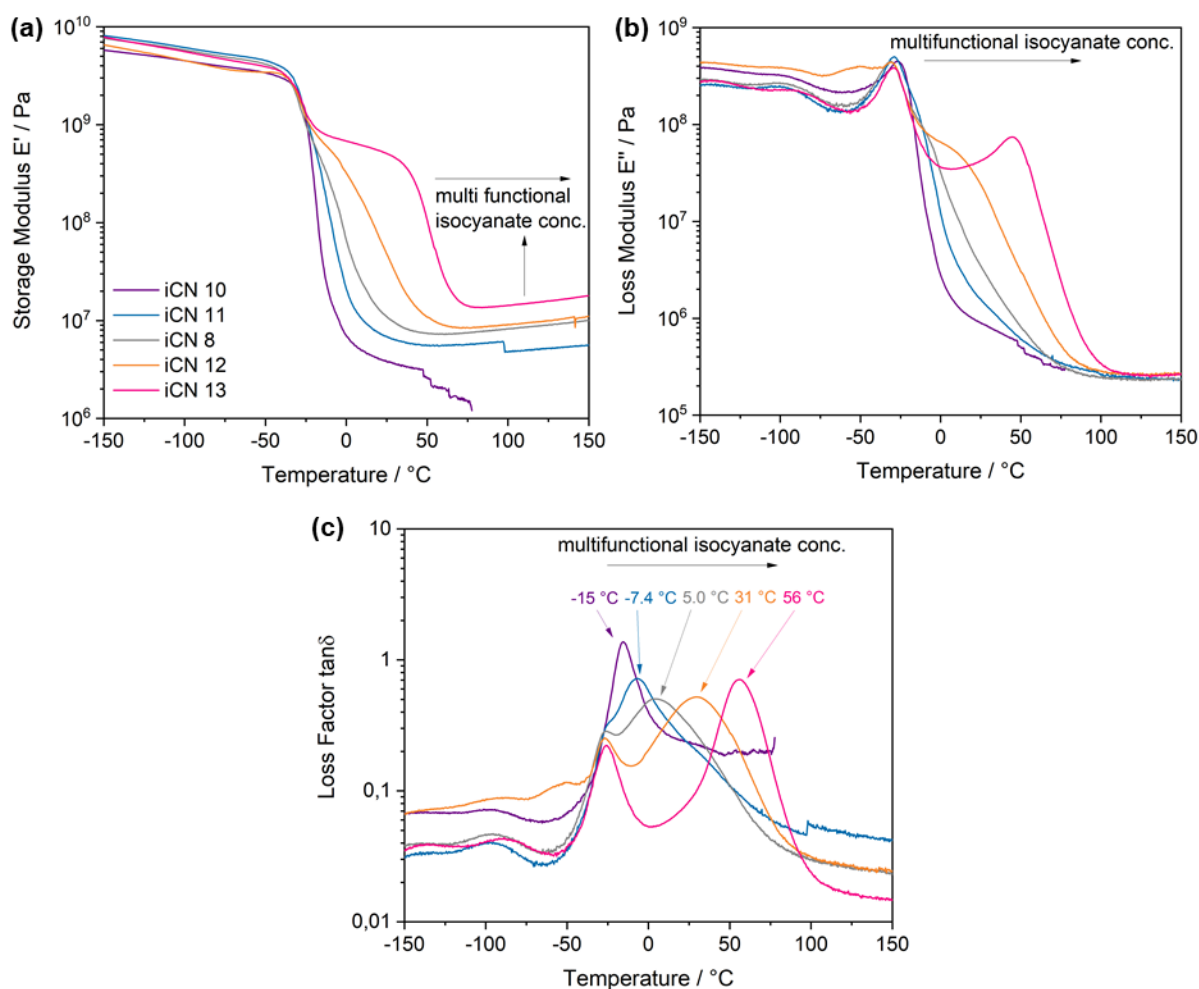

Figure 56. DMA measurements of samples iCN 10 to iCN 13 and iCN 8, showing the effect of an increasing crosslinking density of the second polymer network, at constant acrylate composition. a) the storage modulus, b) loss modulus and c) the loss factor in dependence on the temperature.

The loss factor curve shows a clear dependence on the amount of multifunctional isocyanate. Two distinct glass transition temperatures are observed for all samples, except for iCN 10 that only contains the bifunctional isocyanate as the second polymeric phase. The glass transition

temperature of the softer acrylic phase remains constant at about -25 °C, while with increasing amount of multifunctional isocyanate the second glass transition temperature is shifted from -7.4 °C (iCN 11) to 56 °C (iCN 13). This behavior is related to the formation of a more rigid isocyanate based polymer network. A higher isocyanate content as well as a lower molar mass of the multifunctional isocyanate compared to the bifunctional isocyanate prepolymer, results in the formation of a higher number of urea bonds and crosslink density, which ultimately leads to an increase in the glass transition temperature of the second polymeric phase. As the lower glass transition temperature stays constant, the shift in the glass transition temperature of the high T_g polymeric phase only depends on the composition (crosslinker content) of the second polymeric phase. iCN 10 only shows one distinct glass transition temperature. This behavior is related to an overlapping of the glass transition temperatures of the pure acrylic and isocyanate prepolymer based networks. It is also possible that an improved miscibility of the more polar bifunctional prepolymer with the acrylic phase plays a role, leading to such a decrease in the domain sizes that these are not resolvable anymore by DMA measurements.

Figure 57 shows the phase contrast images of samples iCN 10 to iCN 13, as well as iCN 8. In all cases, except for iCN 10, phase-separated morphologies are obtained, with the harder phase being continuous. For iCN 10, no clear phase separation is observed, hinting towards a good miscibility of the bifunctional isocyanate prepolymer in the acrylate, leading to non-resolvable domains of the two phases. Thus, it is likely that in conjunction with the *tanδ* curve of iCN 10, a molecular interpenetrating network has been formed. Upon addition of the multifunctional isocyanate, phases separate, leading to similar morphologies, independent on the amount of multifunctional isocyanate.
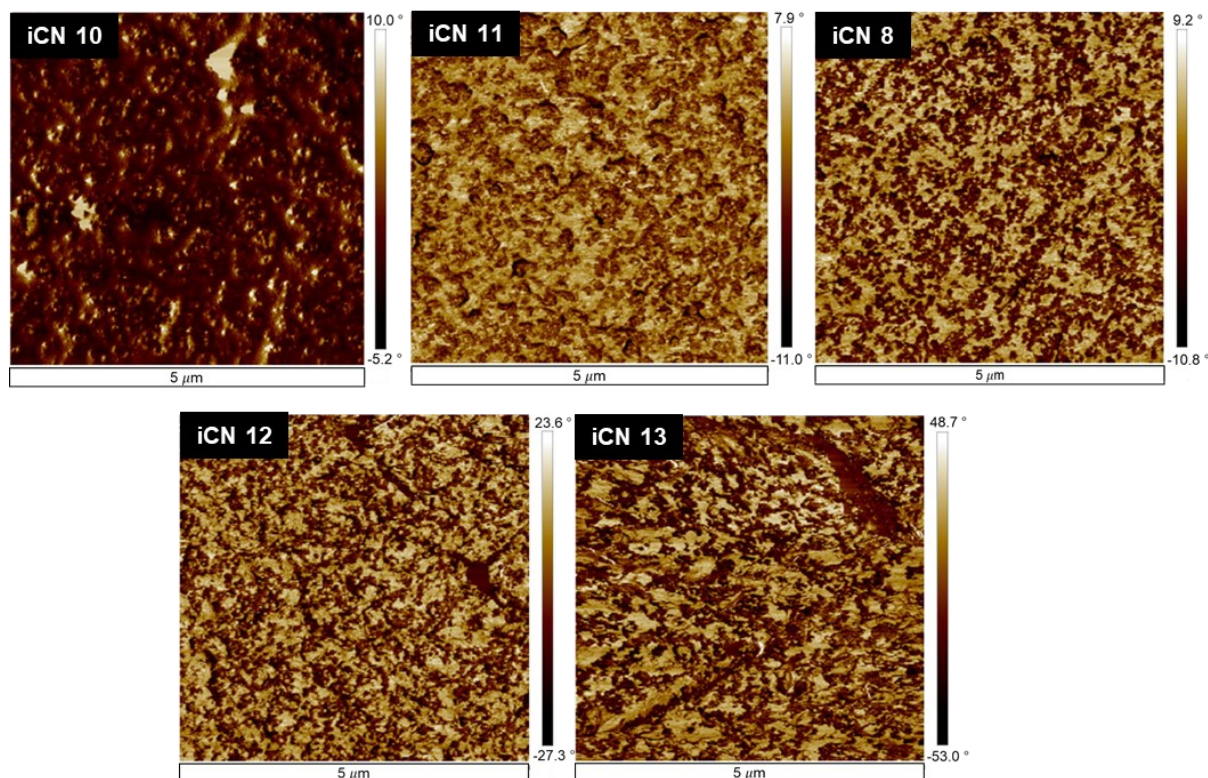
Figure 57. Topographic images of samples iCN 10 to iCN 13, as well as iCN 8, illustrating the effect of varying the composition of the isocyanate based polymeric phase on the morphology at constant acrylate composition.

No significant change in the domain sizes can be observed in iCN 11, 12, 13 and 8, confirming the hypothesis that the polymerization rate of the acrylate is likely to be the main driver for the resulting morphology.

Figure 58 shows the phase distribution of samples iCN 10 to iCN 13 as well as iCN 8. As already stated, iCN 10 shows predominantly soft phase, indicating that the two phases are non-resolvable, which is typical for an interpenetrating network. In all other cases, two distinct peaks can be observed, in which the hard domain peak is slightly higher compared to the soft peak. The peak-to-peak distances, which are an indicator for the degree of phase separation, do not follow a certain trend, which is why no clear statement can be made how the composition of the isocyanate influences the degree of phase separation.
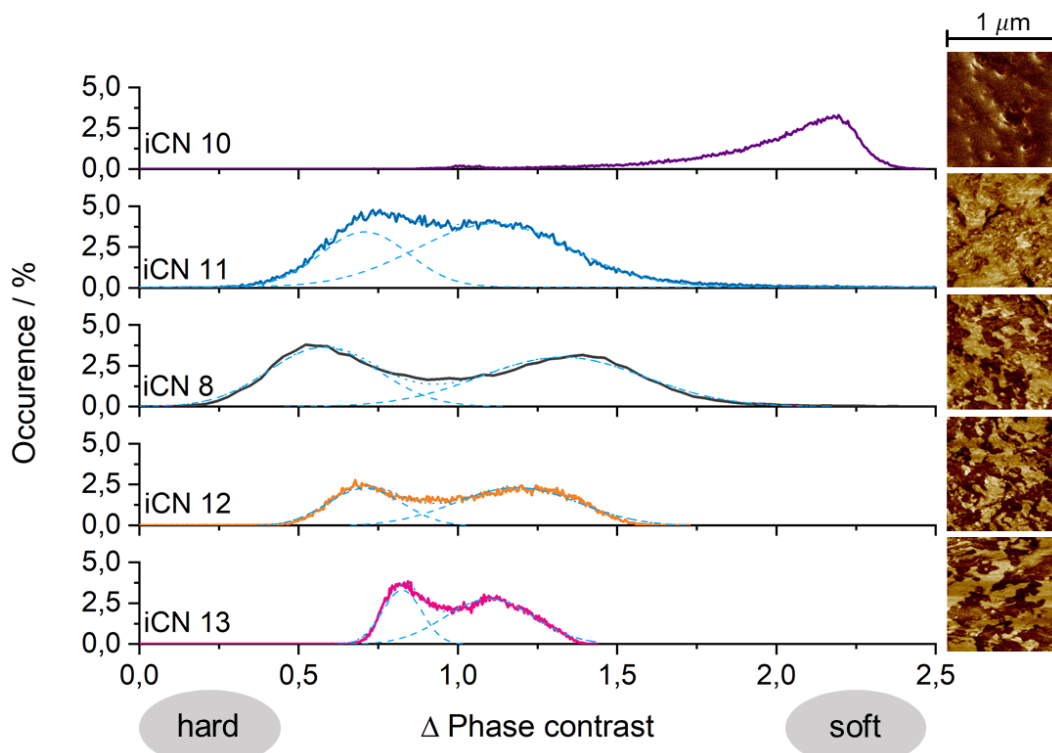
Figure 58. Phase distribution diagram of samples iCN 10 to iCN 13, as well as iCN 8, with corresponding topographic images.

In conclusion, it can be stated that the composition of the acrylic phase is the main influencing factor in directing the continuous phase of the combined networks. The variation in the composition of the second polymeric phase, consisting mainly of the isocyanate components, leads to a change in the thermomechanical properties, as a much harder material evolves upon the addition of the multifunctional isocyanate crosslinker.

A suitable formulation for vat photopolymerization, needs to provide a reasonable viscosity and the ability to form a stable green body. In this light, a high THFA concentration seems to be a good choice in order to obtain a continuous acrylic network, that is likely to result in a stable green body during the printing process. As the main target is to obtain elastomeric-like material properties, it is further important to use low amounts of the multifunctional isocyanate, as this increases the rigidity of the material which contrasts elastomeric material properties. Thus, the acrylic composition of iCN 7 (70 : 30 mono- to diacrylate) in combination with the isocyanate composition of iCN 11 (70 : 30 bifunctional- to multifunctional isocyanate), seems to be a reasonable choice for a suitable printing formulation. In terms of viscosity, all formulations are well suited.

The mechanical properties of the respective samples were further determined by tensile tests, which are presented in the next section.

4.3.3.2   Mechanical Properties

The composition of combined networks has shown to influence the morphology as well as the thermomechanical properties. Tensile tests were further performed on the films to show the influence of the composition on the tensile strength and the elongation at break, which are illustrated in Figure 59. The test specimen were punched out of the films. Five specimen were measured for each sample.
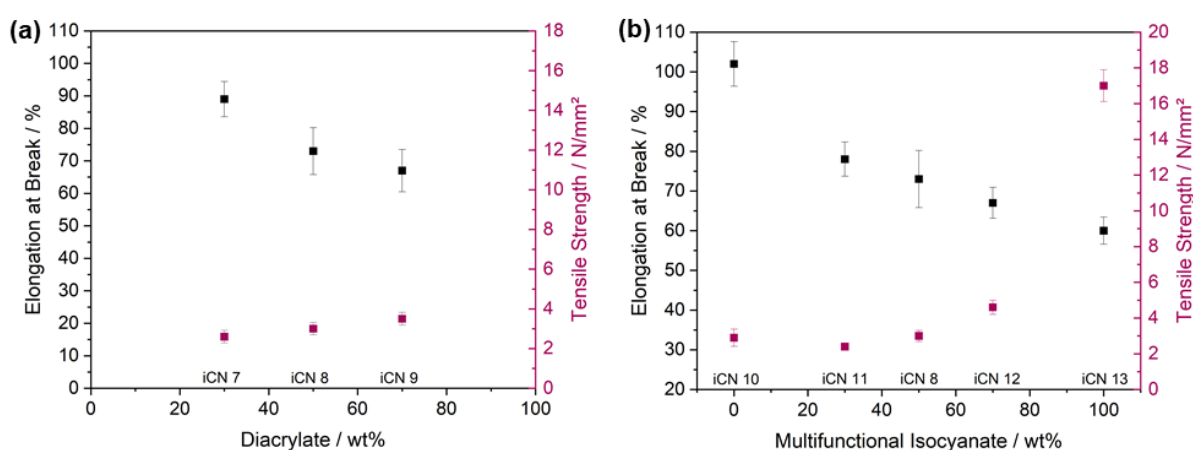

Figure 59. Tensile tests of samples ICN 7 to ICN 13. The elongation at break as well as the tensile strength is given in dependence on a) the amount of diacrylate and b) the amount of multifunctional isocyanate.

In figure Figure 59 a) the elongation at break as well as the tensile strength is given in dependence on the amount of diacrylate. The elongation at break decreases with increasing amount of PEGDA 700. This effect can be explained by the increase in the crosslinking density, which tends to decrease the toughness in the rubber plateau region. At the same time, the tensile strength is slightly increased. Similar effects can be observed when the amount of multifunctional isocyanate is varied. The crosslinking density increases which leads to a decrease in the elongation at break, while the tensile strength increases. The acrylic network AN 2, comprising 50 wt% PEGDA 700 and 50 wt% THFA, possess an elongation at break of 15 % with a tensile strength of 1.3 N·mm^{-2}. In comparison, ICN 8 has an elongation at break of 73 % with a tensile strength of 3 N·mm^{-2}. This means that upon combining the two polymeric networks, the elongation at break was more than quadrupled, while the tensile strength was more than doubled. A strengthening of the acrylic network is thus possible upon combining the two polymeric networks.

4.3.4 3D-Printing of Isocyanate-Acrylate Resins

Based on the investigations shown previously, a high amount of monoacrylate is desired for vat photopolymerization in order to obtain a continuous acrylic phase. With regard to the thermomechanical properties, the material should have a glass transition temperature below use temperature in order to prepare an elastomeric like material in its rubbery state. Accordingly, the first printing trials were based on a THFA to PEGDA 700 ratio of 3 : 2 in combination with a ratio of 3 : 1 of bifunctional to multifunctional isocyanate prepolymer. The overall ratio between acrylate and isocyanate was kept at 1:1.

The photoinitiator of the printing formulation was adapted to the 405 nm light source of the printer. Instead of 2-hydroxy-2-methylpropiophenone (Omnirad 1173), a blend based on three different phenylphosphine oxides (Omnirad BL 750) was chosen, absorbing at 405 nm, with a concentration of 0.5 wt%. The printing process further requires to add an inhibitor to avoid dark curing. Dark curing means the progression of the polymerization reaction in areas adjacent to illuminated areas. For this purpose, 2,5-Bis(5-tert-butyl-2-benzoxazolyl)thiophene was used with a concentration of 0.05 wt%. The role of the inhibitor is mainly to improve the resolution in x,y-direction. To further control the resolution in z-direction, 2′,4′,5′,7′-tetrabromo-3,4,5,6-tetrachlorofluorescein was added as an UV absorber with a concentration of 0.1 wt%. UV absorbers are frequently used in VPP in order to limit the penetration of light to the thickness of one layer, preventing a polymerization below the illuminated voxel.[253] The basic compositions of the two resin formulations, further referred to as P 1 and P 2, are illustrated in Table 16.

Table 16. Basic composition of the two printing formulations P 1 and P 2, with the corresponding viscosities and gel points, determined by UV rheology (NCO 1 and NCO 2: bifunctional isocyanates; allophanate: multifunctional isocyanate; PEGDA 700: diacrylate; THFA: monoacrylate).

m [g]	P 1	P 2
NCO 1	75	–
NCO 2	–	75
Allophanate	25	25
PEGDA 700	40	40
THFA	60	60
η [mPa·s]	233	191
Δt [s]	15	8

The weight ratios between PEGDA 700 and THFA as well as between multifunctional and bifunctional isocyanate are kept constant for both printing formulations. For P 1, NCO 1 is used, which is the prepolymer based on IPDI and pTHF 1000. For P 2, NCO 2 is chosen, which is the biobased prepolymer based on PDI and a polyether carbonate. The viscosities of the two formulations are with 233 mPa·s for P 1 and 191 mPa·s for P 2, ideally suited to be printed by standard vat photopolymerization based printers.

In order to evaluate the printing parameters, photo-rheology was performed first. The light source of the photo-rheometer is 405 nm, which is identical to the light source of the printer. The light intensity of the light source in the printer was measured, enabling to set a similar intensity for the photo-rheology measurements. Additionally the gap of the rheometer was set to 0.1 mm, corresponding to the thickness of one layer in the printing process. The time difference between the exposition to light and the crossover of storage- and loss modulus, further referred to as gel point, functioned as indication to choose the exposure time of the first layer for the printing process. Figure 60 illustrates the results of the photo-rheology measurements. For P 1 the gel point was obtained after 15 s, while for P 2 the gel point was already reached after 8 s (see also Table 16).
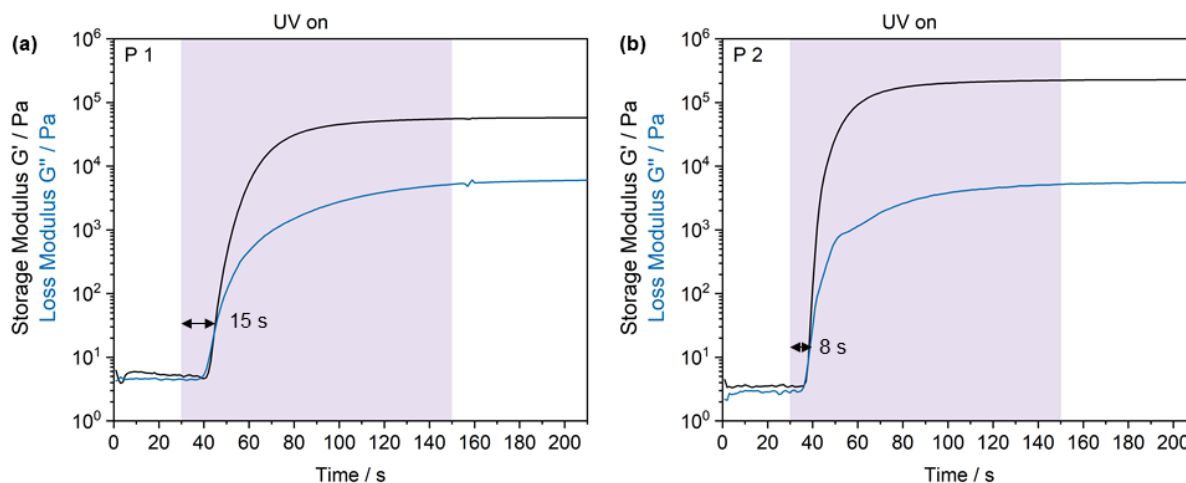

Figure 60. Photo-rheology measurements of printing formulations P 1 and P 2, giving the storage- and loss modulus in dependence on the time and UV exposure.

Tensile bars were chosen as printing objects, to enable the mechanical characterization of the resulting materials. The test specimen were printed flat, in x,y-direction. This has the advantage, that one print job is finished within a few minutes. Due to the fact that the material is soft and only a partially cured green body is obtained after the printing process, it was difficult to print the

tensile bars in z-direction, as the detachment forces during the print job often resulted in the failure of the print job.

Figure 61 schematically shows the manufacturing process of 3D printed tensile bars. At first, a CAD-design file is sliced into multiple layers using appropriate software. The so-called STL file is then sent to the printer, where the printing process is started. After the print job is finished, the printed specimen is removed from the platform. In this case, it is referred to as green body, since the isocyanates did not react during the printing process and still need to be cured in a thermal post-processing step. After 17 h at 100 °C, the final 3D printed tensile bar is obtained. The corresponding printing parameters are given in the experimental section.
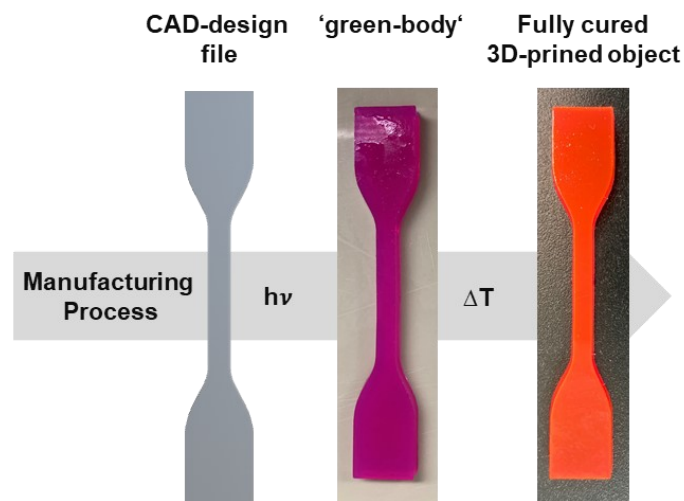

Figure 61. Schematic illustration of the manufacturing process of 3D printed tensile bars from given dual-cure resin formulations.

The color of the printed specimen is related to the fluorescein derivative that has been added as UV absorber to the resin formulation. The color change from the green body to the fully cured 3D printed object is also related to the fluorescein dye, which changes color in dependence on the pH-value as well as the polarity of the polymer matrix.[254] As the target was the preparation of elastomeric like materials, cyclic stress-strain curves were measured. The results are given in the next section.

4.3.4.1 Mechanical Properties

The mechanical properties of the printed tensile bars were measured by cyclic tensile tests in order to determine the stress-strain behavior under cyclic loading. That way, the key characteristics of elastomers, i.e. the reversible deformation after applying a strain force, can be

investigated. The results were correlated to the loss factor, determined by DMA measurements. The corresponding results are illustrated in Figure 62.
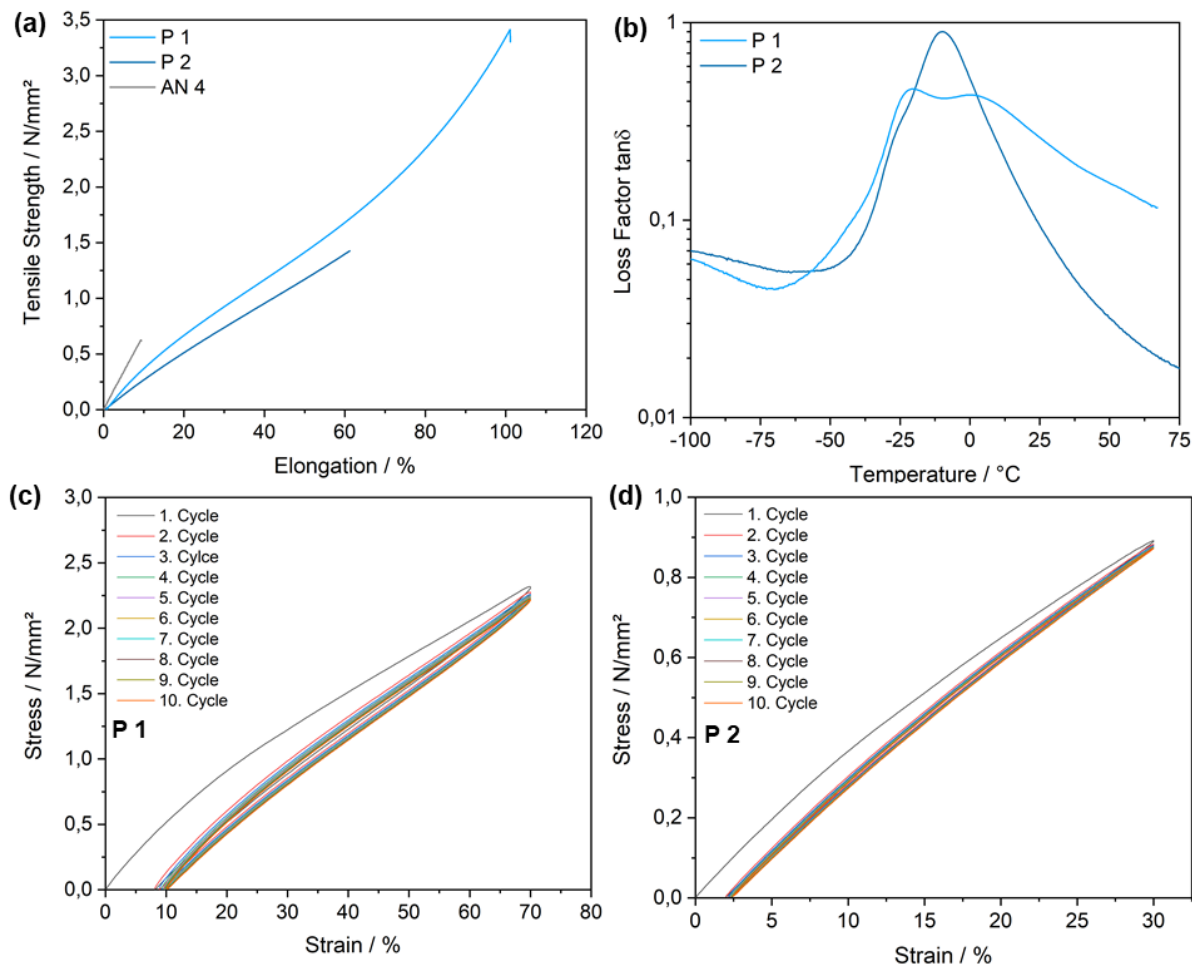

Figure 62. a) depicts the stress-strain behavior of printed tensile test bars of P1, P2 and the reference Ref.1. b) gives the loss factor against temperature determined by DMA measurements of P 1 and P2. c) and d) show the cyclic stress-strain behavior of printed tensile bars for c) P 1 and d) P 2.

In a first step, tensile tests were performed of the printed specimen in order to determine the elongation at break (Figure 62 a). An additional acrylic reference network AN 4 (acrylic network 4) was prepared by a standard UV coating process. It represents the properties of the neat acrylic phase, comprising 40 wt% PEGDA and 60 wt% THFA. In both dual-cure formulations P 1 and P 2, the elongation at break as well as the tensile strength exceed the mechanical properties of AN 4 as can be seen in Figure 62a. This illustrates the feasibility of the dual-cure concept. For P 1, an elongation at break of 101 % (individual value) and a tensile strength of 3.4 N·mm^{-2} was measured, while for P 2, the elongation at break amounts to 63% (individual value), with a tensile strength of 1.4 N·mm^{-2}. The different behavior of P 1 and P 2 can be correlated to the differences

as presented by the loss factor from the DMA curves (Figure 59 b). For P 2, the loss factor is < 0.1 at room temperature, which indicates that the material is already in the rubbery plateau region. In contrast to that, for P 1, the loss factor is > 0.1, i.e. the material behaves more viscoelastic, thus dissipates more energy.

This behavior is further confirmed by the hysteresis loops. The elongation for the respective measurement was chosen based on the preceding tensile tests. As the elongation at break was higher for P 1, a strain of 70 % was chosen, while for P 2, a lower elongation of 30 % was considered to be appropriate for the corresponding tests. The area enclosed by the loading-unloading curves can be regarded as the energy that is dissipated, i.e., the energy absorbed during loading is not fully recovered. The work of deformation is higher for P 1 compared to P 2, which means that in P 1, a larger amount of energy is dissipated during deformation.

Since the work of deformation is comparably low for both materials, it can be stated that both materials show a largely energy elastic deformation behavior. This is of interest for applications in e.g. shoe soles and tires, where the deformation energy should be as low as possible. A significant strengthening of the acrylic network upon combining the two polymeric materials was successfully achieved.

4.3.5 Alternative Post-Processing Option

The main reaction in the dual-cure resin systems described in chapters 4.2 and 4.3 was a polyurea formation, potentially by reaction of the respective diisocyanates with water, instead of the intended trimerization reaction.

Further experiments were performed, in which no catalyst was added to the resin formulation. Instead of a purely thermal post-curing process, the printed specimen were immersed into hot water, to achieve curing. This method is attractive from a toxicological point of view, as no catalyst is needed and additionally, increases the pot-life or open time of the resin formulation. The resin formulation based on P 1 was chosen, which is further referred to as P 1.1 and the thermomechanical properties were evaluated by dynamic mechanical analysis. A comparison between the printed specimens that were cured at elevated temperatures containing the catalyst and the samples cured in hot water without catalyst, was performed in order to check if the two methods can be used interchangeably. The post-processing concept is illustrated in Figure 63.
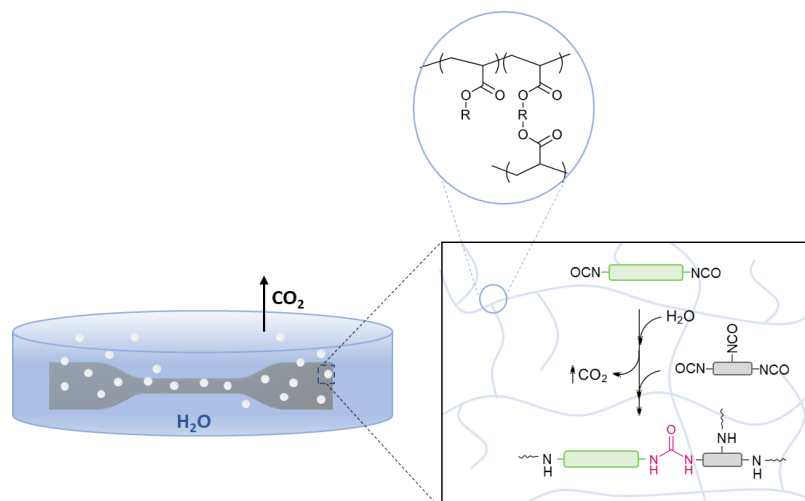
Figure 63. Schematic illustration of a post-processing concept with water and the corresponding reactions taking place.

Time-dependent ATR FT-IR measurements were performed in order to monitor the reaction of the isocyanate groups with water, which are illustrated in Figure 64 a and b. These measurements were performed on the surface as well as inside the printed specimen. For the latter, the printed tensile bar was sliced and placed onto the ATR crystal. As expected, the carbonyl stretching vibration at 2265 cm^{-1} decreases faster on the surface of the printed specimen compared to the inner part. However, after 24 h, all isocyanate groups were converted, also inside the printed part, indicating a full conversion of the isocyanates. It is reasonable to assume, that the acrylic network based on THFA and PEGDA 700 shows some swelling in hot water, providing the reaction partners for a reaction of the isocyanate groups with water also inside the specimen. A potential problem of this reaction path, with regard to shrinkage as well as contamination, could be the migration of the dispersed isocyanate prepolymers into the water phase. Measuring the pH-value of the water phase might be a good indication to determine the migration of the isocyanate out of the printed specimen. Determining the shrinkage of the printed object might also be an alternative to evaluate if the isocyanate prepolymer stays inside the printed specimen.
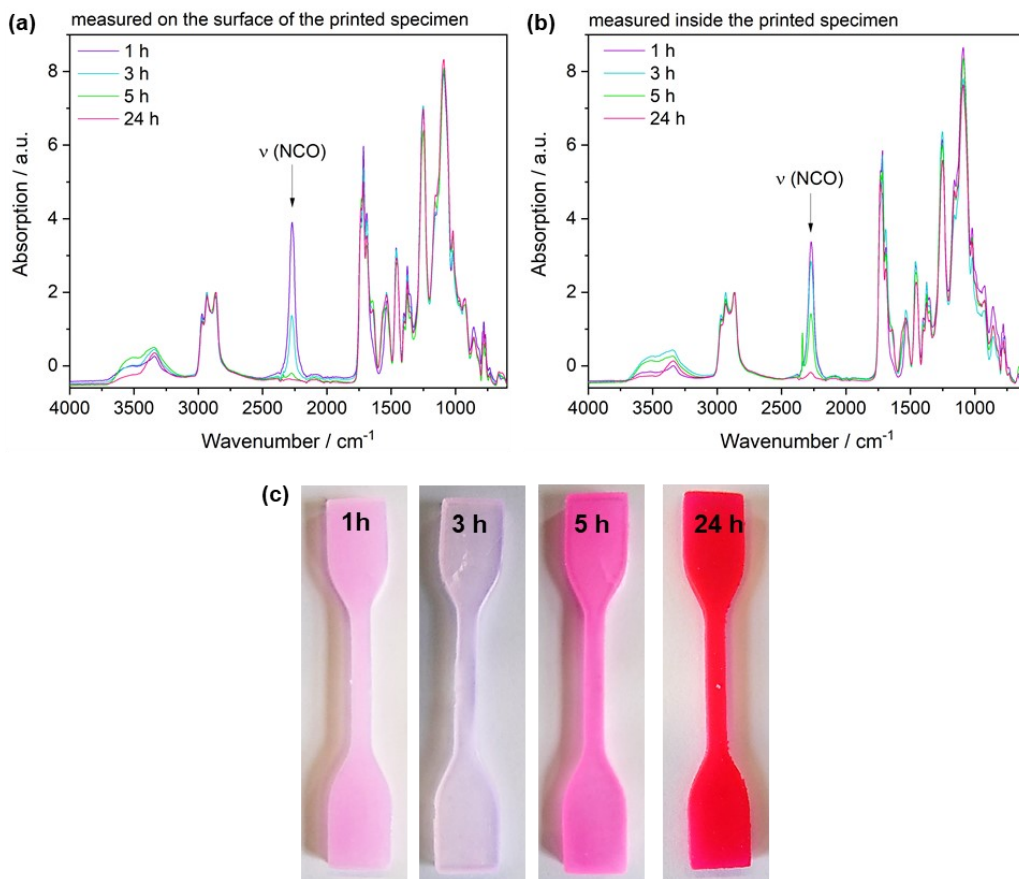
Figure 64. (a) and (b) FT-IR measurements monitoring the progress of the post-processing reaction and (c) images of the printed specimen after 1 h, 3 h, 5 h and 24 h of water exposure of P 1.1.

Figure 64 c shows images of the printed specimen after 1 h, 3 h, 5 h, and 24h of water exposure. An interesting side effect is the change in color upon the progression of the curing reaction. This effect can be related to the fluorescein dye and its ability to change color in dependence on the pH-value and the polarity of the surrounding polymer network.[254]

The thermomechanical properties of P 1.1 were compared to P 1 and are illustrated in Figure 65.

Figure 65. DMA measurements comparing the thermomechanical properties of P 1 and P 1.1.
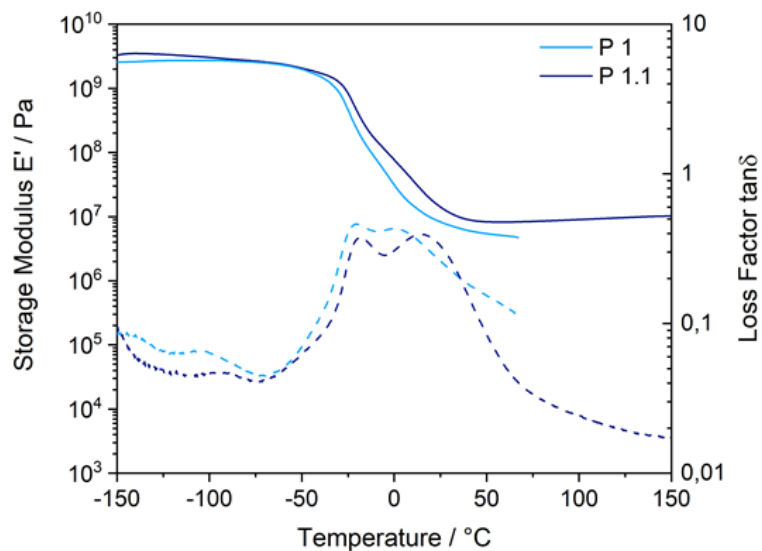
In both cases, two distinct glass transition temperatures can be observed. The lower T_g at about - 22 °C can be attributed to acrylate rich domains while the higher T_g can be related to the respective polyurethane based networks. While there is no shift of the lower T_g, the second glass transition temperature is shifted to higher temperatures for P 1.1, from 6 °C for P 1 to 15 °C for P 1.1. The storage modulus in the rubbery plateau, which gives an indication of the crosslinking density of the corresponding materials seems to be higher for P 1.1 than for P 1. In principle, the crosslinking density of P 1 should be higher than for P 1.1, as at least some isocyanurate ring structures should be present in the networks. This further holds true for the glass transition temperature that should be either similar or lower for P 1.1 than for P 1. It might be the case, that for P 1.1, stronger hydrogen bonding takes place, as it is assumed that more polyurea groups are present that are known for their ability of strong hydrogen bonding.

The results show, that a post-processing with water results in comparable material properties. The advantage is that no catalyst needs to be added to the resin formulation, increasing the stability of the resin and reducing toxicological issues. Especially the latter might be advantageous when the 3D printed objects are considered for skin contact applications, as it is known, that catalysts may trigger skin sensitizations.

4.3.6 Summary

In summary, it was possible to develop a dual-cure concept that enabled the 3D printing of objects with largely energy elastic behavior. It was found that the combination of monomeric acrylates and isocyanate terminated prepolymers yield homogenous mixtures with viscosities below

500 mPa·s, which is ideally suited for VPP. First screening experiments showed that phase-separated networks evolved upon the sequential polymerization of the acrylates and the isocyanates. It was further found, that the intended isocyanurate formation of the isocyanate did not take place, but instead a polyurea formation, presumably by a reaction of the isocyanates with humidity in the curing oven. It was shown that a stable rubbery plateau was only obtained by the addition of a multifunctional polyisocyanate to provide further chemical crosslinking in addition to chain elongation and physical crosslinking by the hydrogen bonds between urea groups. However, the glass transition temperature and the mechanical properties of the 'inverse' combined networks containing multifunctional polyisocyanates were significantly influenced.

A detailed investigation by DMA and AFM showed that by changing the degree of crosslinking of the acrylic phase, influences the morphology. It was found that high fractions of monoacrylate lead to the formation of a continuous acrylate phase, while high fractions of diacrylate resulted in the formation of a continuous polyurea phase. Changing the crosslinking density of the polyurea phase did not lead to a significant change in the morphology, but showed a large impact on the thermomechanical properties. With increasing amount of multifunctional isocyanate, the rigidity of the second polymeric phase increased, as was observed by a shift to higher temperatures of the corresponding glass transition temperature.

Printing trials of these resin formulations were successful and lead to tensile bars with high resolution. The energy elastic behavior was investigated and showed that the materials can be reversibly deformed with only little loss in energy.

It was further shown that it was possible to print and post-process the resin formulation without the addition of a catalyst by simple immersion into hot water, leading to comparable material properties. The post-processing with water represented an easy-to-implement post-processing method and is of potential interest from a toxicological point of view, since it avoids the addition of a potentially critical catalyst.

5 Summary

The combination of acrylate- and polyisocyanate based precursors as main components in novel 3D printing formulations for vat photopolymerization, has shown to provide a versatile tool-box, giving access to materials that cover a broad profile of properties, as schematically summarized in Figure 66.
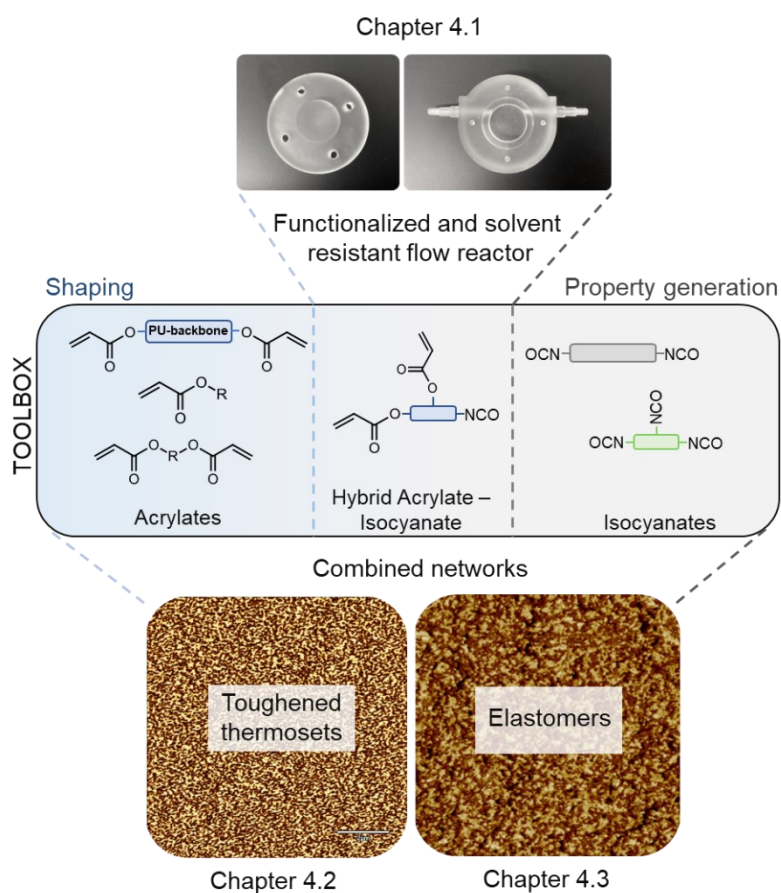
Figure 66. Schematic summary of the achievements presented in this thesis. Dual-cure resin systems based on acrylates and polyisocyanates as well as hybrid isocyanato-acrylates were investigated, yielding solvent resistant and functionalized flow reactors, toughened thermosets as well as elastomeric 3D printed materials.

In all cases, the acrylates were used to create the shape of the 3D printed object by a UV induced radical polymerization, while the desired properties were generated by a subsequent reaction of the isocyanates. The precursors were combined in different ways, adapted to the requirements of the printing process. Difunctional polyurethane acrylates were combined with low viscous polyisocyanates, leading to toughened thermosets. Reversely, difunctional isocyanate

prepolymers were combined with low viscous mono- and difunctional acrylates, resulting in elastomeric material properties. The use of a hybrid precursor in which both functionalities were combined in one molecular structure, was further employed to generate solvent resistant and functionalized 3D printed surfaces, with application as reaction containers in chemical synthesis. These different combinations of acrylates and isocyanates were used to exemplarily show the large variability of the available precursors and the versatility of the dual-cure approach for the development of high performance materials with potential application in vat photopolymerization based printing technologies.

In the first chapter, a flow reactor for chemical synthesis applications was developed with the target to obtain solvent resistance and to enable surface-functionalization. For this purpose, the base resin was provided by a polyurethane acrylate, containing pending reactive isocyanate groups (hybrid acrylate-isocyanate). During the printing process, the isocyanate groups were preserved and thus provided available reactive moieties for a post-reaction with water, which lead to the formation of a polyurea. The solvent stability was tested an clearly outperformed commercially available resins, with regard to solvent uptake as well as degradation. Additionally, high transmittance as well as high temperature stability was obtained. The reactive isocyanate functionalities were further used to functionalize 4-aminobenzophenone on the surface of the 3D printed object. The combination of high solvent resistance with the ability of functionalization with 4-aminobenzophenone was exploited to print a flow-reactor, in which the photooxygenation of citronellol was performed by Renner. The overall concept as well as the most important results are summarized in Figure 67.

In summary, the developed resin is ideally suited for the fabrication of chemical reaction ware, and in combination with the ability of functionalization, provides multiple options to access catalytic surfaces. The successful photooxygenation of citronellol in high turnovers, conducted inside a 3D-printed flow reactor can be regarded as proof of concept. The resins opens up a huge variety of applications.
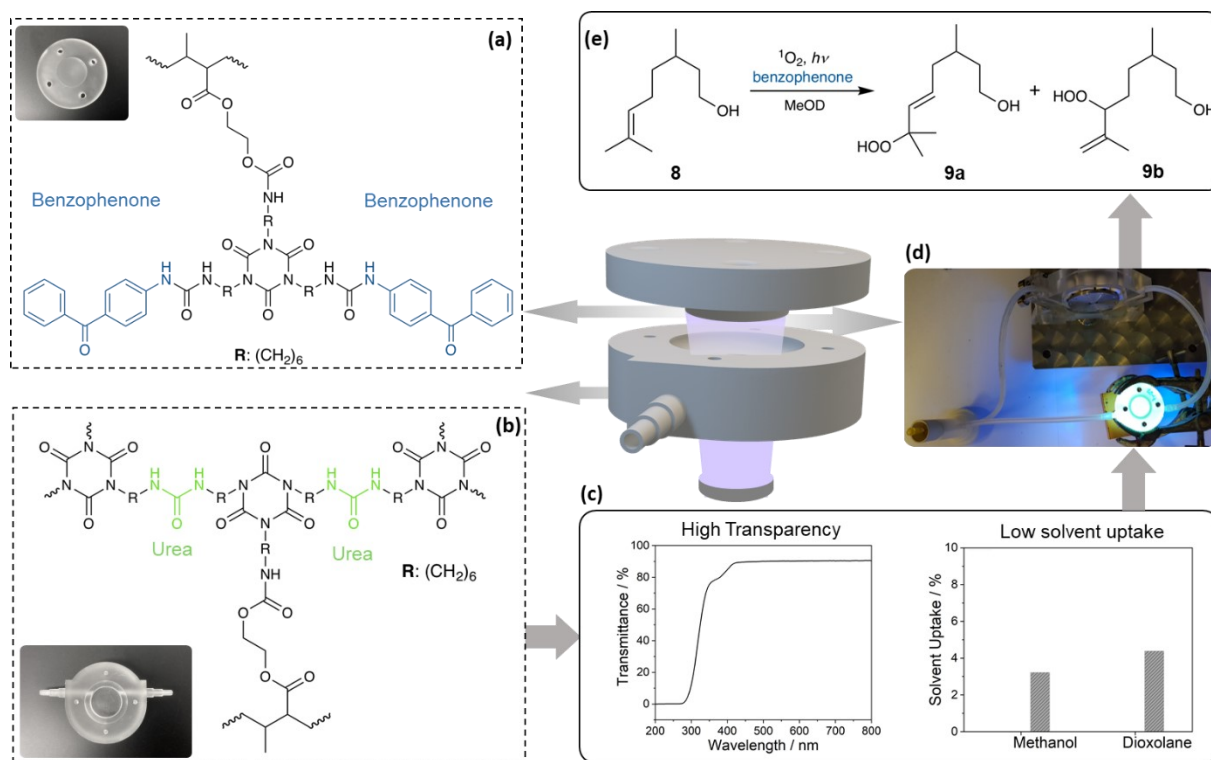
Figure 67. Schematic summary of the concept and results obtained in chapter 4.1. A flow-reactor was printed and post-processed with water (b), yielding high transparency as well as solvent resistance (c). The reactor cover was locally functionalized with 4-aminobenzophenone (a). Combining both parts enabled to conduct the photooxygenation of citronellol in the flow (d) and (e).

In chapter 4.2, well defined polyurethane acrylates (PUA) were synthesized that were combined with a low viscous multifunctional polyisocyanate (allophanate) to yield a dual-cure resin system. The sequential polymerization of the two types of monomers was investigated with different weight ratios of polyurethane acrylate and multifunctional polyisocyanate. It was found that after the UV induced radical polymerization of the PUA, polymerization induced phase separation took place. The second polymerization reaction was performed at elevated temperatures and, against expectation and original design, no pure polyisocyanurate network formation took place, but predominantly a polyurea network was formed, confirmed by FT-IR spectroscopy.

Dynamic mechanical analysis was performed to investigate the thermomechanical properties. It was found that the combined networks were phase-separated with two distinct glass transition temperatures, of which the lower was attributed to the acrylic network and the higher was ascribed to the polyurea network. Theoretical calculations of the storage modulus in dependence on the temperature were performed, using a model that assumes a completely phase-separated morphology. The accuracy of the fit gave an indication on the degree of phase separation, when compared to the experimental DMA data. For high amounts of allophanate, the fit was well suited,

assuming that the phases were almost fully separated. In contrast to that, with decreasing amount of allophanate, intermixing of the two networks took place as the fit was less in line with the experimental DMA results.

This behavior was further proven by AFM measurements. Clearly phase-separated morphologies were obtained for high multifunctional polyisocyanate contents, in which the polyurethane acrylates were present as dispersed particles in a continuous polyurea network. At an even weight ratio of the two networks, both phases were equally present, indicating dual-phase continuity. Further decreasing the amount of multifunctional isocyanate, lead to finely dispersed polyurea particles in a continuous polyacrylate network.

Tensile tests and the calculation of the toughness revealed that it was possible to reinforce the acrylic network upon the incorporation of the isocyanate based particles. Additionally, the polyurethane acrylate particles dispersed in the polyurea network lead to an elastification of the pure polyurea network. The increase in toughness in comparison to the neat polymeric materials was 10-fold for the best material. Thus, the target to obtain a toughened thermoset was successfully achieved.

It was further possible to transfer the concept of toughening via phase separation to vat photopolymerization based printing technologies. First printing trials showed the feasibility of the concept.

In summary, the toughening of photocurable resins by incorporation of a second polymeric phase is highly versatile and especially the combination of acrylates and isocyanates represents multiple options to improve current resin systems for vat photopolymerization. Figure 68 schematically summarizes the concept and the results obtained.
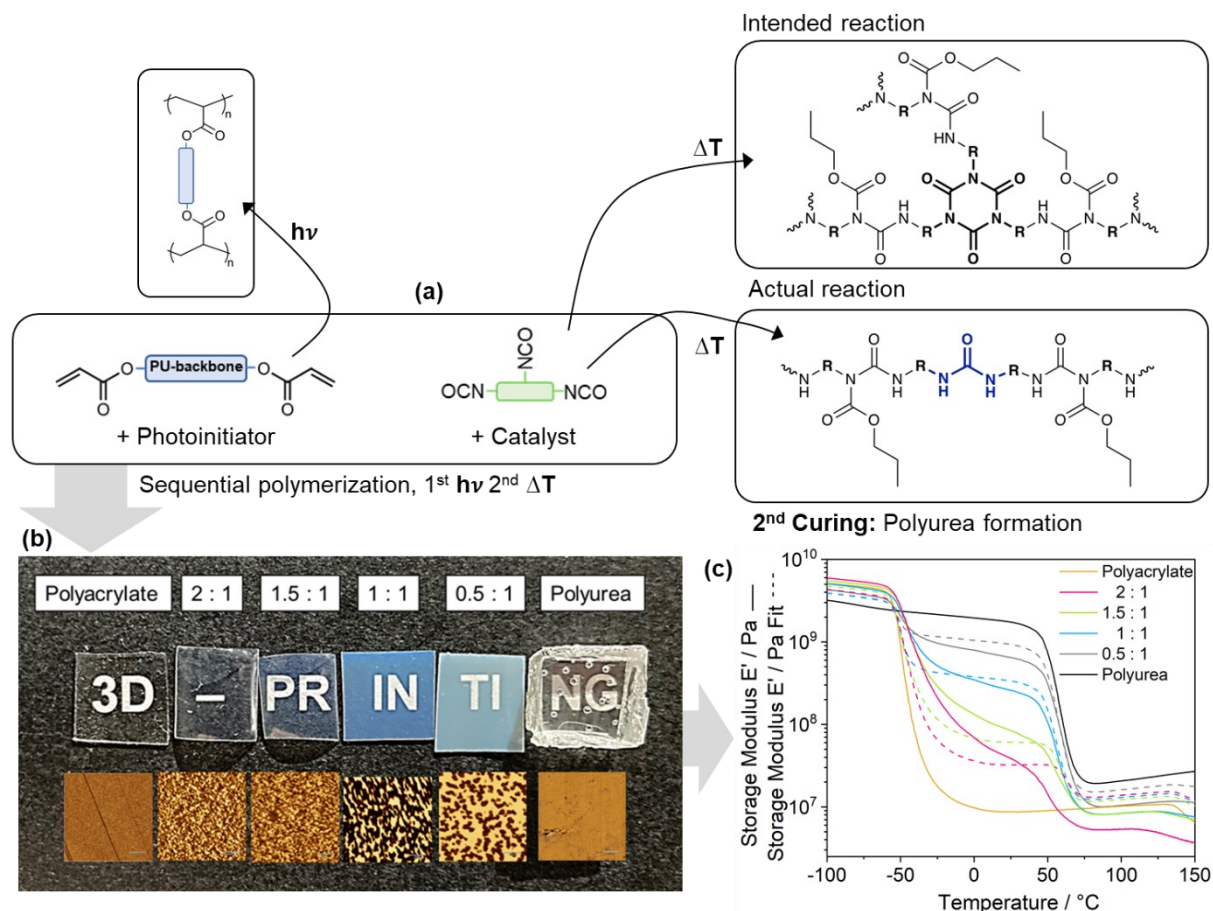
Figure 68. Schematic summary of the results obtained in chapter 4.2. Polyurethane acrylates were mixed and sequentially polymerized with a low viscous HDI based polyisocyanate. The second curing reaction lead to the formation of a polyurea network (a). The monomers were used in different ratios and the resulting combined networks possessed a phase-separated morphology, as determined by AFM (b) and DMA (c).

In chapter 4.3 a printable resin system based on isocyanate terminated prepolymers and low viscous monomeric acrylates was developed. The sequential polymerization of the acrylates and isocyanates lead to combined networks with elastomeric material properties. Structural investigations of the combined networks by FT-IR spectroscopy showed that a polyurea was formed upon the second heat induced reaction of the isocyanates.

The crosslinking density of each polymeric network was systematically varied and the influence on the morphology as well as the thermomechanical properties was investigated. It was found that high amounts of monoacrylate were favorable to obtain phase-separated networks, in which the acrylic network is the continuous phase. High amounts of multifunctional isocyanate did not lead to a significant change in the morphology, but showed a large impact on the thermomechanical properties. With increasing amount of multifunctional isocyanate, the rigidity of the second polymeric phase increased, as was observed by a shift to higher temperatures of the

corresponding glass transition temperature. It was found that low crosslinking densities of both polymeric phases lead to elastomeric material properties.

Printing trials, were successful and lead to tensile bars with high resolution. The energy elastic behavior was investigated and showed that the materials can be reversibly deformed with only little loss in energy. An elongation at break of 101 % and a tensile strength of 3.4 N·mm^{-2} was obtained for a printed specimen.

At last, it was found that the second curing reaction can be performed in hot water instead of the oven and no catalyst needs to be added to the resin formulation. Prints were successfully performed and full through cure and almost identical mechanical properties were obtained in comparison to a catalyst containing resin system. This method represents a promising method for the preparation of 3D printed elastomers. Figure 68 schematically summarized the concept and the results obtained.
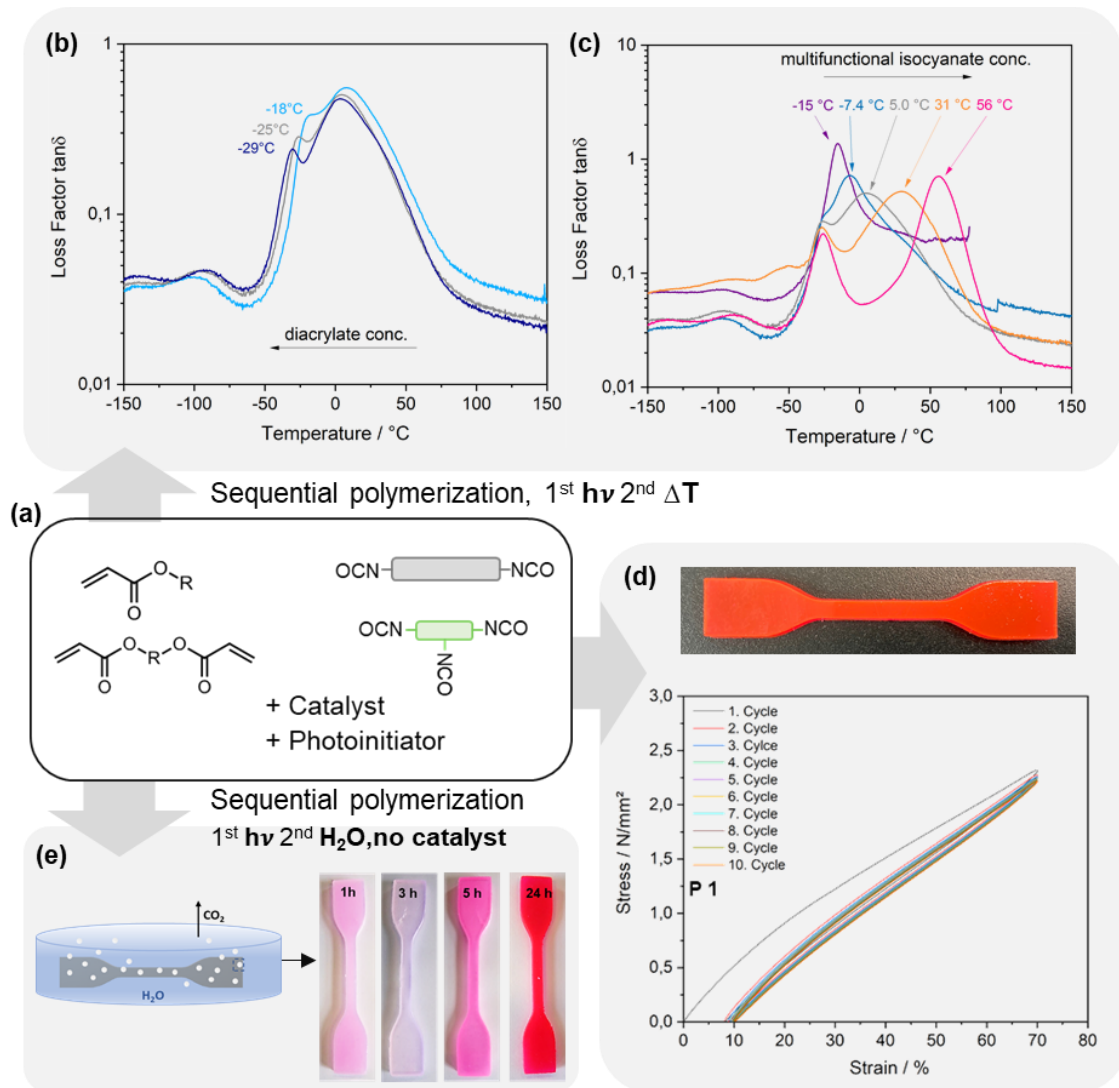
Figure 69. Schematic summary of the results obtained in chapter 4.3. Mono- and difunctional monomeric acrylates were mixed and sequentially polymerized with bi- und multifunctional isocyanates (a). The crosslinking density of both networks was systematically varied to illustrate the influence on the thermomechanical properties (shift in *tanδ*) (b) and (c). Printing trials were successful and the material showed nearly ideal energy elastic behavior (d). Post-processing the material in hot water lead to similar material properties compared to a curing in the oven without water (e).

In conclusion it can be stated that the dual-cure resin systems investigated in this thesis contribute to the continuous improvement of 3D printable materials for VPP and will in the future help to revolutionize the way parts are manufactured.

6 Experimental Part

The following section summarizes the experimental procedures of chapter 4, including the chemicals and characterization methods that were employed.

6.1 List of Chemicals

The chemicals that were used are given in Table 17. Abbreviations, CAS-numbers, purity and manufacturer are given accordingly.

Table 17. List of chemicals that were employed for the experiments conducted in this work.

Name	Abbreviation	CAS	Purity	Manufacturer
Isocyanates				
Desmodur® H	HDI	822-06-0	n.d.	Covestro AG
Desmodur® N3400	Uretdione	–	n.d.	Covestro AG
Desmodur® N3600	Trimer	3779-63-3	n.d.	Covestro AG
Desmodur® XP2860	Allophanate	–	n.d.	Covestro AG
Desmodur® 3200	Biuret	–	n.d.	Covestro AG
Desmodur® 3900	asym. Trimer	–	n.d.	Covestro AG
Isophorone Diisocyanate	IPDI	4098-71-9	n.d.	Covestro AG
Pentamethylene-1,5-diisocyanate	PDI	4538-42-5	n.d.	Covestro AG
Polyols				
Desmophen® C1100	PC 1000	–	n.d.	Covestro AG
Desmophen® 1111 BD	PPG 1000	–	n.d.	Covestro AG
Desmophen® 2061 BD	PPG 2000	–	n.d.	Covestro AG
Cadyon® LC 07	PEC 1000	–	n.d.	Covestro AG
Acrylates				
Dipropyleneglycol diacrylate	DPGDA	57472-68-1	80 % stabilized with MEHQ	abcr
Isobornyl methacrylate	IBOMA	7534-94-3	≤ 100 %	Sigma Aldrich
Polyethylenglycol diacrylate M_n = 700 g mol^{-1}	PEGDA	26570-48-9	contains 100 ppm MEHQ / 300 ppm BHT as inhibitor	Sigma Aldrich
Tetrahydrofurfuryl acrylate	THFA	2399-48-6	contains 500 ppm inhibitor	Sigma Aldrich
2-Hydroxyethylmethacrylate	HEMA	868-77-9	contains ≤250 ppm MEHQ as inhibitor, 97%	Sigma Aldrich
Inhibitors				

Butylhydroxytoluene	BHT	128-37-0	≥ 99%	Sigma Aldrich
2,5-Bis(5-tert-butyl-2-benzoxazolyl)thiophene	BBOT	7128-64-5	99%	abcr
Photoinitiatiors				
Omnirad BL 750	BL 750	–	n.d.	iGM Resins
Omnirad 1173	–	7473-98-5	n.d.	iGM Resins
Catalysts				
Tin(II) ethylhexanoate	$Sn(Oct)_2$	301-10-0	92,5-100%	Sigma Aldrich
Dibutyltin dilaurate	DBTL	77-58-7	95 %	Sigma Aldrich
Others				
2′,4′,5′,7′-tetrabromo-3,4,5,6-tetrachlorofluorescein	–	–	n.d.	Sigma Aldrich
Dibutyl phosphate	–	107-66-4	≥ 97.0%	Sigma Aldrich

6.2 Characterization Methods

The following section summarizes the methods that were employed to analyze and characterize the materials described in chapter 4.

6.2.1 Nuclear Magnetic Resonance Spectroscopy

^{1}H-NMR spectroscopy was performed using a Bruker AV III HD 600 spectrometer. Deuterated benzene (C_6D_6) was used as the solvent. The spectra were evaluated using MestreNova and were calibrated to the chemical shift of C_6D_6 (7.15 ppm).

6.2.2 Fourier Transform Infrared Spectroscopy

FT-IR/ATR spectroscopy was conducted on a Bruker Tensor II, equipped with an ATR (attenuated total reflection) diamond crystal. The evaluation was performed using OPUS Version 7.5 software. For all spectra a baseline correction was performed and the min-max normalization method was applied based on the -CH_2 vibration between 2800 cm^{-1} and 3100 cm^{-1}. For all samples, the absorption, given in arbitrary units (a.u.) was measured.

6.2.3 UV-Vis Spectroscopy

UV-Vis spectroscopy was measured on a PerkinElmer UV/Vis/NIR Spectrophotometer Lambda 950. The samples were measured from 900 nm to 200 nm. Turbidity measurements were performed on a BYK Haze Guard plus.

6.2.4 Gel Permeation Chromatography

Gel permeation chromatography (GPC) measurements were performed on four PSS SDV analytical columns (2 x 50 Å, 5 µm; 2 x 100 Å, 5 µm) using an Agilent HP 1100 series pump and an Agilent 1200 series UV detector (230 nm) with tetrahydrofuran as elution solvent at 35 °C and a flow of 0.6 ml·min^{-1}. The molar masses were determined by comparing the elution volume to a standard calibration based on polystyrene.

6.2.5 Isocyanate Titration

The isocyanate content was determined according to DIN EN ISO 14896. The method represents a type of end-group analysis, in which the isocyanate groups are reacted with a defined excess of dibutyl amine. The amount of unreacted amine can be determined by titration with hydrochloric acid, enabling the back-calculation of the isocyanate content. For this purpose, a defined amount of isocyanate containing sample was dissolved in acetone. The addition of dibutyl amine and the potentiometric titration with hydrochloric acid was performed automatically using a Metrohm Tetrino Plus.

6.2.6 Preparation and UV Curing of Films

For screening experiments, free films were prepared by mixing the corresponding substances, using the speedmixer ARE-250 CE by Thinky for 2 minutes with 2000 rpm. The viscosity of resin formulations was measured using a MCR 51 viscosimeter in a cone-plate configuration CP25-2 by Anton Paar Ltd.. Subsequently, the mixtures were applied onto glass substrates, pretreated with soy lecithin solution (0.5 wt % in ethyl acetate), using a doctoral blade with a 400 µm gap. The films were UV cured using a Superfici UV plus, UV curing machine (Superfici/Elmag, type TU-RE 3000/ Plus), equipped with gallium- and mercury radiation sources. The belt speed was 5 m·min^{-1}, resulting in a total energy intensity of 1300 mJ·cm^{-2}.

The compositions of the resin formulations that were treated accordingly is given in the respective experimental chapter.

6.2.7 3D Printing

Prints were performed on an ASIGA Pro2 75 printer, working with the digital light processing technology. The light source has a wavelength of 385 nm with a total energy input of 10 mW·cm^{-2}. Sliced files were created using the corresponding Composer Software. A minimum amount of resin

formulation of 600 g is needed, in order to guarantee a sufficient backflow of the resin. Further prints were performed on an Anycubic PhotonS working with the digital light processing technology (LCD display), equipped with a 405 nm light source, resulting in an energy input of 5.5 mW·cm^{-2}. Sliced files were created using the corresponding PhotonS software. A minimum amount of resin formulation of 100 g are needed, in order to guarantee a sufficient backflow of the resin.

The general printing process requires to upload the digital construction file into the corresponding printer software. The exposure times of each layer to UV light can be specified as well as the number of so-called bottom- and model layers. Usually, the exposure time of the bottom layers is high, in order to obtain a good adhesion of the object on the build platform. Once the adhesion is obtained, shorter exposure times can be chosen for all other model layers. The corresponding software then creates an STL-file, which contains the information of each layer that will be printed. These information, containing the corresponding printing parameters are then sent to the printer. After pouring the resin into the vat of the printer, the fabrication process can be started.

After printing, the 3D printed object is carefully removed from the build platform and a washing step follows. Depending on the type of resin, the object is post-processed e.g. by temperature.

6.2.8 Atomic Force Microscopy

Atomic force microscopy (AFM) images were obtained under ambient conditions in tapping mode with a NanoScope V multimode atomic force microscope (Bruker Nano Surfaces) using silicon cantilevers with resonance frequencies of 300–400 kHz (model: TESP-V2, Bruker Nano surfaces). The phase scale was set automatically by the software to best visualize phase separation. The absolute degree of phase contrast differed for each measurement. Bearing analysis was performed to normalize the phase contrast. For this purpose, the highest phase contrast in the image was set to zero. Statistical histograms were plotted by measuring the difference between each individual data point and point zero.

6.2.9 Dynamic Mechanical Analysis

Dynamic mechanical analysis (DMA) measurements were performed on a SEIKO SII EXSTAR 6100 DMS with a frequency of 1 Hz. The experiments were carried out from −150 °C to 250 °C with a heating rate of 2 K·min^{-1}. The glass transition temperature (T_g) was determined by evaluation of the peak maximum in the loss factor curve (maximum of *tanδ*).

6.2.10 Differential Scanning Calorimetry

Differential scanning calorimetry (DSC) measurements were performed on a PerkinElmer DSC 500 with an Intracooler 2. The samples were measured from -80 °C to 150 °C with a heating rate of 20 Kmin^{-1}. Three heating cycles were performed for each sample. Sample quantity was about 10 mg for each measurement.

6.2.11 Photo-rheology

Photo-rheology was performed on an Anton Paar Physica MCR301 rheometer, equipped with a heating unit (CTD 450) and Omicron-Laserage (Laserprodukte GmbH „LedHUB®" (High-power LED light engine)) to trigger in situ UV curing.

Measurements were carried out using a plate-plate configuration with a quartz glass plate and a disposable aluminum stamp (d = 25 mm). To determine the gel-points of printing formulations, a measurement profile was performed, with the parameters given in Table 18. In all experiments the UV light was turned on after 30 s of the measurement.

Table 18. Parameters for photo-rheology measurements.

LED / nm	405
Energy density / mWcm^{-2}	5.9
Initial gap / mm	0.1
Frequency / Hz	3
Deformation / %	1

6.2.12 Tensile Testing

Tensile tests were performed on a Zwick Retro with a 2 kN load cell, according to DIN EN ISO 527 at a test speed of 200 mm·min^{-1} and a pre-load of 0.5 N at ambient conditions. S-2 test specimen were punched out from cured films and a five-fold measurement was performed. 3D-printed S-2 test specimen were tested directly after printing and post-processing, without further treatment.

The area below the tensile curves, was determined by using the integration function of the software Origin 2020.

Cyclic loading-unloading measurements on printed specimens were performed on a Zwick Retro with a 500 N load cell. Ten consecutive loading-unloading cycles were performed with a test speed

of 50 mm·min^{-1}. The maximum elongation was selected in dependence on the elongation at break of each sample, determined by standard tensile testing in advance. Relief point of the strain was 0.01 N·mm^{-2}.

6.3 Experimental details for Chapter 4.1

The results presented in this chapter have already been published in the supporting information of Ref.[209]

6.3.1 Synthesis of bifunctional (acrylate and NCO functional) prepolymers

In a typical experiment, the HDI Trimer was heated to 60 °C in a three-neck flask, equipped with a stirrer, a condenser and a thermometer. Subsequently, 500 ppm 2,6-di-tert-butyl-4-methylphenol (butylated hydroxytoluene (BHT)) were added as stabilizer, to prevent a homo-polymerization of the acrylic double bonds. Lastly, 2-(hydroxyethyl) methacrylate was added dropwise in different ratios and the reaction was allowed to take place until the desired isocyanate content was obtained, determined by isocyanate titration measurements. In case of structure number **5**, dibutyltin dilaurate (DBTL, 50 ppm) was added to catalyze the isocyanate hydroxyl reaction. The resulting products were analyzed by NCO-titration and ^{1}H-NMR spectroscopy.

Table 19. Composition of bifunctional (acrylate and NCO-functional) prepolymers.

wt% / #	3	4	5
HDI-Trimer	89.33	80.77	58.36
HEMA	10.62	19.18	41.59
BHT	0.050	0.050	0.050
DBTL	–	–	0.005

The corresponding ^{1}H-NMR analyses are given in Figure 70 for structure **3**, in Figure 71 for structure **4** and in Figure 72 for structure **5**.
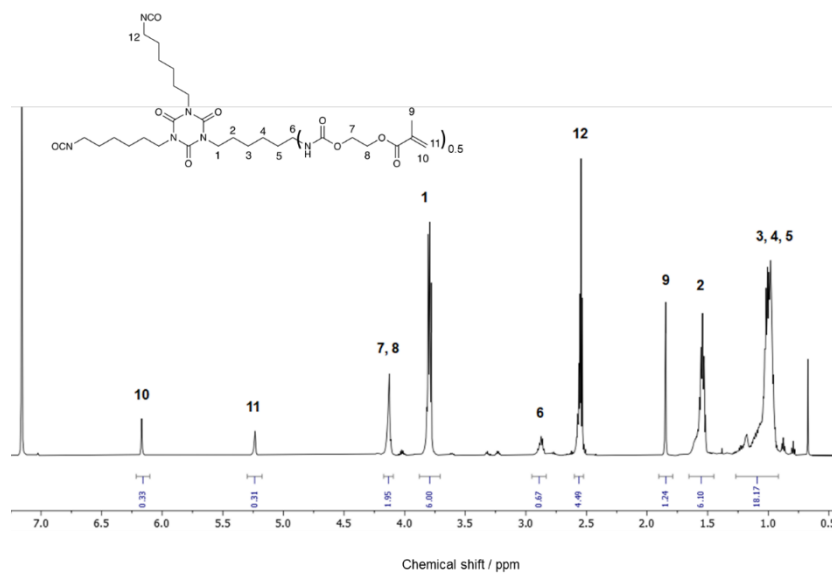
Figure 70. ^{1}H-NMR of structure 3 measured in C_6D_6, δ (ppm): 6.17 (s, 1H, H-10), 5.24 (s, 1H, H-11), 4.15 (m, 2H, H-7, H-8), 3.80 (dd, 6H, H-1), 2.91 (m, 1H, H-6), 2.55 (dd, 5H, H-12), 1.85 (s, 3H, H-9), 1.57 (m, 6H, H-2), 1.17 (m, 6H, H-5), 1.08 (m, 6H, H-3), 1.02 (m, 6H, H-4).

Figure 71. ^{1}H-NMR of structure 4 measured in C_6D_6, δ (ppm): 6.17 (s, 1H, H-10), 5.24 (s, 1H, H-11), 4.15 (m, 4H, H-7, H-8), 3.80 (dd, 6H, H-1), 2.91 (m, 2H, H-6), 2.55 (dd, 4H, H-12), 1.85 (s, 3H, H-9), 1.57 (m, 6H, H-2), 1.17 (m, 6H, H-5), 1.08 (m, 6H, H-3), 1.02 (m, 6H, H-4).
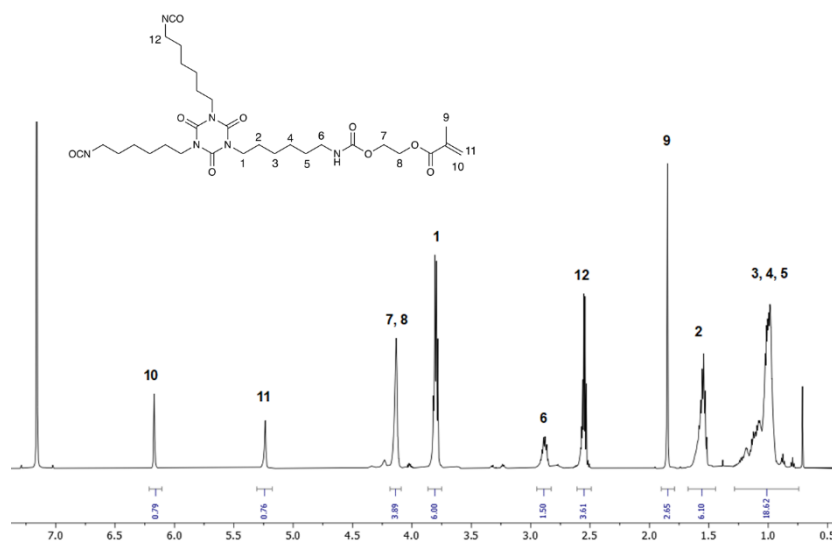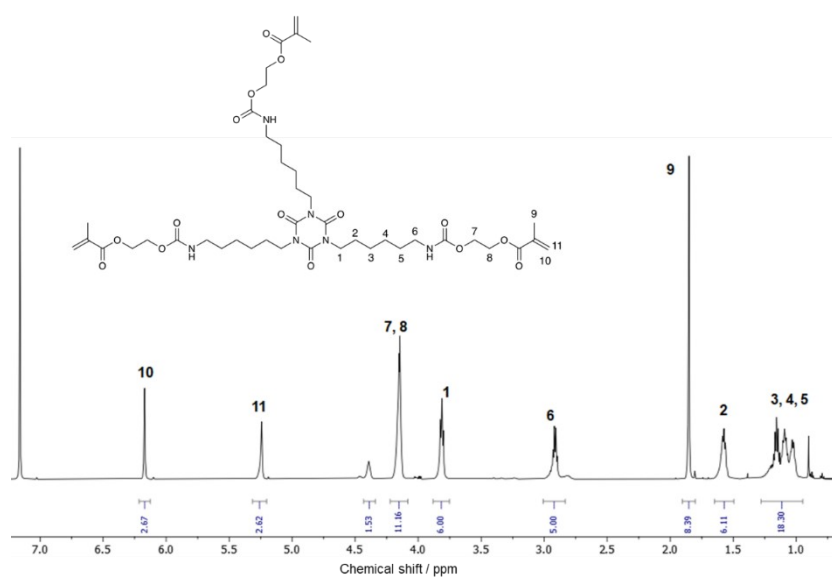
137

Figure 72. ^{1}H-NMR spectrum of structure 5 measured in C_6D_6: δ (ppm): 6.17 (s, 1H, H-10), 5.24 (s, 3H-11), 4.15 (m, 12H, H-7, H-8), 3.80 (dd, 6H, H-1), 2.91 (m, 6H, H-6), 1.85 (s, 9H, H-9), 1.57 (m, 6H, H-2), 1.17 (m, 6H, H-5), 1.08 (m, 6H, H-3), 1.02 (m, 6H, H-4).

6.3.2 Printing Formulation

The as-synthesized structure **3** was diluted with 30 wt% di-(propylene glycol) diacrylate (DPGDA) and different amounts of the photoinitiator Omnirad BL 750 were added, as given in Table 20.

Table 20. Composition of printing formulations.

wt%	Hybrid PUA 1	Hybrid PUA 2
Structure 3	69.7	69.3
DPGDA	29.8	29.7
Omnirad BL 750	0.49	0.99

The corresponding mixtures were homogenized using the speedmixer ARE-250 CE by Thinky for 2 minutes with 2000 rpm and were subsequently poured into the resin bath of the ASIGA Pro2 75 3D printer (details described in chapter 6.2.7). The two resins 'Tough' and 'Durable' of Formlabs were printed as received. Table 21 gives the printing parameters of the four resin formulations. The layer thickness was 100 µm for all prints and the number of bottom layers was three.

Table 21. Printing parameters for the different formulations printed on the ASIGA Pro2 75.

	Bottom exposure time / s	Model layer exposure time / s
Hybrid PUA 1	10	4
Hybrid PUA 2	6	3
Formlabs Tough	18	11
Formlabs Durable	15	8

After printing, *Hybrid PUA 1* as well as *Hybrid PUA 2* were post-processed with water (see chapter 6.3.4) and *Formlabs Tough* and *Durable* were post-cured using UV light. 10 mm x 10 mm x 4 mm cuboids were printed with the four resins and the resulting post-processed cuboids were used to determine the solvent compatibility of the materials. *Hybrid PUA 1* and *Hybrid PUA 2* were further used to print 25 mm x 25 mm x 0.5 mm cuboids, and the resulting post-processed samples were used to measure the transmittance by UV-Vis spectroscopy. *Hybrid PUA 1* was used to print a flow reactor. The corresponding digital models are illustrated in Figure 73.
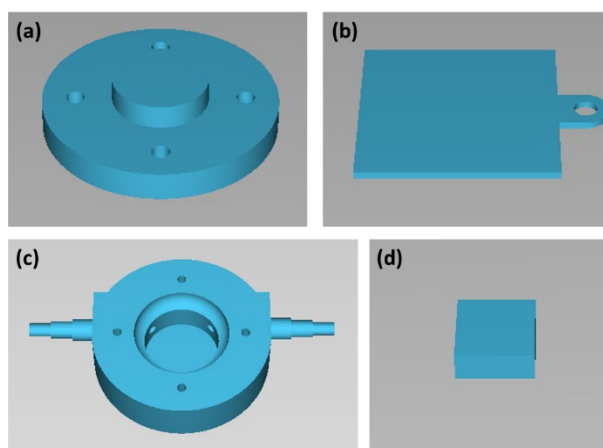

Figure 73. Digital models of a) the reactor cover, b) specimen for UV-Vis measurements, c) the reactor body and d) the specimen for determination of the solvent stability.

6.3.3 Determination of NCO-Content on Printed Parts

The isocyanate content on the surface of 3D-printed parts based on the formulation *Hybrid PUA 1* was determined (before post-processing with water) by titration according to DIN EN ISO 14896 with slight modifications. The surface area A of a 3D printed cuboid was determined using a ruler. 5 mL dibutylamine (DBA) in xylene (0.1 M) were added to the 3D printed cuboid of known size and surface area. Subsequently, 50 mL acetone were added and the mixture was stirred for 5

minutes. Upon addition of three drops phenol red, the excess of DBA was titrated against hydrochloric acid (HCl) (0.1 M), and the isocyanate content on the surface was determined as

$$g/cm^2 \ (NCO) = \frac{(V_B - V_V) \cdot c \ (HCl) \cdot M(NCO)}{A_{3D}} \tag{16}$$

with V_B being the blank consumption of HCl from reference measurements without a sample, V_V being the consumption of HCl during sample titration and A_{3D} being the surface area of the 3D printed sample. Four measurements were performed and the average value was used to determine the concentration of isocyanate groups on the surface of the reactor cover.

6.3.4 Post-Processing with Water

After printing, 3D printed parts based on *Hybrid PUA 1* and *Hybrid PUA 2* were boiled in water for 5 hours or until all isocyanate groups were converted, as determined by FT-IR/ATR-spectroscopy.

6.3.5 Solvent Compatibility

To test the solvent compatibility, 10 mm x 10 mm x 4 mm printed cuboids of post-processed *Hybrid PUA 1* as well as printed cuboids of the commercial resins *Tough* and *Durable* were each immersed in water, ethanol, dichloromethane (DCM), dimethylformamide (DMF), tetrahydrofuran (THF), toluene and acetone for 24 h. The solvent uptake was determined gravimetrically by

$$Solvent \ uptake = \frac{m_s - m_i}{m_i} \cdot 100\% \tag{17}$$

with m_s being the weight of the printed part after swelling in the respective solvent and m_i being the weight before immersion.

6.3.6 Functionalization of the Reactor Cover

To functionalize the reactor cover (printed with *Hybrid PUA 1*) with 4-aminobenzophenone, a concentration of 0.5 mol·L^{-1} of ABP in chloroform was prepared. Subsequently, the surface of the flow reactor cover was wetted with the solution and the reaction was allowed to take place in the oven at 80 °C, for 17 h. After reaction, excess sensitizer was removed by washing the reactor cover

for 10 minutes in an ultrasonic bath using isopropanol as solvent. Subsequently, the reactor cover was placed into hot water, in order to react remaining isocyanate groups.

The printed, post-treated and -functionalized flow-reactor was tested by Melissa Renner at the University of Cologne for the photooxygenation of citronellol. For experimental details see references [209,229]

6.4 Experimental details for Chapter 4.2

6.4.1 Synthesis of polyurethane acrylates

In a typical experiment, the HDI monomer was heated to 100 °C in a four-neck flask, equipped with a stirrer, a condenser and a thermometer under a gentle flow of nitrogen. The corresponding polyols were dehydrated under high vacuum and were neutralized with dibutyl phosphate (250 ppm), before they were added dropwise to the isocyanate using a dropping funnel. The isocyanate was used in a molar excess of 15:1 (isocyanate : polyol). The reaction was allowed to take place for three hours and the conversion was monitored by determination of the remaining isocyanate content using indirect potentiometric titration (see chapter 6.2.5). The composition of the different isocyanate prepolymers is given in Table 22.

Table 22. Compositions of the isocyanate prepolymers.

[wt%]	ISO 1	ISO 2	ISO 3	ISO 4
HDI	71	71	72	56
PC 1000	29	–	–	–
PEC 1000	–	29	–	–
PPG 1000	–	–	28	–
PPG 2000	–	–	–	44
Dibutylphosphate / ppm	250	250	250	250
Resulting NCO-content / %	33.4	33.1	33.4	26.0

Subsequently, the excess amount of HDI was removed using a short-path thin film evaporator, as schematically illustrated in Figure 74.
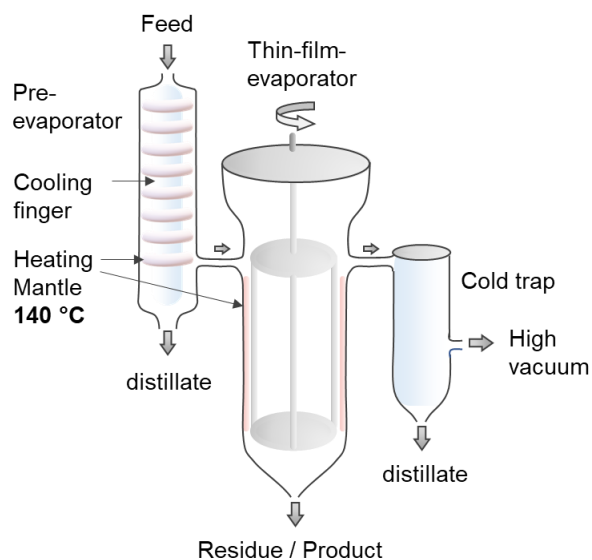
Figure 74. Schematic illustration of a short-path thin film evaporator.

Under vacuum (approx. 0.2 mbar) the mixture was fed dropwise to a pre-evaporator, containing a heating coil and a cooling finger in the middle. The temperature of the heating coil was selected in dependence on the boiling point of the corresponding isocyanate at the respective pressure (140 °C for HDI, 140 °C for PDI and 160 °C for IPDI). The mixture runs along the heating coil and the corresponding isocyanate evaporates followed by condensation on the cooling finger. Subsequently, the pre-evaporated mixture enters the thin-film evaporator where the remaining monomeric isocyanate is separated. A rotating wiper evenly distributes the mixture in the form of a 'thin-film' on a hot glass wall. The resulting large surface area enables to separate even small amounts of residual monomer. The evaporated isocyanate condensates in a cold trap. The isocyanate terminated prepolymer was received as a highly viscous liquid. Depending on the type of isocyanate and polyol used, the prepolymers crystallized upon cooling. The products were analyzed by indirect potentiometric isocyanate titration.

NCO-content: ISO 1: 6.52 %, ISO 2: 6.47 %, ISO 3: 6.29 %, ISO 4: 3.71 %.

Based on the isocyanate content, the NCO equivalent molar mass was determined by

$$NCO(equivalent\ weight) = \frac{42\ \frac{g}{mol} \cdot 100}{NCO\ content\ \%} \left[\frac{g}{mol(NCO)} \right] \tag{18}$$

With the assumption that the as-synthesized isocyanate prepolymers are strictly bifunctional, the number molar mass (M_n) can be calculated.

M_n (titration end-group analysis): ISO 1: 1290 g·mol^{-1}, ISO 2: 1300 g·mol^{-1}, ISO 3: 1340 g·mol^{-1}, ISO 4: 2260 g·mol^{-1}.

In a subsequent synthesis step, the isocyanate terminated prepolymers were reacted with 2-hydroxyethyl methacrylate to yield the corresponding polyurethane acrylates (PUA 1 to PUA 4). For this purpose the prepolymers were heated to 70 °C in a four-neck flask, equipped with a stirrer, a condenser and a thermometer. Butylated hydroxytoluene (BHT, 500 ppm) were added to stabilize the resulting acrylate prepolymer. Dibutyltindilaurate (DBTL, 50 ppm) was added to catalyze the isocyanate hydroxyl reaction. At last, 2-(hydroxyethyl) methacrylate was added dropwise. The reaction was allowed to take place until all isocyanate groups were converted as monitored by NCO-titration. The resulting polyurethane acrylates were analyzed by ^{1}H-NMR spectroscopy, FT-IR spectroscopy and gel permeation chromatography.
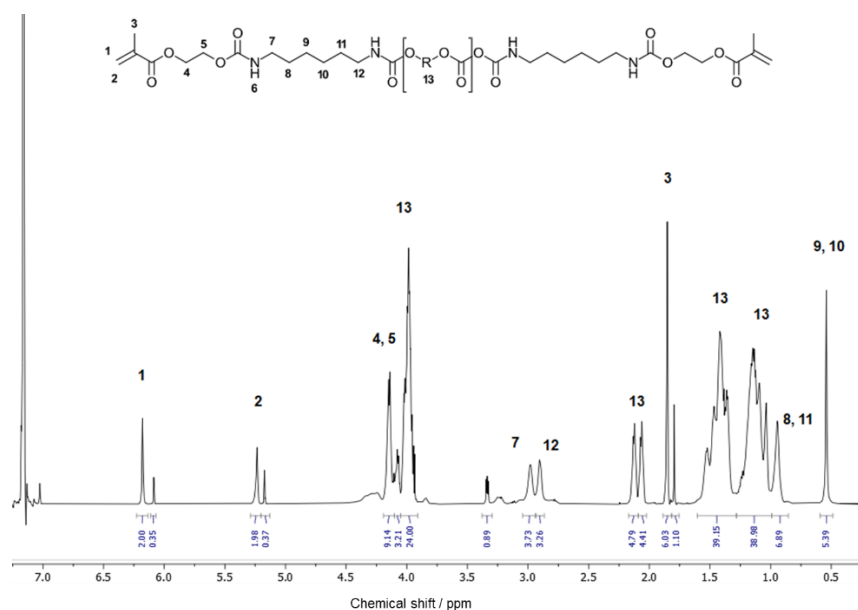
6.4.1.1 Polyurethane acrylate 1

Figure 75. ^{1}H-NMR of PUA 1 measured in C$_6$D$_6$: δ = 6.17 (2H, s, H-1), δ = 5.21 (2H, s, H-2), δ = 5.18 (4H, H-6), δ =4.15 (8H, m, H-4, H-5), δ = 3.97 (24 H, m, H-13), δ = 2.9 (4H, H-7), δ =2.89 (4H, H-12), δ = 2.12 (4H, H-13), δ = 2.12 (4H, H-13), δ = 1.85 (6H, s, H-3), δ = 1.61 - 1.29 (39H, H-13), δ = 1.29 – 1.01 (39H, H-13), δ = 0.96 (8H, s, H-8, H-11), δ = 0.54 (8H, s, H-9, H-10).
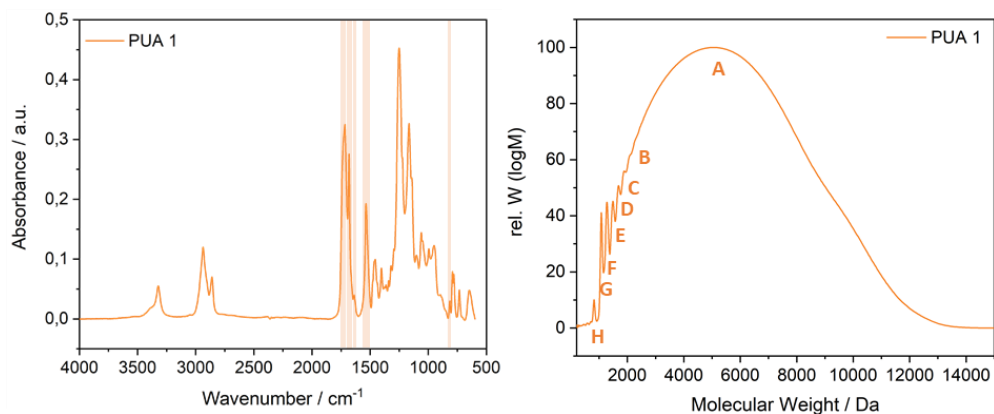
Figure 76. Left: ATR FT-IR spectroscopy, characteristic bands: $\tilde{\nu}$ (C=O, stretching, carbonate) = 1730 cm⁻¹, $\tilde{\nu}$ (C=O, stretching, urethane) = 1715 cm⁻¹, $\tilde{\nu}$ (C=C, stretching, acrylate) = 1637 cm⁻¹, $\tilde{\nu}$ (N-H, def., urethane) = 1535 cm⁻¹, $\tilde{\nu}$ (C=C, def., acrylate) = 814 cm⁻¹. **Right. GPC:** A: 5050 g·mol⁻¹, 71 %; B: 2140 g·mol⁻¹, 7.8 %; C: 1890 g·mol⁻¹, 4.5 %; D: 1690 g·mol⁻¹, 4.5 %; E: 1490 g·mol⁻¹, 4.4 %; F: 1270 g·mol⁻¹, 4.6 %; G: 1080 g·mol⁻¹, 3.2%; H: 820 g·mol⁻¹, 0.9 %; M_n = 2150 g·mol⁻¹, Đ = 1.8.

6.4.1.2 Polyurethane acrylate 2
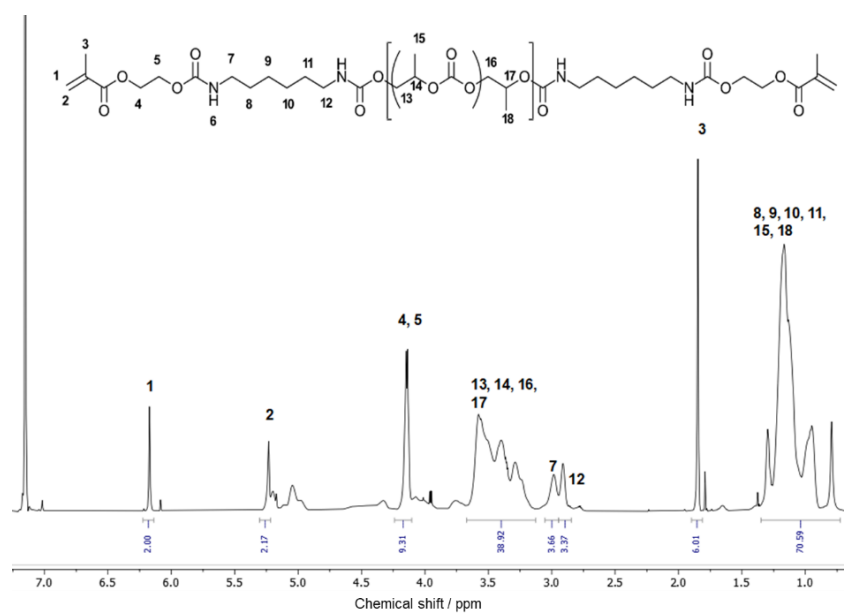
Figure 77. ¹H-NMR of PUA 2 measured in C_6D_6: δ = 6.18 (2H, s, H-1), δ = 5.22 (2H, s, H-2), δ = 5.18 (4H, H-6), δ =4.14 (8H, m, H-4, H-5), δ = 3.12 - 3.59 (39 H, m, H-13, H-14, H-17, H-17), δ = 2.98 (4H, H-7), δ =2.90 (4H, H-12), δ = 1.84 (6H, H-3), δ = 0.7 - 1.30 (75H, m, H-8, H-9, H-10, H-11, H-15, H-18).

Figure 78. Left: FT-IR, characteristic peaks: $\tilde{v}$ (C=O, stretching, carbonate) = 1740 cm^{-1}, $\tilde{v}$ (C=O, stretching, urethane) = 1715 cm^{-1}, $\tilde{v}$ (C=C, stretching, acrylate) = 1637 cm^{-1}, $\tilde{v}$ (N-H, def., urethane) = 1520 cm^{-1}, $\tilde{v}$ (C=C, def., acrylate) = 814 cm^{-1}. **Right: GPC:** A: 2560 g·mol^{-1}, 67 %; B: 4440 g·mol^{-1}, 28 %, C: 870 g·mol^{-1}, 0.9 %; D: 1250 g·mol^{-1}, 1.0 %; M_n = 2350 g·mol^{-1}, Đ = 1.5.

6.4.1.3   Polyurethane acrylate 3
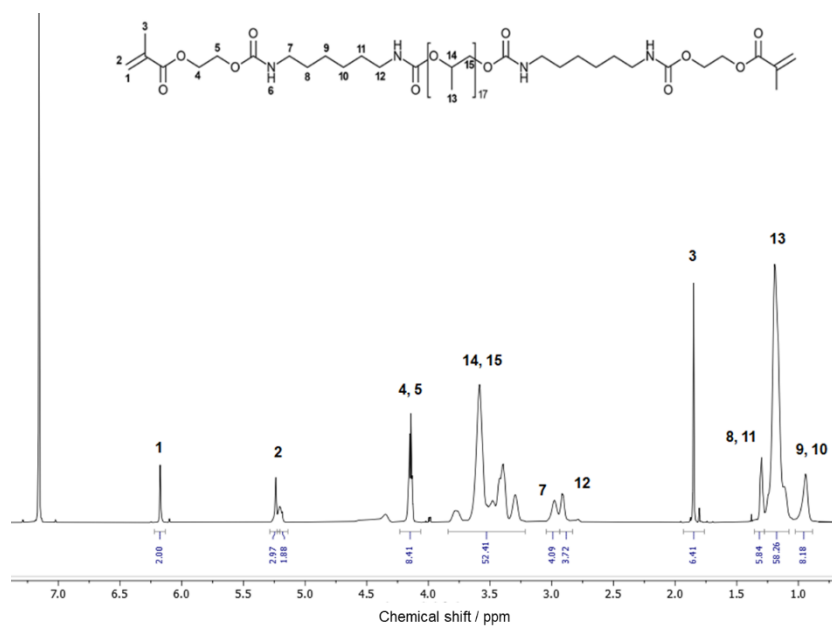
Figure 79. ^{1}H-NMR of PUA 3 measured in C$_6$D$_6$: δ = 6.12 (2H, s, H-1), δ = 5.20 (2H, s, H-2), δ = 5.18 (4H, H-6), δ =4.13 (8H, m, H-4, H-5), δ = 3.50 (56 H, m, H-14, H-15), δ = 2.90 (4H, H-7), δ =2.88 (4H, H-12), δ = 1.82 (4H, H-3), δ = 1.30 (8H, H-8, H-11), δ = 1.19 (56H, m, H-13), δ = 0.92 (8H, H-9, H-10).
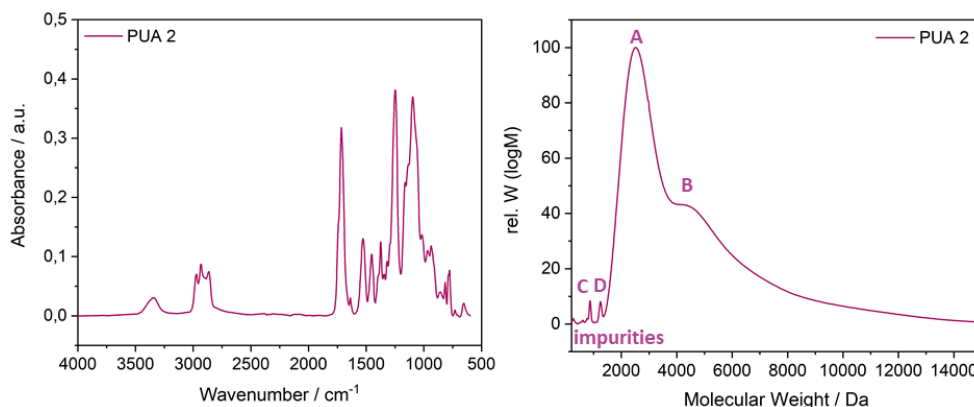
145

Figure 80. Left FT-IR, characteristic peaks: $\tilde{v}$ (C=O, stretching, urethane) = 1720 cm^{-1}, $\tilde{v}$ (C=C, stretching, acrylate) = 1637 cm^{-1}, $\tilde{v}$ (N-H, def., urethane) = 1520 cm^{-1}, $\tilde{v}$ (C=C, def., acrylate) = 814 cm^{-1}. **Right: GPC:** A: 2360 g·mol^{-1}, 80 %; B: 4320 g·mol^{-1}, 13 %; C: 6002 g·mol^{-1}, 2.6 %, D: 867 g·mol^{-1}, 1.2 %; E: 1245 g·mol^{-1}, 1.3 %; M_n = 2290 g·mol^{-1}, Đ = 1.2.

6.4.1.4   Polyurethane acrylate 4
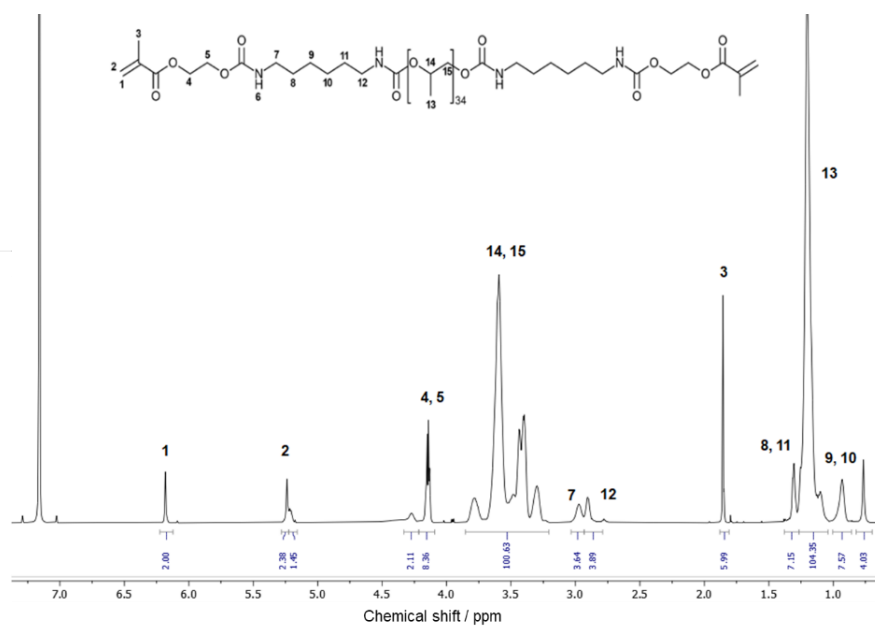
Figure 81. ^{1}H-NMR of PUA 4 measured in C$_6$D$_6$: δ = 6.12 (2H, s, H-1), δ = 5.20 (2H, s, H-2), δ = 5.18 (4H, H-6), δ =4.13 (8H, m, H-4, H-5), δ = 3.50 (105 H, m, H-14, H-15), δ = 2.90 (4H, H-7), δ =2.88 (4H, H-12), δ = 1.82 (4H, H-5), δ = 1.30 (8H, H-8, H-11), δ = 1.19 (105H, m, H-13), δ = 0.92 (8H, H-9, H-10).
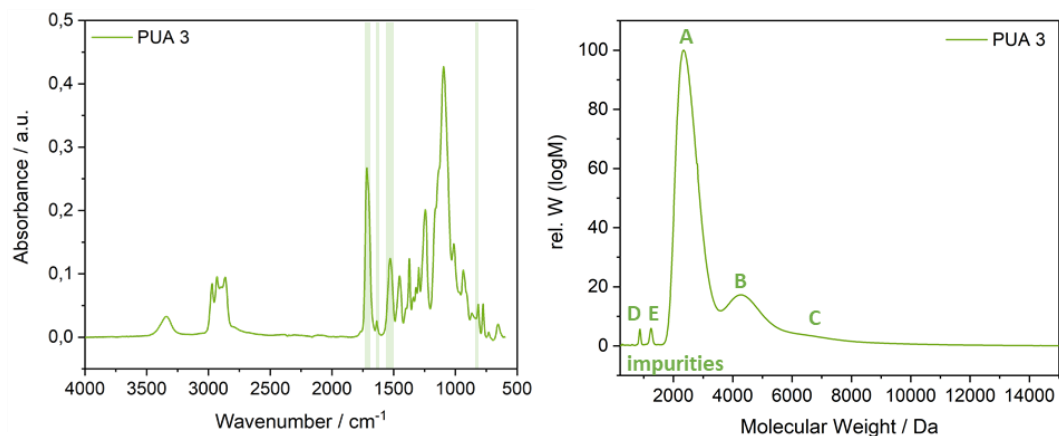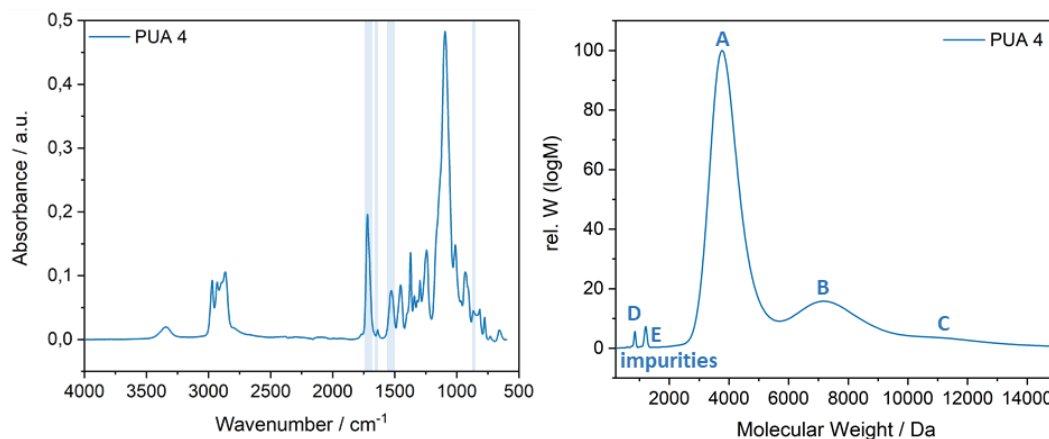
Figure 82. Left: FT-IR, characteristic peaks: $\tilde{v}$ (C=O, stretching, urethane) = 1720 cm^{-1}, $\tilde{v}$ (C=C, stretching, acrylate) = 1637 cm^{-1}, $\tilde{v}$ (N-H, def., urethane) = 1520 cm^{-1}, $\tilde{v}$ (C=C, def., acrylate) = 814 cm^{-1}. **Right: GPC:** A: 3790 g·mol^{-1}, 78 %; B: 7260 g·mol^{-1}, 15 %; C: 9860 g·mol^{-1}, 2.7 %, D: 845 g·mol^{-1}, 1.3 %; E: 1209 g·mol^{-1}, 1.7 %; M_n = 3460 g·mol^{-1}, Đ = 1.3.

6.4.2 Preparation of UV Cured Films

UV cured films of acrylate functional prepolymers were prepared by using the standard UV coating process described in chapter 6.2.6. The composition of the formulations is given in Table 23. After curing the films were removed from the glass substrate and were then analyzed by means of ATR FT-IR spectroscopy, DMA and tensile testing.

Table 23. Composition of crosslinked (CL) acrylate functional prepolymers.

[wt%]	PUA 1 CL	PUA 2 CL	PUA 3 CL	PUA 4 CL
PUA 1	97	–	–	–
PUA 2	–	97	–	–
PUA 3	–	–	97	-
PUA 4	–	–	–	97
Omnirad 1173	3.0	3.0	3.0	3.0
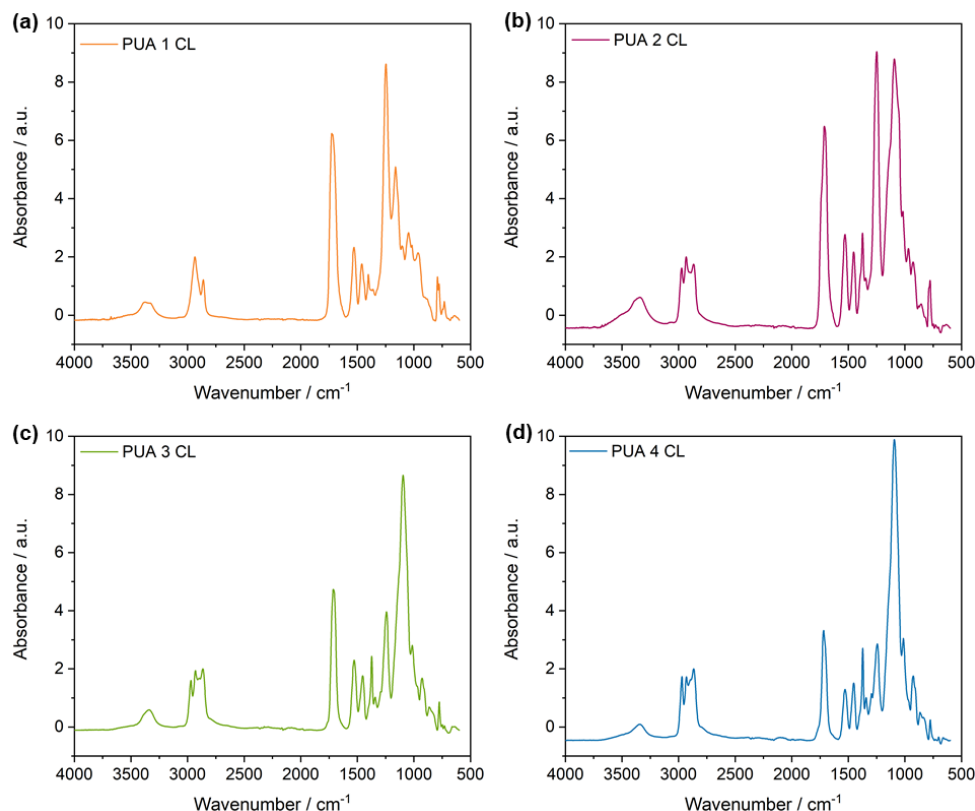
Figure 83. FT-IR spectra of crosslinked (CL) PUA's. **a) PUA 1 CL:** ṽ (C=O, stretching, carbonate) = 1740 cm⁻¹, ṽ (C=O, stretching, urethane) = 1715 cm⁻¹, ṽ (N-H, def., urethane) = 1520 cm⁻¹. **b) PUA 2 CL:** ṽ (C=O, stretching, carbonate) = 1740 cm⁻¹, ṽ (C=O, stretching, urethane) = 1715 cm⁻¹, ṽ (N-H, def., urethane) = 1520 cm⁻¹. **c) PUA 3 CL:** ṽ (C=O, stretching, urethane) = 1720 cm⁻¹, ṽ (N-H, def., urethane) = 1520 cm⁻¹. **d) PUA 4 CL:** ṽ (C=O, stretching, urethane) = 1720 cm⁻¹, ṽ (N-H, def., urethane) = 1520 cm⁻¹.

6.4.3 Preparation of Acrylate – Isocyanate Resins

For the characterization and selection of polyisocyanates as potential diluent of the polyurethane acrylate, formulations were prepared by mixing PUA 4, different low viscous polyisocyanates, Omnirad 1173 (3 wt% with respect to the acrylate) as photoinitiator, as well as tin(II)ethyl hexanoate (0.75 wt% with respect to the isocyanate) as catalyst, using the speedmixer ARE-250 CE by Thinky for 2 minutes with 20000 rpm. The compositions of the formulations are given in Table 24.

Table 24. Preparation of resin formulations.

[wt%]	F1	F2	F3	F4
PUA 4	49.1	49.1	49.1	49.1
Uretdione	49.1	–	–	–
Allophanate	–	49.1	–	–
Asym. Trimer	–	–	49.1	–
Biuret	–	–	–	49.1
Omnirad 1173	1.47	1.47	1.47	1.47
Tin (II) ethylhexanoate	0.37	0.37	0.37	0.37

The viscosity of the resin formulations was measured and the homogeneity was investigated macroscopically.

6.4.4 Preparation of Dually Cured Films

Different amounts of PUA 4 and allophanate were mixed with the photoinitiator Omnirad 1173 (3 wt% with respect to the acrylate) and tin(II)ethylhexanoate (0.75 wt% with respect to the isocyanate) as catalyst using the speedmixer ARE-250 CE by Thinky for 2 minutes with 2000 rpm. As acrylate reference, the PUA 4 was mixed with the photoinitiator (Ref. 2). Two isocyanate based references were prepared. For Ref. 1, the isocyanate was mixed with the catalyst and for Ref. 3, the isocyanate was mixed with water. The corresponding compositions are given in Table 25.

Table 25. Composition for the preparation of combinatorial networks.

[wt%]	Ref. 1	Ref. 2	Ref. 3	CN 1	CN 2	CN 3	CN 4
PUA 4	–	97	–	32.8	49.1	58.8	64.9
Allophanate	99.2	–	95.9	65.7	49.1	39.2	32.6
Omnirad 1173	–	3	–	0.99	1.47	1.8	1.95
Tin (II) ethylhexanoate	0.8	–	–	0.49	0.38	0.30	0.25
Water	–	–	4.1	–	–	–	–

Samples CN 1 to CN 4, as well as Ref. 2 were prepared according to the procedure described in chapter 6.2.6. After UV curing, turbidity measurements of the films on the glass substrate were performed. The measurement of the pure glass substrate was used as reference (see chapter

6.2.3). In a next step, samples CN 1 to CN 4 were placed into the oven at 100 °C for 17 h, to start the second curing reaction. After cooling, the films were removed from the glass substrate.

Ref. 1 and Ref. 3 were prepared using a different method. For Ref. 1 the isocyanate – catalyst mixture was filled into a mold. The mold was fabricated with two glass substrates, both pretreated with soy lecithin solution (0.5 wt% in ethyl acetate). The glass substrates were placed on top of each other with a 3 mm spacer and a silicon tube and were fixed with clamps. The allophanate mixture was then filled into the mold and was cured at 100 °C for 17 h. Subsequently, the crosslinked allophanate was removed from the mold. Ref. 3 was prepared accordingly, except that the allophanate was mixed with water instead of the catalyst.

All samples were analyzed by ATR-FT-IR spectroscopy, DMA, tensile test and AFM.

6.4.5 Digital Light Processing

For printing trials the resin formulation illustrated in Table 26 was prepared by mixing all components using the speedmixer ARE-250 CE by Thinky for 2 minutes with 2000 rpm. The amount of catalyst was 0.75 wt% with respect to the isocyanate component. The amount of photoinitiator was 0.5 wt% with respect to the amount of acrylate and the inhibitor concentration was 0.05 wt% with respect to the acrylate component.

Table 26. Composition of the printing formulation.

[wt%]	CN 2 Printing Formulation
PUA 4	49.7
Allophanate	49.7
Tin (II) ethylhexanoate	0.37
Omnirad BL 750	0.25
BBOT	0.03

All components were mixed in the dark and were poured into the resin vat of the printer.

The bottom exposure time, the normal exposure time, as well as the number of bottom layers was adjusted to achieve appropriate printing conditions. Typically, the bottom exposure time needs to be higher than the actual curing time in order to achieve adhesion of the printed layer on the build platform. The amount of layers that are cured with the bottom exposure time were chosen accordingly. The model layer exposure time, is the time to cure all other layers. Layer thickness was 100 µm for all layers. Tensile bars were selected as printing objects in order to enable a

mechanical characterization of the samples after curing. The printing parameters are given in Table 27.

Table 27. Printing parameters for printing sample CN 2.

Printing Parameters	1	2	3
Bottom exposure / s	17	20	20
Model layer exposure	12	12	15
Number of bottom layers	3	3	3

For printing trial **1**, the adhesion to the build platform of the printed object was not sufficient, which is why the bottom exposure time was increased from 17 s to 20 s. In printing trial **2**, the normal exposure time was too low, which is why in printing trial **3**, the normal exposure time was increased from 12 s to 15 s. The printing parameters were suited to obtain tensile bars, that were carefully removed from the build platform and post cured in the oven at 100 °C for 17 h.

The printed specimen were analyzed by means of DMA and AFM.

6.5   Experimental details for Chapter 4.3

6.5.1   Synthesis of isocyanate functional prepolymers

Isocyanate functional prepolymers were synthesized according to the method described in 6.3.1. In brief, the isocyanate was heated to the corresponding temperature (see Table 28). The polyols were neutralized using dibutyl phosphate (250 ppm) and were slowly added to the isocyanate. After the desired isocyanate content was obtained, as determined by potentiometric titration, the reaction mixture was transferred to a thin-film evaporator. The excess monomeric isocyanate was removed at the temperatures given in Table 28. The resulting isocyanate terminated prepolymers were analyzed by indirect potentiometric titration, rheology, GPC, ^{1}H-NMR spectroscopy and ATR FT-IR spectroscopy.

Table 28. Relevant information for isocyanate terminated prepolymers NCO 1 and NCO 2.

	NCO 1	NCO 2
Isocyanate	IPDI	PDI
Polyol	pTHF	Cardyon LC 07
T (reaction) / °C	120 °C	80 °C

T (thin-film evaporator) / °C	160 °C	130 °C
NCO-content / %	5.3	5.8
Viscosity (at 50 Hz) / mPa·s	13100	7510

6.5.1.1 NCO 1
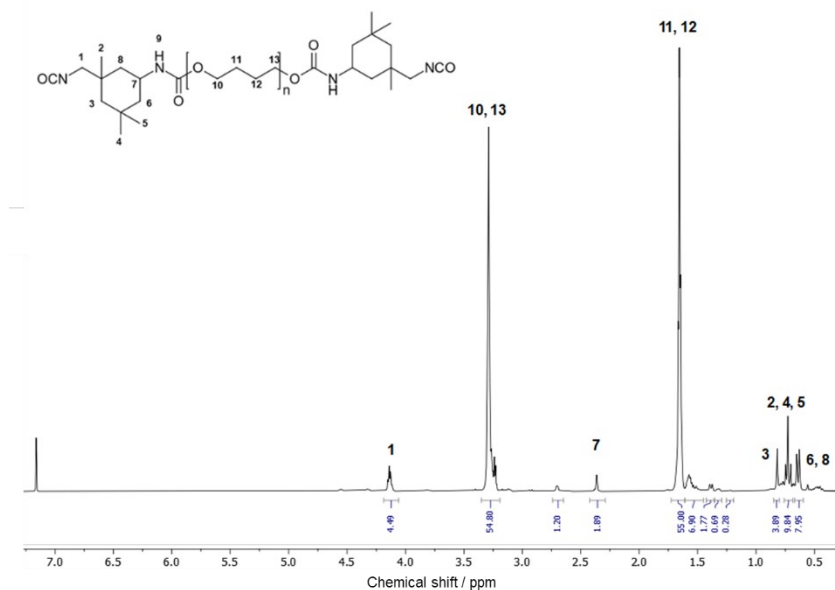
Figure 84. ^{1}H-NMR of NCO 1 measured in C_6D_6): δ = 4.14 (4H, t, H-1), δ = 3.29 (55H, s, H-10, H-13), δ = 2.30 (2H, H-7), δ = 1.66 (55H, m, H-11, H-12), δ = 0.81 (4 H, s, H-3), δ = 0.72 (9H, t, H-2, H-4, H-5), δ = 0.65 (8H, H-6, H-8).
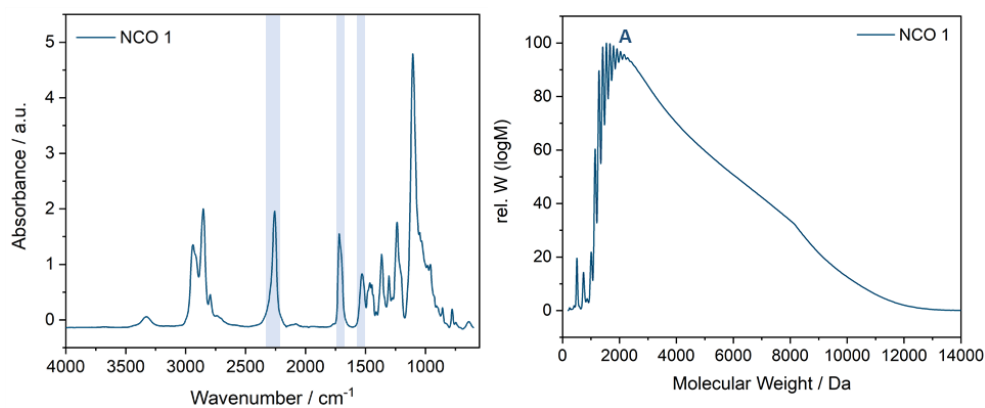
Figure 85. FT-IR spectra of NCO 1, characteristic peaks: $\tilde{v}$ (N=C=O, stretching, isocyanate) = 2265 cm^{-1}, $\tilde{v}$ (C=O, stretching, urethane) = 1721, $\tilde{v}$ (N-H. deformation, urethane) = 1520 cm^{-1}. GPC: A: 3480 g·mol^{-1}.

6.5.1.2   NCO 2
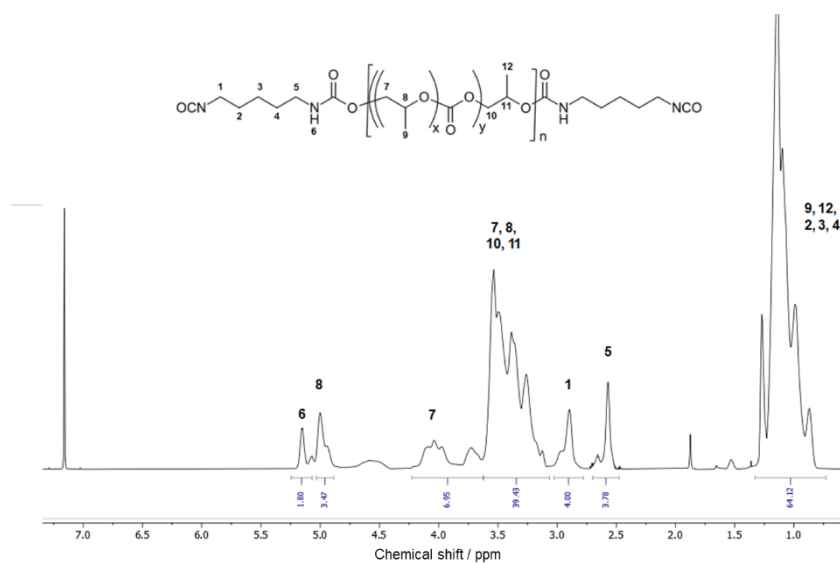
Figure 86. ¹H-NMR of NCO 2 measured in C₆D₆: Only a rough assignment was performed as the exact composition of the polyol employed is not known.
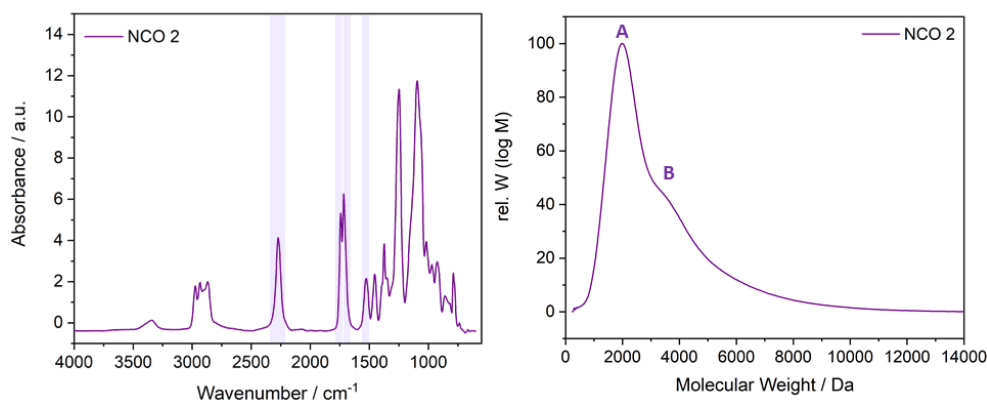
Figure 87. **Left: FT-IR spectra of NCO 1, characteristic peaks:** $\tilde{v}$ (N=C=O, stretching, isocyanate) = 2265 cm⁻¹, $\tilde{v}$ (C=O, stretching, carbonate) = 1740 cm⁻¹, $\tilde{v}$ (C=O, stretching, urethane) = 1721, $\tilde{v}$ (N-H. deformation, urethane) = 1520 cm⁻¹. **Right: GPC: of NCO 1** A: 1940 g·mol⁻¹, B: 3201 g·mol⁻¹.

The isocyanates were trimerized by mixing each isocyanate with tin(II)ethylhexanoate (0.75 wt%) as catalyst. A mold was fabricated with two glass substrates, both pretreated with soy lecithin solution (0.5 wt% in ethyl acetate). The glass substrates were placed on top of each other with a 3 mm spacer and a silicon tube and were fixed with clamps. The isocyanate mixtures were

then filled into the mold and were cured at 100 °C for 17 h. The crosslinked polymer was then removed from the mold and the glass transition temperature was determined by DSC.
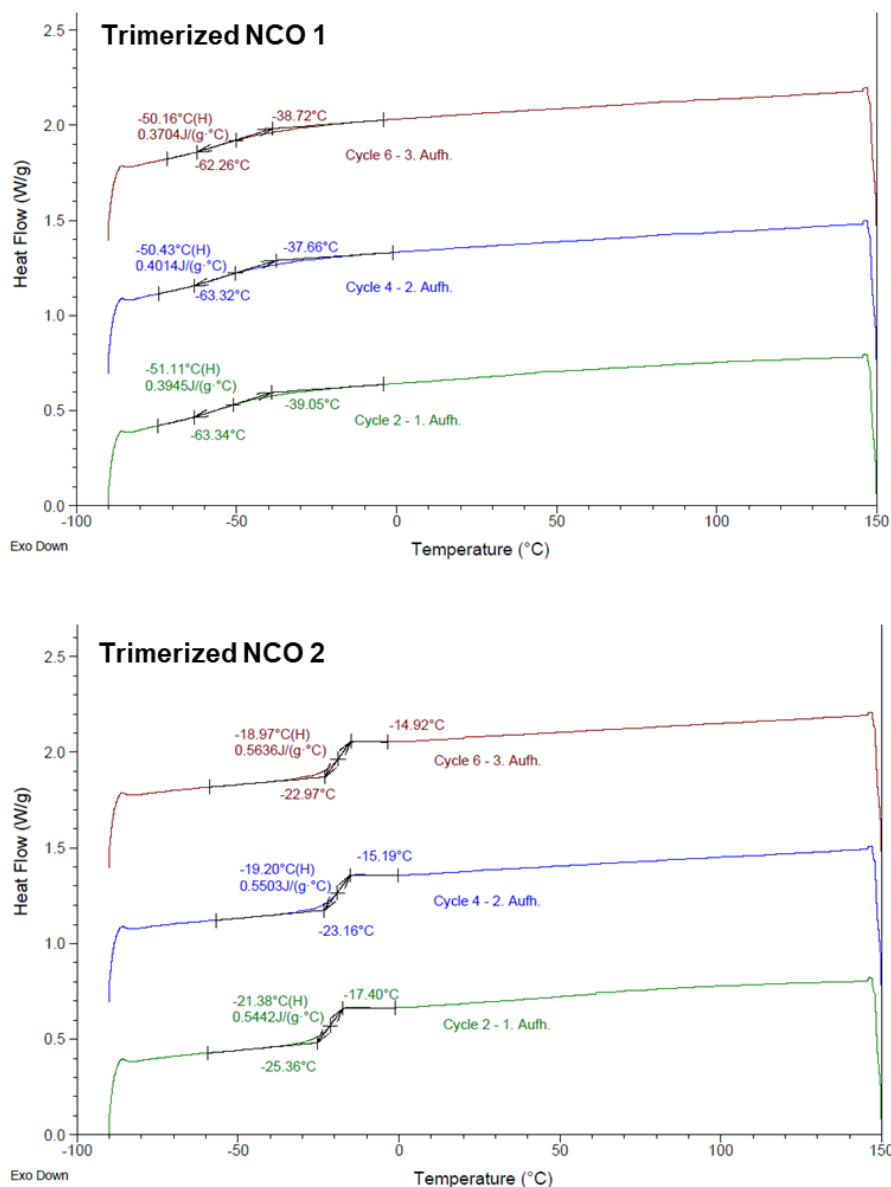
Figure 88. DSC measurements of trimerized NCO 1 (top) and trimerized NCO 2 (below).

6.5.2 Preparation of Dually Cured films

Screening experiments based on dually (UV and temperature) cured films were performed, according to the method described in chapter 6.2.6. The compositions of the corresponding formulations are given in Table 29. AN 1, AN 2, AN 3 and Ref. 2 were removed from the glass

substrates after UV exposure and were ready for analysis. All other samples were placed into the oven at 100 °C for 17 h. ATR FT-IR spectroscopy was used to monitor the quantitative conversion of the isocyanate groups after post-curing.

Ref. 1 was prepared using a different procedure. The mixture of NCO 2 and allophanate was mixed with the catalyst. A mold was fabricated with two glass substrates, both pretreated with soy lecithin solution (0.5 wt% in ethyl acetate). The glass substrates were placed on top of each other with a 3 mm spacer and a silicon tube and were fixed with clamps. The isocyanate mixture was then filled into the mold and was cured at 100 °C for 17 h. The crosslinked polymer was then removed from the mold.

Table 29. Composition of dually cured films.

[wt%]	NCO 1	NCO 2	Allo-phanate	PEGDA 700	THFA	Tin (II) ethylhexanoate	Omnirad 1173
AN 1	–	–	–	-	97.0	–	3.00
AN 2	–	–	–	48.5	48.5	–	3.00
AN 3	–	–	–	97.0	–	–	3.00
AN 4	–	–	–	38.8	58.3	–	2.91
iCN 1	49.1	–	–	29.4	19.6	0.37	1.47
iCN 2	49.1	–	–	19.6	29.4	0.37	1.47
iCN 3	49.1	–	–	39.3	9.8	0.37	1.47
iCN 4	34.4	–	14.7	24.5	24.5	0.37	1.47
iCN 5	24.5	–	24.5	24.5	24.5	0.37	1.47
iCN 6	14.7	–	34.4	24.5	24.5	0.37	1.47
iCN 7	–	24.5	24.5	14.7	34.4	0.37	1.47
iCN 8	–	24.5	24.5	24.5	24.5	0.37	1.47
iCN 9	–	24.5	24.5	34.4	14.7	0.37	1.47
iCN 10	–	49.1	–	24.5	24.5	0.37	1.47
iCN 11	–	34.4	14.7	24.5	24.5	0.37	1.47
iCN 12	–	14.7	34.4	24.5	24.5	0.37	1.47
iCN 13	–	–	10	24.5	24.5	0.37	1.47
Ref. 1	–	49.6	49.6	–	–	0.75	–

AN 1 to AN 3 were analyzed by DSC. Ref. 1 and AN 2 were analyzed by AFM. iCN 1 to iCN 6 were analyzed by DMA. ICN 7 to ICN 13 were analyzed by DMA, AFM and tensile testing. ICN 7 to ICN 9 were further analyzed by photo-rheology. AN 4 was analyzed by tensile testing.
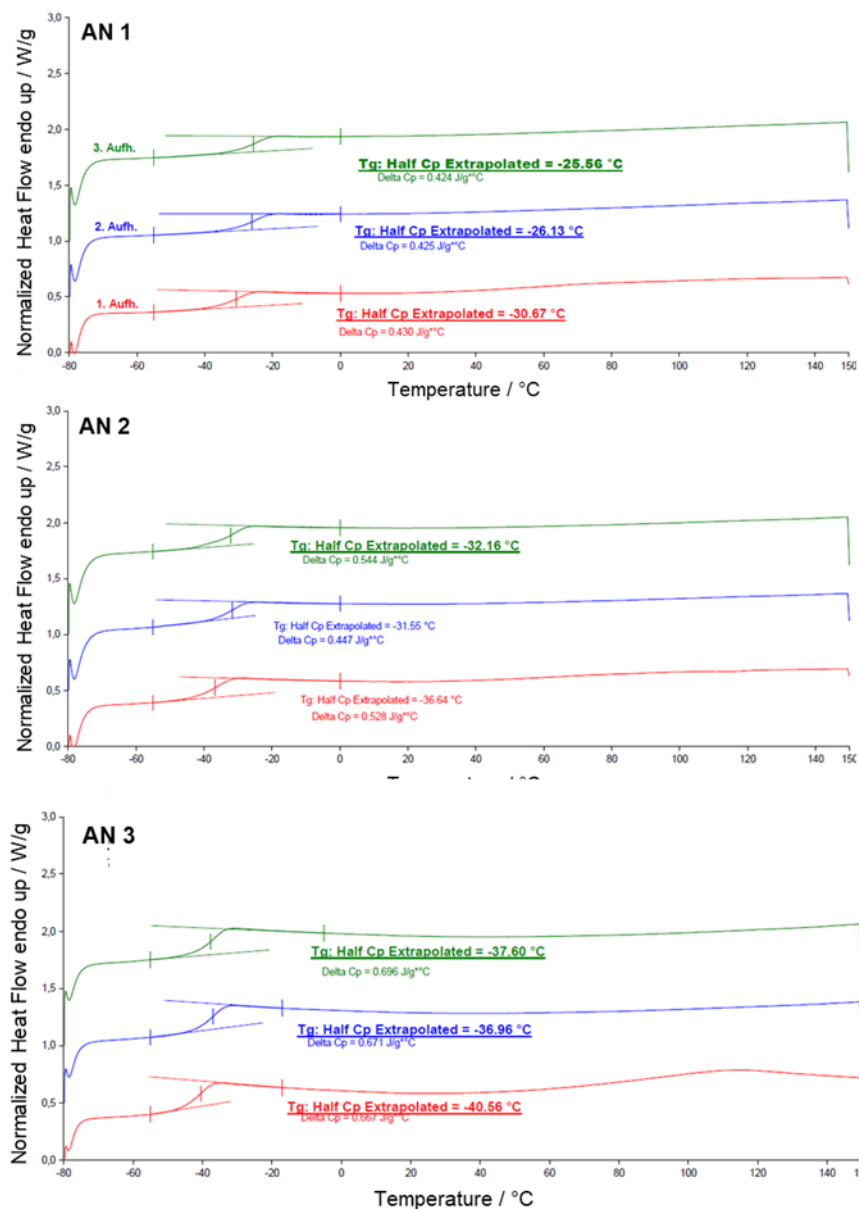
Figure 89. DSC measurements of acrylic networks AN 1 to AN 3.

6.5.3   Digital Light Processing

All prints were performed on an Anycubic PhotonS as described in chapter 6.2.7. The composition of the printing formulations, as well as the viscosity and the corresponding ideal printing parameters are given in Table 30.

Table 30. Composition and printing parameters of printing formulations P 1, P 1.1 and P 2.

m [g]	P 1	P 1.1	P 2
NCO 1	75	75	–
NCO 2	–	–	75
Allophanate	25	25	25
PEGDA 700	40	40	40
THFA	60	60	60
Tin (II) ethylhexanoate	0.5	–	0.5
Omnirad BL 750	0.5	0.5	0.5
BBOT	0.1	0.1	0.1
2′,4′,5′,7′-tetrabromo-3,4,5,6-tetrachlorofluorescein	0.1	0.1	0.1
η [mPa·s]	233	183	191
Δt [s]	15	37	8
Bottom exposure / s	45	60	22
Normal exposure / s	42	55	16
Number of bottom layers	3	3	3

For printing experiments, all components were mixed and poured into the resin vat of the printer. Ideal printing parameters were evaluated starting with the time determined via photo-rheology. S-2 tensile bars were selected as printing objects to enable the mechanical characterization of the material. After printing, the specimen were carefully removed from the build platform and cleaned using a cloth soaked in isopropanol. Subsequently, P 1 and P 2 were placed into the oven for 17 h at 100 °C. P 1.1 was immersed into hot water for 17 h.

The printed tensile bars were analyzed by DMA, tensile testing and cyclic tensile testing.

7 Literature

1.   Hoyle, C. E. & Kinstle, J. F. Radiation curing of polymeric materials. in *ACS Symposium Series* vol. 417 (1990).

2.   Verhoeven, J. W. Glossary of terms used in photochemistry (IUPAC Recommendations 1996). *Pure Appl. Chem.* **68**, 2223–2286 (1996).

3.   Lambert, J. H. *Photometria sive de mensura et gradibus luminis, colorum et umbrae.* (sumptibus vidvae E. Klett, typis CP Detleffsen, 1760).

4.   Beer, A. Bestimmung der absorption des rothen lichts in farbigen flussigkeiten. *Ann. Phys.* **162**, 78–88 (1852).

5.   David, J. No Title. *New Sci.* **64**, 80 (1974).

6.   Hull, C. W. Apparatus for production of three-dimensional objects by stereolithography. vol. US4575330A (1986).

7.   Su, A. & Al'Aref, S. J. Chapter 1 - History of 3D Printing. in (eds. Al'Aref, S. J., Mosadegh, B., Dunham, S. & Min, J. K. B. T.-3D P. A. in C. M.) 1–10 (Academic Press, 2018).

8.   Berman, B. 3-D printing: The new industrial revolution. *Bus. Horiz.* **55**, 155–162 (2012).

9.   Stansbury, J. W. & Idacavage, M. J. 3D printing with polymers: Challenges among expanding options and opportunities. *Dent. Mater.* **32**, 54–64 (2016).

10.   Ngo, T. D., Kashani, A., Imbalzano, G., Nguyen, K. T. Q. & Hui, D. Additive manufacturing (3D printing): A review of materials, methods, applications and challenges. *Compos. Part B Eng.* **143**, 172–196 (2018).

11.   Ligon, S. C., Liska, R., Stampfl, J., Gurr, M. & Mülhaupt, R. Polymers for 3D Printing and Customized Additive Manufacturing. *Chem. Rev.* **117**, 10212–10290 (2017).

12.   Narupai, B. & Nelson, A. 100th Anniversary of Macromolecular Science Viewpoint: Macromolecular Materials for Additive Manufacturing. *ACS Macro Lett.* 627–638 (2020).

13.   Bikas, H., Stavropoulos, P. & Chryssolouris, G. Additive manufacturing methods and modelling approaches: a critical review. *Int. J. Adv. Manuf. Technol.* **83**, 389–405 (2016).

14. Wong, K. V & Hernandez, A. A review of additive manufacturing. *ISRN Mech. Eng.* **2012**, (2012).

15. Dhinakaran, V., Kumar, K. P. M., Ram, P. M. B., Ravichandran, M. & Vinayagamoorthy, M. A review on recent advancements in fused deposition modeling. *Mater. Today Proc.* **27**, 752–756 (2020).

16. O'Neal, B. ABS: Researchers Test Temperature & Speed Settings in FDM 3D Printing. (2019).

17. Picard, M., Mohanty, A. K. & Misra, M. Recent advances in additive manufacturing of engineering thermoplastics: challenges and opportunities. *RSC Adv.* **10**, 36058–36089 (2020).

18. Mark, J. E. *Physical properties of polymers*. vol. 1076 (Springer, 2007).

19. Wikipedia. Duroplaste. (2020).

20. Tieke, B. *Makromolekulare Chemie: Eine Einführung*. (John Wiley & Sons, 2014).

21. Bhowmick, A. K. & Stephens, H. *Handbook of elastomers*. (CRC Press, 2000).

22. Biron, M. *Thermosets and composites*. (Elsevier, 2003).

23. Drobny, J. G. *Handbook of thermoplastic elastomers*. (Elsevier, 2014).

24. Mondschein, R. J., Kanitkar, A., Williams, C. B., Verbridge, S. S. & Long, T. E. Polymer structure-property requirements for stereolithographic 3D printing of soft tissue engineering scaffolds. *Biomaterials* **140**, 170–188 (2017).

25. Melchels, F. P. W., Feijen, J. & Grijpma, D. W. A review on stereolithography and its applications in biomedical engineering. *Biomaterials* **31**, 6121–6130 (2010).

26. Dawood, A., Marti, B. M., Sauret-Jackson, V. & Darwood, A. 3D printing in dentistry. *Br. Dent. J.* **219**, 521–529 (2015).

27. Au, A. K., Huynh, W., Horowitz, L. F. & Folch, A. 3D-printed microfluidics. *Angew. Chemie Int. Ed.* **55**, 3862–3881 (2016).

28. Mendes-Felipe, C., Oliveira, J., Etxebarria, I., Vilas-Vilela, J. L. & Lanceros-Mendez, S. State-of-the-Art and Future Challenges of UV Curable Polymer-Based Smart Materials for Printing Technologies. *Adv. Mater. Technol.* **4**, 1800618 (2019).

29. Champeau, M. *et al.* 4D Printing of Hydrogels: A Review. *Adv. Funct. Mater.* 1910606 (2020).

30. Parra-Cabrera, C., Achille, C., Kuhn, S. & Ameloot, R. 3D printing in chemical engineering and catalytic technology: Structured catalysts, mixers and reactors. *Chem. Soc. Rev.* **47**, 209–230 (2018).

31. Gross, B. C., Erkal, J. L., Lockwood, S. Y., Chen, C. & Spence, D. M. Evaluation of 3D printing and its potential impact on biotechnology and the chemical sciences. *Anal. Chem.* **86**, 3240–3253 (2014).

32. Hurt, C. *et al.* Combining additive manufacturing and catalysis: A review. *Catal. Sci. Technol.* **7**, 3421–3439 (2017).

33. Hartings, M. R. & Ahmed, Z. Chemistry from 3D printed objects. *Nat. Rev. Chem.* **3**, 305–314 (2019).

34. Melchels, F. P. W., Feijen, J. & Grijpma, D. W. A review on stereolithography and its applications in biomedical engineering. *Biomaterials* **31**, 6121–6130 (2010).

35. Wu, C., Yi, R., Liu, Y.-J., He, Y. & Wang, C. C. L. Delta DLP 3D printing with large size. *2016 IEEE/RSJ Int. Conf. Intell. Robot. Syst.* 2155–2160 (2016).

36. Santoliquido, O., Colombo, P. & Ortona, A. Additive Manufacturing of ceramic components by Digital Light Processing: A comparison between the "bottom-up" and the "top-down" approaches. *J. Eur. Ceram. Soc.* **39**, 2140–2148 (2019).

37. Janusziewicz, R., Tumbleston, J. R., Quintanilla, A. L., Mecham, S. J. & DeSimone, J. M. Layerless fabrication with continuous liquid interface production. *Proc. Natl. Acad. Sci.* **113**, 11703–11708 (2016).

38. Tumbleston, J. R. *et al.* Continuous liquid interface production of 3D objects. *Science (80-.).* **347**, 1349–1352 (2015).

39. DeSimone, J. M., Ermoshkin, A., Ermoshkin, N., & Sarnulski, E. T. Continous Liquid Interphase Printing. (2014).

40. IUPAC. Compendum of Chemical Terminology 2nd ed. in (Blackwell Scientific Publications).

41. Christian, D. The use of UV irradiation in polymerization. *Polym. Int.* **45**, 133–141 (1998).

42. Christian, D. UV-radiation curing chemistry. *Pigment Resin Technol.* **30**, 278–286 (2001).

43. Decker, C. Light-induced crosslinking polymerization. *Polym. Int.* **51**, 1141–1150 (2002).

44. Schwalm, R. *UV coatings: basics, recent developments and new applications.* (Elsevier, 2006).

45. Zhang, J. & Xiao, P. 3D printing of photopolymers. *Polym. Chem.* **9**, 1530–1540 (2018).

46. Christian, D. Light-induced crosslinking polymerization. *Polym. Int.* **51**, 1141–1150 (2002).

47. Kaur, M. & Srivastava, A. K. Photopolymerization: A review. *J. Macromol. Sci. - Polym. Rev.* **42**, 481–512 (2002).

48. Jenkins, A. D. Photoinitiators for free radical cationic and anionic photopolymerisation. *Polym. Int.* **49**, 1729 (2000).

49. Fouassier, J.-P. *Photoinitiation, photopolymerization, and photocuring: fundamentals and applications.* (Hanser, 1995).

50. Fouassier, J.-P. & Lalevée, J. *Photoinitiators for polymer synthesis: scope, reactivity, and efficiency.* (John Wiley & Sons, 2012).

51. Dietliker, K. K. & Oldring, P. K. T. *Chemistry and Technology of UV and EB Formulation for Coatings, Inks and Paints: Photoinitiators for Free Radical and Cationic Polymerisation.* (Sita Technology, 1991).

52. Decker, C., Zahouily, K., Decker, D., Nguyen, T. & Viet, T. Performance analysis of acylphosphine oxides in photoinitiated polymerization. *Polymer (Guildf).* **42**, 7551–7560 (2001).

53. Decker, C. Photoinitiated crosslinking polymerisation. *Prog. Polym. Sci.* **21**, 593–650 (1996).

54. Lee, T. Y., Guymon, C. A., Jönsson, E. S. & Hoyle, C. E. The effect of monomer structure on oxygen inhibition of (meth) acrylates photopolymerization. *Polymer (Guildf).* **45**, 6155–6162 (2004).

55.   Atif, M., Bongiovanni, R. & Yang, J. Cationically UV-Cured Epoxy Composites. *Polym. Rev.* **55**, 90–106 (2015).

56.   Lalevée, J., Mokbel, H. & Fouassier, J. P. Recent developments of versatile photoinitiating systems for cationic ring opening polymerization operating at any wavelengths and under low light intensity sources. *Molecules* **20**, 7201–7221 (2015).

57.   Hoyle, C. E. & Bowman, C. N. Thiol–ene click chemistry. *Angew. Chemie Int. Ed.* **49**, 1540–1573 (2010).

58.   Kade, M. J., Burke, D. J. & Hawker, C. J. The power of thiol-ene chemistry. *J. Polym. Sci. Part A Polym. Chem.* **48**, 743–750 (2010).

59.   Uzcategui, A. C., Muralidharan, A., Ferguson, V. L., Bryant, S. J. & McLeod, R. R. Understanding and Improving Mechanical Properties in 3D printed Parts Using a Dual-Cure Acrylate-Based Resin for Stereolithography. *Adv. Eng. Mater.* **20**, 1800876 (2018).

60.   Taormina, G., Sciancalepore, C., Messori, M. & Bondioli, F. 3D printing processes for photocurable polymeric materials: technologies, materials, and future trends. *J. Appl. Biomater. Funct. Mater.* **16**, 151–160 (2018).

61.   Wallin, T. J. *et al.* 3D printable tough silicone double networks. *Nat. Commun.* **11**, 1–10 (2020).

62.   Bagheri, A. & Jin, J. Photopolymerization in 3D printing. *ACS Appl. Polym. Mater.* **1**, 593–611 (2019).

63.   Zhang, B. *et al.* Highly stretchable hydrogels for UV curing based high-resolution multimaterial 3D printing. *J. Mater. Chem. B* **6**, 3246–3253 (2018).

64.   Schimpf, V., Asmacher, A., Fuchs, A., Bruchmann, B. & Mülhaupt, R. Polyfunctional Acrylic Non-isocyanate Hydroxyurethanes as Photocurable Thermosets for 3D Printing. *Macromolecules* **52**, 3288–3297 (2019).

65.   Peng, S. *et al.* 3D Printing Mechanically Robust and Transparent Polyurethane Elastomers for Stretchable Electronic Sensors. *ACS Appl. Mater. Interfaces* **12**, 6479–6488 (2020).

66.   Appuhamillage, G. A. *et al.* 110th Anniversary: Vat Photopolymerization-Based Additive Manufacturing: Current Trends and Future Directions in Materials Design. *Ind. Eng. Chem. Res.* **58**, 15109–15118 (2019).

67. Zhu, X., Lu, G. & Nie, J. Chapter 6 Photopolymerization and its application in 3D printing of customized objects. in *3D Printing with Light* 203–230 (2021).

68. Menard, K. P. & Menard, N. Dynamic mechanical analysis. *Encycl. Anal. Chem. Appl. Theory Instrum.* 1–25 (2006).

69. Chartoff, R. P., Menczel, J. D. & Dillman, S. H. Dynamic mechanical analysis (DMA). *Therm. Anal. Polym. Fundam. Appl.* 387–495 (2009).

70. Menard, K. P. *Dynamic mechanical analysis: a practical introduction*. (CRC press, 2008).

71. Ehrenstein, G. W., Riedel, G. & Trawiel, P. *Thermal analysis of plastics: theory and practice*. (Carl Hanser Verlag GmbH Co KG, 2012).

72. Davis, J. R. *Tensile testing*. (ASM international, 2004).

73. Grellmann, W., Seidler, S. & Anderson, P. I. *Polymer testing*. (Hanser Munich, 2007).

74. Ligon-Auer, S. C., Schwentenwein, M., Gorsche, C., Stampfl, J. & Liska, R. Toughening of photo-curable polymer networks: A review. *Polym. Chem.* **7**, 257–286 (2016).

75. Mark, J. E. & Erman, B. *Rubberlike elasticity: a molecular primer*. (Cambridge University Press, 2007).

76. Treloar, L. R. G. The physics of rubber elasticity. (1975).

77. Dodiuk, H. *Handbook of thermoset plastics*. (William Andrew, 2013).

78. Landel, R. F. & Nielsen, L. E. *Mechanical properties of polymers and composites*. (CRC press, 1993).

79. Herzberger, J., Sirrine, J. M., Williams, C. B. & Long, T. E. Polymer Design for 3D Printing Elastomers: Recent Advances in Structure, Properties, and Printing. *Prog. Polym. Sci.* **97**, 101144 (2019).

80. Rubinstein, M. & Panyukov, S. Elasticity of Polymer Networks. *Macromolecules* **35**, 6670–6686 (2002).

81. Urayama, K. An experimentalist's view of the physics of rubber elasticity. *J. Polym. Sci. Part B Polym. Phys.* **44**, 3440–3444 (2006).

82. Anseth, K. S., Wang, C. M. & Bowman, C. N. Reaction behaviour and kinetic constants for photopolymerizations of multi(meth)acrylate monomers. *Polymer (Guildf).* **35**, 3243–3250 (1994).

83. Atkins, P. W. & De Paula, J. Physical chemistry. (1998).

84. Huang, S.-L. & Lai, J.-Y. Structure-tensile properties of polyurethanes. *Eur. Polym. J.* **33**, 1563–1567 (1997).

85. Flory, P. J. & Fox, T. G. Treatment of intrinsic viscosities. *J. Am. Chem. Soc.* **73**, 1904–1908 (1951).

86. Cooper, A. R. Mechanical Properties of Polymers: The Influence of Molecular Weight and Molecular Weight Distribution. *J. Macromol. Sci. Part C* **8**, 57–199 (1972).

87. Nunes, R. W., Martin, J. R. & Johnson, J. F. Influence of molecular weight and molecular weight distribution on mechanical properties of polymers. *Polym. Eng. Sci.* **22**, 205–228 (1982).

88. Quan, H. *et al.* Photo-curing 3D printing technique and its challenges. *Bioact. Mater.* **5**, 110–115 (2020).

89. Andrade, E. N. da C. The viscosity of liquids. *Nature* **125**, 309–310 (1930).

90. van Bochove, B., Schüller-Ravoo, S. & Grijpma, D. W. Photo-Crosslinked Elastomeric Bimodal Poly(trimethylene carbonate) Networks. *Macromol. Mater. Eng.* **304**, 1–5 (2019).

91. Schüller-Ravoo, S., Feijen, J. & Grijpma, D. W. Preparation of Flexible and Elastic Poly(trimethylene carbonate) Structures by Stereolithography. *Macromol. Biosci.* **11**, 1662–1671 (2011).

92. Sinh, L. H. *et al.* Novel photo-curable polyurethane resin for stereolithography. *RSC Adv.* **6**, 50706–50709 (2016).

93. Gorsche, C., Griesser, M., Gescheidt, G., Moszner, N. & Liska, R. β-allyl sulfones as addition–fragmentation chain transfer reagents: A tool for adjusting thermal and mechanical properties of dimethacrylate networks. *Macromolecules* **47**, 7327–7336 (2014).

94. Gorsche, C. *et al.* Rapid formation of regulated methacrylate networks yielding tough materials for lithography-based 3D printing. *Polym. Chem.* **7**, 2009–2014 (2016).

95. Schwalm, R. *et al.* Tuning the mechanical properties of UV coatings towards hard and flexible systems. *Prog. Org. Coatings* **32**, 191–196 (1997).

96. Decker, C., Masson, F. & Schwalm, R. Dual-curing of waterborne urethane-acrylate coatings by UV and thermal processing. *Macromol. Mater. Eng.* **288**, 17–28 (2003).

97. Bayer, O. Das di-isocyanat-polyadditionsverfahren (polyurethane). *Angew. Chemie* **59**, 257–272 (1947).

98. Akindoyo, J. O. *et al.* Polyurethane types, synthesis and applications-a review. *RSC Adv.* **6**, 114453–114482 (2016).

99. Engels, H. W. *et al.* Polyurethanes: Versatile materials and sustainable problem solvers for today's challenges. *Angew. Chemie - Int. Ed.* **52**, 9422–9441 (2013).

100. Arnold, R. G., Nelson, J. A. & Verbanc, J. J. Recent advances in isocyanate chemistry. *Chem. Rev.* **57**, 47–76 (1957).

101. Ozaki, S. Recent Advances in Isocyanate Chemistry. *Chem. Rev.* **72**, 457–496 (1972).

102. Wurtz, A. Recherches sur les ethers cyaniques et leurs derives. *CR Hebd. Seances. Acad. Sci* **27**, 241 (1848).

103. Hecking, A. *et al.* Polyisocyanate composition based on 1, 5-pentamethylene diisocyanate. (2018).

104. Varma, R. & Varma, D. R. The Bhopal Disaster of 1984. *Bull. Sci. Technol. Soc.* **25**, 37–45 (2005).

105. Laas, H. J., Halpaap, R. & Pedain, J. Zur Synthese aliphatischer Polyisocyanate– Lackpolyisocyanate mit Biuret-, Isocyanurat-oder Uretdionstruktur. *J. für Prakt. Chemie/Chemiker-Zeitung* **336**, 185–200 (1994).

106. Delebecq, E., Pascault, J.-P., Boutevin, B. & Ganachaud, F. On the versatility of urethane/urea bonds: reversibility, blocked isocyanate, and non-isocyanate polyurethane. *Chem. Rev.* **113**, 80–118 (2012).

107. Armistead, J. P., Wilkes, G. L. & Turner, R. B. Morphology of water-blown flexible polyurethane foams. *J. Appl. Polym. Sci.* **35**, 601–629 (1988).

108. Lipshitz, S. D. & Macosko, C. W. Kinetics and energetics of a fast polyurethane cure. *J. Appl. Polym. Sci.* **21**, 2029–2039 (1977).

109. Sonnenschein, M. F. *Polyurethanes: science, technology, markets, and trends*. (John Wiley & Sons, 2021).

110. Silva, A. L. & Bordado, J. C. Recent developments in polyurethane catalysis: Catalytic mechanisms review. *Catal. Rev. - Sci. Eng.* **46**, 31–51 (2004).

111. Chang, M. -C & Chen, S. -A. Kinetics and mechanism of urethane reactions: Phenyl isocyanate–alcohol systems. *J. Polym. Sci. Part A Polym. Chem.* **25**, 2543–2559 (1987).

112. Bloodworth, A. J. & Davies, A. G. 975. Organometallic reactions. Part I. The addition of tin alkoxides to isocyanates. *J. Chem. Soc.* **433**, 5238–5244 (1965).

113. Rand, L., Thir, B., Reegen, S. L. & Frisch, K. C. Kinetics of alcohol–isocyanate reactions with metal catalysts. *J. Appl. Polym. Sci.* **9**, 1787–1795 (1965).

114. Britain, J. W. & Gemeinhardt, P. G. Catalysis of the isocyanate-hydroxyl reaction. *J. Appl. Polym. Sci.* **4**, 207–211 (1960).

115. Guhl, D. Alternatives to DBTL catalysts in polyurethanes—A comparative study. in *Proceedings of the Polyurethanes for High Performance Coatings, European Coatings Conference* (2008).

116. Blank, W. J., He, Z. A. & Hessell, E. T. Catalysis of the isocyanate-hydroxyl reaction by non-tin catalysts. *Prog. Org. Coatings* **35**, 19–29 (1999).

117. Sardon, H. *et al.* Synthesis of polyurethanes using organocatalysis: A perspective. *Macromolecules* **48**, 3153–3165 (2015).

118. Golling, F. E. *et al.* Polyurethanes for coatings and adhesives – chemistry and applications. *Polym. Int.* (2018).

119. Heift, D., Benko, Z., Grützmacher, H., Jupp, A. R. & Goicoechea, J. M. Cyclo-oligomerization of isocyanates with Na(PH2) or Na(OCP) as 'p-' anion sources. *Chem. Sci.* **6**, 4017–4024 (2015).

120. Okumoto, S. & Yamabe, S. A Computational Study of Base-Catalyzed Reactions between Isocyanates and Epoxides Affording 2-Oxazolidones and Isocyanurates. *J. Comput. Chem.* **22**, 316–326 (2001).

121. Driest, P. J., Dijkstra, D. J., Stamatialis, D. & Grijpma, D. W. The Trimerization of Isocyanate-Functionalized Prepolymers: An Effective Method for Synthesizing Well-Defined Polymer Networks. *Macromol. Rapid Commun.* **40**, 1–6 (2019).

122. Widemann, M. *et al.* Structure-Property Relations in Oligomers of Linear Aliphatic Diisocyanates. *ACS Sustain. Chem. Eng.* **6**, 9753–9759 (2018).

123. Flipsen, T. A. C., Steendam, R., Pennings, A. J. & Hadziioannou, G. A novel thermoset polymer optical fiber. *Adv. Mater.* **8**, 45–48 (1996).

124. Bantu, B. *et al.* CO2 and SnII adducts of N-heterocyclic carbenes as delayed-action catalysts for polyurethane synthesis. *Chem. - A Eur. J.* **15**, 3103–3109 (2009).

125. Richter, F. U. 1,4,2-Diazaphospholidine-3,5-diones and related compounds: A lecture on unpredictability in catalysis. *Chem. - A Eur. J.* **15**, 5200–5202 (2009).

126. Ionescu, M. *Chemistry and technology of polyols for polyurethanes.* (iSmithers Rapra Publishing, 2005).

127. Meier-Westhues, H.-U. *Polyurethanes: coatings, adhesives and sealants.* (European Coatings, 2019).

128. Alagi, P. *et al.* Carbon Dioxide-Based Polyols as Sustainable Feedstock of Thermoplastic Polyurethane for Corrosion-Resistant Metal Coating. *ACS Sustain. Chem. Eng.* **5**, 3871–3881 (2017).

129. Von Der Assen, N. & Bardow, A. Life cycle assessment of polyols for polyurethane production using CO 2 as feedstock: Insights from an industrial case study. *Green Chem.* **16**, 3272–3280 (2014).

130. Yilgor, I. & Yilgor, E. Structure-morphology-property behavior of segmented thermoplastic polyurethanes and polyureas prepared without chain extenders. *Polym. Rev.* **47**, 487–510 (2007).

131. Yilgör, I., Yilgör, E. & Wilkes, G. L. Critical parameters in designing segmented polyurethanes and their effect on morphology and properties: A comprehensive review. *Polymer (Guildf).* **58**, A1–A36 (2015).

132. Datta, J. & Kasprzyk, P. Thermoplastic polyurethanes derived from petrochemical or renewable resources: A comprehensive review. *Polym. Eng. Sci.* **58**, E14–E35 (2018).

133. Qi, H. J. & Boyce, M. C. Stress–strain behavior of thermoplastic polyurethanes. *Mech. Mater.* **37**, 817–839 (2005).

134. Driest, P. J. Poly(urethane-isocyanurate) networks. (University of Twente).

135. Wicks, D. A. & Wicks, Z. W. Blocked isocyanates III: Part A. Mechanisms and chemistry. *Prog. Org. Coatings* **36**, 148–172 (1999).

136. Wicks, D. A. & Wicks Jr, Z. W. Blocked isocyanates III: Part B: Uses and applications of blocked isocyanates. *Prog. Org. Coatings* **41**, 1–83 (2001).

137. Bijlard, A. C., Hansen, A., Lieberwirth, I., Landfester, K. & Taden, A. A Nanocapsule-Based Approach Toward Physical Thermolatent Catalysis. *Adv. Mater.* **28**, 6372–6377 (2016).

138. Zöller, T., Iovkova-Berends, L., Dietz, C., Berends, T. & Jurkschat, K. On the reaction of elemental tin with alcohols: a straightforward approach to tin (II) and tin (IV) alkoxides and related tinoxo clusters. *Chem. Eur. J.* **17**, 2361–2364 (2011).

139. Samborska-Skowron, R. & Balas, A. An overview of developments in poly(urethane-isocyanurates) elastomers. *Polym. Adv. Technol.* **13**, 653–662 (2002).

140. Nobuyoshi, S., Tetsuo, Y. & Tanaka, T. Properties of Isocyanurate-Type Crosslinked Polyurethanes. *J. Polym. Sci.* **11**, 1765–1779 (1973).

141. Spirkova, M., Budinski-Simendic, J., Ilavsky, M., Spacek, P. & Dusek, K. Formation of poly(urethane-isocyanurate) networks from poly(oxypropylene)diols and diisocyanate. *Polym. Bull.* **31**, 83–88 (1993).

142. Petrovic, Z. S. & Ferguson, J. Polyurethane Elastomers. *Prog. Polym. Sci.* **16**, 695–836 (1991).

143. Burel, F., Poussard, L., Tabrizian, M., Merhi, Y. & Bunel, C. The influence of isocyanurate content on the bioperformance of hydrocarbon-based polyurethanes. *J. Biomater. Sci. Polym. Ed.* **19**, 525–540 (2008).

144. Moritsugu, M., Sudo, A. & Endo, T. Cyclotrimerization of diisocyanates toward high-performance networked polymers with rigid isocyanurate structure: Combination of aromatic and aliphatic diisocyanates for tunable flexibility. *J. Polym. Sci. Part A Polym. Chem.* **51**, 2631–2637 (2013).

145. Preis, E., Schindler, N., Adrian, S. & Scherf, U. Microporous Polymer Networks Made by Cyclotrimerization of Commercial, Aromatic Diisocyanates. *ACS Macro Lett.* **4**, 1268–1272 (2015).

146. Speckhard, T. A. *et al.* Properties of UV-curable polyurethane acrylates: Effect of reactive diluent. *J. Appl. Polym. Sci.* **30**, 647–666 (1985).

147. Kim, B. K., Lee, K. H. & Kim, H. D. Preparation and properties of UV-curable polyurethane acrylates. *J. Appl. Polym. Sci.* **60**, 799–805 (1996).

148. Koshiba, M., Hwang, K. K. S., Foley, S. K., Yarusso, D. J. & Cooper, S. L. Properties of ultra-violet curable polyurethane acrylates. *J. Mater. Sci.* **17**, 1447–1458 (1982).

149. Kim, B. K., Lee, K. H. & Jo, N. J. Basic Structure-Property Behavior of UV Curable Polyurethane Acrylates. *J. Polym. Sci. Part A Polym. Chem.* **34**, 2095–2102 (1996).

150. Frisch, K. C. & Klempner, D. *Advances in Urethane: Science & Technology.* vol. 14 (CRC Press, 1998).

151. Lin, S. B. *et al.* Properties of UV-cured polyurethane acrylates: Effect of polyol type and molecular weight. *Chem. Eng. Commun.* **30**, 251–273 (1984).

152. Gamardella, F., Sabatini, V., Ramis, X. & Serra, À. Tailor-made thermosets obtained by sequential dual-curing combining isocyanate-thiol and epoxy-thiol click reactions. *Polymer (Guildf).* **174**, 200–209 (2019).

153. Ramis, X., Fernández-Francos, X., De la Flor, S., Ferrando, F. & Serra, A. Click-based dual-curing thermosets and their applications. in *Thermosets: Structure, Properties, and Applications: Second Edition* 511–541 (2018).

154. Tercjak, A. Phase separation and morphology development in thermoplastic-modified thermosets. in *Thermosets: Structure, Properties, and Applications: Second Edition* 147–171 (Elsevier Ltd., 2018).

155. Studer, K., Decker, C., Beck, E. & Schwalm, R. Thermal and photochemical curing of isocyanate and acrylate functionalized oligomers. *Eur. Polym. J.* **41**, 157–167 (2005).

156. Hur, T., Manson, J. A., Hertzberg, R. W. & Sperling, L. H. Fatigue behavior of acrylic interpenetrating polymer networks. II. *J. Appl. Polym. Sci.* **39**, 1933–1947 (1990).

157. Kim, S. C., Klempner, D., Frisch, K. C., Radigan, W. & Frisch, H. L. Polyurethane Interpenetrating Polymer Networks. I. Synthesis and Morphology of Polyurethane-Poly(methyl methacrylate) Interpenetrating Polymer Networks. *Macromolecules* **9**, 258–263 (1976).

158. Sperling, L. H. & Misra, V. The current status of interpenetrating networks. *IPNs around world Sci. Eng.* **1658**, (1997).

159. Gong, J. P., Katsuyama, Y., Kurokawa, T. & Osada, Y. Double-network hydrogels with extremely high mechanical strength. *Adv. Mater.* **15**, 1155–1158 (2003).

160. Shams Es-haghi, S. & Weiss, R. A. Fabrication of Tough Hydrogels from Chemically Cross-Linked Multiple Neutral Networks. *Macromolecules* **49**, 8980–8987 (2016).

161. Lipatov, Y. S. & Alekseeva, T. T. *Phase-separated interpenetrating polymer networks. Advances in Polymer Science* vol. 208 (2007).

162. Liu, Y. Polymerization-induced phase separation and resulting thermomechanical properties of thermosetting/reactive nonlinear polymer blends: A review. *J. Appl. Polym. Sci.* **127**, 3279–3292 (2013).

163. Nevissas, V., Widmaier, J. M. & Meyer, G. C. Effect of crosslink density and internetwork grafting on the transparency of polyurethane/polystyrene interpenetrating polymer networks. *J. Appl. Polym. Sci.* **36**, 1467–1473 (1988).

164. Hasa, E., Stansbury, J. W. & Guymon, C. A. Manipulation of crosslinking in photo-induced phase separated polymers to control morphology and thermomechanical properties. *Polymer (Guildf).* **202**, 122699 (2020).

165. Sperling, L. H. & Mishra, V. The current status of interpenetrating polymer networks. *Polym. Adv. Technol.* **7**, 197–208 (1996).

166. Alemán, J. *et al.* Definitions of terms relating to the structure and processing of sols, gels, networks, and inorganic-organic hybrid materials (IUPAC recommendations 2007). *Pure Appl. Chem.* **79**, 1801–1829 (2007).

167. He, X., Widmaier, J. -M & Meyer, G. C. Kinetics of phase separation in polyurethane/polystyrene semi-1 interpenetrating polymer networks. 2. Microscopy observations and theoretical approach. *Polym. Int.* **32**, 295–301 (1993).

168. Kim, S. C., Klempner, D., Frisch, K. C. & Frisch, H. L. Polyurethane Interpenetrating Polymer Networks. II. Density and Glass Transition Behavior of Polyurethane-Poly(methyl methacrylate) and Polyurethane-Polystyrene IPN'S. *Macromolecules* **9**, 263–266 (1976).

169. Sperling, L. H. Interpenetrating Polymer Networks: An Overview. in *Interpenetrating Polymer Networks* vol. 239 3–38 (American Chemical Society, 2020).

170. Sperling, L. H. & Hu, R. Interpenetrating polymer networks. *Polym. Blends Handb.* 677–724 (2014).

171. Jordhamo, G. M., Manson, J. A. & Sperling, L. H. Phase continuity and inversion in polymer blends and simultaneous interpenetrating networks. *Polym. Eng. Sci.* **26**, 517–524 (1986).

172. Sperling, L. H. Interpenetrating polymer networks and related materials. *J. Polym. Sci. Macromol. Rev.* **12**, 141–180 (1977).

173. Wang, C. L., Klempner, D. & Frisch, K. C. Morphology of Polyurethane- Isocyanurate Elastomers. *J. Appl. Polym. Sci.* **30**, 4337–4344 (1985).

174. Nesterov, A. E. & Lipatov, Y. S. *Thermodynamics of polymer blends*. vol. 1 (CRC Press, 1998).

175. Pötschke, P. & Paul, D. R. Formation of co-continuous structures in melt-mixed immiscible polymer blends. *J. Macromol. Sci. - Polym. Rev.* **43**, 87–141 (2003).

176. Burford, R. P., Markotsis, M. G. & Knott, R. B. Small angle neutron scattering and transmission electron microscopy studies of interpenetrating polymer networks from thermoplastic elastomers. *Nucl. Instruments Methods Phys. Res. Sect. B Beam Interact. with Mater. Atoms* **208**, 58–65 (2003).

177. Tan, S., Zhang, D. & Zhou, E. Use of SAXS to Characterize the Morphology of Poly (polyethylene glycol diacrylate) / Epoxy Resin Interpenetrating Networks. **42**, 90–94 (1997).

178. Burford, R. P., Markotsis, M. G. & Knott, R. B. Real-time SANS study of interpenetrating polymer network (IPN) formation. *Phys. B Condens. Matter* **385–386**, 766–769 (2006).

179. Pfeifer, C. S. *et al.* Tailoring heterogeneous polymer networks through polymerization-induced phase separation: Influence of composition and processing conditions on reaction kinetics and optical properties. *J. Polym. Sci. Part A Polym. Chem.* **52**, 1796–1806 (2014).

180. Konuray, O., Fernández-Francos, X., Ramis, X. & Serra, À. State of the art in dual-curing acrylate systems. *Polymers (Basel).* **10**, 1–24 (2018).

181. Chatani, S., Kloxin, C. J. & Bowman, C. N. The power of light in polymer science: photochemical processes to manipulate polymer formation, structure, and properties. *Polym. Chem.* **5**, 2187–2201 (2014).

182. Carioscia, J. A., Stansbury, J. W. & Bowman, C. N. Evaluation and control of thiol–ene/thiol–epoxy hybrid networks. *Polymer (Guildf).* **48**, 1526–1532 (2007).

183. Bowman, C. N. & Kloxin, C. J. Toward an enhanced understanding and implementation of photopolymerization reactions. *AIChE J.* **54**, 2775–2795 (2008).

184. Velankar, S., Pazos, J. & Cooper, S. L. High-performance UV-curable urethane acrylates via deblocking chemistry. *J. Appl. Polym. Sci.* **62**, 1361–1376 (1996).

185. Decker, C., Viet, T. N. T. & Decker, D. UV-radiation curing of acrylate / epoxide systems. **42**, 5531–5541 (2001).

186. Cai, Y. & Jessop, J. L. P. Decreased oxygen inhibition in photopolymerized acrylate/epoxide hybrid polymer coatings as demonstrated by Raman spectroscopy. *Polymer (Guildf).* **47**, 6560–6566 (2006).

187. Huang, B., Du, Z., Yong, T. & Han, W. Preparation of a novel hybrid type photosensitive resin for stereolithography in 3D printing and testing on the accuracy of the fabricated parts. *J. Wuhan Univ. Technol. Mater. Sci. Ed.* **32**, 726–732 (2017).

188. Schwartz, J. J. & Boydston, A. J. Multimaterial actinic spatial control 3D and 4D printing. *Nat. Commun.* **10**, 1–10 (2019).

189. Shan, J. *et al.* Design and Synthesis of Free-Radical / Cationic Photosensitive Resin Applied for 3D Printer with Liquid Crystal (LCD) Irradiation. *Polymers (Basel).* **12**, 1346 (2020).

190. Hegde, M. *et al.* 3D Printing All-Aromatic Polyimides using Mask-Projection Stereolithography: Processing the Nonprocessable. *Adv. Mater.* **29**, 1701240 (2017).

191. Sirrine, J. M. *et al.* Functional siloxanes with photo-activated, simultaneous chain extension and crosslinking for lithography-based 3D printing. *Polymer (Guildf).* **152**, 25–34 (2018).

192. Scott, P. J. *et al.* Additive Manufacturing of Hydrocarbon Elastomers via Simultaneous Chain Extension and Cross-linking of Hydrogenated Polybutadiene. *ACS Appl. Polym. Mater.* **1**, 684–690 (2019).

193. Kuang, X. *et al.* High-Speed 3D Printing of High-Performance Thermosetting Polymers via Two-Stage Curing. *Macromol. Rapid Commun.* **39**, 1–8 (2018).

194. Griffini, G. *et al.* 3D-printable CFR polymer composites with dual-cure sequential IPNs. *Polymer (Guildf).* **91**, 174–179 (2016).

195. Invernizzi, M., Natale, G., Levi, M., Turri, S. & Griffini, G. UV-assisted 3D printing of glass and carbon fiber-reinforced dual-cure polymer composites. *Materials (Basel).* **9**, (2016).

196. Obst, P. *et al.* Investigation of the influence of exposure time on the dual-curing reaction of RPU 70 during the DLS process and the resulting mechanical part properties. *Addit. Manuf.* **32**, 101002 (2020).

197. Poelma, B. J. & Rolland, J. Can Expand Applications. *Insights* **358**, 1384–1386 (2017).

198. Rolland, J. P. Functional materials for 3D manufacturing using carbon's CLIP technology. *J. Photopolym. Sci. Technol.* **29**, 451–452 (2016).

199. Lu, C., Wang, C., Yu, J., Wang, J. & Chu, F. Two-Step 3 D-Printing Approach toward Sustainable, Repairable, Fluorescent Shape-Memory Thermosets Derived from Cellulose and Rosin. *ChemSusChem* **13**, 893–902 (2020).

200. Zhou, Z. X. *et al.* Synthesis and characterization of a dual-curing resin for three-dimensional printing. *J. Mater. Sci.* **54**, 5865–5876 (2019).

201. Gao, H. *et al.* Mechanically Robust and Reprocessable Acrylate Vitrimers with Hydrogen-Bond-Integrated Networks for Photo-3D Printing. *ACS Appl. Mater. Interfaces* **13**, 1581–1591 (2021).

202. Zhang, B., Kowsari, K., Serjouei, A., Dunn, M. L. & Ge, Q. Reprocessable thermosets for sustainable three-dimensional printing. *Nat. Commun.* **9**, 1–7 (2018).

203. Wang, X. *et al.* i3DP, a robust 3D printing approach enabling genetic post-printing surface modification. *Chem. Commun.* **49**, 10064–10066 (2013).

204. Guo, Q., Cai, X., Wang, X. & Yang, J. "Paintable" 3D printed structures via a post-ATRP process with antimicrobial function for biomedical applications. *J. Mater. Chem. B* **1**, 6644–6649 (2013).

205. Zhang, Y. Post-printing surface modification and functionalization of 3D-printed biomedical device. *Int. J. Bioprinting* **3**, 93–99 (2017).

206. Hoffmann, A. *et al.* New stereolithographic resin providing functional surfaces for biocompatible three-dimensional printing. *J. Tissue Eng.* **8**, 1–9 (2017).

207. Roppolo, I. *et al.* Thiol–yne chemistry for 3D printing: exploiting an off-stoichiometric route for selective functionalization of 3D objects. *Polym. Chem.* **10**, 5950–5958 (2019).

208. Farrer, R. A. *et al.* Selective Functionalization of 3-D Polymer Microstructures. *J. Am. Chem. Soc.* **128**, 1796–1797 (2006).

209. Hansen, A., Renner, M., Griesbeck, A. G. & Büsgen, T. From 3D to 4D printing: A reactor for photochemical experiments using hybrid polyurethane acrylates for vat-based polymerization and surface functionalization. *Chem. Commun.* **56**, 15161–15164 (2020).

210. Liska, R. *et al.* Photopolymers for rapid prototyping. *J. Coatings Technol. Res.* **4**, 505–510 (2007).

211. Zhang, J. & Xiao, P. 3D printing of photopolymers. *Polym. Chem.* **9**, 1530–1540 (2018).

212. Scott, P. J. *et al.* 3D Printing Latex: A Route to Complex Geometries of High Molecular Weight Polymers. *ACS Appl. Mater. Interfaces* **12**, 10918–10928 (2020).

213. Rossi, S., Puglisi, A. & Benaglia, M. Additive Manufacturing Technologies: 3D Printing in Organic Synthesis. *ChemCatChem* **10**, 1512–1525 (2018).

214. Waheed, S. *et al.* 3D printed microfluidic devices: Enablers and barriers. *Lab Chip* **16**, 1993–2013 (2016).

215. Li, F., Macdonald, N. P., Guijt, R. M. & Breadmore, M. C. Increasing the functionalities of 3D printed microchemical devices by single material, multimaterial, and print-pause-print 3D printing. *Lab Chip* **19**, 35–49 (2019).

216. Naderi, A., Bhattacharjee, N. & Folch, A. Digital Manufacturing for Microfluidics. *Annu. Rev. Biomed. Eng.* **21**, 325–364 (2019).

217. Kitson, P. J., Symes, M. D., Dragone, V. & Cronin, L. Combining 3D printing and liquid handling to produce user-friendly reactionware for chemical synthesis and purification. *Chem. Sci.* **4**, 3099–3103 (2013).

218. Symes, M. D. *et al.* Integrated 3D-printed reactionware for chemical synthesis and analysis. *Nat. Chem.* **4**, 349–354 (2012).

219. Kitson, P. J. *et al.* 3D printing of versatile reactionware for chemical synthesis. *Nat. Protoc.* **11**, 920–936 (2016).

220. Zhang, Z., Corrigan, N., Bagheri, A., Jin, J. & Boyer, C. A Versatile 3D and 4D Printing System through Photocontrolled RAFT Polymerization. *Angew. Chemie* **131**, 18122–18131 (2019).

221. Capel, A. J. *et al.* Design and additive manufacture for flow chemistry. *Lab Chip* **13**, 4583–4590 (2013).

222. Kotz, F., Risch, P., Helmer, D. & Rapp, B. E. High-Performance Materials for 3D Printing in Chemical Synthesis Applications. *Adv. Mater.* **31**, 1805982 (2019).

223. Kotz, F. *et al.* Three-dimensional printing of transparent fused silica glass. *Nature* **544**, 337–339 (2017).

224. Kotz, F., Risch, P., Helmer, D. & Rapp, B. E. High-Performance Materials for 3D Printing in Chemical Synthesis Applications. *Adv. Mater.* **31**, (2019).

225. Kotz, F., Risch, P., Helmer, D. & Rapp, B. E. Highly fluorinated methacrylates for optical 3D printing of microfluidic devices. *Micromachines* **9**, 115 (2018).

226. Renner, M. & Griesbeck, A. Think and Print: 3D Printing of Chemical Experiments. *J. Chem. Educ.* **97**, 3683–3689 (2020).

227. Ravelli, D., Protti, S., Neri, P., Fagnoni, M. & Albini, A. Photochemical technologies assessed: the case of rose oxide. *Green Chem.* **13**, 1876–1884 (2011).

228. Schweitzer, C. & Schmidt, R. Physical mechanisms of generation and deactivation of singlet oxygen. *Chem. Rev.* **103**, 1685–1758 (2003).

229. Renner, M. 3D-Drucken von chemischen Experimenten. (2021).

230. Huang, Y., Hunston, D. L., Kinloch, A. J. & Riew, C. K. Mechanisms of Toughening Thermoset Resins. in *Toughened Plastics I* vol. 233 1 (American Chemical Society, 1993).

231. Zhou, Z. X. *et al.* High-Performance Cyanate Ester Resins with Interpenetration Networks for 3D Printing. *ACS Appl. Mater. Interfaces* **12**, 38682–38689 (2020).

232. Flory, P. J. Molecular size distribution in linear condensation polymers1. *J. Am. Chem. Soc.* **58**, 1877–1885 (1936).

233. Pohl, M. *et al.* Dynamics of Polyether Polyols and Polyether Carbonate Polyols. *Macromolecules* **49**, 8995–9003 (2016).

234. Ol'khovikov, O. A., Golubev, V. M. & Gladkovskii, G. A. The viscosity of polypropylene glycol oligomers as a function of temperature and molecular weight. *Polym. Sci. U.S.S.R.* **15**, 2843–2849 (1973).

235. Takayanagi, M., Uemura, S. & Minami, S. Application of equivalent model method to dynamic rheo-optical properties of crystalline polymer. in *Journal of Polymer Science Part C: Polymer Symposia* vol. 5 113–122 (Wiley Online Library, 1964).

236. Kerner, E. H. The Elastic and Thermo-elastic Properties of Composite Media. *Proc. Phys. Soc. Sect. B* **69**, 808–813 (1956).

237. Veenstra, H. *et al.* On the mechanical properties of co-continuous polymer blends: Experimental and modelling. *Polymer (Guildf).* **41**, 1817–1826 (2000).

238. Kolařík, J. Three-dimensional models for predicting the modulus and yield strength of polymer blends, foams, and particulate composites. *Polym. Compos.* **18**, 433–441 (1997).

239. Edwards, S. F. & Vilgis, T. A. The tube model theory of rubber elasticity. *Reports Prog. Phys.* **51**, 243–297 (1988).

240. Roland, C. M. Unconventional rubber networks: Circumventing the compromise between stiffness and strength. *Rubber Chem. Technol.* **86**, 351–366 (2013).

241. Truby, R. L. & Lewis, J. A. Printing soft matter in three dimensions. *Nature* **540**, 371–378 (2016).

242. Deng, Y., Li, J., He, Z., Hong, J. & Bao, J. Urethane acrylate-based photosensitive resin for three-dimensional printing of stereolithographic elastomer. *J. Appl. Polym. Sci.* 1–12 (2020).

243. Patel, D. K. *et al.* Highly stretchable and UV curable elastomers for digital light processing based 3D printing. *Adv. Mater.* **29**, 1606000 (2017).

244. Kuang, X. *et al.* 3D Printing of Highly Stretchable, Shape-Memory, and Self-Healing Elastomer toward Novel 4D Printing. *ACS Appl. Mater. Interfaces* **10**, 7381–7388 (2018).

245. Jeong, G. *et al.* Photocurable Elastomer Composites with SiO 2 -Mediated Cross-Links for Mechanically Durable 3D Printing Materials. *ACS Appl. Polym. Mater.* (2020).

246. Li, X. *et al.* Self-Healing Polyurethane Elastomers Based on a Disulfide Bond by Digital Light Processing 3D Printing. *ACS Macro Lett.* **8**, 1511–1516 (2019).

247. Thrasher, C. J., Schwartz, J. J. & Boydston, A. J. Modular Elastomer Photoresins for Digital Light Processing Additive Manufacturing. *ACS Appl. Mater. Interfaces* **9**, 39708–39716 (2017).

248. van Bochove, B., Schüller-Ravoo, S. & Grijpma, D. W. Photo-Crosslinked Elastomeric Bimodal Poly(trimethylene carbonate) Networks. *Macromol. Mater. Eng.* **304**, 1–5 (2019).

249. Webber, R. E., Creton, C., Brown, H. R. & Gong, J. P. Large Strain Hysteresis and Mullins Effect of Tough Double-Network Hydrogels. *Macromolecules* **40**, 2919–2927 (2007).

250. Etienne, D., Yulan, C., Markus, B., P., S. R. & Costantino, C. Toughening Elastomers with Sacrificial Bonds and Watching Them Break. *Science (80-.).* **344**, 186–189 (2014).

251. Maurya, S. D., Kurmvanshi, S. K., Mohanty, S. & Nayak, S. K. A Review on Acrylate-Terminated Urethane Oligomers and Polymers: Synthesis and Applications. *Polym. - Plast. Technol. Eng.* **57**, 625–656 (2018).

252. Lu, W. *et al.* All acrylic-based thermoplastic elastomers with high upper service temperature and superior mechanical properties. *Polym. Chem.* **8**, 5741–5748 (2017).

253. Kolb, C., Lindemann, N., Wolter, H. & Sextl, G. 3D-printing of highly translucent ORMOCER®-based resin using light absorber for high dimensional accuracy. *J. Appl. Polym. Sci.* **138**, 49691 (2021).

254. Wojciak, S. (Meth) acrylate compositions having a self-indicator of cure and methods of detecting cure. (2005).

Erklärung zur Dissertation

gemäß der Promotionsordnung vom 12. März 2020

„Hiermit versichere ich an Eides statt, dass ich die vorliegende Dissertation selbstständig und ohne die Benutzung anderer als der angegebenen Hilfsmittel und Literatur angefertigt habe. Alle Stellen, die wörtlich oder sinngemäß aus veröffentlichten und nicht veröffentlichten Werken dem Wortlaut oder dem Sinn nach entnommen wurden, sind als solche kenntlich gemacht. Ich versichere an Eides statt, dass diese Dissertation noch keiner anderen Fakultät oder Universität zur Prüfung vorgelegen hat; dass sie - abgesehen von unten angegebenen Teilpublikationen und eingebundenen Artikeln und Manuskripten - noch nicht veröffentlicht worden ist sowie, dass ich eine Veröffentlichung der Dissertation vor Abschluss der Promotion nicht ohne Genehmigung des Promotionsausschusses vornehmen werde. Die Bestimmungen dieser Ordnung sind mir bekannt. Darüber hinaus erkläre ich hiermit, dass ich die Ordnung zur Sicherung guter wissenschaftlicher Praxis und zum Umgang mit wissenschaftlichem Fehlverhalten der Universität zu Köln gelesen und sie bei der Durchführung der Dissertation zugrundeliegenden Arbeiten und der schriftlich verfassten Dissertation beachtet habe und verpflichte mich hiermit, die dort genannten Vorgaben bei allen wissenschaftlichen Tätigkeiten zu beachten und umzusetzen. Ich versichere, dass die eingereichte elektronische Fassung der eingereichten Druckfassung vollständig entspricht."

Publications and Patents

- Hansen, A., Renner, M., Griesbeck, A. G. & Büsgen, T. From 3D to 4D printing: A reactor for photochemical experiments using hybrid polyurethane acrylates for vat-based polymerization and surface functionalization. *Chem. Commun.* **56**, 15161–15164 (2020).

- Hansen, A., Achten, D., Büsgen T. & Griesbeck, A.G. 3D printed elastomers via sequential network formation. *in preparation.*

- Hansen, A., Achten & D. Büsgen T., J. Photo- and thermally curable resin useful for additive manufacturing, EP21174109.5.

- Hansen, A., Achten, D. Büsgen T. & Sütterlin, J. Photo- and thermally curable resin useful in additive manufacturing processes, EP21184735.5.

- Hansen, A., Achten, D., Büsgen, T., Sütterlin, J. & Weickard, J., Photo- and thermally curable resin useful in additive manufacturing processes, EP21202047.3.

Conferences

- Digital poster- and video presentation: "Hybrid polyurethane acrylates for 3D printed reactors featuring solvent resistance, transparency and surface functionalization", Freiburg Macromolecular Colloquium, 26.02.2021.

Die Primärdaten dieser Arbeit sind auf dem Server der Covestro Deutschland AG abgesichert.

Köln, 30.12.2021

Ort, Datum, Unterschrift